



RELAXATION MODELS APPLIED TO PALEOCLIMATE DYNAMICS: SOUTHERN OCEAN MECHANISMS CONTROLLING GLACIAL-INTERGLACIAL CYCLES



CARMEN HERRERO



CARMEN
HERRERO

RELAXATION MODELS APPLIED TO PALEOCLIMATE DYNAMICS: SOUTHERN OCEAN MECHANISMS CONTROLLING GLACIAL-INTERGLACIAL CYCLES

Barcelona
October 2015





D^a MARÍA ISABEL PADILLA LEÓN, SECRETARIA DE LA FACULTAD DE CIENCIAS DEL MAR, ÓRGANO RESPONSABLE DEL PROGRAMA DE DOCTORADO EN OCEANOGRAFÍA, DE LA UNIVERSIDAD DE LAS PALMAS DE GRAN CANARIA.

CERTIFICA


Que el Consejo de Doctores del Programa de Doctorado en Oceanografía, en su sesión de fecha 28 de octubre de 2015, tomó el acuerdo de dar el consentimiento para la tramitación, de la tesis doctoral titulada:

“Relaxation Models Applied To Paleoclimate Dynamics: Southern Ocean Mechanisms Controlling Glacial-Interglacial Cycles ”

presentada por la doctoranda: **D^a Carmen Herrero Navarro**
dirigida por el Doctor D. Antonio García-Olivares Rodríguez

Y para que así conste, a efectos de lo previsto en el Artº 6 del Reglamento para la elaboración, tribunal defensa y evaluación de tesis doctorales de la Universidad de Las Palmas de Gran Canaria, firmo el presente en Las Palmas de Gran Canaria, a veintiocho de octubre de dos mil quince.

| | |

PÁGINA 1 / 1	ID. DOCUMENTO XwwN32p7awxT6rz34GMFFg\$\$			
FIRMADO POR		FECHA FIRMA	ID. FIRMA	
43646105V ISABEL PADILLA LEÓN		29/10/2015 13:05:48	NT10NTY=	

**RELAXATION MODELS
APPLIED TO
PALEOCLIMATE DYNAMICS:
SOUTHERN OCEAN
MECHANISMS CONTROLLING
GLACIAL-INTERGLACIAL CYCLES**

**MODELOS DE RELAJACIÓN APLICADOS A LA
DINÁMICA PALEOCLIMÁTICA: MECANISMOS
DEL OCÉANO AUSTRAL CONTROLANDO LOS
CICLOS GLACIALES-INTERGLACIALES**

Tesis doctoral presentada por

Carmen Herrero Navarro

dirigida por el Dr.

Antonio García-Olivares Rodríguez

para obtener el grado de Doctora por la
Universidad de Las Palmas de Gran Canaria,
Departamento de Física,

DOCTORADO EN OCEANOGRAFÍA

Bienio 2012-2014

En Barcelona, a octubre de 2015

El director

La doctoranda



A la meua família

Contents

12 Preface

14 Acknowledgements

22 Glossary

23..... INTRODUCTION

**30 Chapter 1. RELAXATION MODELS APPLIED TO LATE
PLEISTOCENE CLIMATIC OSCILLATIONS**

33..... 1.1. INTRODUCTION

34..... 1.2. PP04-DERIVED MODELS

37 1.2.1. Biological export production model

43 1.2.2. Two response times for CO₂

44 1.2.3. Two response times for ice volume

46 1.2.4. Oceanic pulse exponentially
dependent on stratification

46 1.2.5. 3τ model

47 1.2.6. Local stratification model

48..... 1.3. MODELS PERFORMANCE

50..... 1.4. DISCUSSION

**56..... Chapter 2. ON THE PHYSICAL MECHANISMS BEHIND
GLACIAL-INTERGLACIAL DYNAMICS**

59..... 2.1. INTRODUCTION

60..... 2.2. RELAXATION MODELS

63..... 2.3. NON-LINEAR ANALYSIS

63 2.3.1. Fourier transform

63	2.3.2. Wavelet transform
73	2.3.3. Phase space portraits
81	2.3.4. Cross recurrence plots
81	2.4. ALTERNATIVE PROXY FOR ICE VOLUME
86	2.5. DYNAMICS OF THE MODELS
94	2.6. OBSERVATIONAL DYNAMICS
99	2.7. DISCUSSION

106..... Chapter 3. IMPACT OF ANTHROPOGENIC CO₂ ON THE NEXT GLACIAL CYCLE

109	3.1. INTRODUCTION
110	3.2. RELAXATION MODELS
111	3.3. ANTHROPOGENIC CO ₂ EMISSIONS
	111..... 3.3.1. Total CO ₂ emission
	114..... 3.3.2. CO ₂ atmospheric response
116	3.4. PROJECTIONS FOR THE NEXT GLACIAL CYCLE
123	3.5. DISCUSSION

128..... Chapter 4. INSIGHT TO MARINE ISOTOPIC STAGE 13 USING LATE PLEISTOCENE RELAXATION MODELS AND SEA LEVEL STACK

131	4.1. INTRODUCTION
132	4.2. RELAXATION MODELS
134	4.3. NON-LINEAR ANALYSIS OF BOTH SIMULATED AND PROXY TIME SERIES
137	4.4. DYNAMICS OF SEA LEVEL RE-CALIBRATED MODELS
137	4.5. DISCUSSION

145..... CONCLUSIONS

150..... **Appendix A. On insolation forcing**

152 **Appendix B. Genetic algorithms for optimization**

155..... **Appendix C. Resumen en castellano**

155..... C.1. INTRODUCCIÓN

162.... C.1.1. Objetivos y estructura de la tesis

163..... C.2. CAPÍTULO 1: MODELOS DE RELAJACIÓN APLICADOS
A LAS OSCILACIONES CLIMÁTICAS

164.... C.2.1. Modelos de relajación

169.... C.2.2. Funcionamiento y dinámica de los modelos

171..... C.3. CAPÍTULO 2: MECANISMOS FÍSICOS TRAS A LA
DINÁMICA DE LOS CICLOS GLACIARESINTERGLACIARES

172.... C.3.1. Modelos 3τ y LS

175.... C.3.2. Dinámica de los modelos

181..... C.4. CHAPTER 3: IMPACTO DEL CO₂ ANTROPOGÉNICO
EN EL PRÓXIMO CICLO GLACIAL

182 ... C.4.1. Emisión de CO₂ y respuesta atmosférica

187.... C.4.2. Proyección para el futuro

193..... C.5. CAPÍTULO 4: ESTUDIO DEL MIS-13 UTILIZANDO MODELOS
DE RELAJACIÓN Y UN STACK DE NIVEL DEL MAR

196 ... C.5.1. Recalibración de los modelos

197.... C.5.2. MIS-13

201..... C.6. CONCLUSIONES

208..... BIBLIOGRAPHY

Preface

This thesis, entitled RELAXATION MODELS APPLIED TO PALEOCLIMATE DYNAMICS: SOUTHERN OCEAN MECHANISMS CONTROLLING GLACIAL - INTERGLACIAL CYCLES, has been funded by the Spanish National Research Council (Consejo Superior de Investigaciones Científicas, CSIC) under the program JAE-Predoc of the «Junta para la Ampliación de Estudios», co-financed by the European Social Fund (FSE).

This work has been performed at the Physical and Technological Oceanography Department of the Institut de Ciències del Mar (ICM-CSIC) at Barcelona, under the guidance of Dr. Antonio García-Olivares, scientist at CSIC. It has been developed in the framework of projects MOC2 (Ocean Climate Memory: mechanisms and paths of surface water formation in the equatorial Atlantic, reference CTM2008-06438, carried out between January 2009 and December 2011), and TIC-MOC (Tipping Corners of the Meridional Overturning Circulation, reference CTM2011-28867, carried out between January 2012 and December 2015). Both projects have been funded by the Ministry of Economy and Competitiveness, Secretary of State of Research, Development and Innovation of the Spanish Government (Ministerio de Economía y Competitividad, Secretaría de Estado de Investigación, Desarrollo e Innovación del Gobierno de España).

This dissertation is structured into a brief introduction, followed by four chapters based on scientific publications, and concludes with a final chapter, stating the main results. Three appendices have been added at the end for clarification of the contents. A total of five scientific papers have been written during the development of this thesis, three of them have been published already and the last two are almost ready to be submitted for publication; a total of eleven conferences have been attended, in which we have participated with six posters and five talks, one of the talks was awarded with L'Océà, a prize to young researchers in Physical Oceanography. Along this research period, a collaborative research stay was done at University of California Santa Barbara, under the guidance of Dr. Lorraine Lisiecki; the derived work is shown at Chapter 4 and it is part of the scientific papers submitted for publication.

Agraiments

Agradecimientos

Acknowledgements

No puc evitar fer una analogia amb un dels mons que millor conec, el de les dues rodes. Un descens pot durar poc, al voltant de 3 minuts, però per poder fer-ho bé has d'haver invertit molt de temps, molt d'esforç i molt de sofriment previ. Diu algú a qui conec bé que la victòria té gust de sang i pols, potser una tesi és quelcom similar. Costa molt de temps i molt d'esforç arribar fins aquí i de vegades, no veus la llum al final del túnel. Però aquí, com a l'esport, has d'entendre molt bé el sacrifici per poder creuar la meta aixecant els braços. I no pots fer-ho sol. No. Necessites molta gent al teu voltant. Aquest petit espai és per tots aquells que m'heu acompanyat en aquesta aventura.

Tot plegat va començar l'any 2007, on jo, estudiant de Física a la UAB, no veia gens clar cap on havia d'anar el meu futur. Suposo que sempre m'ha incomodat no tenir una fita clara davant meu i em trobava en un moment de reflexió profunda, per trobar quin era el meu camí. De vegades, la inspiració arriba quan menys t'ho esperes i la meua va arribar en forma de cançó, conduint un Kia Picanto atrotinat per Menorca.

Batiscafo socialista
redactant informe tràgic,
catedràtic Yuri Puscas
a institut oceanogràfic.
Batiscafo katiuscas
fas un atlas visionari.

Institut Oceanogràfic. Dues paraules que em van fer obrir els ulls. Hi havia vida més enllà de la física teòrica i l'òptica. Hi havia un món macroscòpic, un món menys allunyat de la realitat. Va ser llavors quan l'Oceanografia física va entrar a formar part del meu dia a dia.

Al setembre del 2009, ja amb la carrera pràcticament acabada, vaig prendre la decisió de lluitar per un futur en el món de la recerca. Va ser aleshores quan vaig presentar-me al despatx d'un dels meus professors de la carrera per demanar si podia fer pràctiques amb ell. Aquell professor no era ni més ni menys que l'Antonio García-Olivares, director d'aquesta tesi, tot i que ni ell ni jo no n'érem conscients del llarg camí que ens esperava al davant.

No sabia dir si les oportunitats apareixen soles o són fruit de buscar-les, però al cap de molt pocs dies de començar a fer les pràctiques, em van trucar dient que hi havia una vacant per la beca que havia demanat per anar uns mesos a la Universitat de les Illes Balears, i que inicialment m'havien denegat. Vaig estar sis mesos a Esporles, aprenent de grans investigadors com en Damià Gomis, en Biel Jordà, en Francisco Calafat i sobretot, na Marta Marcos, amb qui vaig tenir el privilegi de treballar activament. Vaig conèixer gent meravellosa amb els que encara, tot i que esporàdicament, compartim trucades i anècdotes: na Chus Alonso, en JuanJo Ensenyat, en GianPa Candini, en Miquel Gomila... Va ser una experiència genial i un bon aprenentatge.

Però tenia clar a on volia estar i aquell lloc era, clarament, l'ICM. Va ser llavors, al setembre del 2010, quan vaig decidir embarcar-me en aquesta gran aventura.

Nada de esto hubiera sido posible sin ti. Gracias Antonio por confiar siempre en mi y ofrecerme la oportunidad de aprender, de crecer, de mejorar y de conocer nuevos aspectos de la vida; gracias por enseñarme y por transmitirme esa gran pasión por la ciencia.

Sense cap mena de dubte l'altre gran suport d'aquesta tesi ha estat en Josep Lluís Pelegrí. Gràcies per donar-me l'oportunitat de treballar amb vosaltres, per ajudar-me dia rere dia a què madurés tant com a investigadora com a persona. Gràcies també per confiar sempre en el meu criteri i per oferir-me grans oportunitats.

Treballar a l'ICM ha estat un grandíssim plaer. No només per què es tracta d'un dels centres de recerca més potents de tot el Mediterrani, si no perquè la gent que el forma es meravellosa. He compartit despatx amb grans persones com l'Evan Mason,

la Patricia De La Fuente, en Miquel Rossell, en Suso Peña, en Sergio Ramírez... tots ells grans investigadors i uns companys excel·lents. També hi ha en Marc Gasser amb el que, tot i no haver coincidit explícitament a un despatx, hi ha una connexió especial; gràcies Marc per totes les converses apassionants que hem tingut i per estar sempre disposat a ajudar o a fer una coca-cola.

L'oficialment extingit DOF (Departament que Organitza més Festes, Claret *et al.* 2011) ha donat pas al DOFT (Departament Organitzador de Festes i Trasllats) però per sort la gent que el forma segueix sent fantàstica. Començant pel «nostre» passadís, amb els dos Jordis (Font i Salat), i l'Emilio García, seguint transversalment amb en Kintxo Salvador, en Pere Fernández, la Maribel Lloret i en Jose Pozo, continuant amb l'Álvaro Víudez, el mejor compañero de despacho que alguien pueda imaginar (mil gracias por aguantarme estos últimos meses), i més endavant amb en Mikhaïl Emelianov i en Jordi Isern. Una planta més amunt trobem en Jose Antonio Jiménez, en Jordi Solé, en Jaume Piera, la Carine Simon, en Miguel Ángel Rodríguez i tot el grup SMOS amb l'Antonio Turiel, en Quim Ballabrera, la Caro Gabarró, en Marcos Portabella, la Maria Piles, la Vero González, la María Belmonte, l'Estrella Olmedo, la Marta Ramírez, la Nina Houreau, la Marta Umbert... i per descomptat, en Fernando Pérez i en Justino Martínez, sempre amb la solució als nostres problemes. Alguns dels que ja han «volat del niu» són en Pedro Llanillo o la Rocio Rodríguez, grandíssimes persones.

Hi ha quatre persones, però, que es mereixen una menció especial, per ordre d'aparició: Paola, Mariona, Maria Rosa i Dorleta. Paola, ha sido un auténtico placer estar a tus espaldas; tienes un gran corazón y una energía aclaparadora, estoy segura que llegarás allí donde te propongas. Gracias, por supuesto, por todos los coffees (aunque yo nunca he tomado café) y por siempre encontrar un hueco para escucharme y darme un buen consejo. La Mariona, ai, Mariona... aquests dies em balla pel cap l'època del B36 i el meu famós «Disfruta, que això només es fa un cop a la vida»; deixam dir-te que se t'ha trobat a faltar per «aquestos lares», però et desitjo que allà on et porti el vent, ja sigui a una banda de l'Atlàntic o a una altra, siguis molt i molt feliç. Maria Rosa, ¿què puc dir-te que no sàpigues?, ha estat un immens plaer poder compartir aquests últims anys al teu costat, parlant de viatges i de noves tec-

nologies; ha estat un gran honor conèixer-te una miqueta més a fons. Per cert, ets la meva millor alumna, sense cap mena de dubte! Gràcies per escoltar-me i aconsellar-me amb la teva immensa saviesa. Dorle, ¿quién nos iba a decir que acabaríamos como dos sin papeles en Salvador de Bahía? Ha sido genial el haberte conocido, eres fantástica y estoy segura que llegarás muy lejos. Gracias por siempre tener una palabra de ánimo a mano y por afrontar la vida con una sonrisa. ¡Viva la biodramina! No, espera, permítame recordar... ¡Ojo, que volcamos!

Per sort, l'ICM no es redueix a un únic departament, hi ha vida social més enllà dels físics i majoritàriament la trobem a Biologia. Als ICM-food, per tots els dinars (amb o sense tuper), coffees, pels cines, per les 4h d'espera a la Crêperie, per les barbacoes i activitats variades... gràcies! Mireia, Elisa, María D. L. F., Xavi, Ramiro, Rachelle, Isabel, Denisse, Carol, Yaiza, Estela, Sdena, Rosana, Norma, AnaMari, Fran C., Laia, Daffne, Cat y por supuesto, Fran A. Habéis hecho que ir a trabajar sea absolutamente fenomenal.

Estimado Sr. Don. Permítame que me dirija a usted en particular para transmitirle mi más sentido agradecimiento. En este tiempo hemos compartido grandes partidas de DS, visto todos los capítulos de Futurama (al menos yo, a usted le ha faltado alguno), comentado grandes películas de la saga Jurassic Park (las buenas y las no tan buenas), ha cambiado usted unas 13 veces de teléfono (todas ellas justificadas), pero lo más importante es que siempre ha estado ahí para animarme cuando más falta ha hecho. Muchos ánimos en este último sprint, tú puedes con esto y más!!! Sin más, me despido. Suya, siempre, una Nobel.

Gràcies també a tot el personal d'administració i serveis, amb la Núria Angosto, l'Eva López, en César García, en Jordi Estaña, en José Fortuño, en Jose María Anguita, en Xavi Leal, la Rosa Cabanillas, la Mariví Martínez de Albéniz i especialment, la Conchita Borruel, qui és capaç de resoldre qualsevol problema. Mil gràcies a tots i a totes per ajudar-nos amb la burocràcia i per aconseguir que l'ICM funcioni «a las mil maravillas». A l' Eli Broglio, gràcies per ajudar-nos amb la divulgació i per organitzar les activitats més divertides i interessants que algú pugui imaginar. A Anita Bonilla de Pelopantón, gracias por ilustrar la ciencia en color y traer un poco de diseño al aburrido mundo científico, y por supuesto, por ser capaz de capturar en

papel mis ideas. És més que possible que m'estigui oblidant més d'un i més d'una, així que mil gràcies a tots i a totes per aquests grandíssims 5 anys.

Evidentment, no tot es redueix a l'ICM. A todo el grupo PalMA, de la Universidad Complutense de Madrid. Gracias Marisa por contestar al correo de una estudiante sin mucha idea diciendo que le gustaba esto de los modelos. Gracias por acogerme, por ofrecerme la oportunidad de trabajar con vosotros y por enseñarme más de cerca el universo CLIMBER. Gracias Jorge y Alex por todas las discusiones apasionantes y por ayudarme a entender un poquito más esto de los modelos, incluso los de hielo. A Rubén, por no ser solo un compañero sino un gran amigo con el que poder comentar la jugada, ¡incluso la del mountain bike! A Etor, por todas las conversaciones apasionantes ya sean de física o de fotografía; a Laura, por su entusiasmo y energía positiva; a Fidel, a Núria, a Edmundo, a Elena, a Ángela, a Jorge N., a Jorge C., y seguro que me estoy dejando a algun@ por el camino. A todo PalMA, gracias, de verdad, por hacerme un huequito semanal esporádicamente en vuestras vidas y por todas esas palmeras de chocolate que hemos compartido (las mejores del mundo mundial, doy fe) y por las que nos quedan por hacer.

Thank you so much to the UCSB for an amazing opportunity. My most sincere gratitude to Lorraine Lisiecki, for welcoming me and offering me the chance to work with her. A special thanks to Vivian Stopples and the administration group, for all the help with the documentation and their warm welcome. Thanks to Rachel Spratt for all the interesting talks, for showing me around and for all the lunches together; to my office-mates, Deborah Khider and Cedric Twardzik, for their help and kindness; to Will Gray, for all the table tennis games (I want my revenge). Also thanks to Frank Kinnaman, for being a great friend in Goleta and for sharing my passion for photography. A huge thanks to the Gans Family, for all the amazing times and for making us feel like home. On the other hand, I'm deeply grateful to all the Intense Family: Steberelli, Dettmers, Herrick, Niermeijer, Bible, Palmer... Thanks so much for being absofrackingly rad #intenseforlife.

Canviem radicalment d'òrbita. Gràcies als amics que he anat fent en cadascuna de les etapes de la meua vida. A la gent del Roser, per compartir amb mi la infància i la joventut; especialment a la Marta, amb qui he compartit grans moments (com

una pizza amb gust de castanya). A les nenes del batxillerat: l'Ester, la Mar, la Cris, l'Anna i la Elena; gràcies per acollir-me quan vaig arribar a una escola desconeguda i fer-me un lloc en les vostres vides. A tota la gent que em va acompanyar al llarg de la vida universitària, especialment als Freaksics: Fran, Laly, Tofu, Tinoco, Guille, Palau, Pablo, Sebas, Sergi, Alberto, Jordi C., Jordi R., Mario, Alba, Laura, Albert... i segur que em deixo a algú; a tots, gràcies. No m'oblido d'aquells que van compartir amb mi les aules per primer cop: en Daniel (junt amb la Julia i l'Èrika), qui ha passat de ser una unitat individual a una molècula de 3 àtoms, amb qui seguim compartint la vida encara que ens separin 19300 km; sembla mentida que amb els anys que han passat i la de coses que han canviat hi hagi certs aspectes de la vida que segueixen igual, com que hi ha converses que malauradament només tú i jo trobem fascinants. And of course, la Sílvia, qui fa massa anys que és lluny però amb qui sempre ens quedarà una màquina de cafè i un «sense got». Als òptics de la UAB i derivats, sempre disposats a fer un sopar, un vídeo o un club de fans: en Menxi (qui té ulleres de putilla) i la Lina, amics d'aquells que sempre ve de gust veure; en Mompi, un dels millors professors que he tingut mai; en David, sempre aventurer i somrient; la Sònia, amb la seva energia positiva i de qui sóc presidenta en superposició del seu club de fans; i per descomptat, dues persones clau: en Bensi i la Car. Albert, ets un crack; deixa'm dir-te que has estat el meu model a seguir a la tesi i hem viscut mil i una aventures, però crec que em quedo amb INVERNAAAALIAAAA i la superposició presidentística (amb el moment estel·lar a l'Abacus, explicant que havíem comprat 100 stands de Quàntic Love i no ens els havien enviat). Car, CarOlid, Carpeta, Cartró i derivats similars... quantes coses hem viscut eh! Car, si algú ens hagués dit en aquella pràctica de col·lisions relativistes tot el que viuríem juntes, no ens l'haguéssim cregut. Gràcies per tots els bons moments, totes les idees esbojarrades, les pelis de Spiderman (i Kill Bill) que hem compartit... i per tots els bons moments que encara estan per venir. A tots els amics bikers, especialment a la Vane i en Miki, qui sempre tenen una estona per ajudar en tot el que faci falta (per quan un sushi?); gràcies per estar sempre al nostre costat, sou molt grans!

Evidentment no hi ha prou espai per anomenar a tothom (tot i que m'he esforçat en mirar de fer-ho), així que gràcies a totes aquelles persones que m'heu acompanyat al llarg de la meva petita història.

Un lugar especial lo reservo a mis padres, Lucía y Emilio, porque sin ellos absolutamente nada de esto hubiera sido posible. Gracias por creer siempre en mí, por enseñarme, por educarme, por darme vuestro apoyo incondicional y también, por malcriarme (y cuánto he disfrutado con ello). Gracias por hacer que me cuestionara las grandes decisiones para estar segura de que era lo que realmente quería (aunque siempre fuera nada más levantarme) y gracias por darme las herramientas necesarias para ser capaz de asumir las consecuencias derivadas. Nada de lo que pueda escribir será suficiente para agradecer todo lo que habéis hecho por mí, pero permitidme insistir: gracias por estar ahí, siempre.

Gracias, también, a la familia que, pese a estar lejos, siempre están al otro lado del teléfono dispuestos a contarme las últimas novedades o dispuestos a compartir los grandes momentos. A Carmina, a los Pepes, a los tíos, a los primos y a los chicos (Victoria, Pablo y Ana), gracias. Y, por supuesto, gracias por todas esas velitas que habéis encendido y que me han iluminado el camino.

A la família Guàrdia - Pascual, per acollir-me a casa seva i fer-me part del seu dia a dia. A l'Antonia i en Josep, a en Dídac i la Mireia, a la Montse i en David, a les iaies Rosita i María, als tiets i als cosins: gràcies.

Last but not least, a en Bernat. Tot va començar a les aules de física, ara ja fa uns quants anys, amb un «nosaltres anem a seure allà, vens?» i des d'aleshores la Terra gira a ritme de pedal. Gràcies per compartir la vida amb mi i fer que cada dia sigui més especial que l'anterior. Gràcies per escoltar-me, per ajudar-me, per animar-me, per fer-me riure cada matí i per fer-me lluitar pels meus somnis. Gràcies per haver cregut sempre en mi i per fer-me ser cada dia millor persona. *I don't know how to put this, but you're kind of a big deal.*

Barcelona, 21 d'octubre de 2015

Glossary

AABW	Antarctic Bottom Water	ITCZ	Intertropical Convergence Zone
ACC	Antarctic Circumpolar Current	LCDW	Lower Circumpolar Deep Water
AMOC	Atlantic Meridional Overturning Circulation	LGM	Last Glacial Maximum
AP	After Present	MOC	Meridional Overturning Circulation
BP	Before Present	NADW	North Atlantic Deep Water
CDW	Circumpolar Deep Water	NH	Northern Hemisphere
CO₂	Carbon dioxide	NMOC	Northern Meridional Overturning Circulation
CRP	Cross Recurrence Plot	ppm	Parts per million
DIC	Dissolved Inorganic Carbon	SH	Southern Hemisphere
EMIC	Earth System Model of Intermediate Complexity	SMOC	Southern Meridional Overturning Circulation
HS1	Heinrich event	SO	Southern Ocean
		YDS	Younger Dryas

Introduction

What is a scientist after all? It is a curious man looking through a keyhole, the keyhole of nature, trying to know what's going on.

— Jacques-Yves Cousteau

Let me start with a fundamental question: why should we study climate? Climate affects our daily life in many ways: on the food we eat, on the houses we live in, on our work, on how we travel... Even affects our culture, our spare time or our health. But all of those are only locally important. What we need to see here is the big picture: climate affects the way all living species have adapted to the biosphere, it is key for our survival, but we are drastically influencing it and we cannot predict the consequences of our actions. It is, then, fundamental to broaden our knowledge on the climate system of Earth, the only home we have ever known, to study the past climatic variability on various time scales to obtain clues that will help society face future climate change. As Carl Sagan foreseen on *Cosmos*, one of his most known books (*Sagan* [1980]):

Our intelligence and our technology have given us the power to affect the climate. How will we use this power? Are we willing to tolerate ignorance and complacency in matters that affect the entire human family? Do we value short-term advantages above the welfare of the Earth? Or will we think on longer time scales, with concern for our children and our grandchildren, to understand and protect the complex life-support systems of our planet? The Earth is a tiny and fragile world. It needs to be cherished.

Paleoclimatology is the science that studies those changes in climate on a really long time scale; as long as the entire history of Earth, 4.54 billion years. It uses data previously preserved on a wide representation of environments (*i.e.* rocks, sediments, ice sheets, corals...) to reconstruct the past state of the Earth climate and its corresponding variability. To find detailed data as old as Earth is almost an impossible task, but we can certainly use a variety of proxy methods to obtain reliable time-series with a time scale of millions of years. In this work, we have used proxy records with a maximum time domain of 5 million years, and our results are reduced to what we may consider the most recent time, only 800,000 years, or in paleoclimate units, 800 kyr.

To understand climate in detail, we should look into all relevant processes of the system, although this might be slightly terrifying, as the number of these processes which must be understood is astonishing. To make it more interesting, the amount of true knowledge that we have is limited and partial. Should we cry on despair? Certainly not. Luckily, paleoclimate, as all sciences, is based on the scientific method, which help us on developing an understanding of reality using terms as mechanism, model and theory. We may describe a theory as a detailed mathematical explanation of phenomena that has sufficient relevance to make predictions from fundamental principles, or in other words, as stated by *Truesdell and Toupin* [1960], a theory is no more than a mathematical model for nature. Truth is, there is no clear path to obtain a reasonable theory of climate in the near future. Rather, we all hope to develop models of climate, in which general conservation principles and assumptions on local mechanisms of feedback allow us to derive mathematical algorithms and predictions that need to be compared with experimental observations. As long as the predictions and the experiments match, we may consider the model valid to describe a reality, a complex object called climate system.

Historically, many inroads have been made to model the structure of long-term climate variability. In the 19th century, Louis Agassiz (*Agassiz* [1838]) proposed for the first time that climate on Earth could have been much colder in older periods of time, at least in the Northern Hemisphere (NH), but under a catastrophist perspective. Later on, Joseph Adhémar (*Adhémar* [1842]) formulated the first astronomical

theory of glacial ages, suggesting that astronomical parameters should modify climate, and explained the position of ice sheets according to the precession of equinoxes, and the subsequent change of location of the perihelion (nearest point to the Sun on Earth orbit) in relation to seasons. Nevertheless, Adhémar formulation was largely criticized, mostly with unfounded arguments, although it had indeed problems. James Croll (*Croll* [1867]) worked on a more elaborated version of this theory, considering the role of eccentricity as a modulation of the precessional forcing, and following Adhémar ideas, insisted on the role of snow accumulation during winters as lead of glaciations. It was on the 20th century when Milutin Milankovitch (*Milankovitch* [1941]) formulated a theory that is still valid nowadays. Croll's main problem was to consider winter as the critical season for the ice sheet evolution, while Milankovitch demonstrated that summer melting is far more important for the ice mass balance, considering summer insolation a key parameter on his theory. Furthermore, Milankovitch considered a third astronomical parameter, the obliquity of the Earth axis (axial tilt), setting the basis of the present astronomical theory of climate.

On the other hand, other hypothesis were developed following a completely different point of view, the geochemical theory. Svante Arrhenius (*Arrhenius* [1896]), inspired by the previous work of Joseph Fourier or John Tyndall, stated the role of CO₂ on climate. He correctly computed how a variation of atmospheric CO₂ levels affects the surface temperature through the greenhouse effect, considering the atmosphere as a carbon reservoir able to control ice ages. Under this perspective, CO₂ and global climate are driving the ice sheet changes, while Milankovitch point of view states that ice sheets controlled by summer northern insolation are the ones driving global climatic changes. Both theories have limitations and problems, and as the reader may suspect, both are essentially valid and not exclusive.

Hays et al. [1976] demonstrated that variations of glacial-interglacials states during the Quaternary may be ultimately caused by changes in parameters of the Earth's orbit (Milankovitch theory), as the astronomical periodicities are found in paleoclimatic records. They also showed that at the obliquity (41 kyr) and precessional bands (23 and 19 kyr) exist a direct climatic response to high latitude summer

insolation forcing, and *Imbrie et al.* [1992] showed that this link between climate and insolation can be interpreted as quasi-linear. But what is certain for 41- and 23-kyr cycles is no longer valid for the major glacial-interglacial cycles with a 100 kyr frequency. These energetic 100-kyr cycles are strongly asymmetric with a slow glaciation state and a fast and abrupt change into interglacial state lasting about 10 kyr called termination. This asymmetry, also known as saw-tooth structure, is really difficult to understand under the astronomical theory; besides, there is no clear link between these main cycles and the eccentricity forcing (100 and 400 kyr frequency) as it is the weakest cycle of the astronomical insolation at a given latitude (measured at the solstice or as a year mean), but it is the most energetic cycle in the observational time series.

This 100-kyr cycle is identified with the Quaternary glacial cycles and, if the astronomical forcing is in fact the driver of the variability, the climatic mechanisms involved are still mostly unknown. Specifically, recent analysis show that glacial-interglacial cycles imply significant changes in the atmospheric CO₂ concentration (180 parts per million (ppm) in glacial period and 280 ppm during interglacial ones), demonstrating that in fact, both historical theories (astronomical and geochemical) are actually valid, interacting in ways that are not yet entirely clear. A combination of ice sheet evolution, driven by astronomical parameters, linked with internal climatic mechanisms producing biogeochemical changes is the most suitable theory nowadays. Some of the most representative models and the different mechanisms and processes affecting climate have been summarized on *Imbrie et al.* [1992, 1993] and more recently on *Paillard* [2015].

The role and mechanisms which involved that increase of atmospheric CO₂ during glacial-interglacial cycles are one of the key points to resolve, and some exchange mechanisms involving the biological or the physical carbon pumps have been proposed to explain it, like the export production on the deep Southern Ocean (SO) or the deep-water ventilation (*Skinner* [2009]). Each of the conceptual approaches has problems explaining the variation in glacial-interglacial CO₂ by itself, which probably suggest that none has operated in complete isolation (*Archer et al.* [2000]; *Sigman and Boyle* [2000]). What seems to be fundamental to explain CO₂ changes

during glacial-interglacial states is the balance between biological sink of exported carbon from the surface-ocean and the returned carbon from deep circulation via physical mechanisms.

The efficiency of deep-water ventilation in glacial and interglacial times could be modified by three major mechanisms:

- (a) Changes in the surface-to-deep mixing rate efficiency (*Toggweiler* [1999]; *Gildor and Tziperman* [2001]) and deep ocean stratification (*Paillard and Parrenin* [2004]; *Watson and Garabato* [2006]), forcing a change in the diapycnal flow of deep CO₂-rich water into surface waters. A stratification-dependent vertical diffusion coefficient appears capable to change also the SO overturning rate with additional consequences on the CO₂ oceanic release (*Bouttes et al.* [2012]).
- (b) Switching on/off of the Antarctic upwelling at Drake Passage latitudes in warm/cold conditions (*Toggweiler et al.* [2006]). Any process producing a stronger wind stress curl at Drake Passage latitudes would cause a stronger upwelling of deep CO₂-rich water at the SO divergence.
- (c) Extended sea ice in the SO produces a capping effect on the CO₂ release to the atmosphere during winters (*Keeling and Stephens* [2001]) and a retardation of the overturning rate in the SO due to sea ice control on the residual circulation (*Watson and Garabato* [2006]; *Fischer et al.* [2010]). This mechanism can be reinforced by the control of sea ice extent on the depth of waters upwelled isopycnally at the Antarctic divergence (*Ferrari et al.* [2014]).

In all three mechanisms, an increased CO₂ release is expected during the change between glacial-interglacial periods, and it is expected to take place mainly in the Southern Hemisphere (SH). Interestingly, recent proxies obtained for the tempera-

ture at Antarctica show a strong correlation between temperature and CO₂ concentrations (*Siegenthaler et al.* [2005]; *Fischer et al.* [2010]). On the other hand, recent interpretations (*Paillard* [2010]) of empirical data (*Bard et al.* [1996]; *Monnin et al.* [2001]) suggest that the atmospheric CO₂ concentration increased for several millennia before the melting of the northern hemisphere ice sheets. Both pieces of evidence support the hypothesis that some of the mechanisms mentioned above, taking place essentially in the SO, could be behind the increase of CO₂ needed to produce glacial-interglacial change.

We may then model the 100-kyr glacial-interglacial cycles as a relaxation oscillation between two different climatic modes, a slow glacial state and a fast deglaciation state, both forced by the insolation and both should include mechanisms that could explain the changes in the atmospheric CO₂. Some simple box models have been proposed as *Pelegrí* [2008] and *Pelegrí et al.* [2013] which take into account changes in overturning rate and biological exportation of CO₂, reproducing approximately sawtooth-like oscillation of last four glacial cycles but in which physical triggers of glacial-interglacial states remain unexplained. More complex models as *Ganopolski et al.* [2010] have shown that Earth system models of intermediate complexity (EMICs) as CLIMBER-2 are able to reproduce the major aspects of glacial cycles under orbital and greenhouse forcing rather realistically. However, the CO₂ forcing has to be introduced independently of the orbital forcing.

Paillard and Parrenin [2004] also proposed a simple relaxation model but taking into account the mechanism of dense water formation in the SO. In this model, the Antarctic ice sheet extent is proposed as a new variable able to link climatic and CO₂ glacial-interglacial changes. The key of their results is the identification of a strong non-linearity in the oceanic source of CO₂ which is controlled by the vertical density structure of the deep ocean. In spite of its simplicity, this model is the first one to accurately reproduce pace and termination times of all glacial-interglacial cycles during Quaternary, as well as the whole set of maxima and minima of the $\delta^{18}\text{O}$ (*Lisiecki and Raymo* [2005]) oscillations observed in the past 5 million years. This may be a sign of the crucial role played by the stratification and southern CO₂ pulse in the onset of glacial-interglacial change.

Nowadays, those mechanisms controlling the variability of the late Pleistocene glacial cycles remain as an outstanding question in the climate sciences. This thesis seeks to broaden the field of relaxation models as a useful tool to examine the internal physical mechanisms of the climate, identifying the main feedbacks and variables involved, such as SO stratification, sea ice extent and carbon oceanic storage; and, also to answer more direct dynamic questions, as to predict the behavior of the future glacial cycle or to explore the dynamics of a particular interglacial. The models obtained predict the ice volume time series of the last 8 glacial cycles with a notable accuracy despite their simplicity: up to 89-90% of correlation with proxy data, which is to our knowledge the highest in the climate literature. The comparison of the models developed in this work with the observational time series have made possible also to suggest a synthetic perspective of the main mechanisms that are probably producing the glacial-interglacial oscillations, and specially the termination events. This synthesis open the way to further analysis with more detailed models such as those of intermediate complexity (EMICs).

A roadmap of the structure of this thesis may be useful to the reader. In Chapter 1 we present a wide representation of relaxation models, with the aim of analyze how several variations of *Paillard and Parrenin* [2004] (PP04) model affect the data fit. The good fit obtained with some PP04-derived models suggests that the mechanisms that these models incorporate may be important factors controlling glacial-interglacial oscillations. In Chapter 2 we focus on identify those mechanisms and dynamics that lead to good data fit and to explore the most plausible physical interpretations of the mathematical expressions. These results have been compared with the state-of-the-art dynamics that supposedly cause glacial-interglacial oscillations, to explore the consistency of our physical interpretation with the observational results. Those relaxation models have been applied to two different scenarios as a useful tool to understand the system: in Chapter 3 have been used to predict the Earth's glacial-interglacial response during the forthcoming 300 kyr, and in Chapter 4 the models have been re-calibrated using a new sea level data stack and are used to understand the dynamics of a very particular interglacial event, the MIS-13. Finally, in Chapter 5 we present the conclusions of the thesis. ┘



Chapter 1

RELAXATION MODELS APPLIED TO LATE PLEISTOCENE CLIMATIC OSCILLATIONS

**Chapter based on the following
published articles:**

*García-Olivares and Herrero [2012],
Fitting the last Pleistocene $\delta^{18}\text{O}$ and
 CO_2 time series with simple box models.
Scientia Marina 76S1:209-218.*

*García-Olivares and Herrero [2013],
Simulation of glacial-interglacial
cycles by simple relaxation models:
consistency with observational results.
Climate Dynamics 41:1307-1331.*

Contents

33.....	1.1. INTRODUCTION
34.....	1.2. PP04-DERIVED MODELS
37.....	1.2.1. Biological export production model
43.....	1.2.2. Two response times for CO ₂
44.....	1.2.3. Two response times for ice volume
46.....	1.2.4. Oceanic pulse exponentially dependent on stratification
46.....	1.2.5. 3τ model
47.....	1.2.6. Local stratification model
48.....	1.3. MODELS PERFORMANCE
50.....	1.4. DISCUSSION

Chapter 1 ⁷

RELAXATION MODELS APPLIED TO LATE PLEISTOCENE CLIMATIC OSCILLATIONS

L

We embarked on our journey to the stars with a question first framed in the childhood of our species and in each generation asked anew with undiminished wonder: What are the stars? Exploration is in our nature. We began as wanderers, and we are wanderers still. We have lingered long enough on the shores of the cosmic ocean. We are ready at last to set sail for the stars.

– Carl Sagan, *COSMOS*

1.1 INTRODUCTION

Some simple relaxation models have been proposed to explain the glacial-interglacial cycles. Particulary, *Paillard and Parrenin* [2004] proposed a model (hereafter PP04) that incorporates very simple parameterizations attempting to represent dense water formation in the SO. Though the model is simple, the results are encouraging because they correctly reproduce the pace and termination times of all the glacial cycles observed.

Here, the PP04 model has been generalized and calibrated to the $\delta^{18}\text{O}$ and CO_2 time series available for the last 800 kyr Before Present (BP) (*Petit et al.* [1999]; *Monnin et al.* [2001]; *Pepin et al.* [2001]; *Lisiecki and Raymo* [2005]; *Siegenthaler et al.* [2005]; *Luthi et al.* [2008]). The objectives of this chapter are:

- (i) to obtain the set of parameters that best fit the late Pleistocene time series in PP04's original model;
- (ii) to investigate several generalizations of Paillard's model by introducing some simple sub-models for the export production, the strength of deep stratification and other mechanisms; and
- (iii) to analyze how the different sub-models affect the data fit.

The next section describes the structure of the initial PP04 model and its best calibrations to the $\delta^{18}\text{O}$ and CO_2 data for the last 800 kyr BP. A biological carbon export rate is next introduced instead of the original mechanism, and the modified model is calibrated and analyzed. An alternative model with two different response times for the CO_2 emission and absorption is also considered. The model is then modified by two different response times for accumulation and ablation of ice, and by adding an exponential oceanic pulse. Next, we compare the patterns found when using different model calibrations, and analyze different mechanisms controlling the oceanic pulse that triggers the deglaciations. Finally, the results and conclusions are summarized.

1.2. PP04 DERIVED MODELS

The set of equations of the original PP04 model are the following:

$$\frac{dV}{dt} = \frac{(V_r - V)}{\tau_V}, \quad 1.1$$

$$\frac{dA}{dt} = \frac{(V - A)}{\tau_A}, \quad 1.2$$

$$\frac{dC}{dt} = \frac{(C_r - C)}{\tau_C}, \quad 1.3$$

$$V_r = -xC - yI_{65} + z, \quad 1.4 \quad \lrcorner$$

$$C_r = \alpha I_{65} - \beta V + \gamma P(-F) + \delta, \quad 1.5 \quad \lrcorner$$

$$F = aV - bA - cI_{60} + d, \quad 1.6 \quad \lrcorner$$

where V and A are dimensionless indexes for non-Antarctic ice volume and extent of Antarctic ice sheet respectively, C is a dimensionless index for atmospheric CO₂, I_{65} is the daily insolation at 65° N on 21 June, $P(F)$ is the deep ocean contribution to the reference CO₂, which in the original model is $P(F) = H(F)$, where H is the Heaviside function ($H = 1$ if $F < 0$; $H = 0$ otherwise), and F is the *salty bottom water formation efficiency* parameter. F increases with ice volume V and decreases when continental shelf areas are reduced (through A) and when I_{60} (daily insolation at 60 S on 21 February) increases.

The main variables V , A , and C tend to decay exponentially to a reference state V_r , V , and C_r in characteristic times τ_V , τ_A and τ_C , respectively. Reference volume (V_r) decreases when C increases, and when I_{65} is high. The CO₂ of reference (C_r) increases when I_{65} is high through parameter α and when the oceanic pulse of CO₂ is on (through parameter γ), and decreases when the ice volume increases. The β parameter represents the feedback between ice volume V and CO₂.

Daily insolations of the last 800 kyr BP are obtained from the *Berger* [1978a] and *Berger and Loutre* [1991] software (Appendix A). We have used negative and positive values when respectively referring to times before present (BP) and after present (AP), where year zero is taken as 1950 AD. Insolations have been normalized with their standard deviations to obtain I_{65} and I_{60} . No lower bound is imposed on the V , C and A variables, which may take positive or negative values because they represent relative and not absolute variations. Note that all results of the model have been normalized by their standard deviation before plotting.

In *Paillard and Parrenin* [2004] no precise tuning of the parameters was performed but a table with central value and range for the parameters was presented. In original PP04, γ parameter had a value of 0.5 due to a mistake. Noticed by Michael Crucifix and Didier Paillard in a later revision, the correct value is 0.7 (Table 1.1).

Three different integration methods were used for the differential equations (Mathematica internal algorithms, Matlab internal algorithms¹ and Predictor-Corrector explicit method with time step of 50 years) and the results were coincident. Given the strong nonlinearity in the variable C dynamics, at least 16000 steps are needed in the latter algorithm to grant that results are independent of the number of steps.

A systematic search of the set of parameters that lead to maximum correlation was implemented around this central case. Correlations of the V and C time series with the (respectively) $\delta^{18}\text{O}$ and CO_2 experimental series available for the last 800 kyr BP were calculated to quantify the maximum observational explained variance, giving us a first approximation of the similarity between simulated and observational time series. The expression for the statistical correlation is

$$\text{cor}[s_1, s_2] = \frac{(s_1 - E[s_1]) \cdot (s_2 - E[s_2])}{(N - 1)\sigma[s_1]\sigma[s_2]}, \quad 1.7$$

where $\text{cor}[s_1, s_2]$ is the correlation between the time series s_1 and s_2 , $E[x]$ is the expected value (mean) of x , the dot symbol denotes scalar product, $\sigma[x]$ is the standard deviation of x , and N is the number of components of arrays s_1 and s_2 .

The correlations obtained are shown in Table 1.1. As can be observed in column 2 of the table, the correlations of the central case of PP04 can be improved from 0.59 and 0.63 to 0.67 and 0.71 for CO_2 and ice volume, respectively, when the α parameter takes the zero value (model PB). This parameter represents a direct forcing

¹Mathematica is a trademark of Wolfram Research and Matlab is a trademark of The MathWorks.

of I_{65} on atmospheric CO_2 and its physical interpretation is not clear, given that the CO_2 response to ice volume is already included in the model. Thus, we have eliminated this parameter from the model hereafter. The second and third panels of Figures 1.1. and 1.2. show the ice volume and CO_2 time series simulated with these two parameter sets. The main difference between the two cases appears in the CO_2 time series, where the oscillations of 41 and 21 kyr in the case with $\alpha = 0$ present a lower amplitude than in the case with $\alpha = 0.15$.

1.2.1. Biological export production model

Martínez-García et al. [2009] observed that the export productivity in the subantarctic Atlantic during glacial stages grew exponentially. This suggests that the export production in the SO could be driven by changes in the supply of iron by dust, which is known to V1 mechanism, is able to generate fits of similar correlation to the ones obtained with the original model (PP04). With this purpose, the oceanic pulse in expression C_r is replaced by an expression that represents the biological rate of carbon exportation of the SO as

$$C_r = \alpha I_{65} - \beta V + B + \delta, \tag{1.8}$$

where

$$B = \begin{cases} \varepsilon(e^{kV} - 1), & V > 0 \\ 0, & V \leq 0 \end{cases}. \tag{1.9}$$

PARAMETERS	PP04	PB	BIO	2τ	4τ	EP	3τ	LS
τ_V	15000	15000	3667	12000	17006	4600	16585	11325
τ_{V_2}	-	-	-	-	3797	1100	3105.5	2325
τ_C	5000	5000	100	800	6796	3040	13505	2793
τ_{C_2}	-	-	-	4500	17667	7600	-	8414
τ_A	12000	10500	-	11333	8089	12000	9004	10266
x	1.3	1.32	0.85	1.29	0.767	1.525	0.905	0.669
y	0.5	0.45	1	0.5	0.442	0.2	0.489	0.527
z	0.8	0.8	0.92	0.85	1.033	0.96	0.946	0.761
α	0.15	-	-	-	-	-	-	0.237
β	0.5	0.496	0.76	0.496	0.406	0.476	0.336	0.793
γ	0.7	0.506	0.49	0.513	1.642	0.46	2.044	1.955
δ	0.4	0.4	0.4	0.434	0.407	0.445	0.228	0.146
a	0.3	0.3	-	0.3	0.395	0.3	0.54	-
b	0.7	0.71	-	0.71	0.8	0.71	1.205	0.936
c	0.01	0.005	-	0.005	-	-	-	0.533
d	0.27	0.27	-	0.27	0.27	0.255	0.483	0.069
ε	-	-	0.8	-	-	-	-	-
k	-	-	0.47	-	-	-	-	-
V_m	-	-	0.5	-	-	-	-	-
λ	-	-	-	-	-	37	-	-
R_V	0.63	0.71	0.58	0.82	0.89	0.85	0.88	0.87
R_C	0.59	0.67	0.45	0.75	0.79	0.77	0.79	0.76

Table
1.1

Central values of the models studied. Columns 2 to 9 correspond to: (2) original *Paillard and Parrenin* [2004] model with $\gamma = 0.7$ (PP04); (3) best fit of previous model (PB); (4) model with biological export production (BIO); (5) model with two relaxation times for C (2τ); (6) model with two relaxation times for C and two relaxation times for V (4τ); (7) model with oceanic pulse exponentially dependent on stratification (EP); (8) model with one relaxation time for C and two relaxation times for V (3τ) and (9) model with local stratification parameters (LS). R_V and R_C represent the correlation between proxy and modeled data for global ice volume, V , and atmospheric CO₂ concentration, C , respectively.

MODELS	DESCRIPTION	NUMBER OF PARAMETERS
PP04	Original <i>Paillard and Parrenin</i> [2004] model with $\gamma = 0.7$	14
PB	Best fit of <i>Paillard and Parrenin</i> [2004] model	13
BIO	Biological rate of exportation included at the CO ₂ reference state	11
2τ	Two different response times for the accumulation and absorption of CO ₂ $\tau_C = \tau_{C_1}$ for the periods where $C < C_r$ and $\tau_C = \tau_{C_2}$ when $C > C_r$	14
4τ	Two different response times for the accumulation and absorption of CO ₂ and two different response times for accumulation and ablation of ice: $\tau_V = \tau_{V_1}$ for periods when $V < V_r$ and $\tau_V = \tau_{V_2}$ when $V > V_r$	14
EP	Oceanic pulse exponentially dependent on stratification	14
3τ	Model with one relaxation time for C and two relaxation times for V	13
LS	Model with local stratification parameters	15

Table 1.2 Description of the different models.

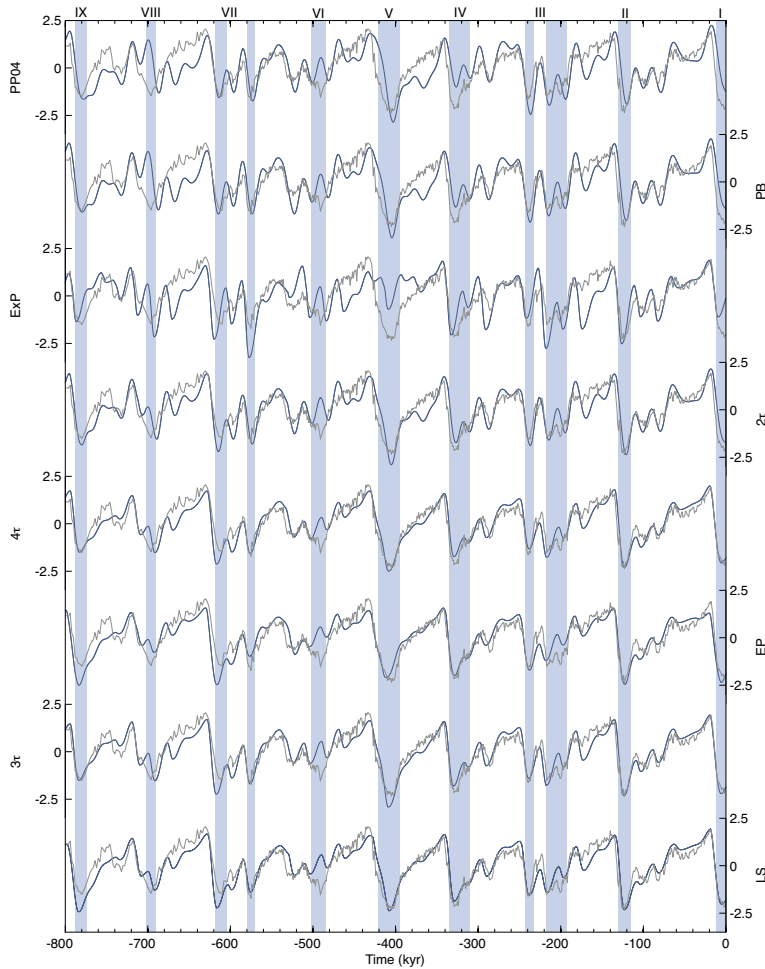


Figure
1.1

Best fits obtained for the ice volume time series. From top to bottom: (1) original *Paillard and Parrenin* [2004] model with $\gamma = 0.7$ (PP04); (2) best fit of previous model (PB); (3) model with biological export production (BIO); (4) model with two relaxation times for C (2τ); (5) model with two relaxation times for C and two relaxation times for V (4τ); (6) model with oceanic pulse exponentially dependent on stratification (EP); (7) model with one relaxation time for C and two relaxation times for V (3τ) and (8) model with local stratification parameters (LS). Proxy records of $\delta^{18}\text{O}$ time series (*Lisiecki and Raymo* [2005]) are superimposed in every panel. Blue bands represent interglacial periods considering benthic $\delta^{18}\text{O}$ below 3.8 per mil.

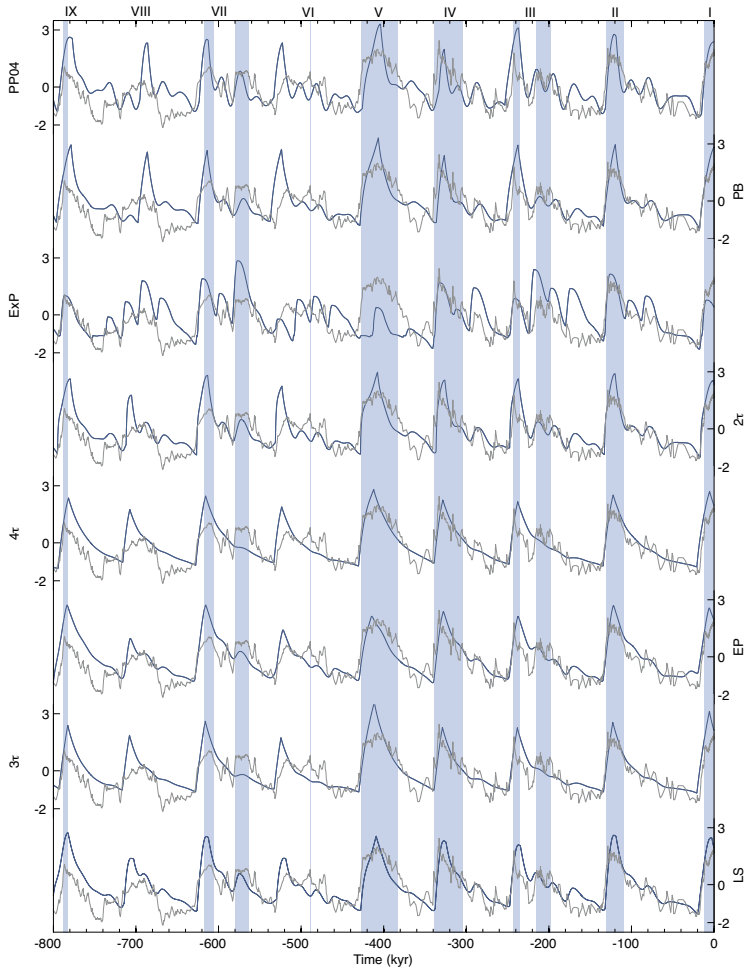


Figure 1.2

Best fits obtained for the CO₂ time series. From top to bottom: (1) original Paillard and Parrenin [2004] model with $\gamma = 0.7$ (PP04); (2) best fit of previous model (PB); (3) model with biological export production (BIO); (4) model with two relaxation times for C (2τ); (5) model with two relaxation times for C and two relaxation times for V (4τ); (6) model with oceanic pulse exponentially dependent on stratification (EP); (7) model with one relaxation time for C and two relaxation times for V (3τ) and (8) model with local stratification parameters (LS). Records of experimental CO₂ time series (Petit et al. [1999]; Monnin et al. [2001]; Pepin et al. [2001]; Siegenthaler et al. [2005]; Luthi et al. [2008]) are superimposed in every panel. Blue bands represent interglacial periods considering experimental CO₂ concentrations above 250 ppm.

However, with this choice the V dynamics is unstable and V increases indefinitely for most of the parameter ε values. This derives from the positive feedback between V and C exportation. To avoid this we assume that $B(V)$ has a bell-shaped form that decreases with V until a V_m value and then increases for very high V values (Figure 1.3). This is equivalent to assuming that an extremely large ice volume would produce a negative effect on the biological activity, possibly because of very low temperatures in the SO. The new expression is

$$B = \begin{cases} -\delta \varepsilon e^{-\left(\frac{0.5(V-V_m)}{\sigma}\right)^2}, & V > 0 \\ 0, & V \leq 0 \end{cases} \quad 1.10$$

where

$$\sigma = k \{1 - \tanh [2(V - V_m)]\}. \quad 1.11$$

In this expression we have assumed that σ decays quickly with V after a certain value V_m .

The best fit obtained with this model (labelled BIO) produces the time series shown in the third panel of Figures 1.1 and 1.2. The correlations are 0.45 and 0.58 for C and V respectively, which are worse than the ones obtained for the other models analyzed. The set of parameter values used is shown in Table 1.1, column 4. For these values, the function $B + \delta$ that represents the exportation-like contribution to the reference carbon C_r , is roughly square-shaped (see Figure 1.3), with a maxima for V values that correspond roughly to interglacials and the first third of glacial periods, a quick decrease to a minimum value for V values corresponding to the remaining glacial period, and an increase to the maximum value afterwards. The decrease is instantaneous instead of exponential but no better fit was found for a gradual exponential decrease of the function.

As can be seen in Figure 1.1, the ice volume is poorly simulated but, even so, many of the ice ages can be identified. The model is able to reproduce qualitatively the nine terminations. However, the terminations VI and V are poorly simulated be-

cause the CO₂ interglacial pulse is underestimated.

The correlation of C with the inorganic carbon data is lower than the correlation of V with the corresponding data, even though a visual inspection could suggest that the C fit is better than the V fit. This probably derives from our tendency to give more importance to coincidence of peaks than to coincidence of other parts of the curve. In this regard, the peaks in V are less apparent than those in C , and are mixed with many secondary peaks.

1.2.2. Two response times for CO₂

A more exhaustive method to obtain the set of parameters that lead to maximum correlation was implemented by using the genetic algorithm included in the Matlab software (see Appendix B for details).

Given that the deep stratification mechanism, as introduced by *Paillard and Parrenin* [2004], generates a fit to the data that is better than the one given by model BIO, we introduced changes in the PP04 model that could improve the correlations obtained in columns 2 and 3 of Table 1.1. Observation of panels 1 and 2 of Figure 1.2 suggests that the correlation between the C time series and the experimental data could increase if the C plot was closer to a triangular sawtooth shape, in particular during glaciations. This shape could possibly be obtained if the response time for the CO₂ absorption was longer than the response time for the CO₂ emission; this may be justified since the climatic state when CO₂ is being absorbed is glacial state, which is very different from the interglacial state of the periods when atmospheric CO₂ is rising. Thus, we used a different relaxation time (τ_{C_2}) for the periods where $C > C_r$. The calibration of this model (labelled 2 τ hereafter) with this additional parameter (column 5 of Table 1.1) generates a best fit with correlations of 0.82 and 0.75 for V and C respectively. As is observed in Figure 1.1 (fourth panel), in this case the V minima obtained at the terminations are deeper than in the previous case (BIO model, third panel) and this produces a graph that is closer to the experimental time series.

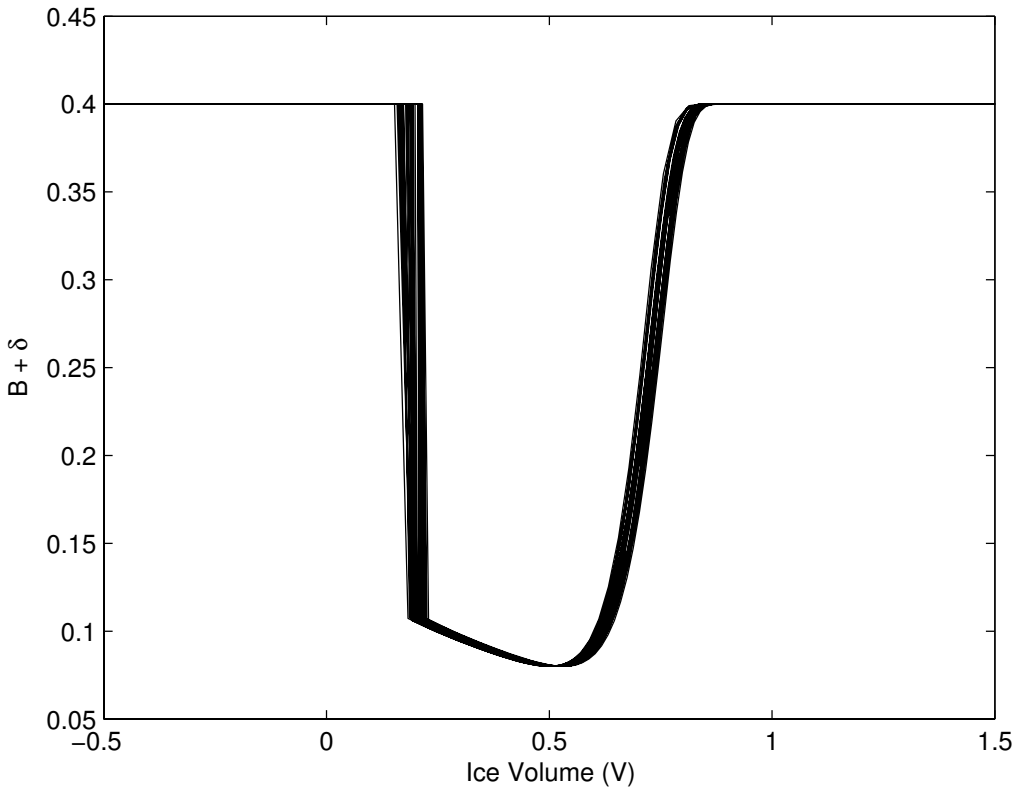


Figure 1.3 Function $B(V) + \delta$ used by the export production model (BIO) in the best fit case.

1.2.3. Two response times for ice volume

By introducing two different response times for accumulation and ablation of ice in model 2τ (τ_V for periods when $V < Vr$ and τ_{V_2} when $V > Vr$), a new model is obtained and is labelled 4τ hereafter.

Two different response times are used, then, for the accumulation and absorption of CO_2 : $\tau_{C_2} = \tau_{C_1}$ for the periods where $C < Cr$ and $\tau_C = \tau_{C_2}$ when $C > Cr$, in

addition to the already mentioned two different response times for accumulation and ablation of ice: $\tau_V = \tau_{V1}$ for periods when $V < V_r$ and $\tau_V = \tau_{V2}$ when $V > V_r$. Physically, two characteristic times for melting (τ_{V2}) and accumulation of ice (τ_{V1}) are justified because they are different processes; specifically, it is necessary that $\tau_{V1} > \tau_{V2}$, because melting is faster than accumulation. However, two response times for emission (τ_{C2}) and absorption (τ_{C1}) of atmospheric CO₂ is harder to explain. *Archer et al.* [2009b] reviewed literature on the carbon cycle and discussed some models, getting to the conclusion that it will take a timescale of 2 to 20 centuries for the ocean to absorb the surplus atmospheric CO₂, and even when the equilibrium would be reached, a substantial fraction (20 - 40%) of this CO₂ would remain in the atmosphere awaiting slower chemicals reactions. These results are apparently coherent with the situation proposed here, where $\tau_{C2} > \tau_{C1}$, but further investigation is needed to have a precise understanding of the long-term carbon cycle and to decide if the long-term emission of CO₂ from soils and oceans has a characteristic time equal or different to the long-term absorption of CO₂.

The best fit of model 4τ has correlations of 0.88 and 0.77 for V and C respectively (column 6 of Table 1.1). Fifth panel of Figures 1.1 and 1.2 shows the simulated V and C time series. The effect of the y parameter (sensitivity to the I_{65} insolation) on the ice volume time-series simulated can be observed. In this case, the y value is 0.44, which is between the 0.2 value of model EP and the 0.5 value of model 2τ . The C series has a saw-shaped form and the 42 kyr oscillations are damped due to the large value of τ_{C2} . This contrasts with model 2τ , where high frequency oscillations in C are more apparent.

The 21 and 42 kyr oscillations in the V time series are also slightly more damped than in model 2τ due to the influence of C on V . The V time series resembles a sawtooth oscillation, as in the experimental data, even though the maximum at -515 kyr is overestimated.

Table 1.1 shows the parameter values corresponding to these model. For this case and the following two, best fits were obtained for values of parameter c that were so small that almost identical correlations could be obtained for a second parameter set with $c = 0$ (no sensitivity to I_{60} forcing).

1.2.4. Oceanic pulse exponentially dependent on stratification

Models derived from PP04 generate oceanic CO₂ pulses $P(F)$ with a strong non-linear dependence on the stratification parameter F , through the Heaviside function: $P(F) = H(F)$. Thus, during the glacial periods the contribution of this term is zero. An alternative way to generate sawtooth like oscillations in the glacial periods could be to allow for some non-zero CO₂ emission when F is positive but small. With this purpose, in this model we have modeled the oceanic pulse (third term in the C_r expression) in a different way,

$$P(F) = \begin{cases} e^{-\lambda F}, & F > 0 \\ 1, & F \leq 0 \end{cases} . \quad \text{1.12}$$

The time series corresponding to the best fit obtained for this model (which is label EP) is shown in sixth panel of Figures 1.1 and 1.2, and the set of parameters used are displayed in the seventh column of Table 1.1. This model also uses four different characteristic times (τ_C , τ_{C_2} , τ_V , and τ_{V_2}).

The correlations for V and C in this case increase to 0.85 and 0.77, respectively. The carbon time series is closer to a sawtooth oscillation than in the previous models. The relatively high damping of the high frequency oscillations (21 and 42 kyr) in the V series derives from the y parameter, or sensitivity to the I_{65} insolation, which takes a small value of $y = 0.2$. Model EP is the one in which the sawtooth-like oscillation is most clearly dominant over the 41 and 21 kyr cycles and, in this aspect, is the one that best fits the experimental time series.

1.2.5. 3τ model

The different scale for uptake and release in our models represents the different sequence of events that take place during glacial and interglacial periods, which

cannot be reproduced in detail by PP04-derived models because of their excessive simplicity in the representation of carbon processes. The 4τ model is, however, not very sensitive to the use of a single τ_C for CO₂ uptake/release, since its best calibration with only 13 parameters gives us correlations of 0.88 and 0.79 for V and C , respectively. The resulting model will be called 3τ hereafter.

As can be observed in the seventh panel of Figure 1.1 (3τ model), many details of the high-frequency oscillations of the experimental ice volume are suitably simulated. The minima at -700 and -575 kyr are similar to the experimental data and the maximum at -220 kyr is closely simulated by this model. The shape of the cycles I, III, IV and VII are also closely simulated. However, 3τ is poor at accurately simulating the minimum of V at -200 kyr (cycle II), the V minimum at -490 kyr and the maximum ice volume at -750 kyr.

1.2.6. Local stratification model

In the previous models, an almost identical optimum can be found with a set of parameters that does not use the I_{60} forcing (i.e. $c = 0$). This forcing was included in PP04 model to take into account possible regional temperature variations which could affect the freezing of surface waters on the Antarctic shelf. Similarly, F dependence on V was introduced to take into account the possible effect of global climate cooling and warming (through V) on regional climate (*Paillard and Parrenin [2004]*). It led us to look for a variable that could represent better than V and I_{60} the regional temperature. This variable was the CO₂, as represented in the model by the variable C , and the new model was called “Local Stratification” (LS) model.

Atmospheric CO₂ can be considered a proxy of Antarctic temperature as shown by the Antarctic deuterium record (*Petit et al. [1999]*; *Luthi et al. [2008]*; *Jouzel et al. [2007]*), so modeled variable C can be considered an approximate proxy of local temperature in the SO. Consequently, the LS sub-model has been developed in which I_{60} insolation has been replaced by variable C , so the expression for F is $F = aV - bA - cC + d$. However, the best fits obtained for this model did not improve those

obtained with $a = 0$. For this reason, we used the final expression (Eq. 1.18) that uses one parameter less. Stratification is thus considered dependent only on regional variables (the extent of Antarctic ice sheet A and SO temperature, related to C). In parallel with it, it was assumed that SO temperature, as represented by variable C , led also the evolution of ice sheet A (Eq. 1.15). This change has no effect on the correlation obtained for V but it improves slightly the correlation obtained for C . The final equations are:

$$\frac{dV}{dt} = \frac{(V_r - V)}{\tau_V}, \quad 1.13$$

$$\frac{dC}{dt} = \frac{(C_r - C)}{\tau_C}, \quad 1.3$$

$$\frac{dA}{dt} = \frac{(-C - A)}{\tau_A}, \quad 1.15$$

$$V_r = -x C - y I_{65} + z, \quad 1.16$$

$$C_r = \alpha I_{65} - \beta V + \gamma H(-F) + \delta, \quad 1.17$$

$$F = -b A - c C + d. \quad 1.18$$

1.3. MODELS PERFORMANCE

The analysis of Table 1.1 gives some hints on the conditions that lead to the best data fits. As can be observed in Figure 1.1, all models have problems to accurately simulate the minimum of V at -200 kyr (cycle II), the timing of the V minimum at -490 kyr (Termination VI) and the maximum ice volume at -750 kyr (except, to some extent, model BIO).

It may be observed that all models have problems simulating the glacial cycle between -600 and -500 kyr, especially the timing of its termination. Inaccurate fitting of the timing of terminations probably derives from limitations of both model and $\delta^{18}\text{O}$ records. A common way of estimating time in paleoclimate records is to stretch, squeeze and shift a record's chronology in order to align it with a template indicative of changes in the Earth's orbital and rotational configuration, a process generally referred to as orbital tuning (*Huybers* [2011]). For this reason, it is not clear that the time scale of the data is better or worse than the time scale of the model (within, let's say, a quarter period of the fastest forcing, the precession, i.e. ± 6 kyr). This is particularly true for the timing of terminations, which apparently are not linearly correlated with the astronomical forcing intensity (see e.g. *Parrenin and Paillard* [2003]). For this reason, a "better fit" of the timing of terminations of the $\delta^{18}\text{O}$ data may not be an improvement, because the data are not necessarily very accurate in their estimation of the precise dates when terminations take place. Time series for the fit error were obtained by subtracting the simulated and experimental time series resulting from dividing every time series by its standard deviation.

The correlations obtained with the EP model do not improve upon the ones obtained with the 4τ model (Table 1.1) so, we can conclude that the results obtained do not justify the introduction of an additional parameter. However, the extra contribution to glacial CO_2 produced in this model makes it possible to fit the experimental CO_2 series with a lower value of the y parameter (sensitivity to I_{65} forcing), which produces a V time series with the high-frequency oscillations more damped. The "texture" of this series, as can be observed in Figures 1.1 and 1.2, resembles that observed in the experimental data.

The performance of 4τ and 3τ models in the simulation of V is quite similar, except for Termination V and the glacial cycle II, where 4τ performs slightly better. For these reasons, 4τ correlation for V is slightly better than 3τ (0.89 instead of 0.88). The use of a different relaxation time for emission and absorption of CO_2 allows 4τ to match CO_2 in glacial cycle V better than 3τ . However, the extreme simplicity of the carbon model shows up in both models though the lack

of high-frequency oscillations in the evolution of C . The LS model has a content of high-frequency variance larger than that of 3τ because it permits a direct forcing of I_{65} to C but its correlation is not better because this variance is frequently out of phase with the observational one.

1.4. DISCUSSION

Starting from the *Paillard and Parrenin* [2004] model, several box models incorporating simple parameterizations of the oceanic CO₂ pumping and response times of carbon and ice volume have been developed. The models' parameters were calibrated to provide the best fit to the $\delta^{18}\text{O}$ and CO₂ experimental time series available for the last 800 kyr BP. The PP04 model is insensitive to the α parameter (direct forcing between I_{65} insolation and CO₂) and the Sun's effect seems to emerge only through the filter of global ice volume. The fit of this model to observational data may be improved if different response times are assumed both for absorption/emission of CO₂ and for ablation/accumulation of ice. Correlations between simulated and experimental time series increase from 0.59 and 0.63 to 0.79 and 0.89 for CO₂ and V , respectively.

Several modifications of the PP04 model that lead to the right timing of the last nine terminations were tested. In particular, the qualitative behavior of the last eight glacial-interglacial cycles may be roughly reproduced with an export production model with export dependent on ice volume (BIO). However, in this model, the best fit corresponded to a dependence between CO₂ export and V that was not exponential as proposed by *Martínez-García et al.* [2009], but a square function. In our formulation, biological export alone was not able to simulate the experimental data as accurately as the other models, even though some kind of biological export of CO₂ is very probably acting in synergy with physical processes in the glacial-interglacial dynamics.

One limitation of the methodology used in this study, common in paleoclimate models, is that there is no distinction between calibration data and validation data. For

this reason, it may be useful to know whether parameter optimizations obtained on half of the data interval lead to nearly the same best estimates. Our models seem to fit better the sawtooth oscillations that climate has shown in the last -400 kyr than the more irregular oscillations occurring between -800 kyr and -400 kyr. In order to include both kinds of dynamics, we used the interval -600 to -200 kyr as calibration data in the LS model. This interval led to a best fit that is coincident with the one shown in the last column of Table 1.1, and the correlations obtained were 0.872 and 0.763, which are slightly better than those obtained for the complete interval (0.866 and 0.757). We have rounded the latter results to two decimal digits in the last column of Table 1.1. When a second and more exhaustive searching is implemented around the values obtained by the genetic algorithm, it is possible to find a different parameter combination with even better correlations (0.884 and 0.774). However, the case is then so tightly fitted to the calibration interval that it fails to reproduce the pace of the whole interval (and correlations drop to 0.43 and 0.22).

On the other hand, the experimental data used ($\delta^{18}\text{O}$: *Lisiecki and Raymo* [2005]; CO_2 : *Monnin et al.* [2001]; *Petit et al.* [1999]; *Siegenthaler et al.* [2005]; *Luthi et al.* [2008]) contain much high-frequency variance, representing (among other things) weather noise, measurement error, and annual-to-centennial climate variability. PP04-derived models do not contain mechanisms able to produce significant variance in these time scales. For this reason, in one of our runs we smoothed the proxy data with a moving average of 2 kyr, and then calibrated the LS model with these time series and the complete interval (-800 kyr, 0 kyr). The correlations obtained were 0.869 and 0.761, respectively, whereas the result with unfiltered data was 0.866 and 0.756, respectively. In conclusion, the smoothing of the experimental time series provides an improvement of less than 1% in the fits of the two variables.

Four models (4τ , EP, 3τ and LS) show a good performance in the simulation of the ice volume observed in the last eight glacial-interglacial cycles and even in many details of that signal belonging to the scale from 23 to 41 kyr. The good fits obtained suggest that density of deep water and its rate of formation may be important factors controlling the oceanic pulse that triggers the deglaciations. *Schmittner* [2007] has confirmed, with a global climate model, the sensitivity of atmospheric CO_2 to processes that affect stratification in SO waters. In our analysis, oceanic pulses that

strongly depend, in a non-linear way, on the deep ocean stratification are necessary to trigger deglaciations. The pulses obtained in the best models are always very close to the Heaviside function proposed by the original work of PP04. Oceanic CO₂ pulses with a duration of between 10 and 20 kyr were found at the beginning of the nine last deglaciations according to the best models analyzed. In addition, different response times for emission and absorption of CO₂ and for accumulation and ablation of ice are necessary to obtain the best fit to the available data. Accumulation and ablation of ice are different physical mechanisms that could have different characteristic times. However, the two response times for emission and absorption of CO₂ are more difficult to explain, as we have said before. To decide whether these two response times correspond to real physical mechanisms, a deeper understanding of the long-term transfer rates in the carbon cycle should be achieved.

Björkström [1979] identified the two slowest response times for the emission of CO₂ to the atmosphere to be related to the remineralization of organic carbon of dead material in soils, and the long travel time of the CO₂ from the deep ocean compartments to the surface. These authors used 1000 year as an order of magnitude for both parameters. *Brovkin et al.* [2002] used the range 400 - 1000 years to model the slow soil response with the CLIMBER-2 paleoclimatic model. The characteristic time of CO₂ absorption in the long-term scales is related to the CO₂ advection from the surface into the deep ocean according to *Björkström* [1979] and it should be, again, of the order of 1000 yr.

Our result $\tau_{C_2} > \tau_C$ could be meaningful if the characteristic time of deep water circulation was longer than the long-term emission time of soils. *Montenegro et al.* [2007] found that 25% of an instantaneous CO₂ release to the atmosphere remains there after 5000 years. *Archer et al.* [2009b] reviewed the literature on the carbon cycle, which agrees that 20% to 35% of an instantaneous CO₂ release remains in the atmosphere in 200 to 2000 years, after equilibration with oceans. Due to oceanic acidification, subsequent dissolution of CaCO₃ increases the uptake capacity of oceans in the scale of 3 to 7 kyr. These results are apparently coherent with the order of magnitude of the τ_{C_2} parameter that we have found. However, more investigation is needed to have a precise understanding of the long-term carbon cycle.

A different problem is deciding what confidence we can give to those models with higher correlations, given that the record used for the past ice volume probably suffers different biases. Indeed, the record is a stack of $\delta^{18}\text{O}$ data from benthic foraminifera, and the ratio $\text{O}^{18}/\text{O}^{16}$ is known to depend on both the isotopic composition and the temperature of the water where the foraminifera develops. *Siddall et al.* [2010] found that ice volume becomes increasingly sensitive to temperature change at low temperatures. *Waelbroeck et al.* [2002] found that the relationship between $\delta^{18}\text{O}$ and ice volume is not linear, since $\delta^{18}\text{O}$ decreased faster than the increase in ice volume at the beginning of the last glaciations, and then progressively more slowly until the ice sheets reached their maximum size. This may produce uncertainties greater than 20% for the ice volume estimations in some periods. Therefore, the models with the largest correlations between predicted ice volume and $\delta^{18}\text{O}$ are not necessarily better than other models with slightly lower correlation because of the uncertainty in the observational data. This is a complex and important question requiring an additional mathematical analysis that we leave for a future work. Fortunately, there is no such problem for CO_2 , which is directly measured in ice cores.

It may be argued that it is not surprising to get good fits (Table 1.1) using models with many parameters. This is particularly true when experimental data are fitted to generic mathematical functions that are dependent on an arbitrary number of parameters. However, it is not so easy to get the same good fit with mathematical expressions that imitate geophysical mechanisms such as feedbacks and pumping rates. An additional outcome from relaxation models of this kind is that they point to specific physical mechanisms that are potentially drivers of the observed changes. Thus, when good fits are obtained with such models, the specific physical mechanisms modeled should be investigated in more detail to confirm them (and not an alternative mechanism producing a similar behavior) as inducers of the observed dynamics.

To sum up, we have obtained eight different fits with ice volume correlations between 0.58 and 0.89 which show a good quantitative and qualitative agreement with the empirical time series, especially 4τ , EP, 3τ and LS; although the warm event of -500 kyr is not properly reproduced by any model. The 4τ model improves the PP04 correlations (0.59 and 0.63) to 0.79 and 0.89 using the same number of parameters

(namely, 14). The EP model uses 15 parameters but the additional parameter, which was aimed at improving the form of the oceanic pulse function, did not improve the correlations and can be considered useless. The 3τ model obtains almost the same correlations as 4τ using only 13 parameters. The LS model (15 parameters) does not improve the correlations of 4τ (which are slightly higher) but incorporates a functional form for stratification F that seems more consistent with both the mechanisms suggested by *Paillard and Parrenin* [2004]. If our aim were to select the model with the best explained variance per parameter, the choice would be 3τ . However, a second objective of this work is to determine whether models with an explained variance similar to the one obtained by 3τ contain parameterizations that can be related as realistically as possible to observed mechanisms. LS can offer a valuable insight into the real meaning of the good performance of PP04-derived models. In the next chapter, the dynamics and mechanisms incorporated in 3τ and LS models will be analyzed and compared. ┘

Chapter 2

ON THE PHYSICAL MECHANISMS BEHIND GLACIAL-INTERGLACIAL DYNAMICS

**Chapter based on the following
published articles:**

*García-Olivares and Herrero [2013],
Simulation of glacial-interglacial cycles
by simple relaxation models: consistency
with observational results. Climate Dy-
namics 41:1307-1331*

*Herrero and García-Olivares [2014],
Non-linear analysis methods applied to
observational and simulated climatic time
series. Proceedings International work-con-
ference On Time Series. Volume 2, p1068-
1080. I.S.B.N: 978-84-15814-97-4*

*Herrero and García-Olivares [2015],
Non-linear analysis methods applied to
observational and simulated climatic time
series. Boletín Geológico Minero, accept-
ed for an ITISE special volume.*

Contents

59.....	2.1. INTRODUCTION
60.....	2.2. RELAXATION MODELS
63.....	2.3. NON-LINEAR ANALYSIS
63.....	2.3.1. Fourier transform
63.....	2.3.2. Wavelet transform
73.....	2.3.3. Phase space portraits
81.....	2.3.4. Cross recurrence plots
81.....	2.4. ALTERNATIVE PROXY FOR ICE VOLUME
86.....	2.5. DYNAMICS OF THE MODELS
94.....	2.6. OBSERVATIONAL DYNAMICS
99.....	2.7. DISCUSSION

Chapter 2 ⁷

ON THE PHYSICAL MECHANISMS BEHIND GLACIAL-INTERGLACIAL DYNAMICS

L

*I don't know anything, but I do know that everything is interesting
if you go into it deeply enough.*

*- Richard P. Feynman,
The Pleasure of Finding Things Out*

2.1. INTRODUCTION

In Chapter 1, PP04-derived models were calibrated to obtain a better fit with experimental time series of $\delta^{18}\text{O}$ and CO_2 available for the last 800 kyr BP. It is observed that the performance of PP04 can be improved if its CO_2 sensitivity to insolation is eliminated and if different response times are considered for absorption and emission of CO_2 , as well as for ablation and accumulation of ice. Correlations between simulated and experimental time series increase from 0.59 to 0.79 for CO_2 , and from 0.63 to 0.89 for ice volume V (4τ model), respectively. According to the models, abrupt CO_2 releases, lasting 10 to 20 kyr, take place at the beginning of the last nine deglaciations.

The good fit obtained with the PP04-derived models, specially with 3τ and LS, suggests that the mechanisms that these models incorporate may be important factors controlling glacial-interglacial oscillations. The objectives of this chapter are:

- (i) to identify the mechanisms and dynamics that have been incorporated in the PP04-derived models, specifically in 3τ and LS, which lead to good data fit;
- (ii) to explore the most plausible physical interpretations of the mathematical expressions incorporated in these models; and
- (iii) to study the extent to which the mechanisms and dynamics previously identified are consistent with state-of-the-art observational results on the dynamics that supposedly cause glacial-interglacial oscillations.

The good data match obtained with this set of models and the analysis of (i) and (ii) reinforce the hypothesis that some specific mechanisms are the main drivers of glacial - interglacial oscillations, pointing at specific mechanisms that deserve further analysis. We begin summing up the structure of the models and continue analyzing their non-linear dynamics using wavelet transform, cross-wavelet transform, wavelet coherence, Fourier analysis, attractors and cross-recurrence plots. Later on, the observational dynamics is evaluated and, finally, we outline the main mechanisms behind the glacial-interglacial oscillations.

2.2. RELAXATION MODELS

As a reminder, the equations of the models that we are going to take in consideration in this chapter are:

3τ		LS	
$\frac{dV}{dt} = \frac{(V_r - V)}{\tau_V},$		$\frac{dV}{dt} = \frac{(V_r - V)}{\tau_V},$	2.1
$\frac{dA}{dt} = \frac{(V - A)}{\tau_A},$		$\frac{dA}{dt} = \frac{(-C - A)}{\tau_A},$	2.2
$\frac{dC}{dt} = \frac{(C_r - C)}{\tau_C},$		$\frac{dC}{dt} = \frac{(C_r - C)}{\tau_C},$	2.3
$V_r = -x C - y I_{65} + z,$		$V_r = -x C - y I_{65} + z,$	2.4
$C_r = -\beta V + \gamma H(-F) + \delta,$		$C_r = \alpha I_{65} - \beta V + \gamma H(-F) + \delta,$	2.5
$F = aV - bA + d,$		$F = cC - bA + d,$	2.6

In these equations the principal dependent variables V , A and C , tend exponentially to reference states V_r , A_r and C_r with characteristic times τ_V , τ_A and τ_C , respectively; these characteristic times and the rest of parameters are specified in Table 1.1. Time series of both models, as well as the proxy data, are shown in Figure 2.1.

There are several differences between models 3τ and LS. One difference is the value used for the reference Antarctic ice sheet (A_r), either $-C$ (representing the inverse effect of Antarctic temperature in Antarctic ice sheet extent) for model LS or V for model 3τ . Another minor difference is the inclusion of I_{65} in model LS when specifying the reference atmospheric CO₂ concentration value, C_r . However, the main difference between both models, is their parameterization of stratification, with F

$= F(V, A)$ in model 3τ and $F = F(C, A)$ in model LS. Both V and C are good proxies for the SO regional temperature and, therefore, either $F = F(V, A)$ or $F = F(C, A)$ are plausibly ways to model the local formation of brines. The fact that the dependence $F = F(V, A)$ performs better than $F = F(C, A)$ may be due to the non-negligible role that V has on stratification through NH - SH teleconnection (García-Olivares and Herrero [2013]) or to a possible larger effect of sea level than Antarctic temperature on brine formation.

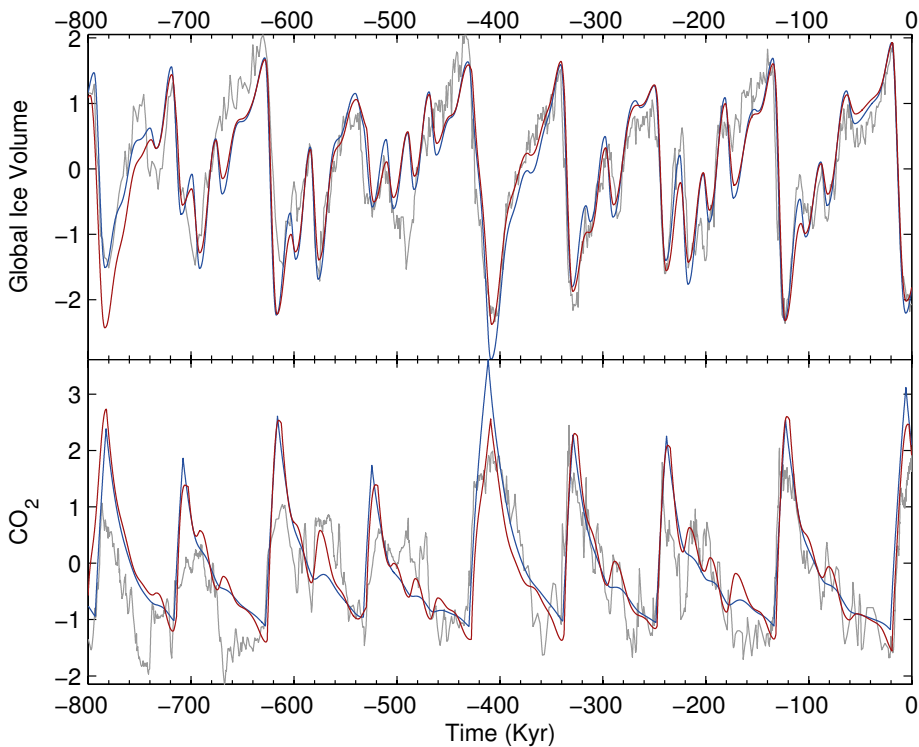


Figure
2.1

Top panel: normalized ice volume as predicted with the 3τ (blue line) and LS (red line) models and proxy $\delta^{18}\text{O}$ records from Lisiecki and Raymo [2005] (grey line). Bottom panel: normalized CO_2 as predicted with the 3τ (blue line) and LS (red line) models and proxy data (Petit et al. [1999]; Indermuhle et al. [2000]; Monnin et al. [2001]; Siegenthaler et al. [2005]; Luthi et al. [2008]) (grey line).

2.3. NON-LINEAR ANALYSIS

2.3.1. Fourier transform

Spectral power of observational and simulated time series are obtained with Fast Fourier Transform (Figure 2.2). As can be observed, frequency content is similar in observational and simulated time series for both the V and C variables. However, $\delta^{18}\text{O}$ has 10% more power content in the band of 100-kyr and 15% more power content in the 41-kyr band than the V predicted by our models. Power in 23-kyr band is small in observational and simulated time-series. Regarding 3τ results, the C observational and simulated spectra are more similar than those for V , in spite of the worse correlations obtained for C . However, LS tends to under predict the 100-kyr power content and to over predict the power in 41 and 23-kyr bands.

2.3.2 Wavelet transform

Wavelet transform, cross-wavelet transform and wavelet coherence are tools that may also be useful for comparing observational and simulated time series, complementing the information obtained from correlation coefficients. Figures 2.3, 2.4 and 2.5 show the wavelet transform of the observational and simulated data. Units in the color bar are wavelet transform power, i.e. $|Wi|^2$, where Wi is the wavelet transform or convolution between the Morlet wavelet function and the time series, and i designates the position of datum number i . The Morlet wavelet is a common choice when using wavelets for feature extraction purposes, because it is reasonably localized in both time and frequency (*Grinsted et al. [2004]*). The thick black line above and below designates the 95% significance level against red noise and the thin black line designates the cone of influence where edge effects might distort the field. The Matlab crosswavelet and wavelet coherence software by *Grinsted et al. [2004]*¹ was used for calculations.

¹Software available at: <http://www.pol.ac.uk/home/research/waveletcoherence>

As shown in Figure 2.3 top and Figure 2.4, the 100-kyr band is the dominant period in both the $\delta^{18}\text{O}$ and V time series of the 3τ and LS models, followed by the 41-kyr band, and power in both frequencies is similarly distributed in observational and simulated series. The $\delta^{18}\text{O}$ time series contains periodicities in the range 1-10 kyr; in contrast, our models do not generate any significant periodicity under 10 kyr. The 23-kyr period is weakly present in both experimental and 3τ time series. The LS and 3τ models show the same patterns in their wavelet diagrams, which are almost indistinguishable from each other.

For CO_2 (Figure 2.3 bottom and Figure 2.5), the power distribution in the simulated and observational time series are similar for the 100-kyr band. Power in the 41-kyr band is somewhat more homogeneously distributed in the observational time series than in the simulated time series. The 23-kyr contribution is weaker in both series and is distributed in a different way in the modeled and observational time series. The difference is greater in the first three cycles, which are relatively difficult to model.

The complex cross-wavelet transform of two time series (Figures 2.6 and 2.7) can be interpreted as the shared power in a given periodicity band (absolute value) and the phase difference between the two series in time frequency space (*Grinsted et al. [2004]*). Lighter purple color indicates greater shared power in that time and periodicity band, and the arrow angle indicates the phase between the observational and simulated series. As can be observed in Figure 2.6, observational and simulated ice volume share a great common power in the 100-kyr and 41-kyr band. In the 100-kyr band, the two periodicities are in phase, but in the 41-kyr band the modeled periodicity tends to lead the observational one at some moments, with a phase between 0 and $\pi/4$. In the 41 and 23-kyr band, the two periodicities tend to be in phase when the common power is high and out of phase when the shared power is low. The two models studied (3τ and LS) show very close patterns in their cross-wavelet transforms for V . Regarding CO_2 (Figure 2.7), the largest shared power is in the 100-kyr band, especially after -500 kyr, when the fit between simulated and observational cycles is somewhat better (see Figure 1.2 and 2.1). In the 41-kyr band the shared power is lower and has relative maxima around -600 kyr, between -400 and -200 kyr and between -150 and -50 kyr. These intervals of good coincidence can be also

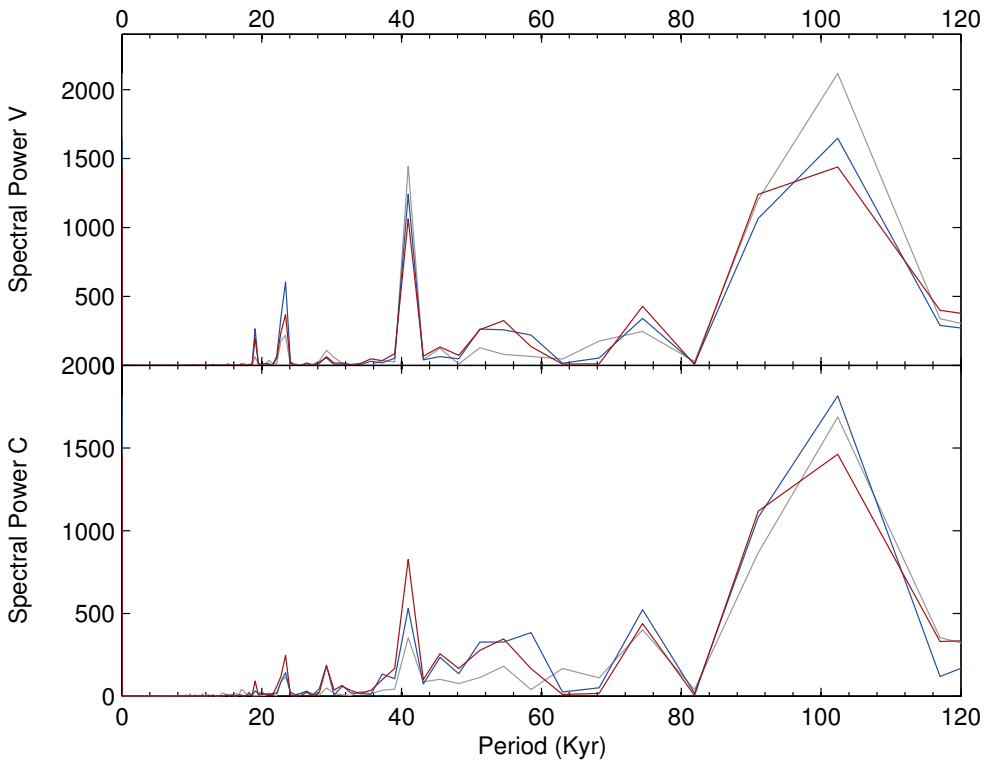


Figure 2.2

At top, spectral power of normalized ice volume as predicted with 3τ model (blue), LS model (red) and proxy $\delta^{18}\text{O}$ records from Lisiecki and Raymo [2005] (grey line); at bottom, normalized CO_2 as predicted with the 3τ (blue line) and LS (red line) models and proxy data (*Petit et al.* [1999]; *Indermuhle et al.* [2000]; *Monnin et al.* [2001]; *Siegenthaler et al.* [2005]; *Luthi et al.* [2008]) (grey line).

observed in Figures 1.1, 1.2 and 2.1 for the LS model. Low shared power is observed in the 23-kyr band, with an out-of-phase pattern in some intervals.

Wavelet coherence of two series can be interpreted as a localized correlation coefficient in time frequency space. It is useful to find locally phase-locked behavior, that is,

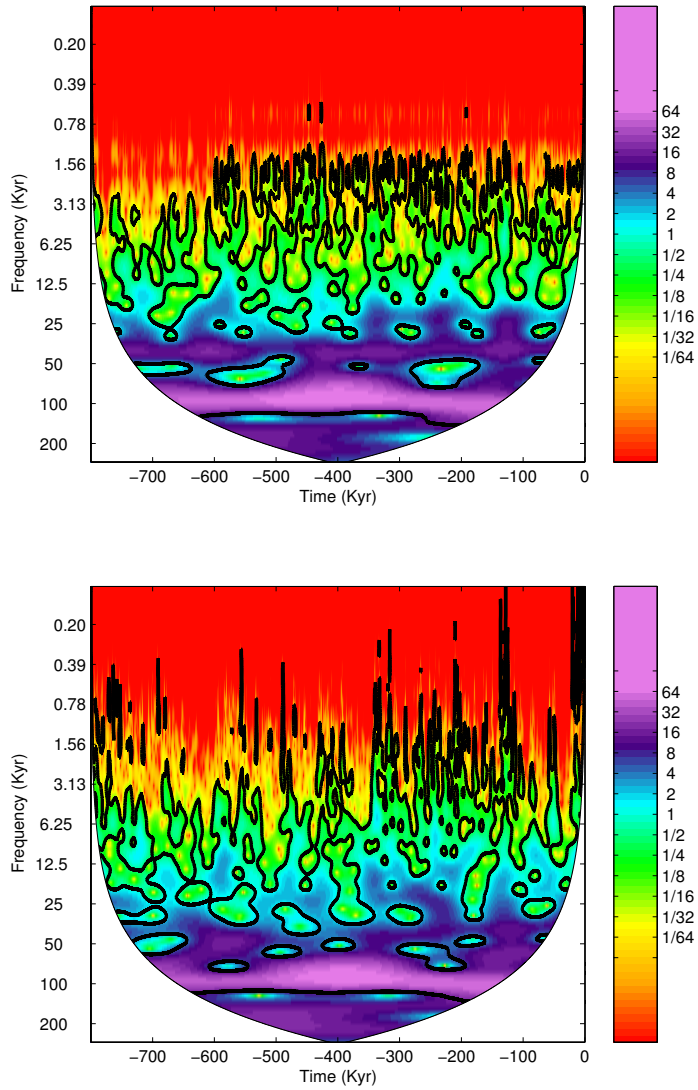


Figure 2.3

Wavelet diagram of proxy $\delta^{18}\text{O}$ records from *Lisiecki and Raymo* [2005] (top) and proxy CO_2 data from *Petit et al.* [1999]; *Indermuhle et al.* [2000]; *Monnin et al.* [2001]; *Siegenthaler et al.* [2005]; *Luthi et al.* [2008] (bottom).

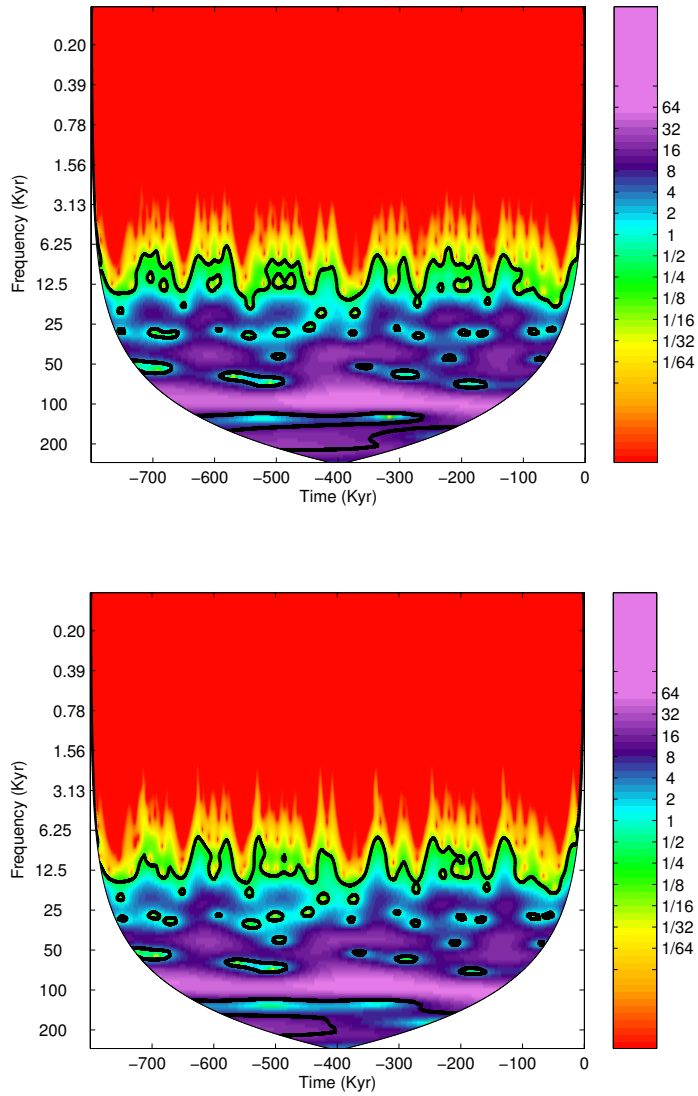


Figure 2.4

Wavelet diagram of the simulated V time series with 3τ model (top) and LS model (bottom).

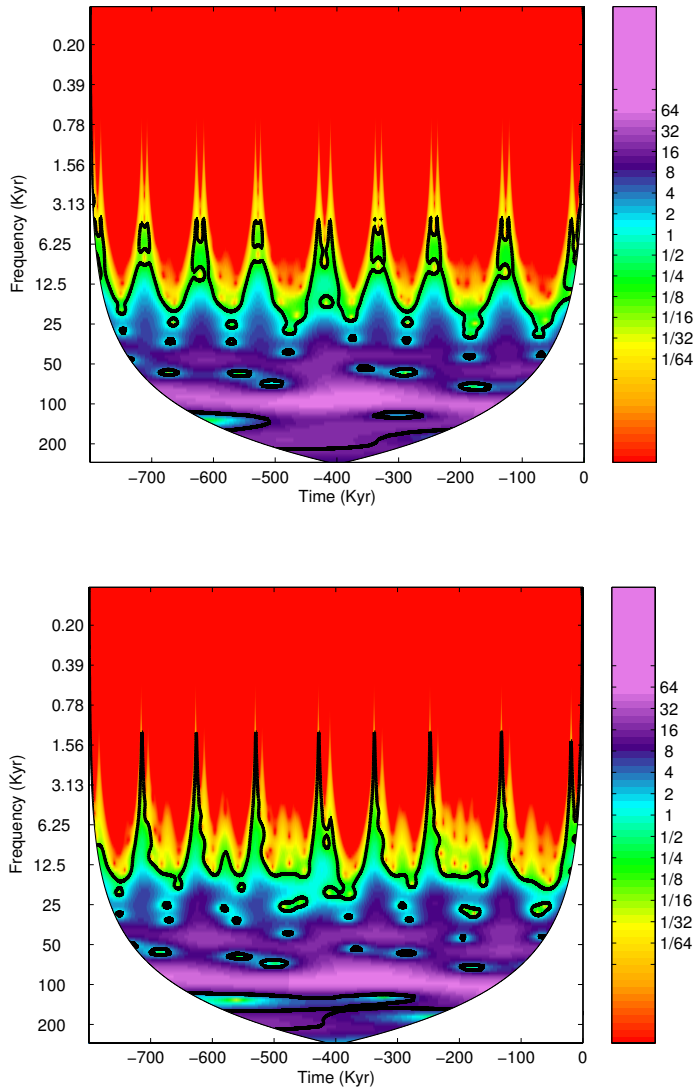


Figure 2.5 Wavelet diagram of the simulated C time series with 3τ model (top) and LS model (bottom).

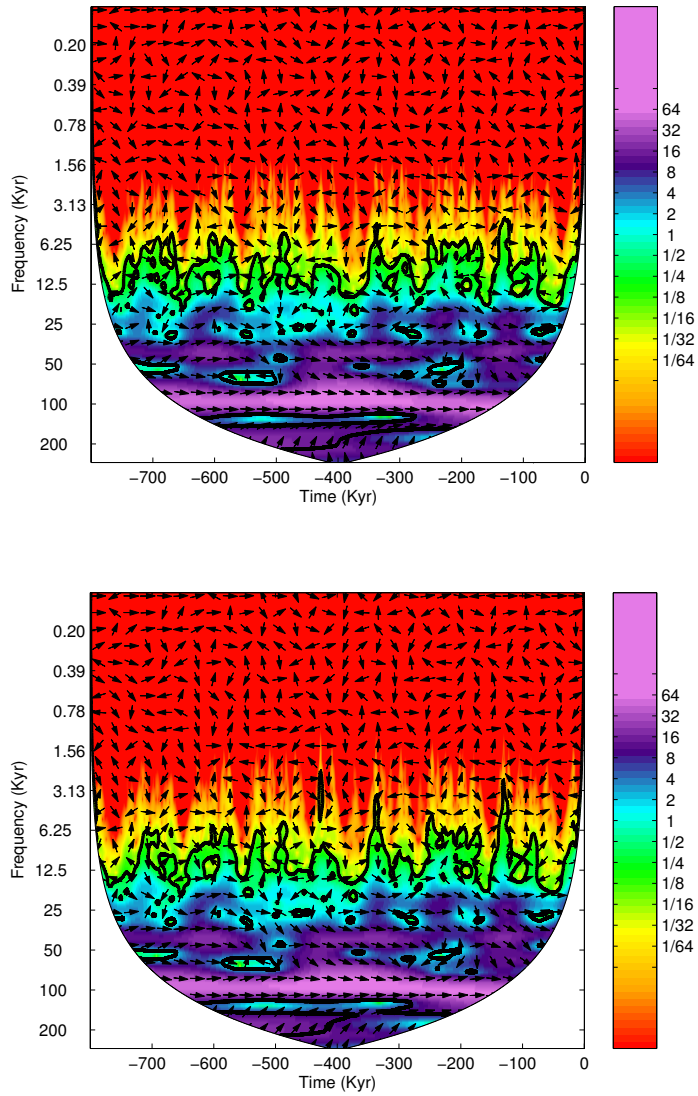


Figure 2.6

Cross-wavelet transform between proxy $\delta^{18}\text{O}$ records from *Lisiecki and Raymo* [2005] and simulated V time series with 3τ model (top) and LS model (bottom).

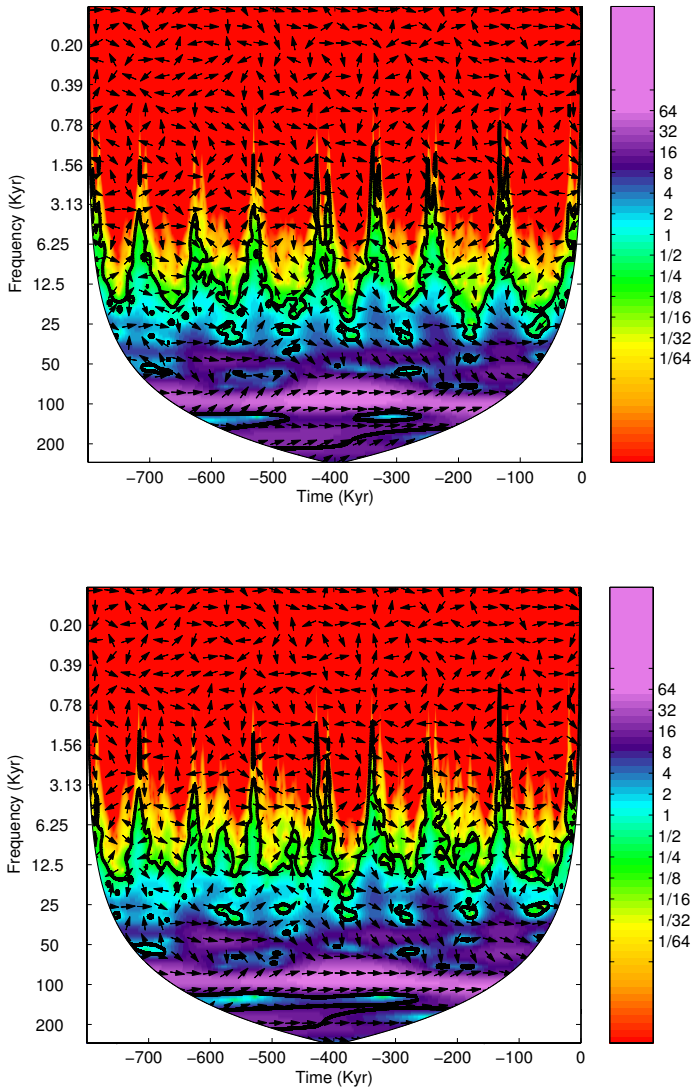


Figure 2.7

Cross-wavelet transform between proxy CO₂ data from *Petit et al.* [1999]; *Indermuhle et al.* [2000]; *Monnin et al.* [2001]; *Siegenthaler et al.* [2005]; *Luthi et al.* [2008] and simulated C time series with 3τ model (top) and LS model (bottom).

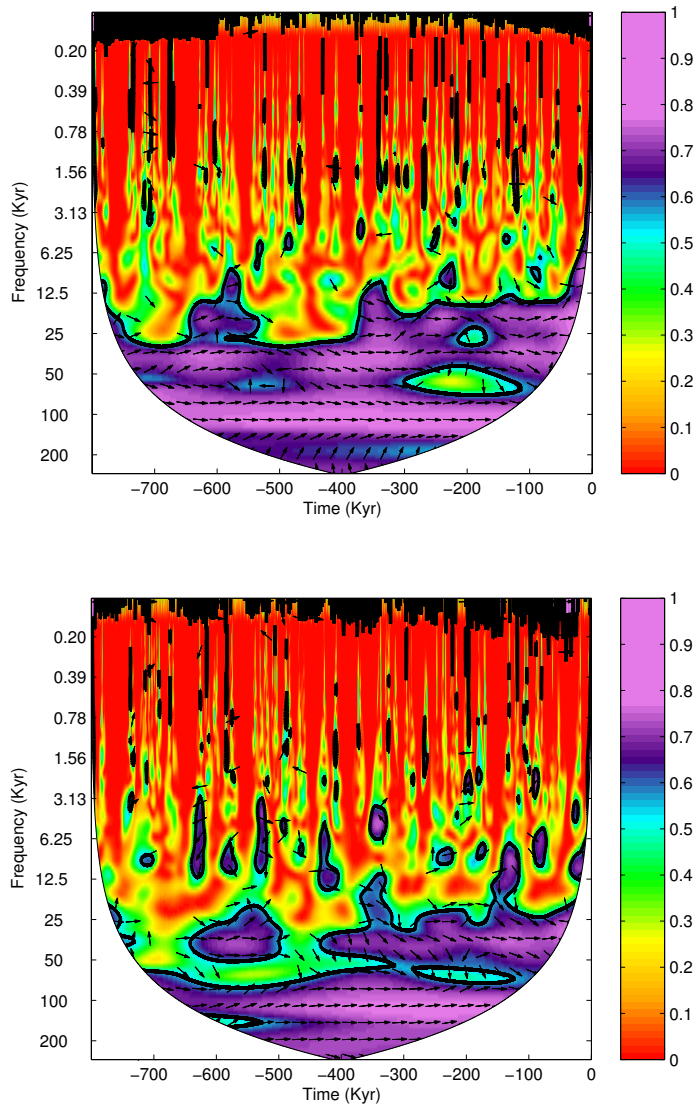


Figure 2.8

Wavelet Coherence between proxy $\delta^{18}\text{O}$ records from *Lisiecki and Raymo* [2005] and simulated V time series with 3τ model (top) and LS model (bottom).

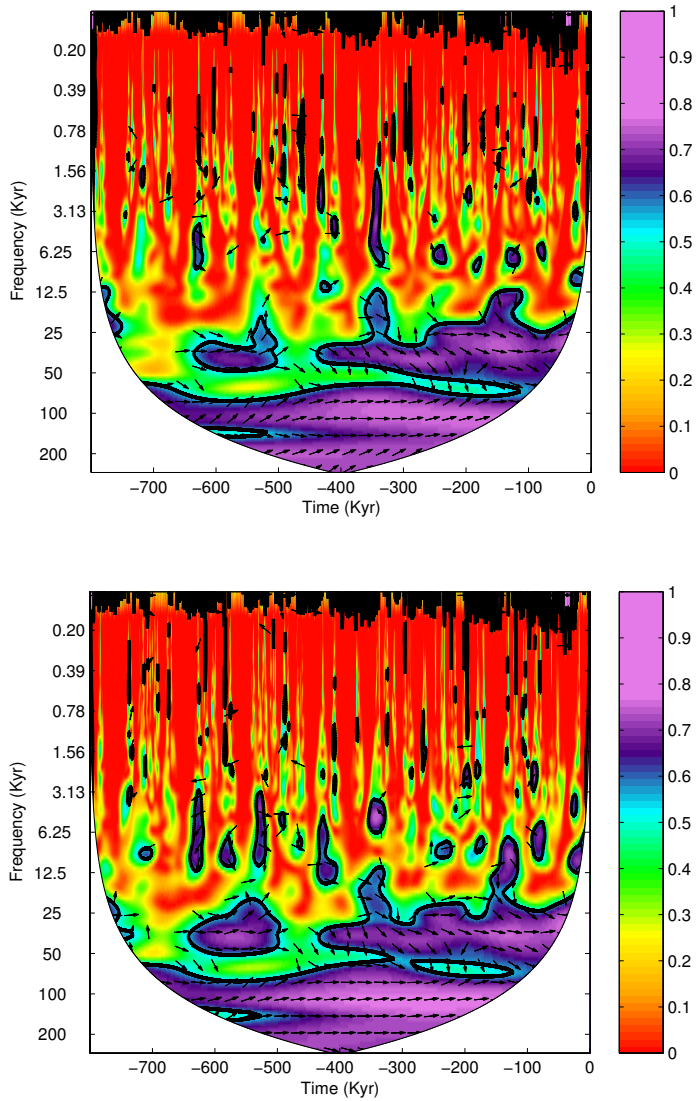


Figure
2.9

Wavelet Coherence between proxy CO₂ data from *Petit et al.* [1999]; *Indermuhle et al.* [2000]; *Monnin et al.* [2001]; *Siegenthaler et al.* [2005]; *Luthi et al.* [2008] and simulated C time series with 3τ model (top) and LS model (bottom).

moments in which both series oscillate with the same frequency and a given phase difference. Figure 2.8 shows the wavelet coherence of the $\delta^{18}\text{O}$ and the simulated V series for 3τ and LS and Figure 2.9 shows the wavelet coherence of the observational CO_2 and the simulated C series for the same models. It can be observed that the correlations of V for the two models are always in phase, are larger than 0.9 in the 100-kyr band for all times and are especially high in the four last cycles (-400 kyr to 0). In the 41-kyr band the simulated and observational series oscillate together with a correlation that exceeds 0.9 around -600 kyr, between -400 and -350 kyr, and is always greater than 0.7 between -130 and -90 kyr. The coherence is not significant between -750 and -630 kyr and between -540 and -380 kyr, corresponding to intervals in which the models are worse at matching the observational series (see Figures 1.1 and 2.1).

Regarding CO_2 (Figure 2.9), in the two models the coherence at the 100-kyr band is in phase and high after -500 kyr and weaker and out of phase before -500 kyr coinciding with the first glacial cycles (see also Figure 2.2), which are more difficult to simulate. In the 41-kyr band the coherence is high in roughly the same intervals as in the V series, and in the 23-kyr band it is practically inexistent. This can be attributed to the combined effects of high-frequency damping produced by parameter τ_C (and/or τ_{C_2} in LS) and poor representation of the carbon dynamics by PP04-derived models.

2.3.3. Phase space portraits

Phase space portraits and embedding attractor techniques can also be useful for quantifying the performance of a simulated time series in matching the dynamical properties of an observational time series. Time series of 16000 linearly interpolated, equally spaced data are used to reconstruct the attractors. To avoid autocorrelated effects we use the method of mutual information (*Marwan et al.* [2007]), a well-established measure to detect nonlinear dependencies within a time series, which estimates an optimal time lag of 1433 for V and 1371 for C . The first step

is to see whether the attractor of the observational time series is embedded in a phase space with the same dimensionality as the predicted time series. To estimate the embedding dimension, we use the method of false nearest neighbor (*Kennel et al.* [1992]), which examine the variation of the number of neighbors in a time-series trajectory as a function of the dimension to obtain an estimate of the real embedding dimension. The dimensionality D obtained for the observational time series was $D = 4$ and the dimensionality D_S obtained for the simulated time series was $D_S = 3$. The difference may be due to the existence of some independent variable not taken into account by the model that generates the oscillations of a period < 2 kyr in $\delta^{18}\text{O}$. A moving average of the observational series with a 2-kyr window produced a smoothed time series which generates a dimensionality coincident with the one of the simulated time series ($D = D_S = 3$); reconstructed attractors for the smoothed $\delta^{18}\text{O}$ and CO_2 time series are displayed in Figures 2.10 and 2.11, respectively.

Figures 2.12 and 2.13 show the attractor obtained for 3τ and LS models for simulated ice volume and Figures 2.14 and 2.15 show the same for CO_2 . The embedded attractors of proxy and simulated data are not identical but present a certain similarity in form, and the amplitude of the phase space is close for V ; in the C case, the form is not that similar but the amplitude is equivalent. PP04-derived models are forced externally by I_{65} insolation, and a similar astronomical forcing is supposed to act on the climate system. In any externally forced dynamical system, one of the dimensions has to be the phase of the external forcing, ϕ , which allows the system to become autonomous through the equation $d\phi/dt = 1$. Two additional variables, v_1 and v_2 , remain available, so our three variables V , C and A must be considered as dependent on v_1 and v_2 : $V = V(v_1, v_2)$, $C = C(v_1, v_2)$ and $A = A(v_1, v_2)$. These attractors (Figures 2.10 to 2.15) and the series that they produce bear some resemblance to the Duffing dynamical system, which is also a three-dimensional externally forced nonlinear oscillator with an embedded strange attractor (*Kovacic and Brennan* [2011]).

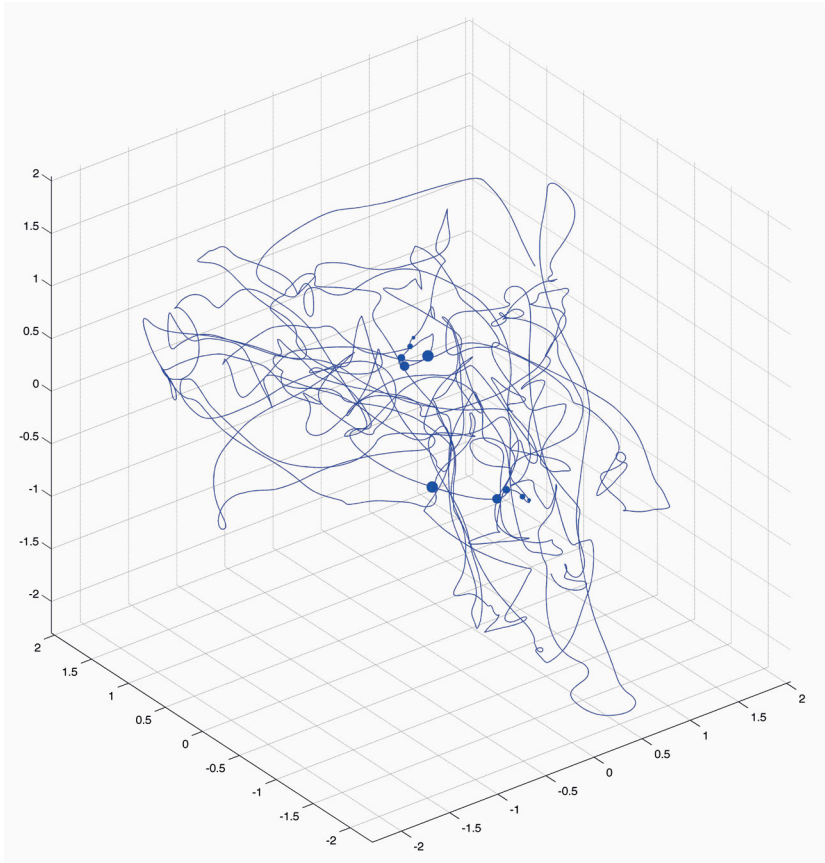


Figure
2.10

Embedded attractor of the smoothed proxy $\delta^{18}\text{O}$ records from *Lisiecki and Raymo* [2005].

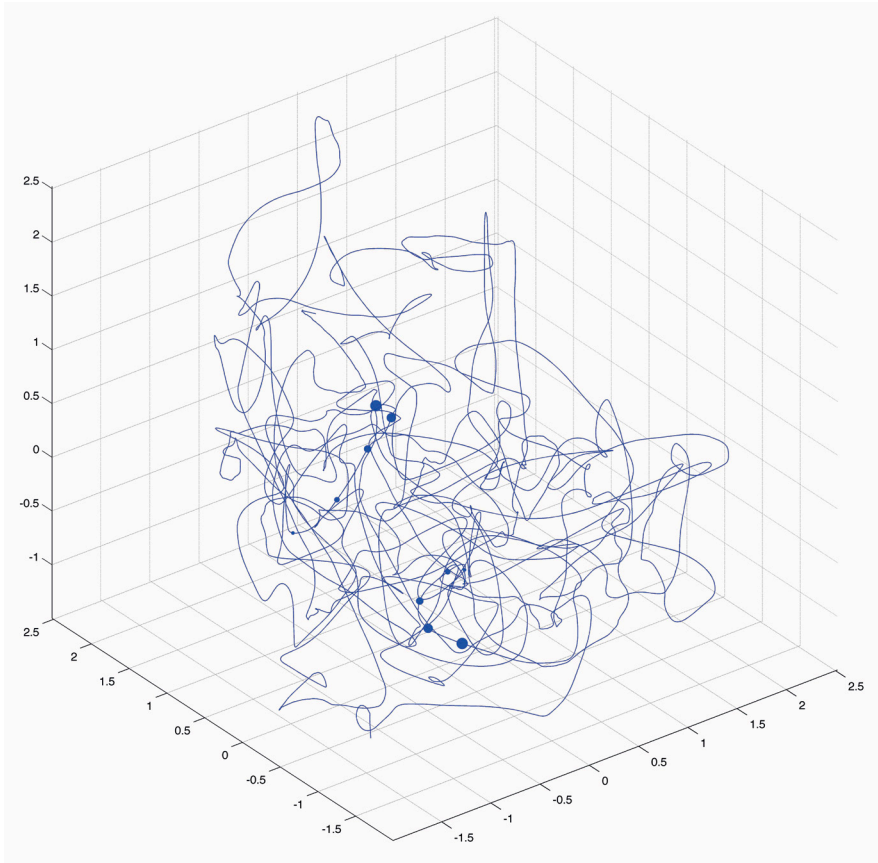


Figure
2.11

Embedded attractor of the smoothed proxy CO₂ data from *Petit et al.* [1999]; *Indermuhle et al.* [2000]; *Monnin et al.* [2001]; *Siegenthaler et al.* [2005]; *Luthi et al.* [2008].

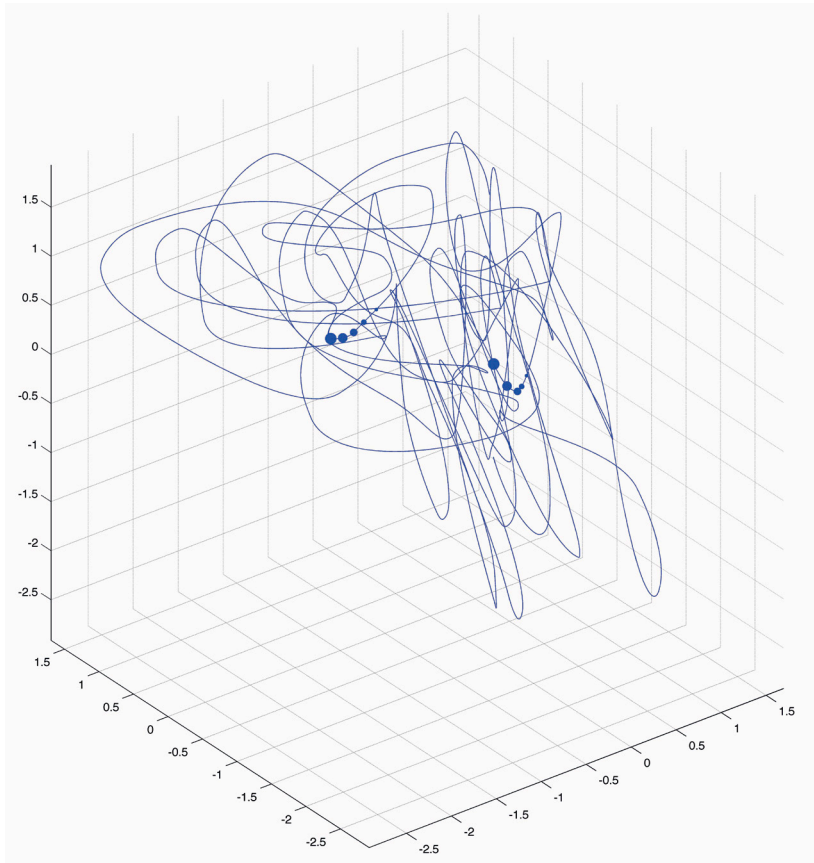


Figure 2.12 Embedded attractor of the simulated V time series with 3τ model.

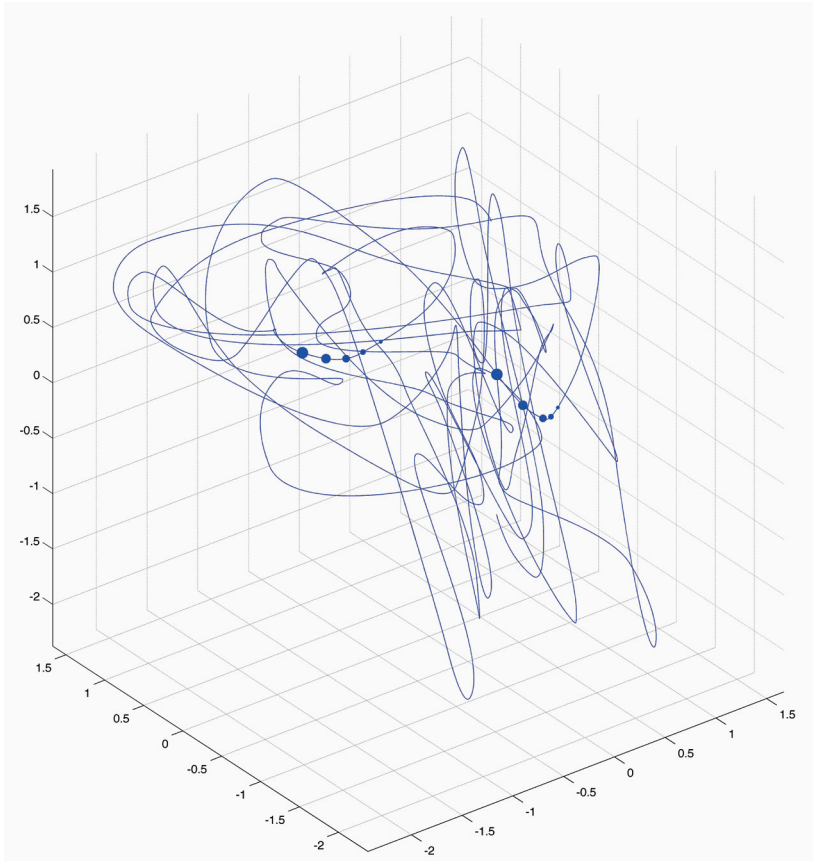


Figure
2.13

Embedded attractor of the simulated V time series with LS model.

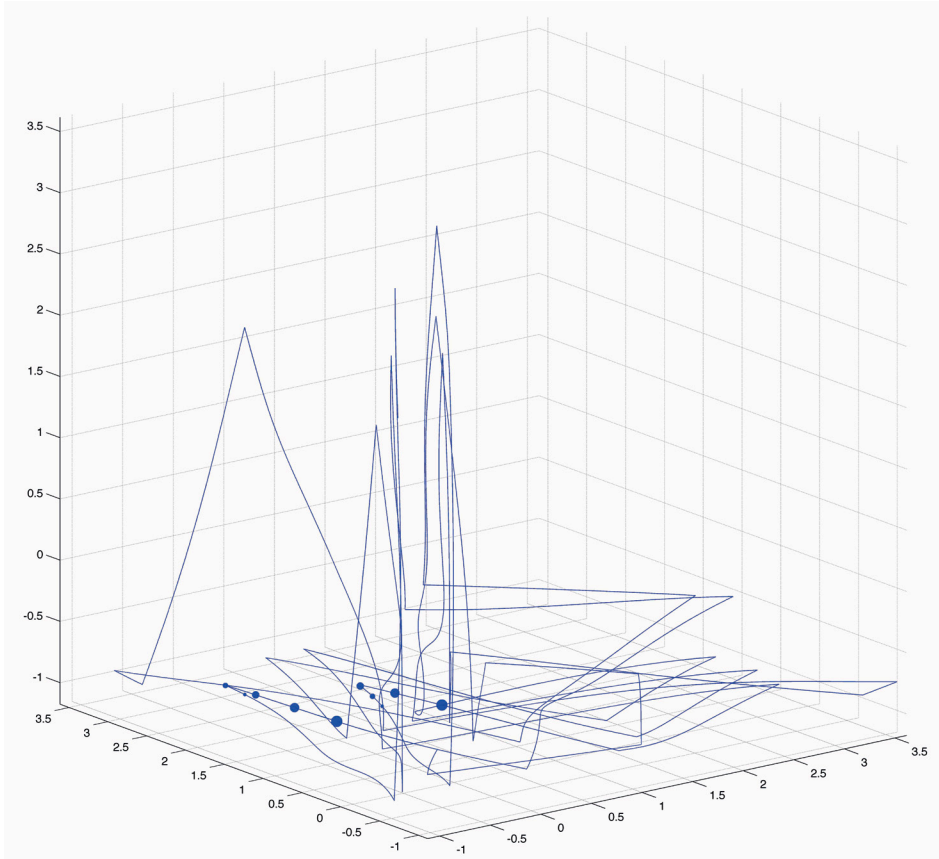


Figure 2.14 Embedded attractor of the simulated C time series with 3τ model.

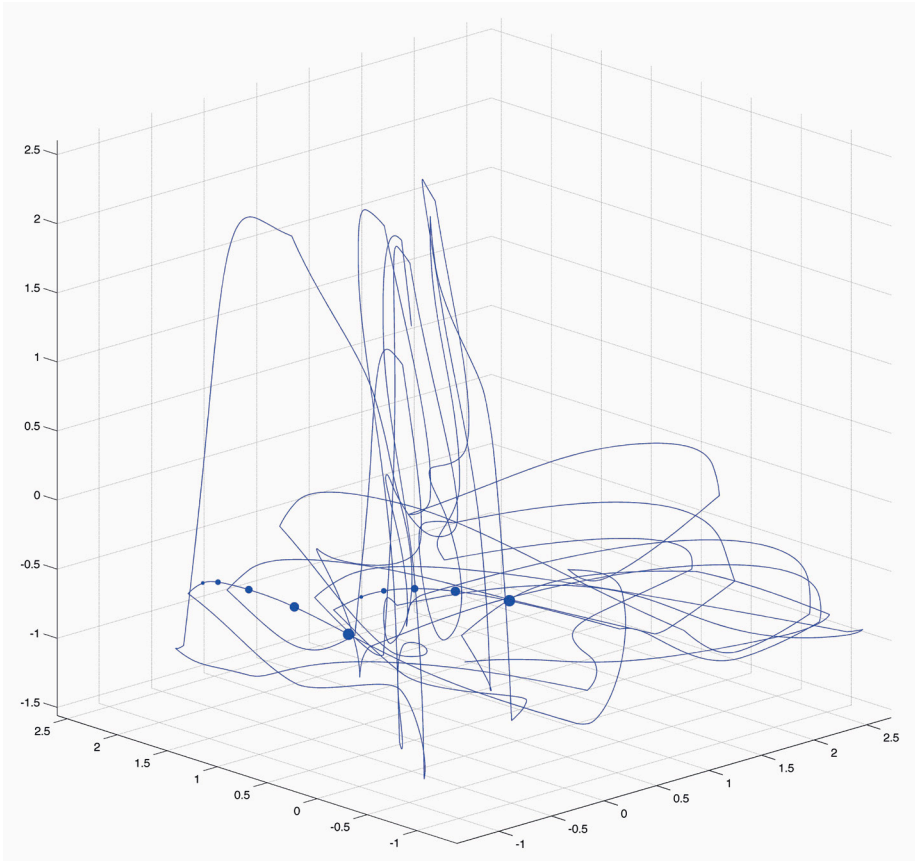


Figure
2.15

Embedded attractor of the simulated C time series with LS model.

2.3.4. Cross recurrence plots

We then obtained the cross recurrence plot (CRP) of observational and simulated trajectories which, despite its name, does not represent recurrences but rather the conjunctures of states of the two systems. The CRP reveals all the times when the phase space trajectory of the first system visits roughly the same region in the phase space where the phase space trajectory of the second system is (*Marwan et al.* [2007]). Figures 2.16 to 2.19 show the CRP obtained with the above parameters for the simulated series of V and C obtained by the models. The Matlab tool created by *Marwan et al.* [2007] was used. Last glacial cycle does not show up because this period data is smaller than D times l , where D is the dimension ($D = 3$) and l is the lag ($l = 1433$ for V and $l = 1371$ for C). We can see that the persistent intervals of good coincidence between the V and $\delta^{18}\text{O}$ series (Figure 2.1) coincide with intense black patches in Figures 2.16 and 2.17, especially spots following Termination IX and Termination VII, $5000 < N < 6000$, $7000 < N < 9000$, $9200 < N < 9500$, $10500 < N < 11000$ and $11500 < N < 12500$ (Terminations are shown in Figures 1.1 and 1.2). Many patterns occurring in the main diagonal appear deformed in lines and columns, indicating that both series are cyclical and the way in which $V(t)$ coincides with $\delta^{18}\text{O}(t)$ at time t shows similarity to the way in which $V(t)$ coincides with $\delta^{18}\text{O}(t-T)$, where T is the 100-kyr period. Roughly 85% of the time the predicted and observational V trajectories are neighbors at a distance of 0.46 times the standard deviation of the phase space. The C trajectories are much more poorly simulated, with the predicted and observational trajectories coinciding less than 50% of the time (Figures 2.18 and 2.19). However, the dynamics in the intervals when the CO_2 is maximum is normally well simulated, which seems to be sufficient to allow the V dynamics to obtain a good similarity to the observational dynamics.

2.4. ALTERNATIVE PROXY FOR ICE VOLUME

As pointed out in Chapter 1, the *Lisiecki and Raymo* [2005] record is a stack of $\delta^{18}\text{O}$ data from benthic foraminifera, and the $\text{O}^{18}/\text{O}^{16}$ ratio is known to depend on

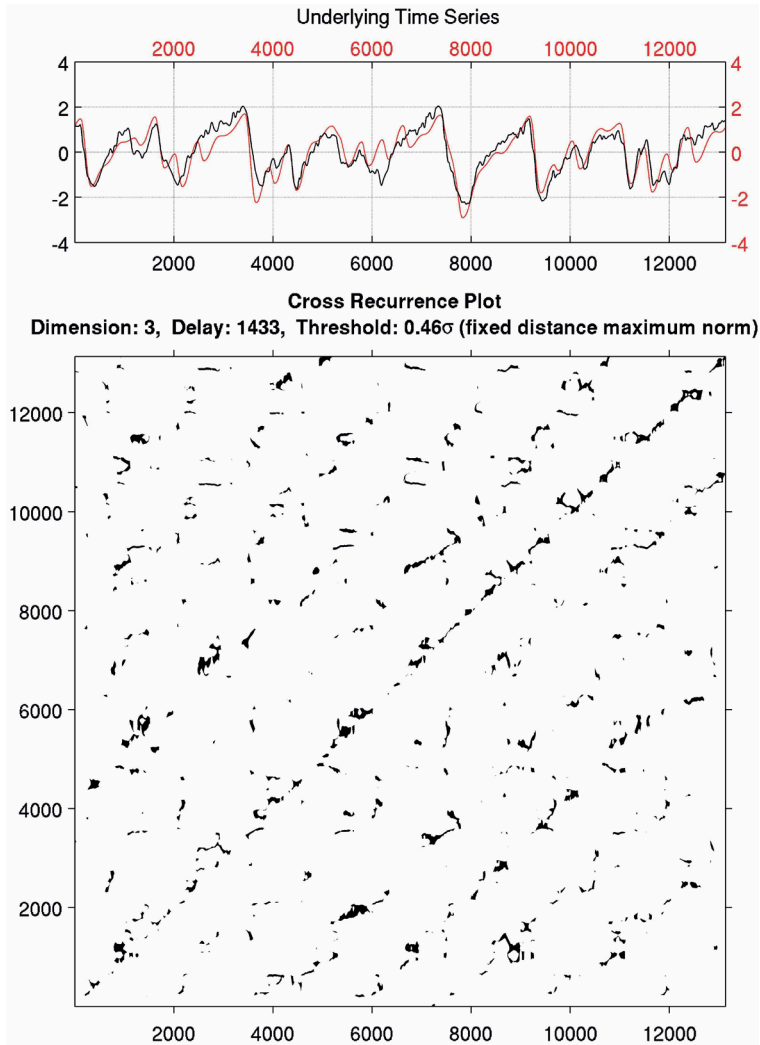


Figure 2.16

Cross-recurrence plots obtained for smoothed proxy $\delta^{18}\text{O}$ records from *Lisiecki and Raymo* [2005] and simulated V time series with 3τ model.

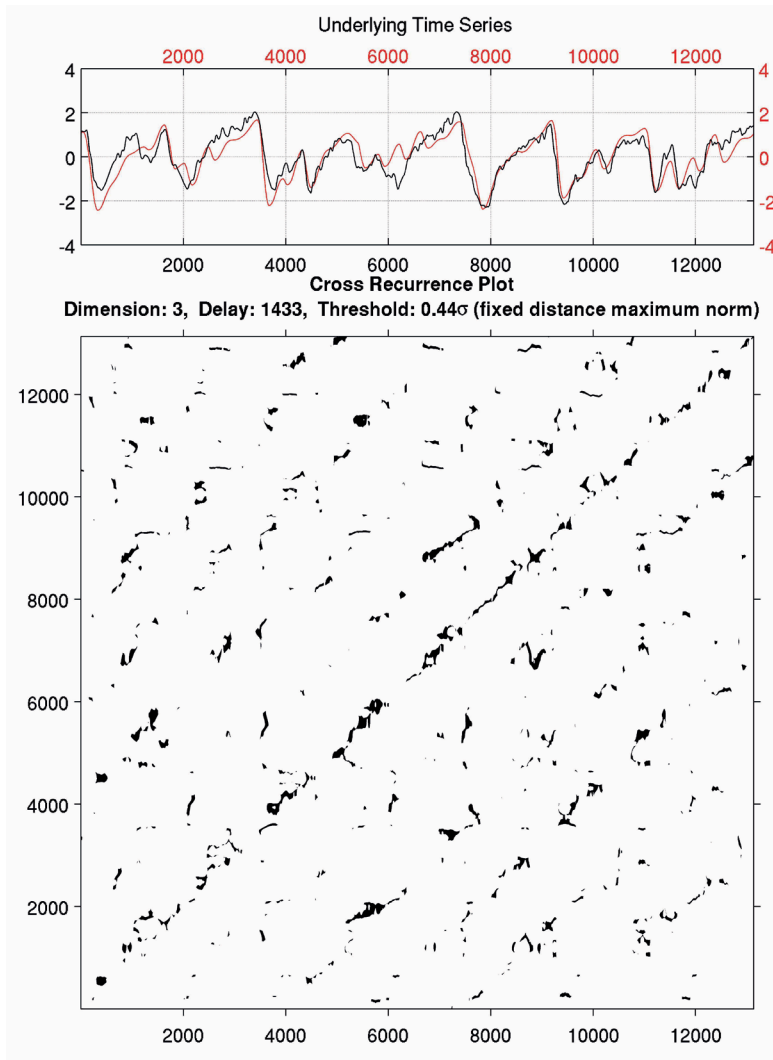


Figure 2.17

Cross-recurrence plots obtained for smoothed proxy $\delta^{18}\text{O}$ records from Lisiecki and Raymo [2005] and simulated V time series with LS model.

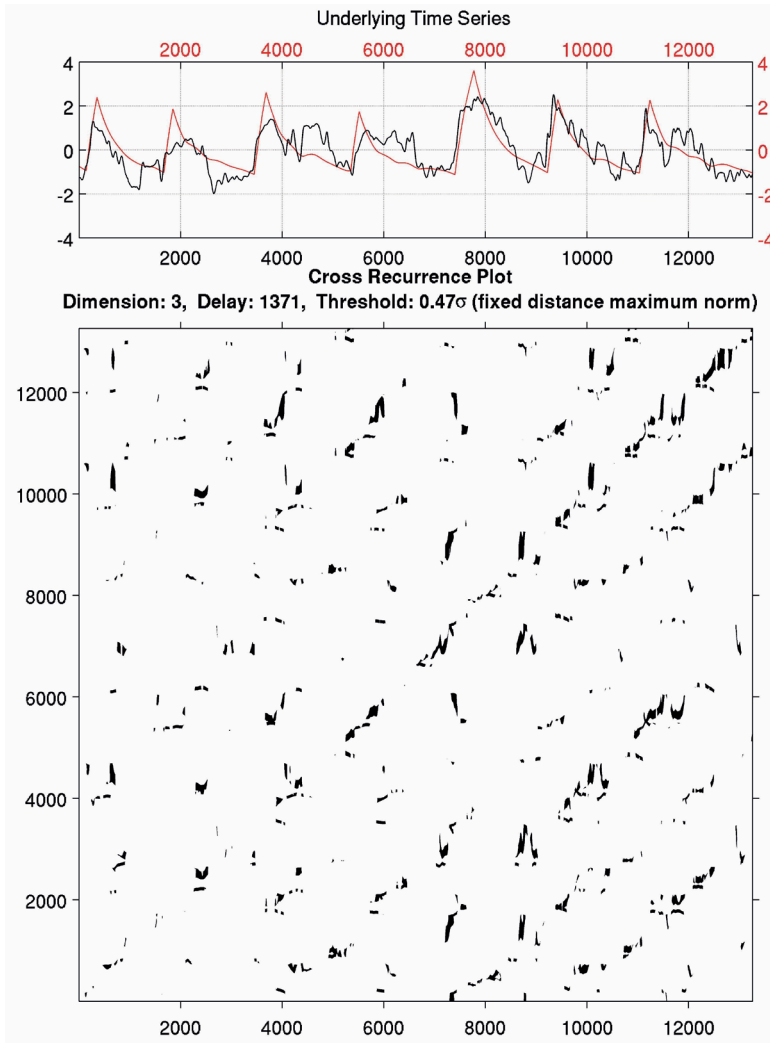


Figure
2.18

Cross-recurrence plots obtained for smoothed proxy CO₂ data from *Petit et al.* [1999]; *Indermuhle et al.* [2000]; *Monnin et al.* [2001]; *Siegenthaler et al.* [2005]; *Luthi et al.* [2008] and simulated C time series with 3τ model.

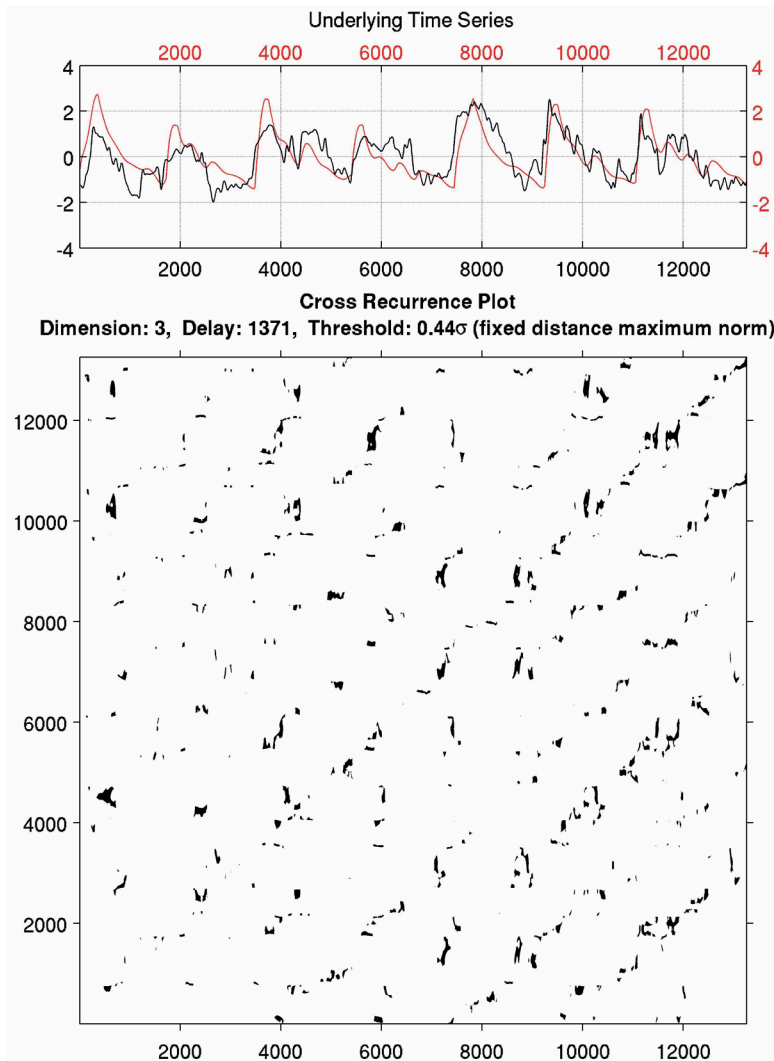


Figure 2.19

Cross-recurrence plots obtained for smoothed proxy CO₂ data from *Petit et al.* [1999]; *Indermuhle et al.* [2000]; *Monnin et al.* [2001]; *Siegenthaler et al.* [2005]; *Luthi et al.* [2008] and simulated time series with LS model.

both the isotopic composition and the temperature of the water where foraminifera developed. *Waelbroeck et al.* [2002] found that the relationship between $\delta^{18}\text{O}$ and ice volume is not linear, since $\delta^{18}\text{O}$ decreases faster than the increase in ice volume at the beginning of the last glaciations, and then progressively more slowly until the ice sheets reached their maximum size. This may produce uncertainties of 20% for the ice volume estimations at the beginning of glaciations. Consequently, there is some risk of over-interpretation when model parameters are adjusted to fit that isotopic record tightly. If that error was assumed to take place during 20 kyr at the beginning of each glacial period, it would cause a 7% loss of explained variance or a 4% loss of correlation. This is slightly above the correlation differences in the models that we have studied, so their performance must be considered equivalent within the observational uncertainty.

Bintanja et al. [2005] tried to eliminate the temperature effects from the $\delta^{18}\text{O}$ series by using a model for air and deep ocean temperatures. The resulting sea-level time series can be used as an alternative to $\delta^{18}\text{O}$. When we calculate the correlations between this time series and the V predicted by our models, we obtain the surprising result that they increase from 0.88 to 0.90 for 3τ and from 0.87 to 0.89 for LS. This shows that the calibration of our selected models to an isotopic series with experimental biases has produced a robust result in spite of the observational uncertainty, although a non-negligible component is that Bintanja's time series is slightly smoother than $\delta^{18}\text{O}$. In Figure 2.20 the V predicted by the 3τ and LS models is compared with sea level time series (*Bintanja et al.* [2005]) and $\delta^{18}\text{O}$ records (*Lisiecki and Raymo* [2005]). In the bottom panel, the power spectrum of all series is shown. As can be observed, the behavior of the 3τ and LS models compared with *Bintanja et al.* [2005] sea level is good, reinforcing the robustness of the fits implemented. Although the correlation improves, the results do not offer any new dynamical insights.

2.5. DYNAMICS OF THE MODELS

A common feature of PP04-derived models is their lack of sensitivity to the I_{60} forc-

ing. This result could be interpreted in three alternative ways:

- (i) Our function $F(V, A)$ is an approximate representation of stratification but I_{60} is not a good proxy for Southern Ocean temperature.
- (ii) Stratification and/or CO₂ release in the SO is not controlled by regional temperatures.
- (iii) Release of CO₂ in the SO is not controlled by stratification and the function $F(V, A)$ in our models represents a different process.

A possible interpretation belonging to group (iii) is that A might represent sea ice instead of the ice-sheet area and that $F(V, A)$ could be a proxy for a rate of emission of CO₂ that is controlled directly by sea ice area, A , and SO deep temperature. SO deep temperature could be controlled by NH temperature (through V) more strongly than by I_{60} . One possible mechanism able to produce this effect was proposed by *Gildor and Tziperman* [2001]: stratification in the SO is composed of cold, fresh water above warm, salty water. Glacial conditions in the NH cool the North Atlantic Deep Water (NADW) and, consequently, via the southward flow and upwelling of NADW, lower the deep temperature in the SO. Because of the permanent ice cover over Antarctica, surface ocean temperature in the SO near Antarctica is

$$\frac{dA}{dt} = \frac{(V - A - cI_{60})}{\tau_A}. \quad \text{2.7}$$

close to freezing point during the entire glacial cycle, so it cannot cool very much even during glacial conditions. Glacial conditions therefore increase the density of deep SO water but not of surface SO water and this strengthens the vertical stratification there. As a result, vertical mixing in the SO is expected to be reduced. This mechanism implies that temperature changes in the NH (supposedly correlated with global ice volume V) lead to the CO₂ changes in the SH. This mechanism is plausible

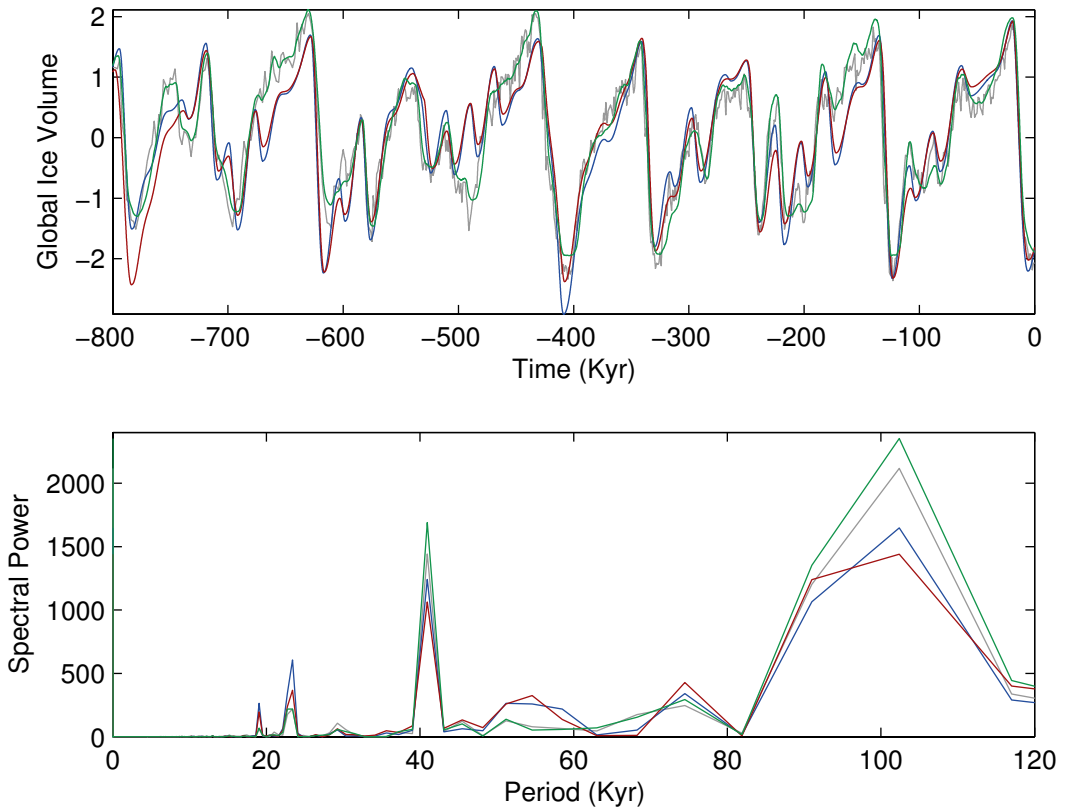


Figure 2.20

Top panel: normalized ice volume as predicted with the 3τ (blue line), LS (red line) models, proxy $\delta^{18}\text{O}$ records from Lisiecki and Raymo [2005] (grey line) and Bintanja et al. [2005] sea-level time series (green line). Bottom panel: power spectrum of normalized ice volume as predicted with 3τ model (blue), LS model (red), proxy $\delta^{18}\text{O}$ records from Lisiecki and Raymo [2005] (grey line) and Bintanja et al. [2005] sea-level time series (green line).

but interpreting F as a model for such mechanism is uncertain, because correlation between V and North Atlantic temperature time series (*Bard [2003]*) is low, only 0.64 for the last 800 kyr.

On the other hand, to determine whether A is sensitive to I_{60} , Equation 2.2 of the model 3τ was modified as

However, the best fits obtained after this change did not improve upon those obtained by our 3τ model, showing that Equation 2.2 is also insensitive to I_{60} .

These results are consistent with the following conclusions: a variable A that follows the evolution of V with a delay of 5 to 7 kyr seems necessary to obtain good fits. This variable can be interpreted, as *Paillard and Parrenin [2004]* do, as the ice sheet extent on the Antarctic shelf, but it can also be interpreted as the whole SO ice extent since the capping effect (*Keeling and Stephens [2001]*) and the control of A on the residual circulation act in the same direction as the deep stratification. CO₂ release to the atmosphere in the SO may be controlled by either stratification or sea ice extent, or by both. However, neither of the two corresponding variables in our models (F and A) seems to be sensitive to I_{60} insolation. The conclusion is that either some of these mechanisms are not sensitive to SO temperature, which is difficult to conceive, or I_{60} is not a good proxy for SO temperature.

Huybers and Denton [2008] pointed out an important fact that had gone unperceived and can bring new light to these conclusions: Antarctic summer duration is highly correlated with I_{65} insolation. In addition, it is plausible that the Antarctic climate remains in near radiative equilibrium with local heat accumulation, which is controlled by summertime duration. In contrast, northern changes are mediated through the response of the northern ice sheets, which are much more sensitive to insolation at the solstice (I_{65}) than to summertime duration. Thus, SO temperature could be a crucial variable that has influence on the southern sea ice or the density of deep water, or both; but this southern temperature does not need to be controlled via teleconnection with the north, it may respond to some regional astronomical forcing different to I_{60} .

The correlation between the observational CO₂ time series we use and the Antarctic temperature inferred from the EPICA dome by *Jouzel et al.* [2007] for the past 800 kyr is 0.89. Thus, the good performance of the LS model, where $F = F(C, A)$, and the fact that C is a good proxy of Antarctic temperature, suggest that formation of Antarctic deep waters may be controlled only by ice sheet extent and regional temperature.

The good performance of the 3τ , and even 4τ , models and their functional form $F(V, A)$ could suggest that stratification is partly controlled by the temperature of the NADW upwelling, through V and the teleconnection mechanism of *Gildor and Tziperman* [2001]. This contribution could exist but it cannot be large because of the modest correlation between the $\delta^{18}\text{O}$ and North Atlantic sea surface temperature (0.64). More plausibly, $F(V, A)$ is another way to suitably represent stratification in PP04-derived models, since the correlation of $\delta^{18}\text{O}$ with Antarctic temperature is almost as high as that of CO₂ (0.86 instead of 0.89). More importantly, the 3τ model simulates V with a far better correlation (0.88) than that of C (0.79) and therefore the correlations between its simulated C and $-V$ and the Antarctic temperature are very similar: 0.78 and 0.77, respectively. Thus, V is a good proxy of SO regional temperature and the expression $F(V, A)$ is plausibly a suitable way to model the local formation of brines, as $F(C, A)$ is. The fact that $F(V, A)$ performs somewhat better than $F(C, A)$ could be attributed to the additional (even small) contribution that V has over stratification (through teleconnection) and C does not, or, perhaps, to a larger effect of sea level over brine formation than local temperature has. The fact that sea level affects the area of the Antarctic shelf, where brines are produced, supports this second possibility.

The LS model, which uses the expression $F(C, A)$, needs a direct forcing of I_{65} on C . Model 3τ , which uses $F(V, A)$, doesn't need it, but it has the direct forcing I_{65} on the V variable. This suggests that PP04-derived models need a quick response of regional SO temperature to I_{65} rising, as quick as $\tau_{V_2} \cong 3$ kyr in 3τ and $\tau_{C_2} \cong 3$ kyr in LS. The coincidence of these two scales reinforces our interpretation of $-V$ and C in F as proxies of SO regional temperatures.

Figure 2.21 shows the time variation of I_{65} (top), V (second panel), A (third panel), C (fourth panel) and F (bottom) simulated by the 3τ (blue line) and LS (red line)

models for the two last glacial cycles. Due to the effect of τ_C , C responds to the I_{65} variations with a certain delay. For this reason, every maximum (minimum) of I_{65} in the figure is followed by a maximum (minimum) of C 5 kyr later. The variations of C are reflected in the F variable which has its maxima and minima in counter-phase with C . On the other hand, A responds to C by following its long-term trend (with a delay of 7 kyr approximately) but damping its high-frequency oscillations. When C is low, as in the glacial maximum, A is large, and F is close to the trigger $F < 0$. In this situation, any new maximum in I_{65} causes a decrease in F (through C and A) that triggers the oceanic CO₂ pulse, starting the deglaciation. In the case of 3τ , an almost parallel description can be made using variable V instead of C .

The double condition for generating a deglaciation is thus the coincidence of a maximum of I_{65} in a period when V is large. This double condition was observed and incorporated by Paillard in some previous models (Paillard [1998]).

Figure 2.22 shows the relative contributions to CO₂ levels of the mechanisms involved, as functions of time, for the 3τ model (top) and LS model (bottom). The blue line represents the $\gamma - \beta V$ term in Equation 2.5; the red line represents the deep ocean contribution ($H(-F)$) in the same equation to the change in C_r . An inertial contribution, defined as the instantaneous difference between C and its asymptotic value C_r , has been included as a green line.

In the 3τ and LS models, C_r maintains a monotonous growth after -135 kyr. First, following the abrupt increase in C_r caused by the connection of the oceanic pulse; then, following the increase in C_r caused by the positive feedback T-CO₂ (V-CO₂ in our models). The slope of this CO₂ increase depends on the rate of decrease of V , which responds to a combination of astronomical forcing and greenhouse feedback. In these models the period during which the CO₂ increases is approximately the period when the oceanic pulse is connected. However, the introduction of a direct forcing of I_{65} on C_r in the LS model allows the deglaciations to start with a shorter oceanic release of CO₂. This interchangeability between a fraction of the oceanic release and other sources of CO₂ taking place at moments of astronomical warming (as the termination periods usually are) stems ultimately from the extreme simplicity of the CO₂ release mechanisms incorporated in the PP04-derived models. After

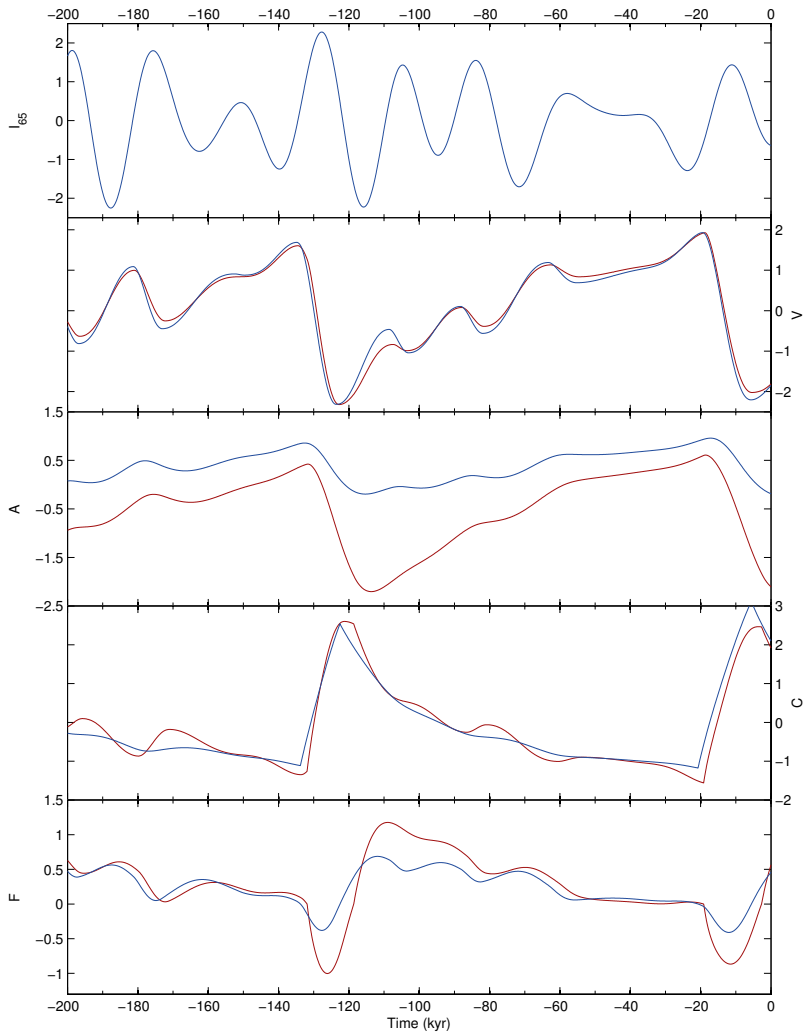


Figure
2.21

Time variation of I_{65} (top), V (second panel), A (third panel), C (fourth panel) and F (bottom) simulated by the 3τ (blue line) and LS (red line) models for the two last glacial cycles.

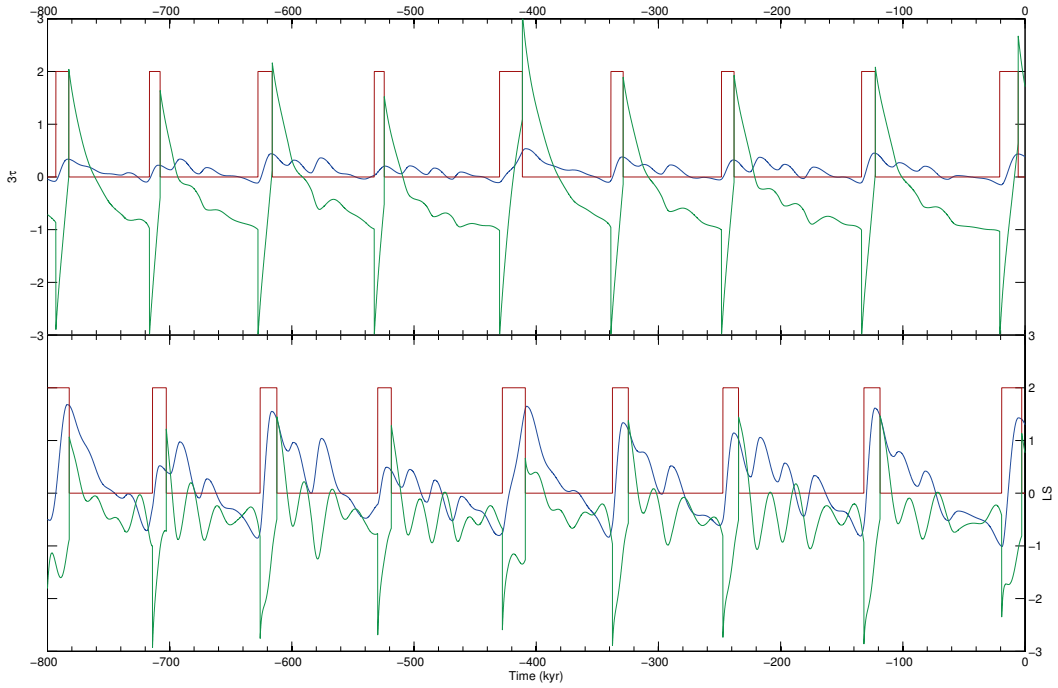


Figure 2.22

Relative contributions to CO₂ levels of the mechanisms involved, as functions of time, for the 3τ model (top) and LS model (bottom). The blue line represents the $\delta - \beta V$ term in Equation 2.5; the red line represents the deep ocean contribution ($H(-F)$) in the same equation to the change in C_r . An inertial contribution, defined as the instantaneous difference between C and its asymptotic value C_r , has been included as a green line.

the end of the oceanic pulse and astronomic contributions, C is mainly above its asymptotic level and starts to decrease towards glacial levels.

Two main conclusions can be extracted from this analysis:

- (i) The oscillation in V that characterizes the termination periods is essentially produced by the same positive feedbacks, CO_2 - T and T - CO_2 , that characterize any other oscillation triggered by insolation change; however, this oscillation has stronger slopes in both C_r and V_r because of the extra contribution generated by the oceanic pulse.
- (ii) A rather abrupt oceanic release of CO_2 (similar to a rectangular pulse) seems necessary to initiate a deglaciation; this release is controlled by the deep-water formation variable, F , which depends mainly on V and A (3τ model), or on C and A (LS model); and V , A and C are driven in the last term by I_{65} insolation.

2.6. OBSERVATIONAL DYNAMICS

The dynamics and change of overturning, and its impact on CO_2 variation during glacial cycles, remain controversial (*Sigman et al.* [2010]). However some facts are well established and widely accepted.

First, the deep ocean has northern and southern meridional overturning circulations (NMOC and SMOC) which have been described as:

- (i) A long loop (NMOC) dominated by NADW, which is relatively poor in dissolved CO_2 because of high photosynthetic consumption.
- (ii) A short loop (SMOC) dominated by Antarctic Bottom Water (AABW) which is richer in CO_2 (*Toggweiler et al.* [2006]; *Watson and Garabato* [2006]).

The existence of the SMO loop seems to depend crucially of diapycnal mixing (*Haertel and Fedorov* [2011]). Both loops mix in the interior around the Antarctic continent to form Circumpolar Deep Water (CDW), which comes up to the surface along the southern part of the Antarctic Circumpolar Current (ACC). This upwelling is forced mainly by the divergence of Ekman pumping at the surface, centered to lie at approximately 65°S today (*Toggweiler* [1999]), which is driven by the mid-latitude westerlies. Any change in either zonal wind stress curl or latitude of the westerly wind belt should reduce the deep water content of the Meridional Overturning Circulation (MOC) and plausibly its intensity (*Toggweiler et al.* [2006]). However, NMOC intensity in the SO seems to be the sum of the mean Ekman transport and opposing mean eddy transport over the ACC. The residual northward transport is strongly controlled by heat gain of the waters traveling northward (*Karsten and Marshall* [2002]).

Second, temperatures are close to freezing at all sites in the glacial ocean, but the deep SO (at sites located within present AABW spreading pathways) was much more saline than today, which implies a density anomaly between the deep and surface SO waters that is three times larger than nowadays (*Adkins et al.* [2002]; *Watson and Garabato* [2006]). This evidence could be a consequence of increased brine rejection in Antarctica in combination with reduced recirculation of AABW to the surface (*Fischer et al.* [2010]).

Third, overturning was nearly, or completely, eliminated during the coldest deglacial interval in the North Atlantic region, beginning with the catastrophic iceberg discharge Heinrich event HS1, 17500 years ago (*McManus et al.* [2004]), coinciding with the first major step in Antarctic warming (*Barker et al.* [2009]). Some terminations have started in coincidence with Heinrich events (*Cheng et al.* [2009]). In Terminations I (T-I) and III the same sequence is observed: a Heinrich event at the end of the glacial period (HS1 in T-I), followed by an interstadial (Bolling-Allerod in T-I), lasting 1800-2000 years, then a second stadial (Younger Dryas (YDS) in T-I) and then the final deglaciation (Holocene in T-I).

Coupled general circulation models for glacial conditions show very little change in the strength of the zonal wind stress on the SO and weak shifts in the location of

the westerlies belt (*Fischer et al.* [2010]). However, observations of wind and rain patterns in HS1 and YDS suggest that the Inter-tropical Convergence Zone (ITCZ) and trade winds shifted southward (*Peterson et al.* [2000]; *Leduc et al.* [2009]; *Saiikku et al.* [2009]; *Wang et al.* [2004]; *Griffiths et al.* [2009]). Two warming pulses in the SH coincided with HS1 and YDS, respectively, suggesting a north-south connection mechanism such as the bipolar seesaw suggested by *Broecker* [1998]. The $^{231}\text{Pa}/^{230}\text{Th}$ ratios from core GGC5 off the Bermuda Rise (*McManus et al.* [2004]) reflect a strong reduction in Atlantic overturning circulation during HS1 and a moderate reduction during YDS. In contrast, biogenic opal flux in the SO, interpreted as a proxy for changes in upwelling south of the Antarctic Polar Front (*Anderson et al.* [2009]) shows an increase in upwelling during HS1, a decrease during the Bolling-Allerod period and a further increase in overturning during YDS. This suggests that the shut-down in the Atlantic MOC (AMOC) removed a source of dense water to the ocean interior and that this “density vacuum” (*Broecker* [1998]) precipitated an increase in AABW formation to fill that vacuum (*Sigman et al.* [2010]).

These pieces of evidence have been interpreted similarly by different authors (see *Cheng et al.* [2009]; *Denton et al.* [2010]; *Shakun et al.* [2012]). The sequence of events would start with a rising boreal summer insolation controlled mainly by inclination and precession cycles (*Huybers* [2011]). This insolation produces a gradual northern warming in the presence of a massive, isostatically depressed NH ice sheet which has growth gradually for 80-100 kyr. In these conditions, an ice instability mechanism makes the Laurentide, Greenland and European sheets ablate and collapse locally, producing a strong meltwater pulse into the North Atlantic, which initiates a Heinrich event. This slows the AMOC and lowers the south-north Atlantic heat flux, with stadial conditions in the north and southern warming and southward movement of climatic zones in the SH. The above three studies agree that this sequence is the deglacial trigger.

A number of mechanisms are potentially able to connect this trigger with an increased release of CO_2 in the SO and subsequent atmospheric CO_2 rise:

- (i) Southward movement of climatic zones could include a southward shift in the westerlies, resulting in enhanced wind-driven

upwelling on the Antarctic divergence (*Marchitto et al.* [2007]). This would promote ventilation of CDW and the observed productivity peak (*Anderson et al.* [2009]), would erode the Antarctic salinity-driven stratification and would thus facilitate the formation of deep water in Antarctica (*Toggweiler et al.* [2006]). The importance of this mechanism deserve further investigation, as recent studies have shown an oscillatory behavior of AMOC between weak and strong states due to variations on the density gradient in the Atlantic Ocean, derived from variations of CO₂ and strength of SO winds (*Banderas et al.* [2015]).

- (ii) Warming of the SO could melt sea ice, leading to an increase in ventilation as a result of enhanced residual northward transport and also to degassing effects. As suggested by *Fischer et al.* [2010], the increase and decrease in sea ice coverage could have modulated the annual net heat gain of the SO surface, and the reduced buoyancy gain would have weakened the MOC during glacial periods through its control of the residual circulation. This would have limited the upwelling of CO₂-enriched deep water, acting in the same direction as the capping effect that winter ice extent is assumed to have on deep-water outgassing of CO₂ (*Stephens and Keeling* [2000]).
- (iii) Warming associated with southerly shifts could reduce Patagonian glaciation, lowering the flux of dust and iron from Patagonia to the SO. This would reduce the efficiency of the biological pump (*Martin and Fitzwater* [1988]).
- (iv) Increased CO₂ release from Antarctic divergence would decrease the concentration of dissolved inorganic carbon (DIC) and thus increase the carbonate ion concentration in the deep ocean. This would increase the burial rate of calcium carbonate, forcing a decrease in whole-ocean alkalinity, decreasing solubility and putting an additional fraction of CO₂ into the

atmosphere. According to *Sigman et al.* [2010], this carbonate compensation in cooperation with switch on/off of deep water formation or a degassing effect is able to account for 40 ppm of $p\text{CO}_2$ difference between interglacial and glacial conditions. It is probable that neither Antarctic overturning nor gas exchange were completely shut off/on. However, more complete nutrient consumption and lower export of organic matter have been observed in the Antarctic during glacial periods, suggesting a reduced supply of nutrients and water from the deep to the surface ocean (*Sigman et al.* [2010]). Thus, overturning decreased in the glacial SO while productivity did not decrease as much as the nutrient supply from below did, making $p\text{CO}_2$ decrease as a result. This mechanism would have complemented the previous ones, generating the atmospheric $p\text{CO}_2$ difference of 40 ppm.

- (v) In the sub-Antarctic zone, the sinking flux of organic matter was greater in glacial periods than today, with some evidence for more complete nutrient consumption (*Sigman et al.* [2010]). The effect of this zone on alkalinity and availability of nutrients at low-latitudes is great, reaching 40 ppm for the $p\text{CO}_2$ glacial-interglacial difference (*Hain et al.* [2010]).

As observed by *Sigman et al.* [2010] the declines in atmospheric $p\text{CO}_2$ to their minima during peak ice ages tend to occur over tens of thousands of years and/or in steps. This may result from the progressive activation of different $p\text{CO}_2$ reducing processes (*Hain et al.* [2010]). In particular, the Antarctic cooling early in the last ice age, 115 kyr BP, has been interpreted as reduced Antarctic overturning or increased sea-ice suppression of gas exchange (*Peacock et al.* [2006]) with an additional fraction of CO_2 uptake due to ocean cooling. In contrast, the second major decline in atmospheric $p\text{CO}_2$, 70 kyr BP, coincides with a major dust flux increase in Antarctic and sub-Antarctic zones (*Martínez-García et al.* [2009]), which may have caused iron fertilization of the SO (*Watson et al.* [2000]). Additionally, this period may have suffered the sharpest

transition from NADW to GNAIW formation (*Hodell et al.* [2003]), which may have improved the ability of the deep SO to lower atmospheric pCO₂ (*Sigman et al.* [2010]).

2.7. DISCUSSION

To what extent are PP04-derived models consistent with the observational dynamics summarized in last section? First, the sequence of activation of processes that release CO₂ during the terminations, suggested by the triggering sequence mentioned above, is very different to the sequence of steps that reduce CO₂ during glacial times, and this difference generates the typical saw-tooth shape of the CO₂ glacial-interglacial oscillations. The lack of a complete model for the biological and carbonate pumps in the PP04-derived models makes it impossible to precisely reproduce the series of events that characterize glacial periods, and using different relaxation times for moments of increasing and decreasing CO₂ is the easiest way to take into account this asymmetry and to reproduce the double slope cycle. When a single relaxation time τ_C is used ($\tau_{C_2} = 0$) in the LS calibration, the correlation obtained for V decreases by less than 1% (0.85 instead of 0.86) but the correlation for C decreases by 8% (0.68 instead of 0.74) because of the far more abrupt ups and downs of the simulated C during the glacial periods. The 3τ model is much less sensitive to this τ_{C_2} parameter, and maintains a very high correlation when it is eliminated (0.88 and 0.79, for V and C , respectively, in the 3τ model). We thus obtain a model with almost the same correlations as 4τ and with one parameter less than PP04. The good performance in relation to PP04 must be attributed only to the introduction of a different time for accumulation (τ_V) and for ablation of ice (τ_{V_2}).

Though the glacial decay is only roughly simulated by PP04-derived models, the precise fitting of pace and intensity of interglacial CO₂ that these models generates is sufficient to obtain a good match of the ice volume evolution.

The term cI_{60} has been removed from Equation 2.6 in 3τ model as one conclusion of this study is that PP04-derived models are not sensitive to I_{60} southern insolation. In these models, C seems to be a much better proxy of Antarctic temperature than I_{60}

is. This indirectly reinforces the claim of *Huybers and Denton* [2008] that Antarctic temperature is not sensitive to insolation during a particular summer day and that it could be sensitive to another kind of variable, such as austral summer duration.

The stratification function, F , is a crucial variable of PP04-derived models, which must be interpreted as stratification produced by density difference between AABW and NADW with a possible minor contribution from stratification produced by density difference between NADW and surface water. F controls the upwelling of CO₂ in a nonlinear way: an abrupt oceanic release of CO₂ similar to a rectangular pulse of 10 to 20 kyr, very sensitive to F , is necessary in these models to generate the terminations. Mixing rates may decrease as density differences increase (*Watson and Garabato* [2006]) if we use the internal wave parameterization for the vertical mixing coefficient suggested by *Gargett* [1984]. If the density difference between AABW and NADW is small, the blending process of the two water masses may be more efficient and a larger fraction of the AABW wells up with the mixed Lower Circumpolar Deep Water (LCDW) into the two loops of the meridional overturning circulation (NMOC and SMOC). *Bouttes et al.* [2012] have shown the plausibility of this stratification-dependent mechanism with a model of intermediate complexity.

The changes in ocean circulation associated with westerlies, deep ocean stratification, expansion of sea ice, variation of AMOC efficiency, together with variations of biological uptake and carbonate compensation seems to be the main drivers for the CO₂ atmospheric difference between glacial and interglacial states. *Ferrari et al.* [2014] has recently proposed a new mechanism able to link Antarctica sea ice expansion with the temperature drop, the rearrangement of deep water masses and the change of circulation in LGM, proving that they are not independent mechanisms, but feedbacks. The precise mechanism is lead by the isopycnals of the SO, which control the upwelling and mixing of AABW and NADW, separating the NMOC and SMOC cells. The slope and position of this isopycnal change according with the expansion of summer sea ice, mixing actively AABW and NADW in the interglacial period, but confining the mixing-driven upwelling of abyssal waters at the LGM, closing the SMOC and preventing the mixing of NADW and AABW. As a result, AABW filled oceans basins up to 2 km depth, instead of the present 4 km depth.

This closed abyssal overturning cell would act as a ocean storage of carbon. This approach, considers the expansion of quasi-permanent sea ice in the SH as the driver of the termination. This suggest that sea ice extent may have an effect on the CO₂ release intensity which works in the same direction than stratification during glacial and interglacial periods; therefore, we cannot discard a possible parallel contribution of sea ice area in the intensity of the CO₂ release.

PP04-derived models need a quick response of regional SO temperature (represented by C in LS and by $-V$ in 3τ) to I_{65} rising, as quick as $\tau_{V2} \cong 3$ kyr in 3τ and $\tau_C \cong 3$ kyr in LS. The real climate system could produce a quick response of this kind during deglaciations by the bipolar seesaw mechanism (*Broecker* [1998]).

A is another crucial variable for this kind of models and follows the evolution of V and C with a delay of about 5-7 kyr. This dependence shows that A is sensitive to Antarctic temperature, and the delay suggests that it represents the extent of ice sheet on Antarctic shelves and not on SO sea ice extent. Polynyas are the places where most of the brine is produced and are located between the ice sheet edges and sea ice. Thus, the position of ice- sheet boundaries is crucial for the rate and density of the deep water formed. According to *Anderson et al.* [2002], the Antarctic ice-sheet edge was close to the continental slope in the Last Glacial Maximum (LGM) and it started to retreat onto the continent some thousand years after the LGM on most of the shoreline. This delay seems to be coherent with the delay obtained for the A variable in our calibrations. Therefore, PP04-derived models reinforce an interpretation of the oceanic CO₂ release during deglaciations as controlled by the deep stratification rather than by a capping effect.

As can be observed in Figure 2.21, A takes about 80 to 100 kyr to reach a level that makes stratification become critical ($F < 0$). Therefore, the 100-kyr period (main frequency of glacial cycles) must be considered as internally generated by the climate system. More specifically, it must be interpreted as the characteristic time needed for the Antarctic ice sheet to reach the continental slope. The observations of *Anderson et al.* [2002] on the advance and retreat of ice shelves are not in disagreement with this time scale, but additional observations are needed to contrast this prediction of PP04-derived models.

According to *Tziperman et al.* [2006], many of the models that best fit glacial oscillations have a “phase locking” between a Milankovitch frequency ω_m and an internal cyclicity ω_i . Frequently, a good fit can be obtained when the quotient ω_m/ω_i is a rational number. However, this good fit does not imply that the mechanisms represented by the model are the correct ones. Phase locking is a necessary condition but not a sufficient one. However, *Tziperman et al.* [2006] conclude that “the actual glacial cycles may also be similarly phase locked to the Milankovitch forcing”. That is, this property is probably also one of the climate system itself. If this is so, showing nonlinear phase locking is a good –though not sufficient– feature for a correct paleoclimate model.

What should be sufficient? There is no clear mathematical criterion for deciding. However, if the right mechanisms were to be incorporated in a model with nonlinear locking, we would expect the model to display the following features:

- (i) Its predictions should have high correlations with the experimental time series.
- (ii) It should reproduce the ups and downs of the experimental time series in the scales between thousand to million years better than other models of similar complexity.
- (iii) It should generate time series with frequency composition and embedding dynamics similar to the observational ones.

However, ultimately, only the experimental confirmation that the proposed mechanisms are really acting would be a definitive sufficient condition.

The visual inspection of Figure 2.1 as well as the good correlations obtained show that our models offer great improvements in criteria (i) and (ii) in comparison with other simple models studied in the literature. The wavelet analysis and phase space portraits show that the models that we have discussed here satisfy the third criteria, at least for variable V . On other hand, the pace of orbital timescale is well simulated

for V and C , but in the sub-orbital timescales the phasing of C is poorly matched in many periods that include the deglaciations (Figure 2.9). In addition, the cross-recurrence analysis shows that the short term coherence between simulated and observational CO_2 is only sporadic, indicating that both time series do not follow the same dynamical behavior (Figures 2.18 and 2.19). However, in the deglacial periods the two carbon series become dynamically close. Finally, neither simulated C nor V match the observations on timescales 1-10 kyr, which are the timescales where the first events of the deglacial trigger take place.

The most important conclusion of this study is that a detailed dynamics of CO_2 is of little relevance to obtain very good agreement between simulated ice volume and $\delta^{18}\text{O}$. All that is needed is a nonlinear instability that is reached after 80-100 kyr and that enables that even a modest sub-orbital variation may trigger a sudden release of atmospheric CO_2 . This nonlinear instability seems to be controlled by V or C (here interpreted as Antarctic temperature) and by A (interpreted as Antarctic ice sheet) in PP04-derived models. More specifically, Antarctic cooling would press toward greater stratification because a cooler regional temperature would precondition the surface layer temperature making easier the water column on the shelf to get the -1.9 to -2°C needed for freezing and brine formation. On the other hand, ice sheet extent would tend to block the active polynyas, producing an opposite effect. With the progress of glaciation the latter effect would become dominant and would place the system close to instability, due to the decrease in stratification.

A precise simulation of the detailed set of events constituting the deglacial trigger would require adding some model for the North Atlantic ice sheet instability to our models as well as more complex carbon models. PP04-derived models produce good fits in spite of their simplicity in the modeling of oceanic CO_2 release, which is made to depend only on stratification. The other contributions (carbonate compensation, shoaling or deepening of NADW formation, change of productivity in SO and slowing down of SO overturning) are not included in the model, but should be included in future improvements to obtain a closer representation of all the physical processes that are apparently involved.

Heinrich events seem to belong to a cyclic process of calving with a recurrence peri-

od much shorter than deglaciations (*Bond and Lotti [1995]*). However, according to the interpretations of *Cheng et al. [2009]*; *Denton et al. [2010]*; *Shakun et al. [2012]*, Heinrich events are able to produce large iceberg discharges and long stadials only when ice sheets become large enough. Long stadials are needed to produce a strong CO₂ oceanic release able to start the termination according to *Denton et al. [2010]*. However, large oceanic CO₂ emissions can be produced only if stratification has weakened at the end of the glacial period (*Burke and Robinson [2012]*; *Martinez-Boti et al. [2015]*) for the lack of brine formation (*Paillard and Parrenin [2004]*; *Bouttes et al. [2012]*) or may be weakened by the expected SO upwelling activation. Ultimately, stratification change plausibly controls a large fraction of the oceanic CO₂ release and is synchronous with other mechanisms which contribute an additional fraction in warm periods, such as biological and carbonate pumps in the sub-Antarctic zone and sea ice extent which controls the residual circulation (*Hain et al. [2010]*; *Sigman et al. [2010]*) and the depth of upwelled water (*Ferrari et al. [2014]*). In this regard, stratification may play the same role as an “order parameter” (*Haken [1987]*) plays in a synergetic nonlinear change. └



Chapter 3

IMPACT OF ANTHROPOGENIC CO₂ ON THE NEXT GLACIAL CYCLE

**Chapter based on the following
published articles:**

*Herrero, García-Olivares and Pelegrí [2014],
Impact of anthropogenic CO₂ on the next
glacial cycle. Climatic Change 122:283-298*

Contents

109	3.1. INTRODUCTION
110	3.2. RELAXATION MODELS
111	3.3. ANTHROPOGENIC CO ₂ EMISSIONS
		3.3.1. Total CO ₂ emission
		3.3.2. CO ₂ atmospheric response
116	3.4. PROJECTIONS FOR THE NEXT GLACIAL CYCLE
123	3.5. DISCUSSION

Chapter 3 ⁷

IMPACT OF ANTHROPOGENIC CO₂ ON THE NEXT GLACIAL CYCLE

L

You think man can destroy the planet? What intoxicating vanity. Let me tell you about our planet. Earth is four-and-a-half-billion-years-old. There's been life on it for nearly that long, 3.8 Billion years. Bacteria first; later the first multicellular life, then the first complex creatures in the sea, on the land. Then finally the great sweeping ages of animals, the amphibians, the dinosaurs, at last the mammals, each one enduring millions on millions of years, great dynasties of creatures rising, flourishing, dying away – all this against a background of continuous and violent upheaval. Mountain ranges thrust up, eroded away, cometary impacts, volcano eruptions, oceans rising and falling, whole continents moving, an endless, constant, violent change, colliding, buckling to make mountains over millions of years. Earth has survived everything in its time. It will certainly survive us [...] If we're gone tomorrow, the earth will not miss us.

- Michael Crichton, *Jurassic Park*

3.1. INTRODUCTION

Following Paillard and Parrenin [2004], several relaxation models, based on simple parameterizations of deep ocean stratification, have been recently developed (García-Olivares and Herrero [2012, 2013]). Two of these models, 3τ and LS, have good skills reproducing the conditions during the last 8 glacial cycles (Chapter 1). The 100-kyr glacial-interglacial periodicity is internally generated through three

coupled variables: atmospheric CO₂ concentration, global ice volume and the extension of the Antarctic ice shelf; an important mechanism is the advance and retreat of Antarctic ice as it controls, through brine formation, the deep-ocean stratification and, thus, its capacity to retain CO₂ (Chapter 2).

In this chapter we will use the two models, 3τ and LS, to predict the Earth's glacial-interglacial response during the forthcoming 300 kyr. In Section 3.2 the models' good performance on reproducing past climates is illustrated. In Section 3.3, taking into account the history and predictions of anthropogenic CO₂ emissions, the fraction that remains in the atmosphere is specified. In Section 3.4 the models are applied to project the future climate with and without this anthropogenic CO₂ pulse. A discussion of our results, comparing them with those from other models, is presented in Section 3.5 as well as some brief conclusions.

3.2. RELAXATION MODELS

As we have seen in Chapter 1 and 2, the models, using the parameters in Table 1.1, are able to reproduce the climatic maxima and minima observed from 800 kyr BP to the present for both ice volume and CO₂ (Figures 1.1, 1.2 and 2.1), as well as some of the observed suborbital periodicities (Figure 2.2). Cross-wavelet coherence and cross-recurrence analyses (*Grinsted et al.* [2004]; *Marwan and Kurths* [2002]; *Marwan et al.* [2007]) using proxy and simulated time series show that both model and proxy records display similar dynamics (Figures 2.3 to 2.19).

These results strongly endorse the idea that the relaxation models, despite their simplicity, do include some of the key mechanisms that are behind Pleistocene climatic oscillations. In fact, the models structure mimic some of the major feedbacks that are plausibly taking place in the mechanisms controlling the climate system, such as the effect of northern insolation at the solstice on ice volume, the CO₂ – temperature feedback (through ice volume V), the ice volume – CO₂ sources feedback, and the emission of deep-ocean CO₂ as a function of stratification (the variable F) in both models, which depends on sea level (SO temperature, represent-

ed by C in LS model) and Antarctic ice sheet extent. Additional details on these mechanisms, and the way the models represent them, can be found in *Paillard and Parrenin* [2004], *Paillard* [2010] and *García-Olivares and Herrero* [2013].

Under these considerations, and provided the anthropogenic CO₂ pulse is properly represented, the models may be used to predict its effect on the perturbation of the natural sequence of glaciations and terminations.

3.3. ANTHROPOGENIC CO₂ EMISSIONS

3.3.1. Total CO₂ emission

A crucial first step is to estimate how much anthropogenic CO₂ will be emitted to the atmosphere. With this objective we use the historical record of burning fossil fuels (*Boden et al.* [2010]), complemented with data for the last years obtained from the Global Carbon Project¹. The annual rate of fossil fuels emission, E in (Gt yr⁻¹), is approximated through the following Lorentz function:

$$E = \frac{U b e^{-b(t - tp)}}{[1 + e^{-b(t - tp)}]^2}, \tag{3.1}$$

where U represents the Ultimate Recoverable Resources (URR) of fossil fuels in gigatons of carbon equivalent (Gtce), tp is the year of peak fossil fuels emission (yr), and $Ub/4$ is the corresponding peak rate of fossil fuels emission (Gtce yr⁻¹). Only two of the three parameters are independent, e.g. given either the total area under the curve (U) or the year for peak emissions (tp) we select the other two parameters by numerically searching the best least square fit of the data to Equation 3.1.

¹<http://www.globalcarbonproject.org/carbonbudget>

The Intergovernmental Panel on Climate Change (IPCC) published a Special Report on Emission Scenarios (SRES) that contains 40 scenarios for future fossil fuel production to assess future climate change (*SRES* [2000]). For example, the SRES A1 set uses an average accumulated carbon emission between 1750 and 2100 AD of approximately 1995 Gtce, and the A1F1 extreme scenario implicitly assumes 4100 Gtce of URR, according to the Hubbert linearization done by *Berg and Boland* [2013]. However, these scenarios are based on simple extrapolations of present emission rates with no consideration on actual URR values. *Höök et al.* [2010] and *Berg and Boland* [2013] show that this report is based on unreasonably optimistic expectations about future fossil fuel production which do not take into account realistic estimates for proven and probable fossil fuels reserves. In order to obtain a realistic estimate for *U* we have used the analysis of both *Laherrere* [2006] and the *Energy Watch Group* [2007] on the URR for the three main fossil fuels (coal, oil and gas).

The *Energy Watch Group* [2007] estimates 479 Gt for bituminous coal and anthracite, 272 Gt for sub-bituminous coal, and 158 Gt for lignite. Assuming 92%, 40% and 66% of carbon respectively for these three minerals, we obtain approximately 558 Gtce and the peak of coal-derived CO₂ emissions on year 2042 AD. The analysis of *Laherrere* [2006] gives an estimate of 3000 Gb for all kind of oils (Gb = Gigabarrel, one oil barrel is very close to 159 liters of oil), which amounts to 353 Gtce if we use the conversion factor recommended by EPA²: 0.118 tons of carbon per barrel. The International Energy Agency (*IEA* [2010, 2012]) recognizes that conventional oil production is at or very close to a maximum since 2006 AD and that this production will hardly increase much more, which amounts to an implicit recognition of the oil peak arrival (*Laherrere* [2012a]). Regarding gas, *Laherrere* [2006] predicts an URR of 9100 Tcf, which amounts to about 120-132 Gt of carbon. Recently, *Laherrere* [2012b] has updated the URR coal estimate to 750 gigatons of oil equivalent (Gtoe). Using a carbon content of 25.7 tce/TJ for average coal, in the upper range of reported values (*Gassan-zade* [2004]), this amounts to 808 Gtce. Given these considerations, the total fossil fuels URR amounts to approximately 1300 Gtce, being this our best estimate for the integrated anthropogenic emission of carbon.

² <http://www.epa.gov/greenpower/pubs/calcmeth.htm>

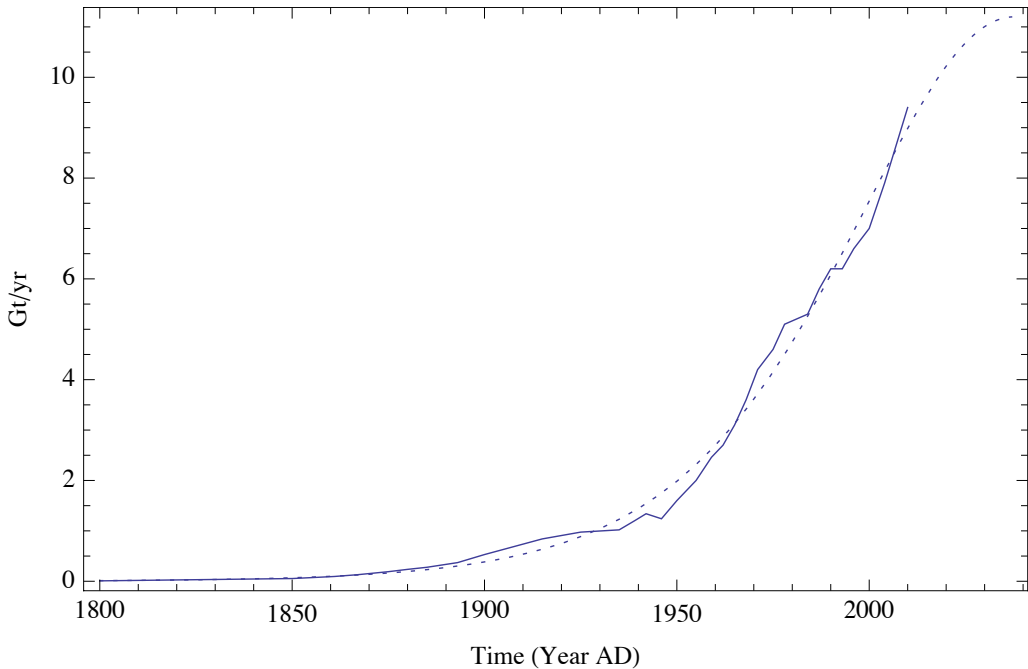


Figure 3.1 Historical data of fossil fuels emissions during the 1800-2010 period (continuous line) and slightly modified Lorentz function such that the area until 2010 equals the accumulated historical emissions (dashed line).

Figure 3.1 shows the historical data on fossil fuels emissions during the 1800 to 2010 AD period and the corresponding fit using a Lorentz function (Equation 3.1), obtained setting $U = 1300$ Gt, which corresponds to a peak emissions on year 2037 AD. This fit has been done such that the integrated carbon emission at 2010 AD has exactly the same area than the historical time-series until 2010 AD (dashed lines in Figures 3.1 and 3.2). This modified Lorentz function is the one we use to produce the full time series for the accumulated anthropogenic emission of fossil fuels (Figure 3.2). The peak of emissions occurs in year 2037 AD, coincident with the inflection point in the accumulated curve, and tends to zero near year 2324 AD, when the accumulated emissions reach their maximum values.

3.3.2. CO₂ atmospheric response

The relatively fast, at the 10 to 100 yr scale, anthropogenic CO₂ emission will lead to a rise in atmospheric concentration but it will also produce an increased storage rate into the ocean, ground vegetation, trees, detritus and soil (*Kheshgi and Jain [2003]*). Our models do not include this type of relatively rapid feedback climatic mechanisms. To take them into account we require a transfer function of accumulated carbon emissions (A_c , in Gt) to atmospheric CO₂ concentration (pCO₂, in ppmv). With this objective we turn to the global compartmental model ISAM (*Jain et al. [1994]; Kheshgi and Jain [2003]*), which may be interactively run online³.

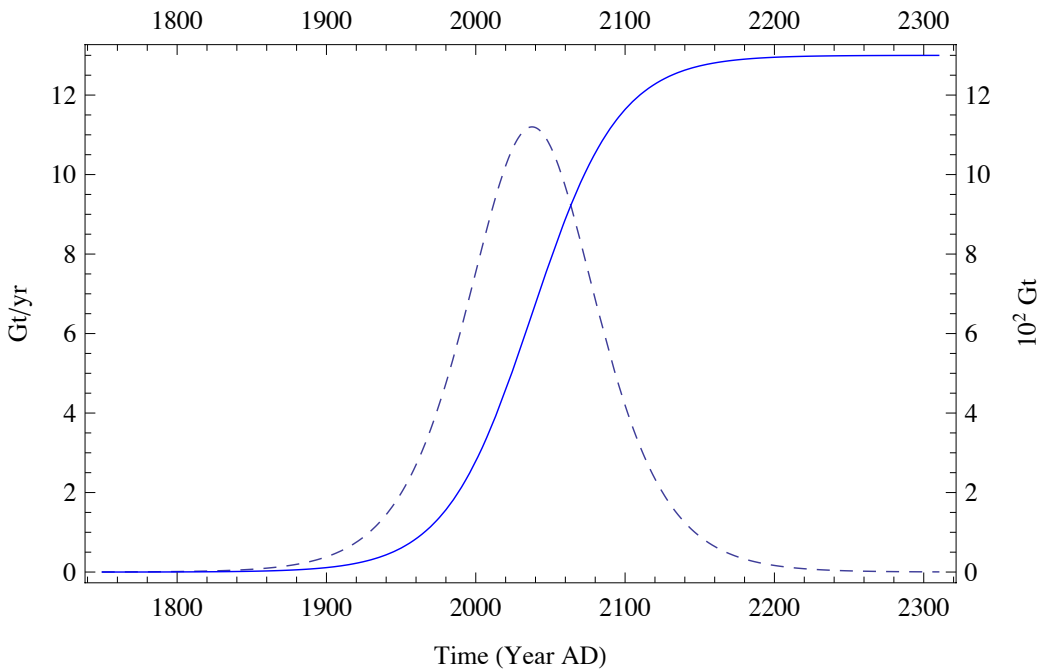


Figure 3.2 Modified Lorentz function illustrating the anthropogenic carbon release per year (dashed line) and the accumulated carbon release (solid line).

In this model, the rates of transfer from the atmosphere to the above five compartments have been calibrated to match the average projections (by six dynamic global-vegetation models and 10 coupled ocean-atmosphere models) for CO₂ uptake between years 2000 and 2200 AD.

In order to obtain the A_c to pCO₂ transfer function, we use the ISAM model with the A1T scenario parameters, as proposed by the IPCC (*SRES* [2000]). We run the ISAM model for values of URR between 0 and 3000 Gt, at increasing URR intervals of 100 Gt, replacing the fossil fuels input of A1T scenario with the modified Lorentz function. For each URR value we obtain the corresponding atmospheric response; these final response points are then linearly interpolated in order to have a continuous curve (Figure 3.3). The corresponding transfer function should be adequate to model the short-term (at decadal and century time scales) response in the range from 0 to 3000 Gt; in particular, it may be used to model the results with our URR best estimate, $U = 1300$ Gt (Figures 3.1 and 3.2). Note that contributions from future deforestation are considered by the ISAM model, therefore they are reflected in the transfer function of Figure 3.3.

We may now finally estimate the time evolution of the anthropogenic atmospheric CO₂ pulse. The historical data of atmospheric concentrations is used for the period between 1750 and 2010 AD. Thereafter, and until the end of the anthropogenic emission in year 2324 AD, the atmospheric CO₂ is estimated using the predicted accumulated emissions from the modified Lorentz function (Figures 3.1 and 3.2) and the transfer function as deduced from the ISAM model (Figure 3.3). In this way the accumulated carbon emission is 361 Gt in year 2010 AD, 642 Gt in year 2037 AD, and reaches a maximum value of 1300 Gt by year 2324 AD, and the atmospheric concentrations at those dates can be obtained from the corresponding ordinates in Figure 3.3.

³<http://climate.atmos.uiuc.edu/isam2>

3.4. PROJECTIONS FOR THE NEXT GLACIAL CYCLE

Before making a projection for the next 300 kyr we must take into consideration if there are other plausible mechanisms which are not incorporated in our models. In this work we consider two potential contributions: the very well established weathering compensation mechanism and the less known emission of methane from clathrates. We have chosen these two mechanisms not only because they are indeed relevant effects but also because they are illustrative of the sort of modifications that feedback mechanisms may cause in the Pleistocene dynamics.

According to *Archer and Ganopolski* [2005], the silicate weathering cycle will cause that 7% of the anthropogenic CO₂ will still remain in the atmosphere 100 kyr after an anthropogenic perturbation. This implies that, after ending the anthropogenic emission, about 9% of the CO₂ concentration will decay with a time constant of approximately 400 kyr. We take into consideration this non-linear buffer (ocean carbon chemistry) effect by simply assuming that 91% of the anthropogenic perturbation will follow the dynamics given by Equations 2.1 to 2.6, while the remaining 9% will have a long-term decay, with a 400 kyr time decay constant. A similar approach was used by *Paillard* [2006].

Archer et al. [2009a] have studied the greenhouse effect expected to occur in the next 10 kyr as the rising temperatures lead to the emission of a fraction of the methane clathrates from continents and shelves. Their projection has a large uncertainty related to determining the critical fraction of methane bubbles that are able to reach the ocean surface. Taking this fraction as 2.5% and considering a scenario of 1000 Pg of carbon emission, sufficiently close to the one used in our models, he predicts an increase of 0.4 – 0.5°C related to the escape of methane during some 10 kyr. Taking a climate sensitivity of 3°C for a doubling of CO₂, the effect of the predicted methane emission, C_{met} , is equivalent to 40.5 ppmv of CO₂ concentration during a period of about 10 kyr. We have introduced this contribution in our projections by assuming that C_{met} (additional equivalent CO₂ concentration derived from methane) grows linearly from 0 to 40.5 ppmv between 0 and 2 kyr, remains constant between 2 and 10 kyr, and decreases linearly from 40.5 ppmv to 0 between 10 and 20 kyr.

Following these considerations, we are now ready to start the projection. The model equations are integrated forward, with the anthropogenic carbon emission scenario in Figure 3.2 as the initial condition and properly forced by the insolation at 65°N (*Berger* [1978b]), to predict the evolution of the interglacial-glacial transitions during the next 300 kyr. In order to obtain a CO₂ projection in dimensional units (ppmv), rather than the model non-dimensional units, a concentration of 280 ppmv is assumed for year 1750 AD and a dimensional scale is obtained by considering the range of atmospheric concentrations in the Taylor Dome Ice Core between the last glacial maximum (181 ppmv) and year 1750 AD (280 ppmv) (*Indermuhle et al.* [2000]). Similarly, in order to transform from model ice volume to benthic $\delta^{18}\text{O}$ (per mil), the conversion used is

$$V = (V_{normalized} + \text{std}(\delta^{18}\text{O})) + \text{mean}(\delta^{18}\text{O}), \quad \mathbf{3.2}$$

where $V_{normalized}$ is the modeled ice volume normalized with its own standard deviation and mean. All other variables remains non-dimensional as there is no dimensional scale available for their transformation.

The projection for the next 300 kyr is computed for both unperturbed and perturbed conditions using either the 3τ or LS models; Figure 3.4 illustrates, as an example, the predicted evolution of atmospheric CO₂ following the anthropogenic CO₂ pulse. Both models display an exponential decay in atmospheric CO₂, with characteristic time decay somewhat longer for 3τ than for LS. The two models, despite having different parameterizations for ocean stratification and ice sheet evolution, do produce a very similar outcome for the following glacial cycle. Hereafter, we will focus on the future projection obtained with the 3τ model, a comparison of both models shows analogous results.

Figure 3.5 shows the CO₂ evolution predicted by model 3τ following the anthropogenic short-term pulse, after adding the long-term weathering compensation mechanism and further including methane emissions from clathrates. It may be observed that in all cases the timing for the next interglacials does not substantially change. The main effect is caused by the weathering compensation which causes somewhat

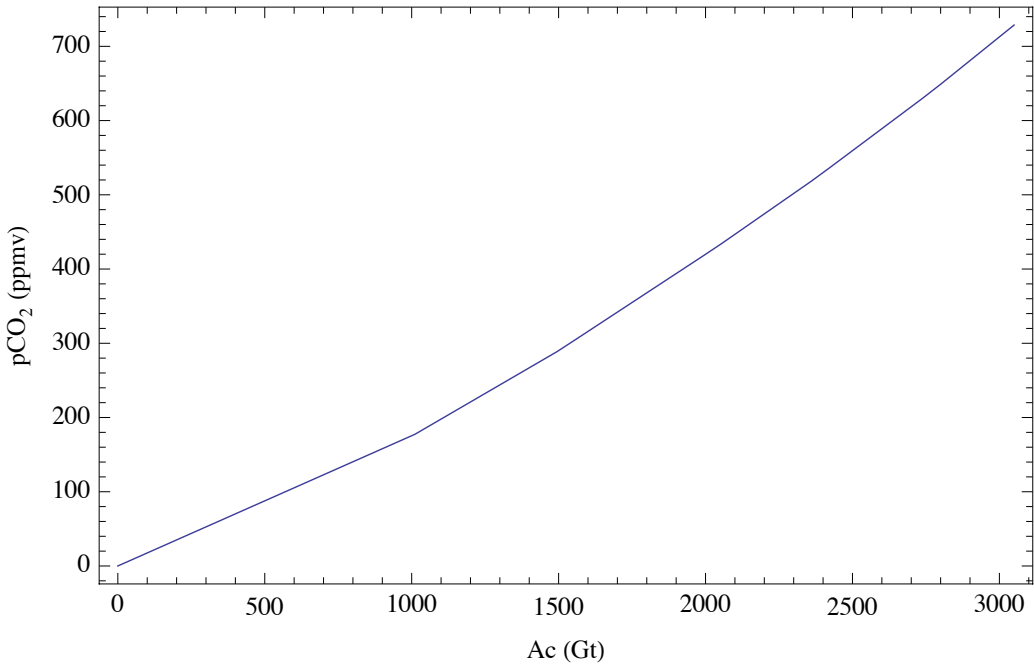


Figure 3.3

Relation between the accumulated anthropogenic carbon emissions (Ac) and the atmospheric CO₂ concentration (pCO_2). The data is obtained from an aggregate of A1T scenarios (*SRES* [2000]) as predicted by model ISAM (*Jain et al.* [1994]), available at <http://climate.atmos.uiuc.edu/isam2/>, for every possible value of URR.

higher concentrations and a slightly longer duration of the present interglacial. The effect of the methane emission is much reduced except for a relatively short plateau in CO₂ values after ending the anthropogenic pulse.

The introduction of the anthropogenic CO₂ pulse clearly perturbs the natural cycle for all four model variables during the forthcoming 300 kyr (Figure 3.6). Notice that the values for variables I_{65} , V , A and F in Figure 3.6 are relative variations, only C has been translated to physical units (ppmv); further note that a minimum bound for V has been set to an additional 10 meters sea level rise with respect to year zero, which corresponds to a melting about 30% higher than the Greenland ice sheet (*IPCC* [2001]) and, for this reason, V doesn't take values under $-0.93/ -1.94$ for $3\tau/LS$ models.

A comparison between the different panels in Figure 3.6 illustrates the influence of I_{65} on the sequence of events, as discussed with detail in Chapter 2 and *García-Olivares and Herrero* [2013]. In both the perturbed and unperturbed simulations, a V minimum (maximum) is produced a few thousand years after every positive (negative) peak in I_{65} . During a glaciation, the long-term increase in V produces an increase in A which tends to decrease the F value (due to the inverse dependence of F on A , Equation 2.6). The transit to the interglacial relies heavily on F turning negative (through the Heaviside function in Equation 2.5): F reaches negative values only during periods of advanced glaciation because at these times A is also large. In these situations, peaks in I_{65} lead to relative minima in V and a subsequent decrease in both A and F , which may induce negative F values that trigger the oceanic CO_2 emission. The condition to generate a deglaciation is, thus, the coincidence of a maximum of I_{65} in a period when V is large, as we have seen previously in Chapter 2.

The model predicts a maximum CO_2 concentration of 519 ppmv in 2300 AD followed by an exponential decay. To define interglacial conditions we use two simple criteria (*Crucifix* [2011]): CO_2 concentrations above 250 ppm and benthic $\delta^{18}\text{O}$ below 3.8 per mil; the CO_2 criterion has been used also by *IPCC* [2007]. According to the CO_2 criterion the current interglacial would end 40 kyr AP (35 kyr AP) for 3τ (LS), and according to the $\delta^{18}\text{O}$ criterion it would end 46 kyr AP (40 kyr AP) for 3τ (LS). Therefore, the length of this interglacial would be 54 – 47 kyr (according to the CO_2 values) and 58 – 50 kyr (according to the $\delta^{18}\text{O}$) as predicted by the 3τ and LS models. This interglacial would be followed by a glacial period lasting until 113 kyr AP.

The model also predicts the disappearance of the next interglacial unperturbed age, which should start at 64 kyr AP. This is due to the abnormally reduced ice volume and ice sheet area predicted for the present interglacial, which takes long to recover. The ice sheet, A , follows the evolution of V with a delay of about 7 kyr (Equation 2.2 and τ_A value in Table 1.1). The F function, however, turns negative only when A is large enough (due to the high value $b = 1.205$). At 64 kyr AP, V decreases (C rises) in response to the positive forcing of the I_{65} insolation but A is not high enough for F to become negative. If V and A were large,

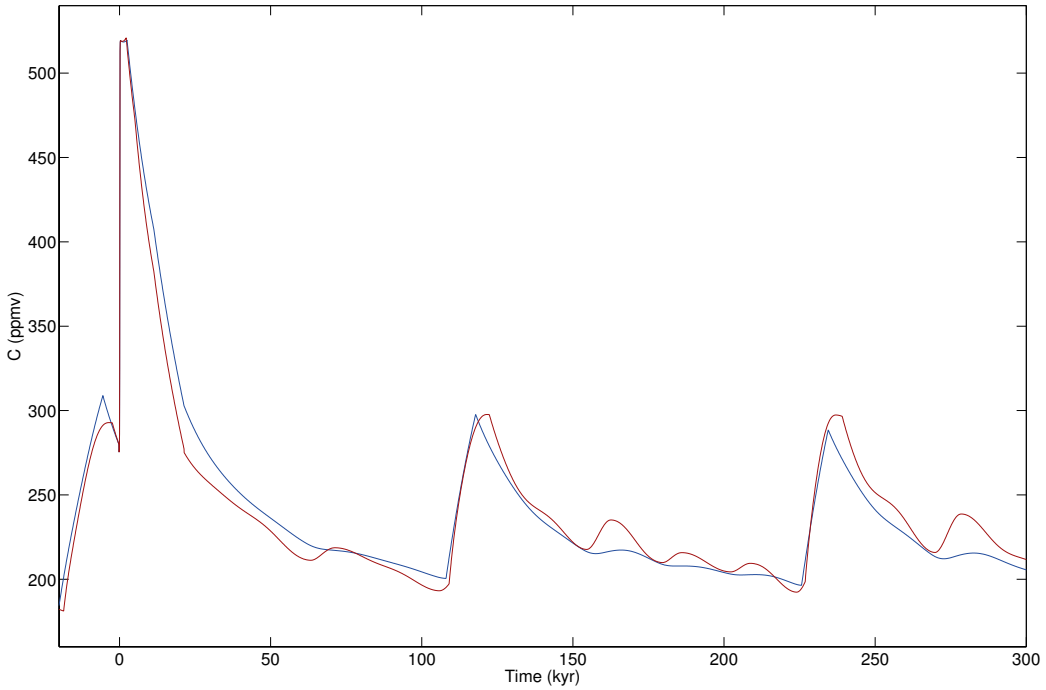


Figure 3.4

Prediction of the dimensional atmospheric CO₂ concentration for the next 300 kyr using, as an initial condition, the anthropogenic carbon release scenario shown in Figure 3.2. The blue and red lines correspond to the projection by the 3τ and LS models, respectively.

as occurs in the unperturbed case, F would be close to the threshold value ($F = 0$) and the decrease of V (rise of C) at that time would drive F to negative values, triggering the oceanic pulse. This delayed recovery of the ice volume V (and A) is caused by the anthropogenic pulse introduced in the model, which produces 20 kyr of abnormally high greenhouse effect. Under these conditions V needs a longer time to reach the glacial maximum and the next glacial cycle moves 44 kyr forward in time. At 235 kyr AP perturbed and unperturbed interglacials coincide again and the further evolution of all variables remain in phase, suggesting the recovery of the natural periodicity.

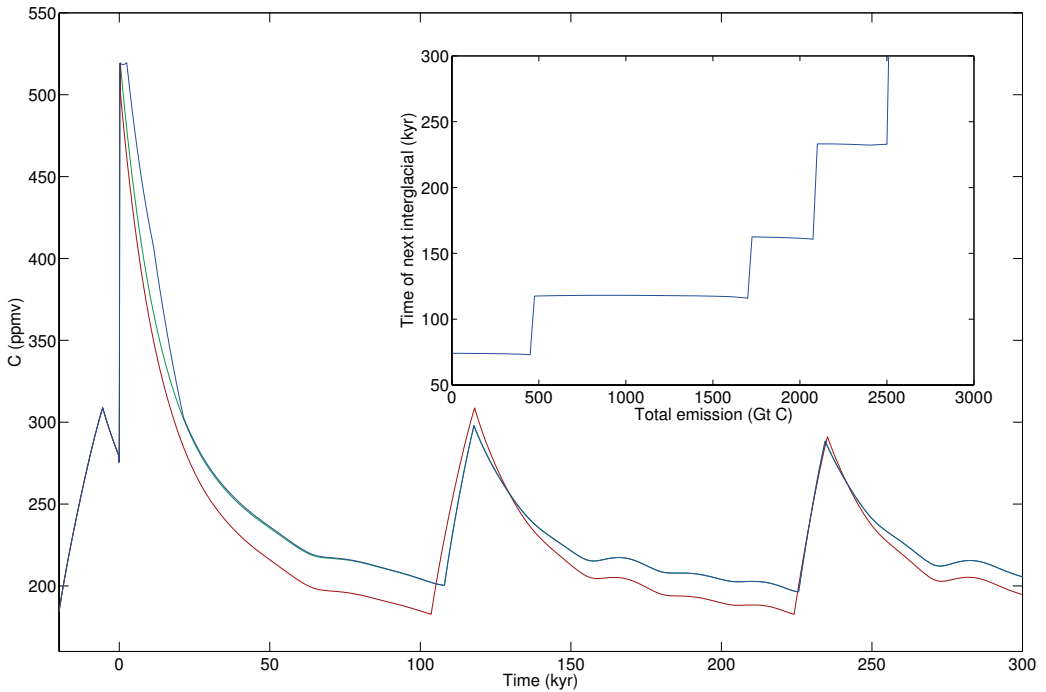


Figure 3.5

Dimensional atmospheric CO₂ concentration for the next 300 kyr as predicted by model 3τ following the anthropogenic short-term pulse (red line), after adding the long-term weathering compensation (green line), and after further incorporating the methane emissions from clathrates (blue line). The inset shows how the start of the next interglacial shifts depending on the total emissions of carbon.

We have also explored how sensitive are the model results, in particular the starting time for the next interglacial cycle, to different URR values. One main result is that a progressive increase in the anthropogenic pulse leads to smaller, with lower CO₂ values, interglacial cycles. A quite relevant result is that the timing for the next interglacial will change discretely as U exceeds different threshold values (inset in Figure 3.5). For example $U = 475$ Gt represents the URR threshold beyond which the next interglacial will experience a delay of 44 kyr; the following thresholds will occur at 1725 and 2100 Gt, with corresponding additional delays of 42 and 72 kyr (inset in Figure 3.5).

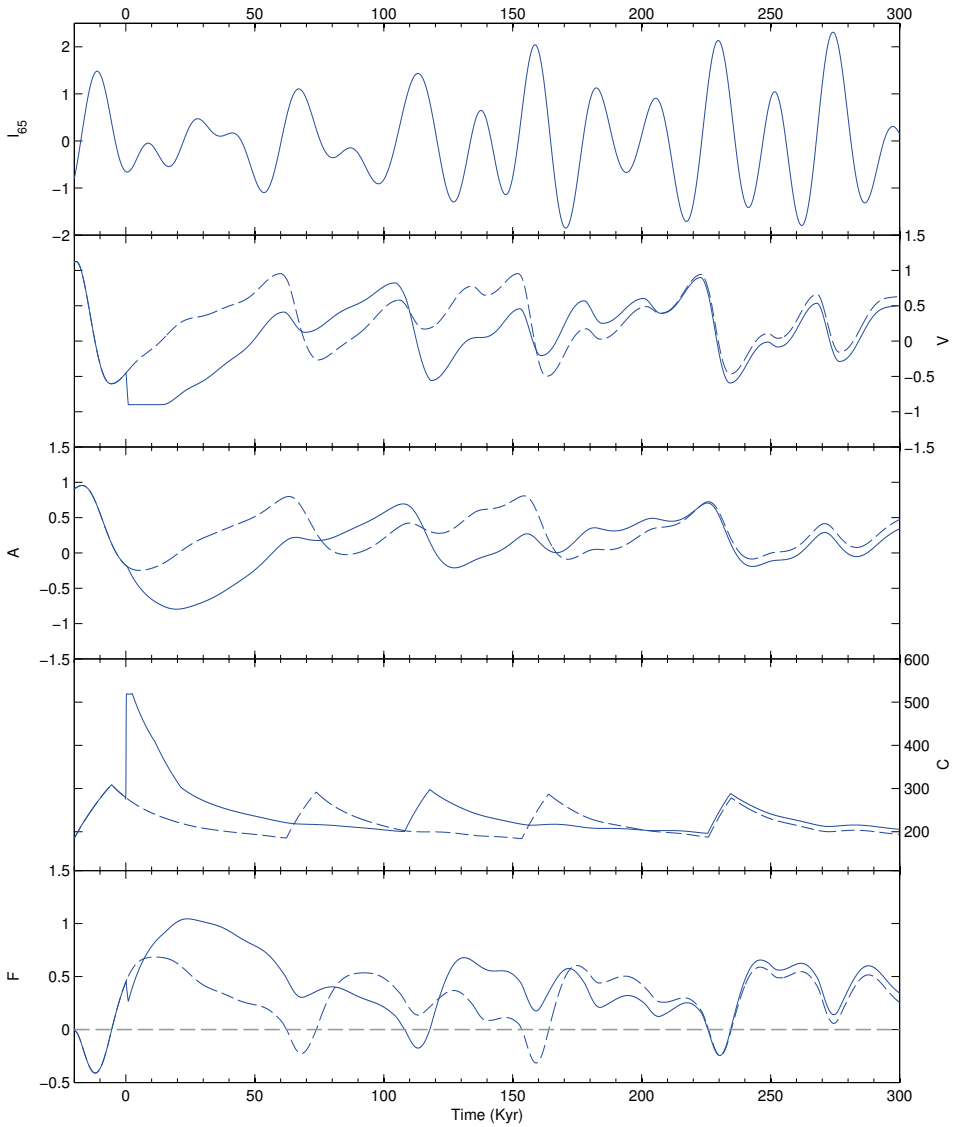


Figure 3.6

Prediction of climatic variables for the future 300 kyr as obtained using the 3τ model (including weathering compensation and methane emissions). The top panel shows the I_{65} insolation time series and all other four panels present the projection of normalized ice volume (second panel), normalized extension of Antarctic ice sheet (third), dimensional atmospheric CO₂ concentrations, (fourth) and stratification function (bottom), with (solid line) and without (dashed line) the anthropogenic perturbation in all cases.

3.5. DISCUSSION

It may be argued that the carbon mechanisms in our models are too simplistic to represent adequately the interglacial of 400 kyr BP, which is the closest natural analogue of the present interglacial (*Loutre and Berger* [2000]). This is partially true, since the CO₂ plateau near 400 kyr BP is not reproduced by our models, which always produce saw-teeth shapes for the CO₂ evolution. However, if we apply the *Crucifix* [2011] CO₂ and $\delta^{18}\text{O}$ criteria, the models do reasonably well. According to $\delta^{18}\text{O}$ the duration of the 400 kyr BP interglacial is 26 kyr from to the proxies, 21 kyr from to model LS and 27 kyr from model 3τ ; the corresponding CO₂ durations are 44 kyr (proxy), 27 kyr (LS) and 35 kyr (3τ). The duration for the 400 kyr interglacial is similar, as estimated either from model 3τ or the proxies. In addition, Figure 2.1 shows that near 400 kyr BP the shape of the glacial termination and the beginning of the interglacial are well simulated by both LS and 3τ . This endorses the potential of our models (particularly, model 3τ) to anticipate the duration of the present unperturbed interglacial with equally good behavior.

Loutre and Berger [2000] predict that the present interglacial is destined to last about 55 kyr if the CO₂ concentrations are maintained at constant levels above 220 ppmv. That long interglacial duration is supposedly due to the configuration of the astronomic forcing, which is similar to the one occurred in the interglacial of 400 kyr BP. With a CO₂ level of 210 ppmv they foresee an interglacial lasting until 15 kyr AP; with 220 ppmv they predicted the glacial conditions would start 17 kyr AP and the interglacial conditions would return between 27 and 54 kyr AP. The comparison with our results is difficult, because our models depend on three characteristic times of CO₂ absorption after the interglacial peak, making CO₂ not to remain constant in time. If we use the $\delta^{18}\text{O}$ criterion, the end of the present unperturbed interglacial is estimated at 12.5 kyr AP, the estimate becomes 8 kyr AP if the CO₂ criterion is used (for both 3τ and LS models). Thus, the duration of the unperturbed interglacial as predicted by our models (20 kyr - 25 kyr for CO₂ - $\delta^{18}\text{O}$) is less than *Loutre and Berger* [2000] estimate for CO₂ concentrations above 220 ppmv, but similar to their prediction with CO₂ concentration of 210 ppmv.

After adding the anthropogenic perturbation, the 3τ model predicts a slow decay of the greenhouse effect so that the interglacial conditions remain until 40-46 kyr AP, which is shorter than predicted by *Loutre and Berger* [2000] (55 kyr) for their high-CO₂ concentration (≤ 210 ppmv) scenario, and longer than the duration of previous interglacials (30 kyr or less according to *Winograd et al.* [1997]).

Our prediction of the following interglacial is not strongly dependent on the exact value of the CO₂ initial condition in the range of 475-1700 Gt (inset in Figure 3.5). When URR is equal or larger than 1725 Gt, the models predict a very slow V , A and F recovery, so that the interglacial at 118 kyr AP is lost and the next interglacial takes place in coincidence with the following obliquity maximum at 160 kyr AP. For URR between 2100 and 2500 Gt, the recovery is even slower, shifting the next interglacial to 232 kyr AP and for URR equal or larger than 2525 Gt the next interglacial is totally lost until at least 300 kyr AP. This would be the case with the most extreme IPCC scenarios (such as A1F1 and A1G AIM); however, we consider those scenarios with URR above 2100 Gt as unrealistic.

Our projection also displays some interesting resemblances with *Mysak* [2008] forecast, carried out with the McGill Paleoclimate Model, an EMIC. If we set the interglacial conditions to correspond to CO₂ concentrations above 250 ppmv (*IPCC* [2007]), our 3τ model does show an interglacial lasting until 46 kyr AP. This is close to *Mysak's* prediction (*Mysak* [2008]), who found that the next glacial inception occurs 50 kyr AP.

On the other hand, our prediction differs substantially from the results of the intermediate complexity model by *Archer and Ganopolski* [2005]. Their carbon model, based on *Archer* [2005], includes very plausible geochemical mechanisms for ocean acidification and CaCO₃ response operating in the scale of 10 kyr and 100 kyr. However, their evolution of atmospheric pCO₂ does not account for the sort of natural pCO₂ variability that drives the glacial/interglacial cycles, and only focuses on the geochemical mechanisms that credibly affect the anthropogenic perturbation. The lack of mechanisms for the geophysical absorption of CO₂ at time scales of 10 kyr, such as the ice volume - CO₂ feedback, probably results in predictions for the atmospheric pCO₂ that are substantially higher than ours. For a total carbon

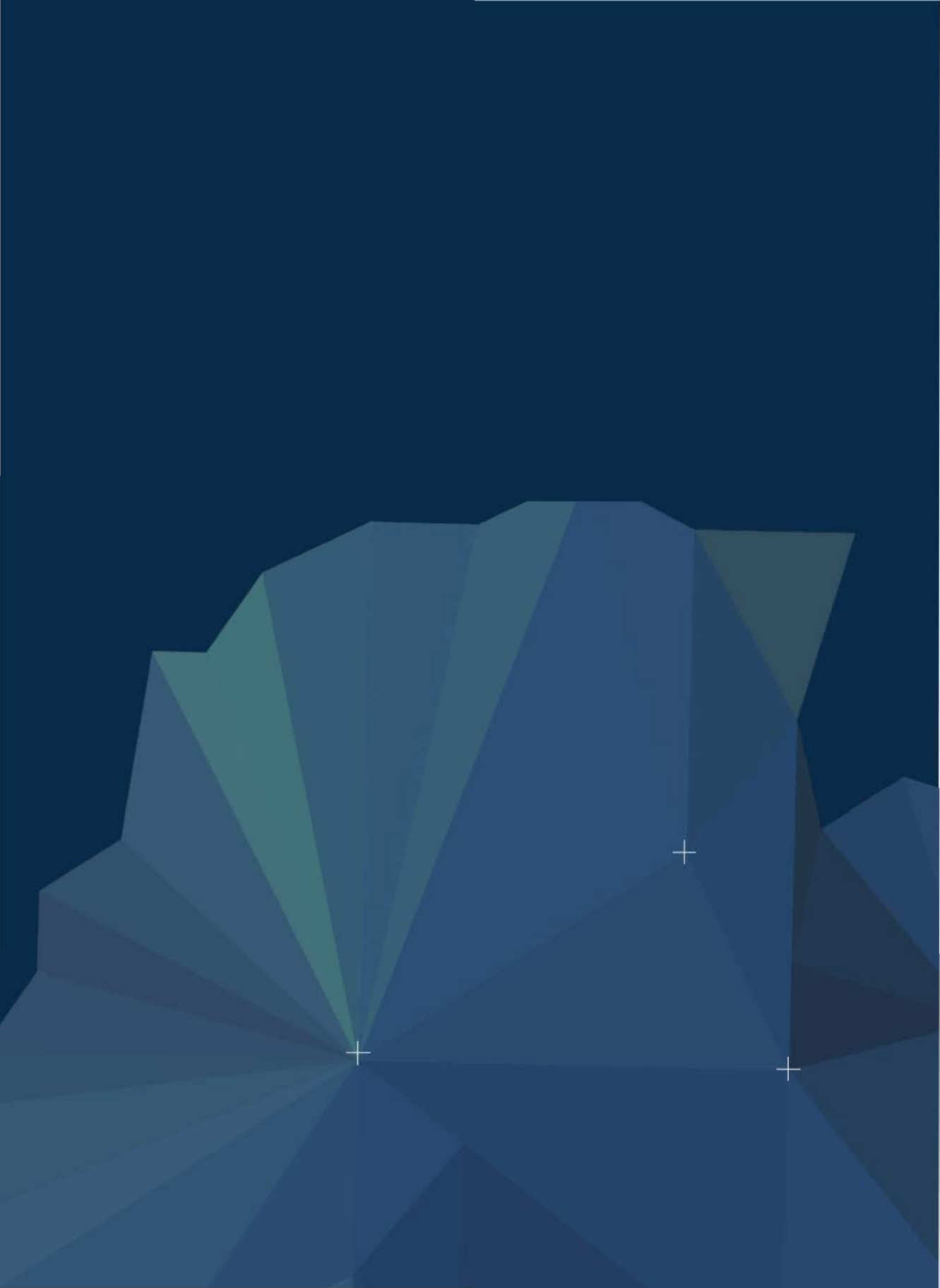
emission of 1000 Gt, their model forecasts the current interglacial period to last for another 130 kyr AP. In contrast, we project a much smaller effect of the anthropogenic pulse, with the atmospheric CO₂ decreasing below interglacial levels in 40-46 kyr (according to 3τ) and reaching the minimum glacial levels in about 100 kyr, resulting in a delay of the next interglacial stage by 44 kyr.

The differences between the results of *Archer and Ganopolski* [2005] and *Mysak* [2008] arise from the different hypotheses on the long-term fate of atmospheric CO₂, which is made depend exclusively on geochemical mechanisms in the former, and is externally imposed in the latter. In comparison, in our models the rate of decay for most of the atmospheric CO₂, except for the relatively small anthropogenic fraction (9%) which is assumed to obey a long-term weathering adjustment, is obtained through fitting the model equations to the observed CO₂ and global ice volume variations during the past glacial cycles. The time decay constants obtained in this way lie between 8400 and 13500 yr (Table 1.1). Our underlying assumption, therefore, is that the internal dynamics of the Earth system will remain the same, either with or without the anthropogenic CO₂ pulse, except for the relatively small fraction with a weathering-related slow decay.

In this work we have illustrated an application of two simple relaxation-type models (*García-Olivares and Herrero* [2013]) to predict the future evolution of global Earth variables during the next 300 kyr, with and without the atmospheric CO₂ perturbation caused by anthropogenic fossil fuels emissions.

The abnormally high thermal perturbation of the current interglacial will lead to a delay in the future advance of the ice sheet over the Antarctic shelf. As a result, the relative maximum of boreal insolation 65 kyr AP will have no effect on the stability of the developing glaciation. However, the following insolation peak (115 kyr AP) will take place in an appropriate state of the climate system and will be sufficient to induce the new deglaciation. The next glacial maximum will take place about 105 kyr AP and the following interglacial will be delayed forward in time by 44 kyr in relation to unperturbed conditions. Our models projections depend on the URR value, being very stable in the 475 to 1700 Gt range; for URR equal or larger than 1725/2100 Gt the next interglacial is expected to begin 160/232 kyr AP.

Our projection on the evolution of the Earth's climate may be compared with those from intermediate complexity models for the Earth System, with appealing similarities in one case (*Mysak* [2008]) but with differences in another instance (*Archer and Ganopolski* [2005]). We believe that simple coupled models have the fundamental attribute that, despite their simple structure, retain the principal Earth's climatic interactions, being capable of accounting for the natural evolution of an externally imposed atmospheric CO₂ pulse. Nevertheless, in order to confirm this claim, our results should be compared with those obtained from an Earth System model which includes fully interactive long-term global carbon dynamics. Once this is proven, simple coupled models may become a helpful tool to examine the future evolution of climate under different scenarios of anthropogenic fossil fuels emissions. **L**



Chapter 4

INSIGHT TO MARINE ISOTOPIC STAGE 13 USING LATE PLEISTOCENE RELAXATION MODELS AND SEA LEVEL STACK

**Chapter based on the following
published articles:**

*Herrero, Lisiecki and García-Olivares [2015],
Insight to Marine Isotopic Stage 13 using
late Pleistocene relaxation models and sea
level stack. In preparation.*

Contents

131	4.1. INTRODUCTION
132	4.2. RELAXATION MODELS
134	4.3. NON-LINEAR ANALYSIS OF BOTH SIMULATED AND PROXY TIME SERIES
137	4.4. DYNAMICS OF SEA LEVEL RE-CALIBRATED MODELS
137	4.5. DISCUSSION

Chapter 4 ⁷

INSIGHT TO MARINE ISOTOPIC STAGE 13 USING LATE PLEISTOCENE RELAXATION MODELS AND SEA LEVEL STACK

L

It seems to me that the natural world is the greatest source of excitement; the greatest source of visual beauty; the greatest source of intellectual interest. It is the greatest source of so much in life that makes life worth living.

- David Attenborough

4.1. INTRODUCTION

As we have seen in previous chapter, glacial-interglacial oscillations of late Pleistocene climate (last 800 kyr) reveal a characteristic 100-kyr ice-age cycle, assumed to be mainly derived from orbital parameters and from internal feedbacks of the climate system (*Hays et al.* [1976]; *Archer et al.* [2000]; *Paillard* [2010, 2015]).

Following *Paillard and Parrenin* [2004], several relaxation models, based on simple parameterizations of deep ocean stratification, have been developed (*García-Olivares and Herrero* [2012, 2013]). Two of these models, 3τ and LS, have good skills reproducing the conditions during the last eight glacial cycles (Chapter 1). The 100-kyr glacial-interglacial periodicity is internally generated through three coupled variables: atmospheric CO₂ concentration, global ice volume and the extension of the Antarctic ice shelf (for a detailed dynamics, see Chapter 2)

$\delta^{18}\text{O}$ data from benthic foraminifera (*Lisiecki and Raymo [2005]*) may be used as a proxy for ice volume (*Shackleton et al. [2000]*; *Shakun et al. [2015]*; *Waelbroeck et al. [2002]*), although the $\text{O}^{18}/\text{O}^{16}$ ratio is known to depend on both the isotopic composition and temperature of the water where foraminifera develop. *Waelbroeck et al. [2002]* found that the relationship between $\delta^{18}\text{O}$ and ice volume is not linear, causing some uncertainties in the ice volume variations.

Global ice volume changes derived from growth and retreat of continental ice sheets may be associated with sea level variations in the glacial-interglacial cycles (*Chappell and Shackleton [1986]*; *Waelbroeck et al. [2002]*; *Lambeck et al. [2014]*), a proxy with less uncertainties. Some reconstructions of sea level from ocean sediment core data have been performed using different proxies and models, each of them limited by measurement error, local variations in salinity and temperature, and assumptions particular to each technique. *Spratt and Lisiecki [2015]* have compiled a wide representation of these reconstructions, developing a sea level stack, which represents the eustatic sea level record more accurately than each of the individual reconstructions.

In this work, we use *Spratt and Lisiecki [2015]* sea level stack to analyze and identify differences between $\delta^{18}\text{O}$ and sea level as proxy data for the ice volume. In next section, the models are presented and some non-linear methods are applied in Section 4.3 to outline the differences between $\delta^{18}\text{O}$ and sea level stack. Section 4.4 shows the recalibration and optimization of 3τ and LS models to the new set of sea level data, and the discussion of the results, as well as some brief conclusions, are presented in last section.

4.2. RELAXATION MODELS

There are several differences between models 3τ and LS (Figure 4.1, bottom panel). One difference is the value used for the reference Antarctic ice sheet, either $-C$ (representing the inverse effect of Antarctic temperature in Antarctic ice sheet extent) for model LS or V for model 3τ . Another minor difference is the inclusion of I_{65} in model LS when specifying the reference atmospheric CO_2 concentration value, C_7 .

However, the main difference between both models, is their parameterization of the ocean state, with $F = F(V, A)$ in model 3τ and $F = F(C, A)$ in model LS. Both V and C are good proxies for the Southern Ocean (SO) regional temperature and either $F = F(V, A)$ or $F = F(C, A)$ are plausibly ways to model the local formation of brines. The fact that the dependence $F = F(V, A)$ performs somewhat better than $F = F(C, A)$ may be due to the non-negligible role that V has on stratification through teleconnections (*García-Olivares and Herrero [2013]; Gildor and Tziperman [2001]*) or to a possible larger effect of sea level than Antarctic temperature on brine formation (Chapter 2).

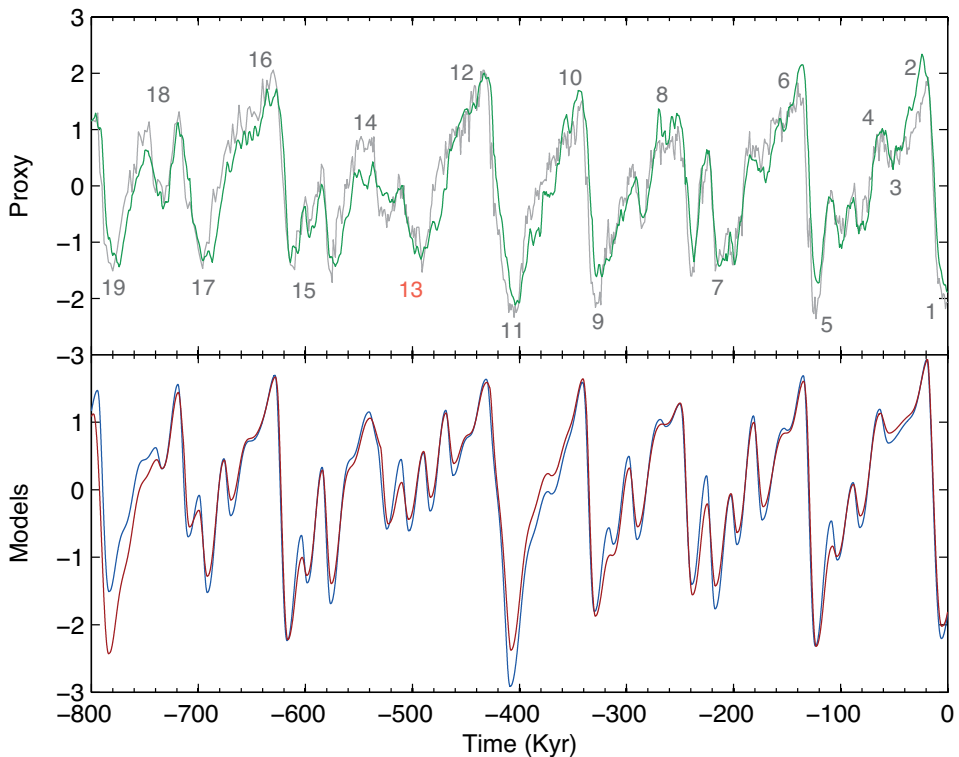


Figure 4.1 Top panel: proxy $\delta^{18}\text{O}$ records from *Lisiecki and Raymo [2005]* (grey line) and sea level stack from *Spratt and Lisiecki [2015]* (green line); numbers represent Marine Isotopic Stage labels for the early Pliocene from *Lisiecki and Raymo [2005]*. Bottom panel: normalized ice volume as predicted with the 3τ (blue line) and LS (red line) models.

The best-fit correlations are 0.87/0.88 (between $\delta^{18}\text{O}$ and modeled V) and 0.76/0.79 (between the reconstructed atmospheric CO_2 concentration and modeled C) for models LS/ 3τ . The parameter values that lead to the best data fit for either model are shown in Table 4.1.

The two different proxies, $\delta^{18}\text{O}$ records from *Lisiecki and Raymo* [2005] and sea level stack from *Spratt and Lisiecki* [2015], have similar dynamics but the timing of deglaciations is slightly shifted in all cases, as well as depth of glacial cycles, specially in the first four cycles (from -800 to -400 kyr) (Figure 4.1, top). The difference is, somehow, more evident around -500 kyr where the sea level data reconstruct the cycle with less variance. A comparison between sea level stack and benthic $\delta^{18}\text{O}$ has been performed in *Spratt and Lisiecki* [2015], showing that the relationship between benthic $\delta^{18}\text{O}$ and sea level is well-described by a linear function in the first four cycles (from -800 to -400 kyr) and a quadratic function in the last cycles (from -400 to 0 kyr).

4.3. NON-LINEAR ANALYSIS OF BOTH SIMULATED AND PROXY TIME SERIES

Some non-linear analysis have been performed to analyze internal frequencies of each time series. Spectral power of observational and simulated time series are obtained with Fast Fourier Transform (Figure 4.2). The sea level stack has more power than any other series in the 100-kyr band, but the power in the 41-kyr band is visibly lower than any other time series. As it seems, the sea level stack tends to over predict the power for long wave frequencies and to under predict it for short wave frequencies when compared with $\delta^{18}\text{O}$ data.

The complex cross-wavelet transform of two time series can be interpreted as the shared power in a given periodicity band (absolute value) and the phase between the two series in time frequency space (*Grinsted et al.* [2004]). Lighter purple color indicates greater shared power in that time and periodicity band, and the arrow angle indicates the phase between the observational and simulated series. It is in-

interesting to see that in the main 100-kyr band the shared power is maximum (as expected) and the phase is really similar for all three cases (Figure 4.3), but the most interesting features are the blue spots in the 41-kyr band at the sea level and $\delta^{18}\text{O}$ case. Apparently, there are some significant differences between both proxies around -500 and -250 kyr, in terms of obliquity content, which made both proxies dynamically different at those times.

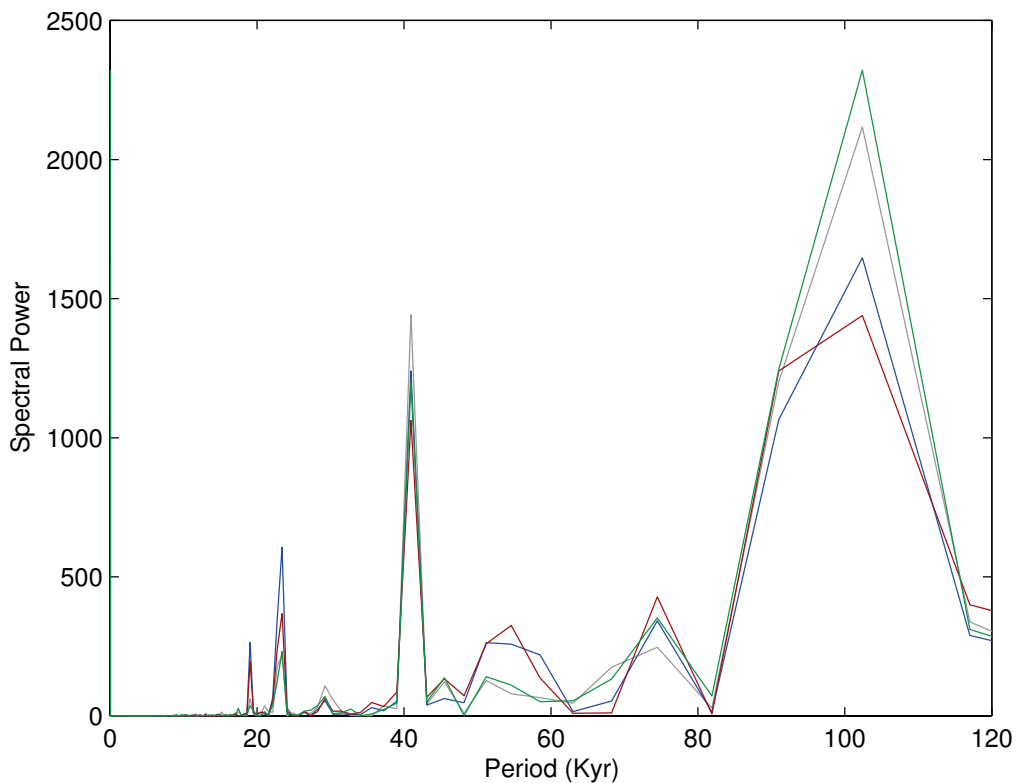


Figure 4.2 Spectral power of normalized ice volume as predicted with 3τ model (blue), LS model (red), proxy $\delta^{18}\text{O}$ records from Lisiecki and Raymo [2005] (grey line) and Spratt and Lisiecki [2015] sea-level stack (green line).

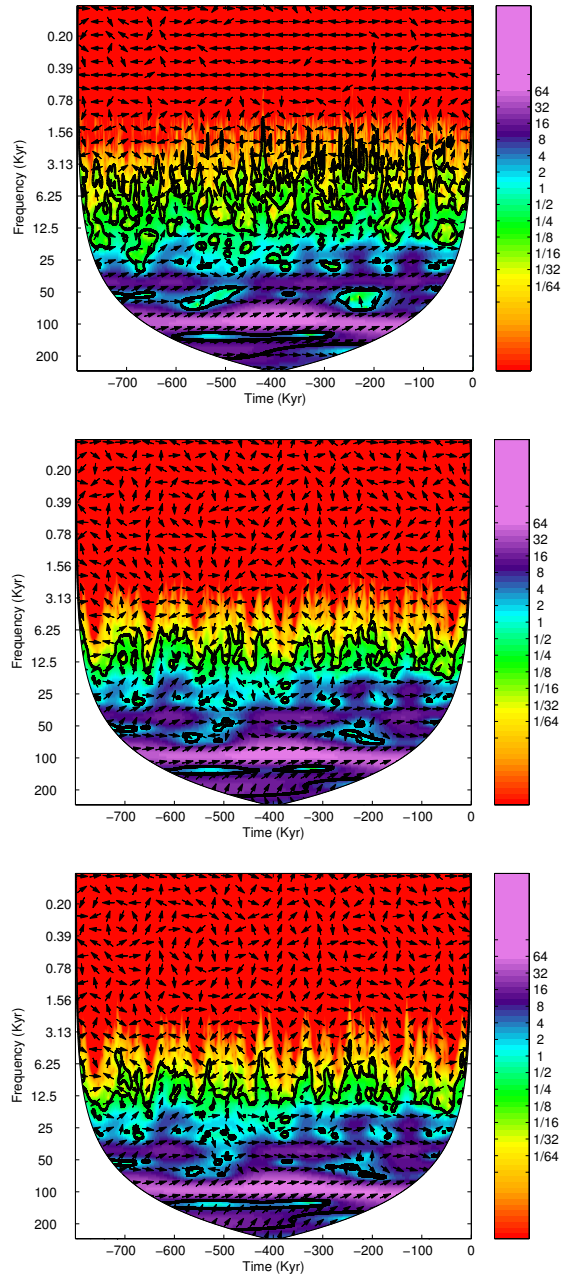


Figure 4.3

Cross-wavelet transform between proxy sea level stack from *Spratt and Lisiecki* [2015] and $\delta^{18}\text{O}$ records from *Lisiecki and Raymo* [2005] (top), simulated V time series with 3τ model (middle) and LS model (bottom).

4.4. DYNAMICS OF SEA LEVEL RE-CALIBRATED MODELS

Considering the existing dynamic differences between the sea level stack and the benthic $\delta^{18}\text{O}$, a new calibration has been done for both 3τ and LS models using the sea level (SL) stack from *Spratt and Lisiecki* [2015]. This has derived in new 3τ and LS models, called $3\tau_{SL}$ and LS_{SL} hereafter.

The comparison between parameter values of all models is shown in Table 4.1. The correlations between the original models and the new recalibrate models do not change much; for V , the correlation has increased from 0.88 (3τ) to 0.89 ($3\tau_{SL}$), just 1%, while there is no change for the LS/ LS_{SL} case. For C , however, the correlation has slightly decreased in both cases from 0.79 (3τ) to 0.77 ($3\tau_{SL}$) and from 0.76 (LS) to 0.73 (LS_{SL}), a 2% and a 3% respectively. This change in the correlation should not be important, as the uncertainties in the $\delta^{18}\text{O}$ may produce an over interpretation of the data, meaning that these correlation differences of less than 4% are included under the observational uncertainty. Nevertheless, the most remarkable feature of these new optimizations is a double peak shown in the $3\tau_{SL}$ ice volume around -500 kyr. This double peak was not present in the original 3τ models, and it is not shown in any LS model, suggesting that there are a significant dynamic difference between both proxies and/or both models.

4.5. DISCUSSION

Marine Isotopic Stage 13 (MIS-13) interglacial occurred approximately 500,000 years ago (-500 kyr). It is of particular interest, as it suffered severe summer monsoons simultaneously with increasing marine oxygen isotope and decreasing Antarctic ice core records in temperature compared to other interglacials (*Yin and Guo* [2008]; *Lang and Wolff* [2011]; *Muri et al.* [2012, 2013]). All of these anomalies indicate a warm Northern Hemisphere (NH) and a cool Southern Hemisphere (SH), and consequently a strong asymmetry of hemispheric climates during MIS-13 (*Guo et al.* [2009]).

The stratification and deep water formation in 3τ and $3\tau_{SL}$ models, where $F = F(V, A)$, is partly controlled by the temperature of the North Atlantic Deep Water (NADW) upwelling and partly by sea level, thus these models are more affected by the NH temperature changes and variations of global sea level. On the other hand, LS and LS_{SL} models have $F = F(C, A)$, suggesting that the formation of Antarctic Bottom waters (AABW) and stratification may be controlled only by Antarctic ice sheet extent and regional temperature, all local variables of the SH.

Benthic $\delta^{13}C$ data from *Lisiecki* [2010] can be considered a good proxy for deep ocean carbon storage, or consequently, a proxy for deep stratification. Figure 4.5 show the $\delta^{13}C$ data from *Lisiecki* [2010] and ocean parameter, F , for both $3\tau_{SL}$ and LS_{SL} . The models represent more accurately the last four glacial cycles (from -400 to 0 kyr), where F is slightly shifted on the stratification, rather than the first ones (from -800 to -400 kyr), where F is clearly different than $\delta^{13}C$. This behavior points out that F , which is in control of the CO₂ pulse and hence triggers the deglaciation, might not be representing only the stratification as *Paillard and Parrenin* [2004] suggested. *Ferrari et al.* [2014] suggest that large oceanic CO₂ emissions are related to the Antarctic ice cover. Both mechanisms (stratification and Antarctic ice cover) may be represented under F in our models, suggesting that in the first four glacial cycles the two mechanisms are out of synchrony, while in the last four cycles are acting on the same direction. Further research is needed to understand the mechanisms controlling oceanic CO₂ emissions and the cause of the MIS-13 anomaly.

MIS-13 is a good case to evaluate this possible double dependence of F , as the two peaks in CO₂ are more like plateaus, rather than the common saw-tooth. This might be caused by the stratification and Antarctic ice cover acting out of phase: the weakened stratification will produce a vertical CO₂ pulse to trigger the deglaciation, but as the temperature is specially low in this interglacial, the Antarctic ice cover is abnormally wide and acts as a cover for the expected CO₂ outgassing, controlling the amplitude of the pulse. Both models have very similar shapes but LS_{SL} shows a more deep state ($F < 0$) in all interglacials, specially in MIS-13. It does show the starting of a double peak in MIS-13, but the first deglaciation is very light and does not produce enough CO₂ pulse to change the state, maintaining the

PARAMETERS	3τ	$3\tau_{SL}$	LS	LS _{SL}
τ_V	16585	20525.6	11325	15996.6
τ_{V_2}	3105.5	5826.5	2325	3179
τ_C	13505	8824.5	2793	2933.2
τ_{C_2}	-	-	8414	10069.4
τ_A	9004	11110	10266	13757.8
x	0.905	1.547	0.669	0.544
y	0.489	0.923	0.527	0.344
z	0.946	1.704	0.761	1.531
α	-	-	0.237	0.907
β	0.336	0.255	0.793	0.985
γ	2.044	1.538	1.955	2.242
δ	0.228	0.549	0.146	0.514
a	0.54	0.727	-	-
b	1.205	1.586	0.936	1.877
c	-	-	0.533	0.928
d	0.483	0.51	0.069	0.418
R_V	0.88	0.89	0.87	0.87
R_C	0.79	0.77	0.76	0.73

Table 4.1 Parameter values used for the original 3τ and LS models, and the new recalibration $3\tau_{SL}$ and LS_{SL} models. R_V and R_C represent the correlation between proxy and modeled data for global ice volume, V , and atmospheric CO₂ concentration, C , respectively.

glacial period (Figure 4.6). Afterwards, the system is dynamically ready to change the state, producing a deep and strong interglacial. This deep interglacial state is more stable and generates a CO₂ pulse strong enough to change permanently from glacial to interglacial. In the $3\tau_{SL}$ case, the deep ocean stratification parameter is more unstable (close to the tipping point $F = 0$) and although the first CO₂ pulse

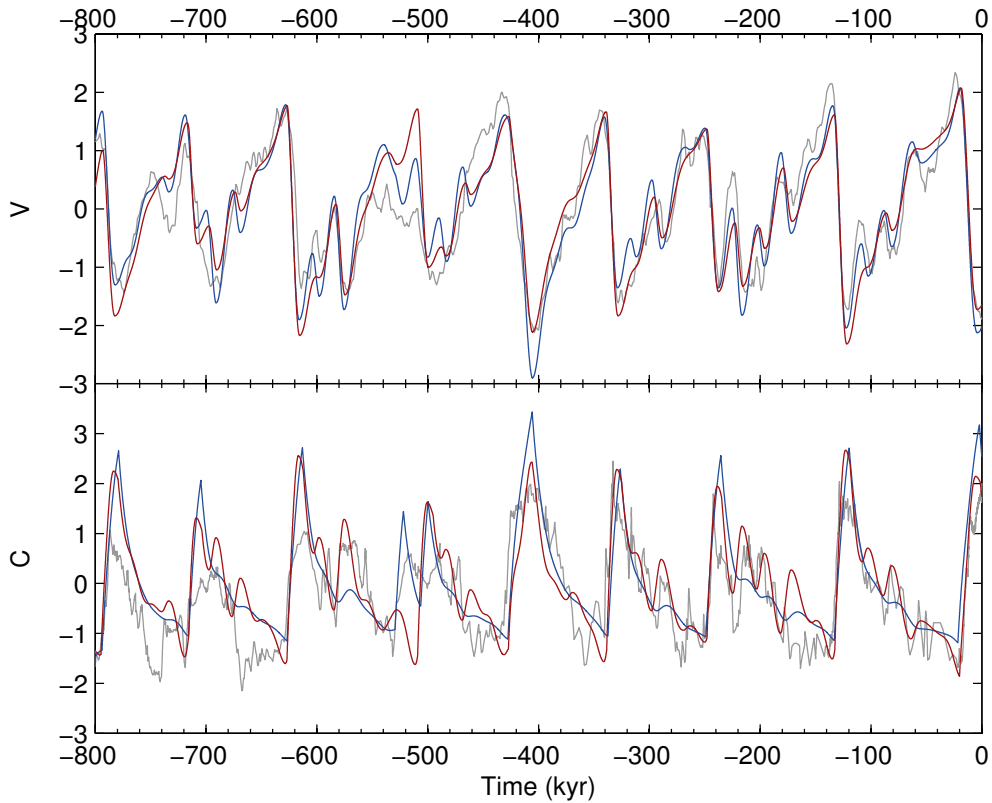


Figure
4.4

Top panel: best fit obtained after the optimization between *Spratt and Lisiecki* [2015] sea level stack (grey line) and $3\tau_{SL}$ model (blue line), LS_{SL} model (red line). Bottom panel: best fit obtained for the CO_2 time series after the optimization: $3\tau_{SL}$ model (blue line), LS_{SL} model (red line) and experimental CO_2 time series from *Petit et al.* [1999]; *Monnin et al.* [2001]; *Pepin et al.* [2001]; *Siegenthaler et al.* [2005]; *Luthi et al.* [2008] (grey line).

generates a change of state, it is not strong enough to maintain it, retreating back to an additional glacial state. The second pulse is slightly stronger, finally generating a stable change of state.

LS_{SL} first attempt to change the state may not be strong enough because it does not capture the asymmetry of hemispheres, as the F parameter is only affected by

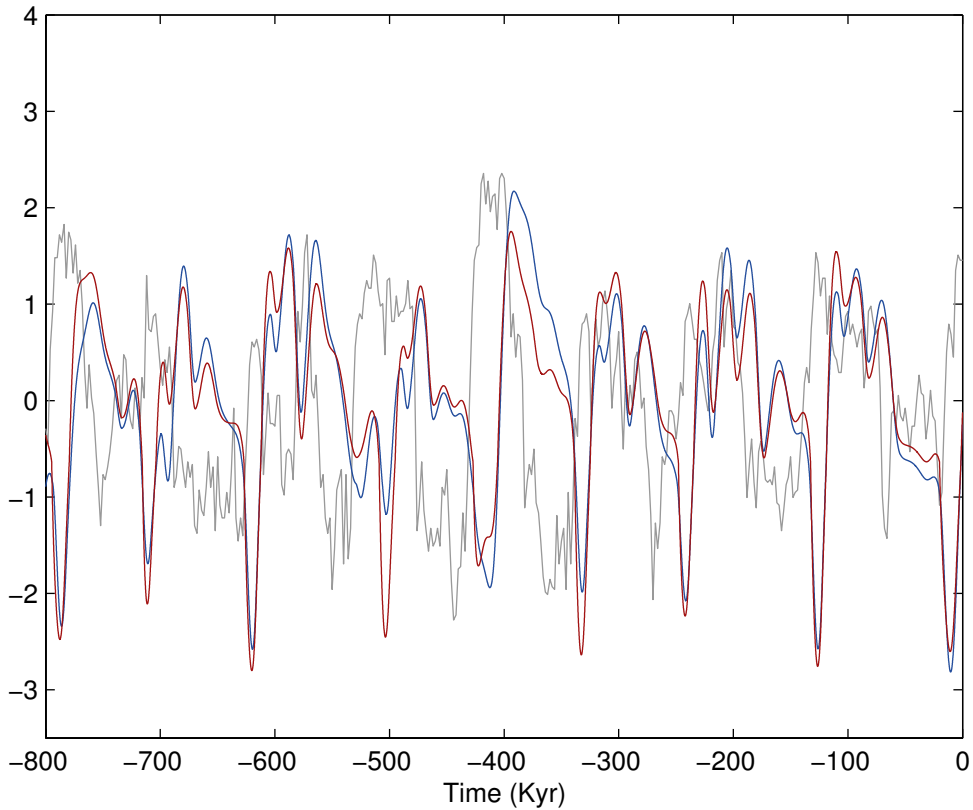


Figure 4.5 Deep ocean stratification parameter, F , derived from $3\tau_{SL}$ model (blue line), LS_{SL} model (red line) and $\delta^{13}C$ gradient from *Lisiecki* [2010](grey line).

SH variables. $3\tau_{SL}$ on the other hand, is affected by the dynamics of both NH and SH, capturing the asymmetry between hemispheres which produces a more unstable deep ocean stratification through a teleconnection of NADW (*García-Olivares and Herrero* [2013]; *Gildor and Tziperman* [2001]).

In this work, we have compared two simple relaxation-type models (*García-Olivares and Herrero* [2013]) with *Spratt and Lisiecki* [2015] sea level stack to analyze and identify differences between $\delta^{18}O$ (*Lisiecki and Raymo* [2005]) and sea level as proxy

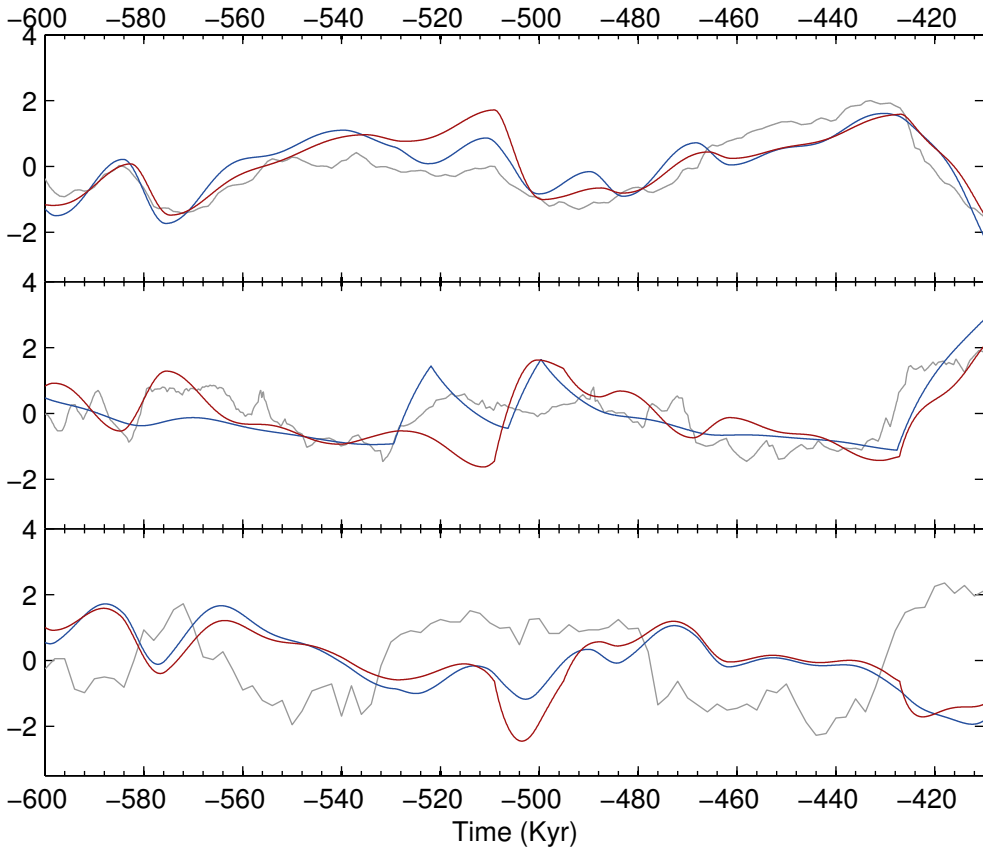


Figure
4.6

Top panel shows ice volume fits: $3\tau_{SL}$ model (blue line) and LS_{SL} model (red line), derived from the optimization to Spratt and Lisiecki [2015] sea level stack (grey line). Best fit obtained for the CO₂ time series: $3\tau_{SL}$ model (blue line) and LS_{SL} model (red line), compared with experimental CO₂ time series from Petit et al. [1999]; Monnin et al. [2001]; Pepin et al. [2001]; Siegenthaler et al. [2005]; Luthi et al. [2008] (grey line) are shown at the middle panel. Deep ocean stratification parameter, F , derived from $3\tau_{SL}$ model (blue line), LS_{SL} model (red line) and $\delta^{13}C$ gradient from Lisiecki [2010] (grey line) are shown at bottom panel.

data for the ice volume. The recalibration of the models with the sea level stack has outlined the different dynamics of the models in a very particular interglacial event, the MIS-13.

The comparison of benthic $\delta^{13}C$ data from *Lisiecki* [2010] with the ocean state parameter, F , shows a mismatch in the first cycles (from -800 to -400 kyr), suggesting that F might represent not only the deep stratification (as suggested by *Paillard and Parrenin* [2004]) but also other variables, like the Antarctic ice sheet (as pointed out by *Ferrari et al.* [2014]), which probably play an important role in the deglaciations. On the last cycles (from -400 to 0 kyr), F seems to be in good pace with the stratification, although slightly shifted, suggesting that both mechanisms (stratification and Antarctic ice cover) are acting in the same direction.

The inability of LS_{SL} on reproducing the double CO_2 peak at MIS-13 may be due to the dependence of F on local variables, which unable F to capture an asymmetry between hemispheres. On the other hand, $3\tau_{SL}$ correctly reproduces this double peak and seems more accurate capturing the dynamics of MIS-13, suggesting that the parametrization $F = F(V, A)$, affected by both NH and SH dynamics, performs better and it is more appropriate to simulate the climate system dynamics. ┌

+

Conclusions

We on Earth have just awakened to the great oceans of space and time from which we have emerged. We are the legacy of 15 billion years of cosmic evolution. We have a choice: We can enhance life and come to know the universe that made us, or we can squander our 15 billion-year heritage in meaningless self-destruction. What happens in the first second of the next cosmic year depends on what we do, here and now, with our intelligence and our knowledge of the cosmos.

– Carl Sagan, *COSMOS*

In this final chapter I will briefly revise the results presented in this thesis. In Chapter 1 several relaxation models incorporating a wide representation of physical mechanisms, like the oceanic CO₂ pumping or the response times of carbon and ice volume, have been developed. The models' parameters have been calibrated to provide the best fit to the $\delta^{18}\text{O}$ and CO₂ experimental time series available for the last 800 kyr BP. We have described eight different sub-models, all derived from the original *Paillard and Parrenin* [2004], to evaluate how those different parameterizations affect the data fit. Some of those mechanisms like the biological exportation production or an exponential CO₂ oceanic pulse does not offer new insights. On the other hand, the sub-models with different response times for accumulation and ablation of ice, and/or emission and absorption of CO₂, show a good quantitative and qualitative agreement with the empirical time series, especially 4τ , EP, 3τ and LS, suggesting that different relaxation times are a possible way to reproduce the asymmetry in the glacial cycles and that the mechanisms that these models incorporate may be important factors controlling glacial-interglacial oscillations.

The 4τ model improves the PP04 correlations (0.59 and 0.63) to 0.79 and 0.89 using 14 parameters. The EP model uses 15 parameters but the additional parameter, which was aimed at improving the form of the oceanic pulse function, did not improve the correlations and can be considered useless. The 3τ model obtains almost the same correlations as 4τ using only 13 parameters. The LS model (15 parameters) does not improve the correlations of 4τ (which are slightly higher) but incorporates a functional form for stratification F that seems more consistent with the mechanisms suggested by *Paillard and Parrenin* [2004]. 3τ is, then, the model with the best explained variance per parameter, and LS, having a explained similar variance, contain parameterizations that can be related to the observed mechanisms. Both models offer a valuable insight into the real meaning of the good performance of PP04-derived models, and deserve further analysis.

In Chapter 2, the dynamics and mechanisms incorporated in 3τ and LS models have been analyzed and compared, to explore the most plausible physical interpretations of the mathematical expressions. First, we have evaluated their non-linear dynamics using wavelet transform, cross-wavelet transform, wavelet coherence, Fourier analysis, attractors and cross-recurrence plots. We have, then, identified the mechanisms and dynamics that lead to good data fit and we have compared the results with the observational dynamics that supposedly cause glacial-interglacial oscillations.

We have demonstrated that, in fact, relaxation models are a useful tool to analyze and study the physical mechanisms of the climate system, as well as to identify feedbacks and the involved variables. We have shown that the models are not sensitive to the southern insolation; rather, they respond to a different variable, C , which seems to be a much better proxy of Antarctic temperature. One important conclusion is that the detailed dynamics of CO_2 are not important to obtain a good match between the models and the proxy data. What is really important is a nonlinear instability, reached after 80 - 100 kyr (allowing V to reach a maximum level), allowing any modest increase of the insolation to cause a release of atmospheric CO_2 .

Variable F is crucial in the models. We have pointed out that an abrupt oceanic release of CO_2 , similar to a rectangular pulse of 10 to 20 kyr, is necessary to trigger the termination, and F is the non-linear control of this upwelling of CO_2 . It can be

described as a deep ocean control parameter. We believe that F can be physically considered the stratification synchronously combined with the biological and carbonate pumps in the sub-Antarctic zone, and with the sea ice extent which controls the residual circulation and the depth of upwelled water.

A precise simulation of the detailed set of events constituting the deglacial trigger would require adding some parameterization for the North Atlantic ice sheet instability to our models as well as more complex carbon dynamics. PP04-derived models produce good results in spite of their simplicity in the modeling of oceanic CO₂ release, and to obtain a closer representation of all the physical processes involved in the climate system, more mechanisms should be included in future versions.

In Chapter 3 we have illustrated an application of the relaxation models, useful too to answer more direct dynamic questions. We have used 3τ and LS models to predict the future evolution of global Earth variables during the forthcoming 300 kyr, with and without the atmospheric CO₂ perturbation caused by anthropogenic fossil fuels emissions.

The anthropogenic CO₂ pulse produces 20 kyr of abnormally high greenhouse effect, involving a delay in the future advance of the ice sheet over the Antarctic shelf. As a result, the corresponding peak of northern insolation, causing a termination in the unperturbed scenario, will have no effect on the stability of the developing glaciation. However, the following insolation peak will take place in an appropriate state of the climate system and will be sufficient to induce the new deglaciation, moving, accordingly, the next glacial cycle 44 kyr forward in time. After three cycles, perturbed and unperturbed interglacials coincide again and the further evolution of all variables remain in phase, suggesting the recovery of the natural periodicity. On the other hand, a progressive increase in the anthropogenic pulse leads to smaller, with lower CO₂ values, interglacial cycles, and the timing for the next interglacial will change discretely as U exceeds different threshold values.

In Chapter 4 the models have been re-calibrated using a new sea level data stack and are used to understand the dynamics of a very particular interglacial event, the MIS-13. We have compared 3τ and LS models with *Spratt and Lisiecki [2015]* sea

level stack to analyze and identify differences between $\delta^{18}\text{O}$ (*Lisiecki and Raymo* [2005]) and sea level as proxy data for the ice volume.

The comparison of the deep ocean parameter, F , with a proxy of deep stratification (benthic $\delta^{13}\text{C}$ data, *Lisiecki* [2010]) shows a mismatch in the first cycles (from -800 to -400 kyr), suggesting that F might be representing not only the deep water formation but also other variables, like the Antarctic ice sheet. On the last cycles (from -400 to 0 kyr), F seems to be in good pace with the stratification, although slightly shifted, suggesting a representation of a mixed state of the deep ocean. This reinforces the results of Chapter 2, where F represents not only the stratification but also the sea ice extent.

The appearance (or not appearance) of a double CO_2 peak at MIS-13 in our models, suggest that the parametrization $F = F(V, A)$, affected by both NH and SH dynamics, is more appropriate to simulate the climate.

We may then assess that relaxation models can be extremely useful tools to characterize the complex climate system, and helpful to examine specific questions as the future evolution of climate under different scenarios of anthropogenic fossil fuels emissions. Relaxation models may contribute to broaden the knowledge of the mechanisms controlling the variability of the late Pleistocene glacial cycles; nevertheless, their results should be compared with those obtained from an intermediate complexity model, which should include conservation equations, realistic geometry and long-term global carbon dynamics. The analysis of the present results under the complementary perspective given by these complex models would be a natural continuation of this thesis. **L**




Appendix

150.....	Appendix A. On insolation forcing
152	Appendix B. Genetic algorithms for optimization
155.....	Appendix C. Resumen en castellano

A. ON INSOLATION FORCING

We have used *Berger* [1978a] and *Berger and Loutre* [1991] software to calculate insolation time series at different latitudes, covering a time domain from last 800 kyr to the next 300 kyr in time steps of 100 years. We have used negative and positive values when respectively referring to times before present (BP) and after present (AP), where year zero is taken as 1950 AD. In Chapters 1, 2 and 4 we have taken into account only the past time (last 800 kyr) but in Chapter 3 we have made some projections, using the next 300 kyr domain.

Two sets of insolation data has been developed for the past time. On one hand, insolation regarding one single day of the year at one specified latitude, this is Northern Hemisphere summer insolation (65°N) on 21st June, named I_{65} , and on the other hand, late Austral summer insolation (60°S) on 21st February, named I_{60} (Figure A.1).

For Chapter 3, a new set of Northern Hemisphere summer insolation (65°N) on 21st June has been calculated, this time considering the whole time domain (from -800 to $+300$ kyr), shown in Figure A.2. 

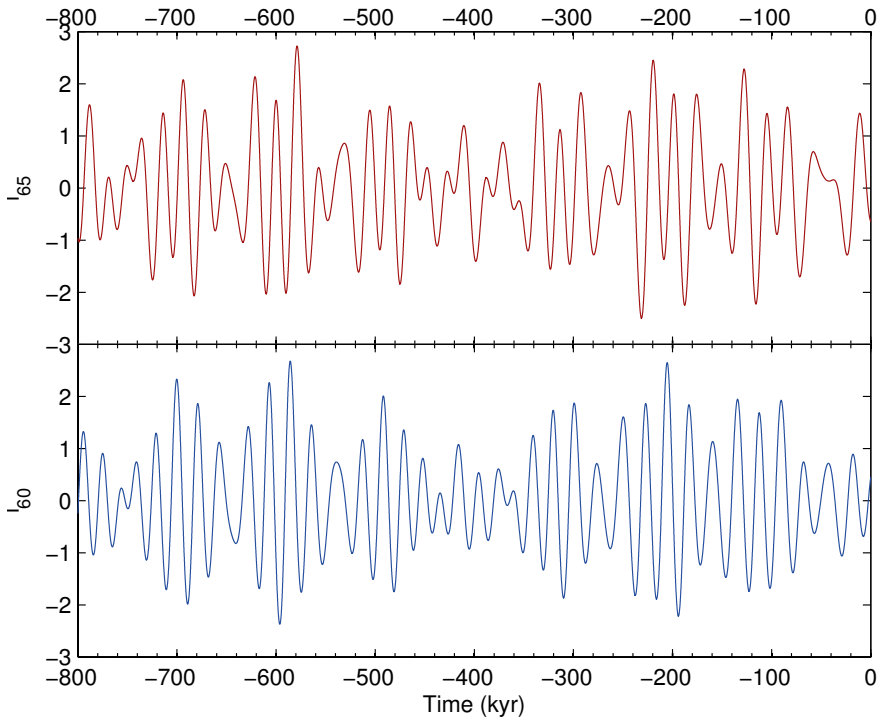


Figure A.1 Northern Hemisphere summer insolation (top) and late Austral summer insolation (bottom) for the past 800 kyr

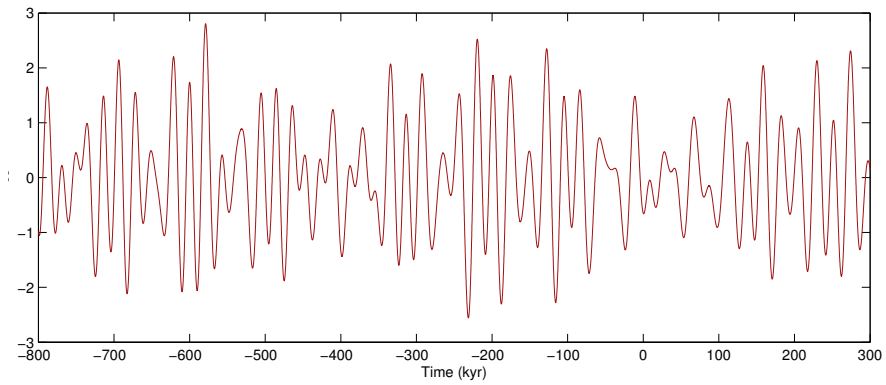


Figure A.2 Northern Hemisphere summer insolation (65°N) from the last 800 kyr to the next 300 kyr.

B. GENETIC ALGORITHMS FOR OPTIMIZATION

To perform optimizations of mathematical expressions, we have implemented a multi-objective genetic algorithm with the aim of maximize correlation between experimental and modeled data. This has been done with Global Optimization Toolbox from Matlab¹.

First of all, we must answer a key question: what exactly is a genetic algorithm?

According to *Charbonneau* [2002], genetic algorithms are, fundamentally, a class of search techniques that use simplified forms of the biological processes of selection/inheritance/variation.

This optimizers are based on natural selection, which states that individuals better adapted to their environment, i.e., for whatever reason better at obtaining food, avoiding becoming lunch, and finding/attracting/competing for mates, will, on average, leave behind more offspring than their less apt colleagues.

¹Matlab is a trademark of The MathWorks.

For natural selection to lead to evolution, two more essential ingredients are required:

1- inheritance: offspring must retain at least some of the features that made their parents fitter than average, otherwise evolution is effectively reset at every generation.

2- variability: at any given time individuals of varying fitnesses must coexist in the population, otherwise natural selection has nothing to operate on.

To better understand the mechanism, here we show a genetic optimization problem based in our model. One is given a model that depends on a set of parameters u (like 3τ), and a functional relation $f(u)$ that returns a measure of quality, or fitness, associated with the corresponding model; in our case, this function is the correlation between the modeled output and the experimental data. The optimization task usually consists in finding the “point” u^* in parameter space corresponding to the model that maximizes the fitness function $f(u)$; in our case, we search in a parameter space of 11 to 15 coordinates, depending on the model. We now define a population as a set of Np realizations of the parameters u .

A top-level view of a basic genetic algorithm is then as follows:

- 1- Randomly initialize population and evaluate fitness of its members (parents).
- 2- Breed selected members of current population to produce offspring (child) population (selection based on fitness).
- 3- Replace current population by offspring population.
- 4- Evaluate fitness of new population members.
- 5- Repeat steps (2) through (4) until the fittest member of the current population is deemed fit enough.

The crucial singularity lies with step 2: *Breeding*. It is in the course of breeding that information is passed and exchanged across population members through mechanisms as crossover (also called recombination) and mutation. As the name suggests, crossover is a process of taking more than one parent solutions and mix them to produce a child. In the mutation, some parents are randomly change to produce some variations in evolution (just as mutation works in natural environment).

This is how genetic algorithm works from a very simplified point of view. We have used this technique to set all parameters (11 to 15, depending on the case) that form the model in order to find the combination that maximizes the correlation. **L**

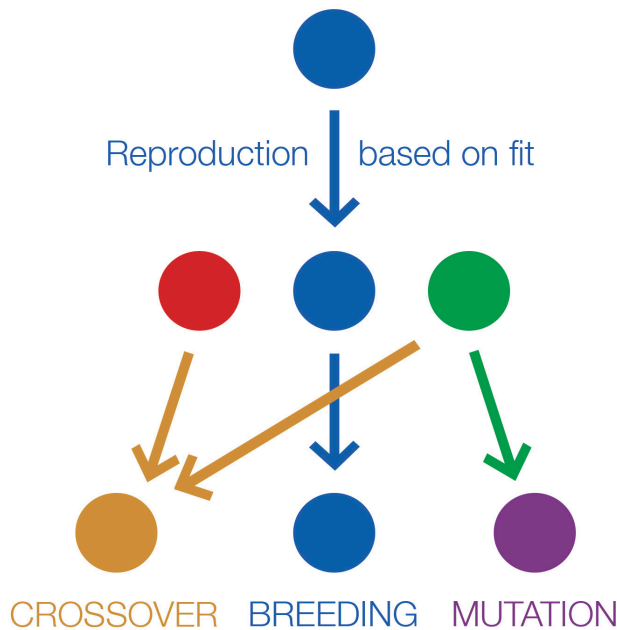


Figure A.2 Visual inspection of genetic algorithm work flow. **L**

C. RESUMEN EN CASTELLANO

C.1. INTRODUCCIÓN

Permítanme comenzar con una pregunta fundamental: ¿por qué debemos estudiar el clima? El clima afecta a la vida cotidiana de muchas maneras: en la comida que comemos, en las casas en que vivimos, en nuestro trabajo, en la forma en que viajamos... Incluso afecta a nuestra cultura, nuestro tiempo libre o nuestra salud. Pero esto es tan solo localmente importante. Lo que tenemos que ver aquí es el conjunto: el clima afecta la manera en que todas las especies vivas se han adaptado a la biosfera, es clave para nuestra supervivencia, pero estamos influenciándolo de manera drástica y no podemos predecir las consecuencias de nuestras acciones. Es, por tanto, fundamental ampliar nuestro conocimiento sobre el sistema climático de la Tierra, el único hogar que hemos conocido, para estudiar la variabilidad climática pasada en diferentes escalas de tiempo con el objetivo de obtener pistas que ayudarán a la sociedad a afrontar el futuro cambio climático. Como Carl Sagan predijo en *Cosmos*, uno de sus libros más conocidos (Sagan [1980]):

"Nuestra inteligencia y nuestra tecnología nos han dado el poder de afectar el clima. ¿Cómo vamos a usar este poder? ¿Estamos dispuestos a tolerar la ignorancia y la complacencia en los asuntos que afectan a toda la familia humana? ¿Valoramos ventajas a corto plazo por encima del bienestar de la Tierra? ¿O vamos a pensar en escalas de tiempo más largas, con la preocupación por nuestros hijos y nuestros nietos, para entender y proteger los complejos sistemas de soporte de vida de nuestro planeta? La Tierra es un mundo pequeño y frágil. Necesita ser cuidado."

La paleoclimatología es la ciencia que estudia los cambios en el clima en una escala de tiempo muy larga; tan larga como toda la historia de la Tierra, 4.54 mil millones de años. Utiliza datos previamente conservados en una amplia representación de ambientes (como rocas, sedimentos, hielo, corales ...) para reconstruir el estado más antiguo del clima de la Tierra y su correspondiente variabilidad. Encontrar datos detallados tan antiguos como la Tierra es prácticamente una tarea imposible, pero sin duda se puede usar una variedad de métodos para obtener series temporales fiables con una escala de tiempo de millones de años. En este trabajo, hemos utilizado registros con un dominio de tiempo máximo de 5 millones de años, y los resultados se reducen a lo que podríamos considerar el tiempo más reciente, solamente 800000 años, o en unidades paleoclimáticas, 800 ka.

Para entender el clima en detalle, debemos mirar en todos los procesos relevantes del sistema, aunque esto puede ser un poco aterrador, ya que el número de estos procesos que deben ser entendidos es asombroso. Para hacerlo más interesante, la cantidad de conocimiento cierto que tenemos es limitado y parcial. ¿Debemos llorar de desesperación? Ciertamente no. Por suerte, el paleoclima, como todas las ciencias, se basa en el método científico, que nos ayuda en el desarrollo de una comprensión de la realidad utilizando términos como mecanismo, el modelo y la teoría. Podemos describir una teoría como una explicación matemática detallada de los fenómenos que tiene relevancia suficiente para hacer predicciones a partir de los principios fundamentales, o en otras palabras, según lo declarado por *Truesdell and*

Toupin [1960], una teoría no es más que un modelo matemático para la naturaleza. La verdad es que no hay un camino claro para obtener una teoría razonable del clima en el futuro cercano. Más bien, todos esperamos para desarrollar modelos de clima, en el que los principios e hipótesis sobre los mecanismos locales de retroalimentación nos permitan derivar algoritmos matemáticos y predicciones que deben ser comparados con las observaciones experimentales. Mientras las predicciones y los experimentos coinciden, podemos considerar el modelo válido para describir una realidad, un objeto complejo denominado sistema climático.

Históricamente, se han hecho muchos avances para modelar la estructura de la variabilidad del clima a largo plazo. En el siglo XIX, Louis Agassiz (*Agassiz* [1838]), propuso por primera vez que el clima en la Tierra podría haber sido mucho más frío en períodos anteriores de tiempo, al menos en el hemisferio norte (NH), pero bajo una perspectiva catastrofista. Más tarde, Joseph Adhémair (*Adhémair* [1842]) formuló la primera teoría astronómica de las edades glaciales, sugiriendo que los parámetros astronómicos pueden modificar el clima, y explicó la posición de las capas de hielo de acuerdo con la precesión de los equinoccios, y el posterior cambio de ubicación del perihelio (punto más cercano a la órbita del Sol en la Tierra) en relación con las estaciones. Sin embargo, la formulación Adhémair fue criticada ampliamente, sobre todo con argumentos infundados, aunque tenía, ciertamente, problemas. James Croll (*Croll* [1867]) trabajó en una versión más elaborada de esta teoría, teniendo en cuenta el papel de la excentricidad como una modulación de la precesión, y siguiendo las ideas Adhémair, insistió en el papel de la acumulación de nieve durante el invierno como la clave de las glaciaciones. Fue en el siglo XX, cuando Milutin Milankovitch (*Milankovitch* [1941]) formuló una teoría que sigue siendo válida hoy en día. El principal problema de Croll fue considerar el invierno como la temporada crítica para la evolución del manto de hielo, mientras que Milankovitch demostró que la fusión de verano es mucho más importante para el balance de masa de hielo, teniendo en cuenta la insolación de verano un parámetro clave en su teoría. Además, Milankovitch considera un tercer parámetro astronómico, la oblicuidad del eje de la Tierra (inclinación axial), sentando las bases de la presente teoría astronómica del clima.

Por otro lado, otras hipótesis se desarrollaron desde un punto de vista completamente diferente, como la teoría geoquímica. Svante Arrhenius (*Arrhenius* [1896]), inspirado en la obra anterior de Joseph Fourier o John Tyndall, confirmó el papel de CO₂ en el clima. Él correctamente calculó cómo una variación de los niveles de CO₂ atmosférico afecta a la temperatura de la superficie a través del efecto invernadero, teniendo en cuenta la atmósfera como un depósito de carbono capaz de controlar las edades de hielo. Bajo esta perspectiva, el CO₂ y el clima mundial están impulsando los cambios capas de hielo, mientras que el punto de vista de Milankovitch implica que capas de hielo controladas por la insolación en verano en el norte son los que impulsan los cambios climáticos globales. Ambas teorías tienen limitaciones y problemas, y como el lector puede sospechar, ambas son esencialmente válidas y no excluyentes.

Hays et al. [1976] demuestran que las variaciones de glaciares-interglaciares estados durante el Cuaternario se pueden causar en última instancia por los cambios en los parámetros de la órbita de la Tierra (la teoría de Milankovitch), ya que las periodicidades astronómicas se encuentran en los registros paleoclimáticos. También muestran que en la oblicuidad (41 ka) y bandas de precesión (23 y 19 ka) existe una respuesta climática directa al forzamiento de la insolación a altas latitudes e *Imbrie et al.* [1992] muestran que este vínculo entre el clima y la insolación puede ser interpretado como cuasi-lineal. Pero lo que es seguro para los ciclos de 41- y 23-ka ya no es válido para los principales ciclos glaciares-interglaciales con una frecuencia de 100 ka. Estos ciclos energéticos de 100 ka son fuertemente asimétricos con un estado de glaciación lento y un cambio rápido y abrupto en el estado interglacial que dura unos 10 ka llamado terminación. Esta asimetría, también llamada estructura de diente de sierra, es realmente difícil de entender bajo la teoría astronómica; además, no existe una relación clara entre estos principales ciclos y la excentricidad (100 y 400 ka de frecuencia), ya que es el ciclo más débil de la insolación astronómica en una latitud dada (medida en el solsticio o como un año medio), pero es el ciclo más energético en la serie de observaciones.

Este ciclo de 100-ka se identifica con los ciclos glaciales del cuaternario y, si el for-

zamiento astronómico es, de hecho, el conductor de la variabilidad, los mecanismos climáticos implicados son aún en su mayoría desconocidos. En concreto, análisis recientes muestran que los ciclos glaciales-interglaciales implican cambios significativos en la concentración de CO₂ en la atmósfera (180 partes por millón (ppm) en período glacial y 280 ppm durante los interglaciares), lo que demuestra que, de hecho, ambas teorías históricas (astronómica y geoquímica) son realmente válidas, interactuando en formas que aún no están del todo claras. Una combinación de la evolución capa de hielo, impulsado por parámetros astronómicos, vinculada con los mecanismos climáticos internos que producen cambios biogeoquímicos es la teoría más adecuada hoy en día. Algunos de los modelos más representativos y los diferentes mecanismos y procesos que afectan el clima han sido sintetizábamos en *Imbrie et al.* [1992, 1993] y más recientemente en *Paillard* [2015].

El papel y los mecanismos que implicó que el aumento del CO₂ atmosférico durante los ciclos glaciales e interglaciales son uno de los puntos clave para resolver, y se han propuesto algunos mecanismos de intercambio, como las bombas físicas o biológicas, para explicarlo, como la producción para la exportación en el Océano Austral (SO) profundo o la ventilación de aguas profundas (*Skinner* [2009]). Cada uno de los enfoques conceptuales tiene problemas para explicar la variación de CO₂ glacial-interglacial por sí mismos, lo que probablemente sugiere que ninguno ha operado en completo aislamiento (*Archer et al.* [2000]; *Sigman and Boyle* [2000]). Lo que parece ser fundamental para explicar los cambios de CO₂ durante los estados glaciales-interglaciales es el equilibrio entre la biológica de carbono exportado de la superficie del océano y el carbono que regresar de la circulación profunda a través de mecanismos físicos.

La eficiencia de la ventilación de aguas profundas en tiempos glaciales e interglaciales podría ser modificado por tres mecanismos principales:

- (a) Cambios en la eficiencia de tasa de mezcla superficie-profundidad (*Toggweiler* [1999]; *Gildor and Tziperman* [2001]) y la estratificación del océano profundo (*Paillard and Parrenin* [2004]; *Watson*

and Garabato [2006]), obligando a un cambio en el flujo diapirico del agua profunda rica en CO₂ en aguas superficiales. Un coeficiente de difusión vertical dependiente de la estratificación parece capaz de cambiar también la tasa de overturning en el SO con consecuencias adicionales sobre la liberación oceánica de CO₂ (Bouttes et al. [2012]).

- (b) Cambio de off / on del afloramiento de la Antártida en latitudes del Drake Passage en condiciones de frío / calor (Toggweiler et al. [2006]). Cualquier proceso que produce un estrés de viento mayor en las latitudes del Drake Passage provocaría una fuerte surgencia de agua rica en CO₂ de profundidad en la divergencia del SO.
- (c) La extensión de hielo marino en el SO produce un efecto de limitación sobre la liberación de CO₂ a la atmósfera durante los inviernos (Keeling and Stephens [2001]) y un retraso de la tasa de vuelco en el control de hielo SO debido a la mar en la circulación residual (Watson and Garabato [2006]; Fischer et al. [2010]). Este mecanismo puede ser reforzado por el control de la extensión del hielo marino en la profundidad de las aguas afloradas isopícnicamente en la divergencia antártica (Ferrari et al. [2014]).

En los tres mecanismos, se espera un aumento de la liberación de CO₂ durante el cambio entre los períodos glaciales-interglaciales, y se espera que tenga lugar principalmente en el hemisferio sur (SH). Curiosamente, proxies recientes obtenidos para la temperatura a la Antártida muestran una fuerte correlación entre las concentraciones de temperatura y de CO₂ (Siegenthaler et al. [2005]; Fischer et al. [2010]). Por otra parte, las interpretaciones recientes (Paillard [2010]) de los datos empíricos (Bard et al. [1996]; Monnin et al. [2001]) sugieren que la concentración de CO₂ en la atmósfera aumentó durante varios milenios antes de la fusión del hemisferio norte capa de hielo. Ambas piezas de evidencia apoyan la hipótesis de que algunos

de los mecanismos mencionados anteriormente, que tiene lugar esencialmente en el SO, podrían estar detrás del aumento del CO₂ necesario para producir el cambio glacial-interglacial.

Podemos, por tanto, modelar los ciclos glaciales-interglaciales 100-ka como una oscilación de relajación entre dos modos climáticos diferentes, un estado glacial lento y un estado deglaciación rápido, forzados por la insolación y ambos deben incluir mecanismos que puedan explicar los cambios de CO₂ en la atmósfera. Algunos modelos de cajas simples se han propuesto como *Pelegrí* [2008] y *Pelegrí et al.* [2013], que tienen en cuenta los cambios en la frecuencia y la exportación biológica de CO₂, reproduciendo la oscilación de los últimos cuatro ciclos glaciales en forma de dientes de sierra pero en el que los factores desencadenantes físicos de estados glaciales-interglacial permanecen sin explicación. Más modelos complejos como *Ganopolski et al.* [2010] han demostrado que los modelos de complejidad intermedia (EMIC) como CLIMBER-2 son capaces de reproducir los principales aspectos de los ciclos glaciales bajo forzings orbitales y de efecto invernadero de forma realista. Sin embargo, el CO₂ tiene que ser introducido independientemente del forzamiento orbital.

Paillard and Parrenin [2004] también propuso un modelo simple relajación, pero teniendo en cuenta el mecanismo de formación de agua densa en el SO. En este modelo, la extensión del hielo de la Antártida se propone como una nueva variable capaz de vincular los cambios glaciales-interglaciales climáticos y de CO₂. La clave de sus resultados es la identificación de una fuerte no linealidad en la fuente oceánica de CO₂ que es controlada por la estructura vertical de la densidad de las profundidades del océano. A pesar de su simplicidad, este modelo es el primero para reproducir con precisión ritmo y terminación de tiempos de todos los ciclos glaciales-interglaciales durante el Cuaternario, así como a toda la serie de máximos y mínimos del $\delta^{18}\text{O}$ (*Lisiecki and Raymo* [2005]) observados en los últimos 5 millones de años. Esto puede ser una señal del papel crucial que desempeña la estratificación y el pulso oceánico de CO₂ en el inicio del cambio glacial-interglacial.

C.1.1. Objetivos y estructura de la tesis.

Hoy en día, los mecanismos que controlan la variabilidad de los ciclos glaciales del Pleistoceno permanecen como una cuestión pendiente en las ciencias climáticas. Esta tesis pretende ampliar el campo de los modelos de relajación como una herramienta útil para examinar los mecanismos físicos internos del clima, identificando los principales feedbacks y las variables involucradas, tales como la estratificación del SO, la extensión del hielo marino o el almacenamiento de carbono oceánico; y, también para responder a preguntas dinámicas más concretas, como para predecir el comportamiento del futuro ciclo glacial o para explorar la dinámica de un interglacial particular. Los modelos obtenidos predicen las series de tiempo de volumen de hielo de los últimos 8 ciclos glaciales con una precisión notable a pesar de su simplicidad: de un 89 a un 90% de correlación con datos indirectos, que es a nuestro entender la más alta en la literatura. La comparación de los modelos desarrollados en este trabajo con las series de observacionales han hecho posible, también, sugerir una perspectiva sintética de los principales mecanismos que probablemente producen las oscilaciones glaciales-interglaciales, y especialmente los eventos de terminación. Esta síntesis se abre el camino para avanzar en el análisis de los modelos más detallados, como los de complejidad intermedia (EMIC).

Una hoja de ruta de la estructura de esta tesis puede ser útil para el lector. En el capítulo 1 presentamos una amplia representación de los modelos de relajación, con el objetivo de analizar cómo varias variaciones del modelo de *Paillard and Parrenin* [2004] (PP04) afectan al ajuste de datos. El buen ajuste obtenido con algunos modelos derivados de PP04 sugiere que los mecanismos que incorporan estos modelos pueden ser factores importantes que controlan las oscilaciones glaciales-interglaciales. En el capítulo 2 nos centramos en identificar esos mecanismos y dinámicas que llevan a buen ajuste de los datos y se exploran las interpretaciones físicas más plausibles de las expresiones matemáticas. Estos resultados se han comparado con el state-of-the-art que supuestamente causan oscilaciones glaciales-interglaciales, para explorar la consistencia de nuestra interpretación física con los resultados obser-

vacionales. Esos modelos de relajación se han aplicado a dos escenarios diferentes como una herramienta útil para entender el sistema: en el capítulo 3 se han utilizado para predecir la respuesta glacial-interglacial de la Tierra durante los próximos 300 ka, y en el capítulo 4 los modelos han sido recalibrados usando un nuevo stack de datos del nivel del mar y se utilizan para comprender la dinámica de un evento interglacial muy particular, los MIS-13. Por último, en el capítulo 4.5 se presentan las conclusiones de la tesis.

C.2. Capítulo 1:

MODELOS DE RELAJACIÓN APLICADOS A LAS OSCILACIONES CLIMÁTICAS

Se han propuesto algunos modelos simples de relajación para explicar los ciclos glaciales- interglaciales. Particularmente, *Paillard and Parrenin* [2004] propuso un modelo (PP04 en adelante) que incorpora parametrizaciones muy simples que representan la formación de agua densa en el SO. Aunque el modelo es simple, los resultados son alentadores, ya que reproducen correctamente los tiempos de ritmo y de terminación de todos los ciclos glaciares observados.

Aquí, el modelo PP04 se ha generalizado y calibrado para las series climáticas disponibles de $\delta^{18}\text{O}$ y CO_2 de los últimos 800 ka antes del presente (BP) (*Petit et al.* [1999]; *Monnin et al.* [2001]; *Pepin et al.* [2001]; *Lisiecki and Raymo* [2005]; *Siegenthaler et al.* [2005];

Luthi et al. [2008]). Los objetivos de este capítulo son obtener el conjunto de parámetros que mejor se adapten a las series de tiempo observacionales con el modelo original PP04; investigar varias generalizaciones del modelo de Paillard introduciendo algunos submodelos simples como la exportación, la estratificación u otros mecanismos; y analizar cómo los diferentes submodelos afectan el ajuste de datos.

C.2.1. Modelos de relajación.

Las ecuaciones del modelo original PP04 son las siguientes:

$$\frac{dV}{dt} = \frac{(V_r - V)}{\tau_V}, \quad \text{c.1}$$

$$\frac{dA}{dt} = \frac{(V - A)}{\tau_A}, \quad \text{c.2}$$

$$\frac{dC}{dt} = \frac{(C_r - C)}{\tau_C}, \quad \text{c.3}$$

$$V_r = -x C - y I_{65} + z, \quad \text{c.4}$$

$$C_r = \alpha I_{65} - \beta V + \gamma P(-F) + \delta, \quad \text{c.5}$$

$$F = a V - b A - c I_{60} + d, \quad \text{c.6}$$

donde V y A son índices adimensionales para el volumen de hielo global y la capa de hielo Antártico respectivamente, C es un índice adimensional del CO_2 atmosférico, I_{65} es la insolación diaria a 65°N el 21 de junio, $P(F)$ es la contribución del océano profundo al CO_2 de referencia, el cual en el modelo original es $P(F) = H(-F)$, donde H es la función de Heaviside ($H = 1$ si $F < 0$; $H = 0$ en cualquier otro caso), y F es el parámetro de eficiencia de formación de agua profunda.

PARÁMETROS	PP04	PB	BIO	2τ	4τ	EP	3τ	LS
τ_V	15000	15000	3667	12000	17006	4600	16585	11325
τ_{V_2}	-	-	-	-	3797	1100	3105.5	2325
τ_C	5000	5000	100	800	6796	3040	13505	2793
τ_{C_2}	-	-	-	4500	17667	7600	-	8414
τ_A	12000	10500	-	11333	8089	12000	9004	10266
x	1.3	1.32	0.85	1.29	0.767	1.525	0.905	0.669
y	0.5	0.45	1	0.5	0.442	0.2	0.489	0.527
z	0.8	0.8	0.92	0.85	1.033	0.96	0.946	0.761
α	0.15	-	-	-	-	-	-	0.237
β	0.5	0.496	0.76	0.496	0.406	0.476	0.336	0.793
γ	0.7	0.506	0.49	0.513	1.642	0.46	2.044	1.955
δ	0.4	0.4	0.4	0.434	0.407	0.445	0.228	0.146
a	0.3	0.3	-	0.3	0.395	0.3	0.54	-
b	0.7	0.71	-	0.71	0.8	0.71	1.205	0.936
c	0.01	0.005	-	0.005	-	-	-	0.533
d	0.27	0.27	-	0.27	0.27	0.255	0.483	0.069
ε	-	-	0.8	-	-	-	-	-
k	-	-	0.47	-	-	-	-	-
V_m	-	-	0.5	-	-	-	-	-
λ	-	-	-	-	-	37	-	-
R_V	0.63	0.71	0.58	0.82	0.89	0.85	0.88	0.87
R_C	0.59	0.67	0.45	0.75	0.79	0.77	0.79	0.76

Tabla C.1 Valores centrales de los modelos estudiados. R_V y R_C representan la correlación entre los datos observados y los modelos para el volumen global V y el C , respectivamente.

MODELOS	DESCRIPCIÓN	NÚMEROS DE PARAMETROS
PP04	Modelo original <i>Paillard and Parrenin</i> [2004] con $\gamma = 0.7$	14
PB	Mejor ajuste de <i>Paillard and Parrenin</i> [2004]	13
BIO	Exportación biológica en el CO ₂ de referencia	11
2τ	Diferente tiempo de emisión y absorción de CO ₂ y $\tau_C = \tau_{C_1}$ cuando $C < C_r$ $\tau_C = \tau_{C_2}$ cuando $C > C_r$	14
4τ	Diferente tiempo de emisión y absorción de CO ₂ y diferente tiempo para la acumulación y ablación de hielo:: $\tau_V = \tau_{V_1}$ cuando $V < V_r$ y $\tau_V = \tau_{V_2}$ cuando $V > V_r$	14
EP	Pulso oceánico dependiente de la estratificación	14
3τ	Modelo con un tiempo de relajación para C y dos tiempos de relajación para V	13
LS	Modelo con parámetros locales de estratificación	15

Tabla C.2 Descripción de los modelos

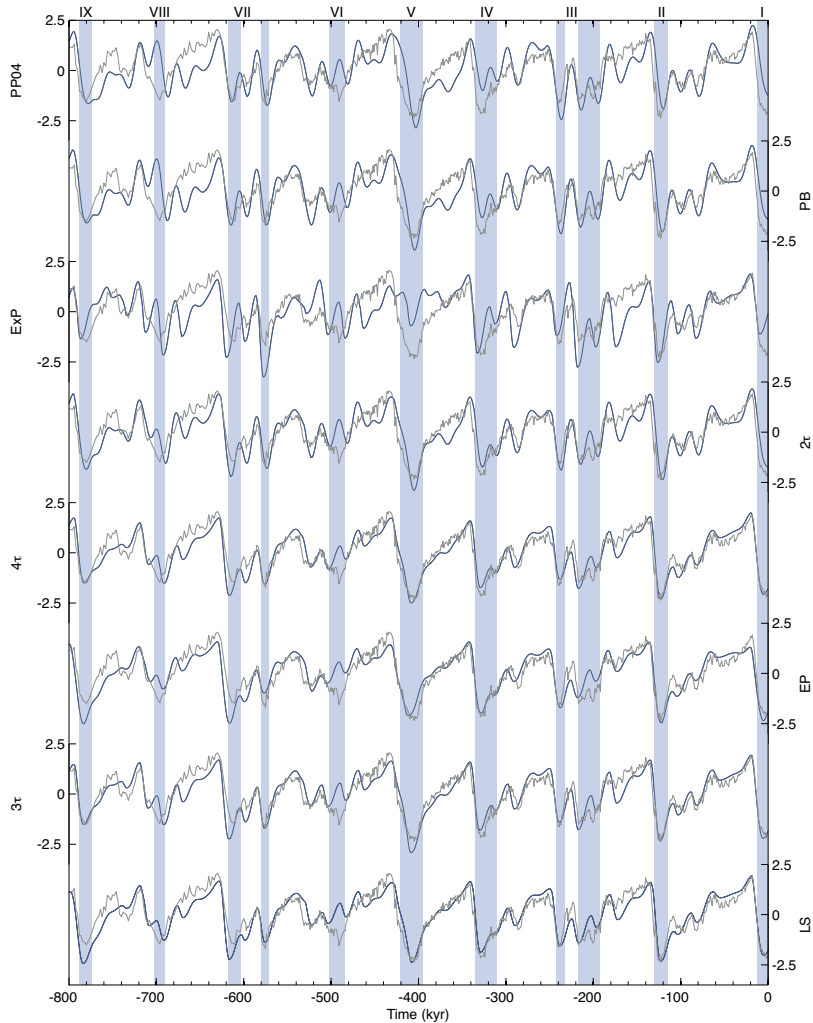


Figure
C.1

Resultados obtenidos para las series de volumen de hielo. De arriba a abajo: (1) modelo original de Paillard and Parrenin [2004] con $\gamma = 0.7$ (PP04); (2) mejor ajuste del modelo anterior (PB); (3) modelo con exportación biológica (BIO); (4) modelo con dos tiempos de relajación para C (2τ); (5) modelo con dos tiempos de relajación para C y dos tiempos de relajación para V (4τ); (6) modelo con un pulso oceánico exponencialmente dependiente de la estratificación (EP); (7) modelo con un tiempo de relajación para C y dos tiempos de relajación para V (3τ) y (8) modelo con parámetros de estratificación local (LS). Datos de $\delta^{18}\text{O}$ (Lisiecki and Raymo [2005]) superpuestos en cada panel. Las bandas azules representan los periodos interglaciales considerando $\delta^{18}\text{O}$ por debajo de 3.8 per mil.

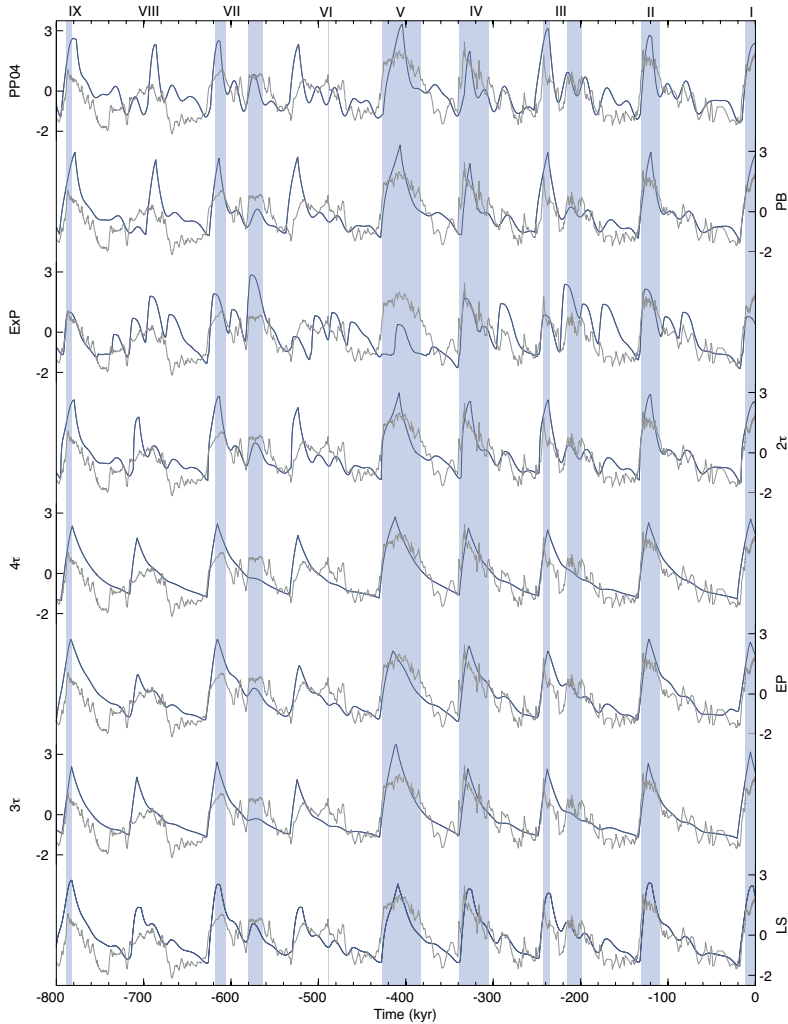


Figure
C.2

Resultados obtenidos para las series de CO_2 . De arriba a abajo: (1) modelo original de *Pailard and Parrenin* [2004] con $\gamma = 0.7$ (PP04); (2) mejor ajuste del modelo anterior (PB); (3) modelo con exportación biológica (BIO); (4) modelo con dos tiempos de relajación para C (2τ); (5) modelo con dos tiempos de relajación para C y dos tiempos de relajación para V (4τ); (6) modelo con un pulso oceánico exponencialmente dependiente de la estratificación (EP); (7) modelo con un tiempo de relajación para C y dos tiempos de relajación para V (3τ) y (8) modelo con parámetros de estratificación local (LS). Datos de CO_2 experimental (Petit et al. [1999]; Monnin et al. [2001]; Pepin et al. [2001]; Siegenthaler et al. [2005]; Luthi et al. [2008]) superpuestos en cada panel. Las bandas azules representan los periodos interglaciales considerando concentraciones de CO_2 superiores a 250 ppm.

Las principales variables V , A , y C tienden a decaer exponencialmente a un estado de referencia V_r , V , y C_r en unos tiempos característicos τ_V , τ_A and τ_C , respectivamente.

Las insolaciones diarias de los últimos 800 ka se obtienen a partir de *Berger* [1978a] y *Berger and Loutre* [1991]. Hemos utilizado los valores negativos y positivos en referencia a los tiempos antes del presente (BP) y después de presente (AP), donde el año cero se toma como 1950 AD. Las insolaciones se han normalizado con sus desviaciones estándar para obtener I_{65} y I_{60} . Todos los resultados del modelo han sido normalizados por su desviación estándar antes de ser representados.

C.2.2. Funcionamiento y dinámica de los modelos

A partir de *Paillard and Parrenin* [2004], se han desarrollado varios modelos de cajas que incorporan parametrizaciones simples de los tiempos de bombeo de CO_2 y de respuesta oceánicos de carbono y volumen de hielo. Los parámetros de los modelos han sido calibrados para proporcionar el mejor ajuste a los datos experimentales de $\delta^{18}\text{O}$ y CO_2 disponibles para los últimos 800 ka. El modelo PP04 es insensible al parámetro α y el efecto del Sol parece emerger sólo a través del filtro de volumen de hielo global. El ajuste de este modelo a los datos observacionales se puede mejorar si se asumen diferentes tiempos de respuesta tanto para la absorción / emisión de CO_2 y para la ablación / acumulación de hielo. Las correlaciones entre las series simuladas y experimentales aumenta de 0.59 y 0.63 a 0.79 y 0.89 para el CO_2 y el V , respectivamente.

Varias modificaciones del modelo PP04 que conducen a la sincronización correcta de las últimas nueve terminaciones han sido probadas. En particular, el comportamiento cualitativo de los últimos ocho ciclos glaciales-interglaciales puede ser reproducido con un modelo de exportación con depende del volumen de hielo (BIO). Sin embargo, en este modelo, el mejor ajuste correspondió a una dependencia entre la exportación de CO_2 y V que no fue exponencial, como propuso *Martínez-García et al.* [2009], sino con una función cuadrada. En nuestra formulación, la exportación

biológica por sí sola no es capaz de simular los datos experimentales con la misma precisión que los otros modelos, a pesar de que algún tipo de exportación biológica de CO₂ está muy probablemente actuando en sinergia con los procesos físicos en la dinámica de los glaciares-interglaciares.

Cuatro modelos (4τ , EP, 3τ and LS) muestran un buen ajuste en la simulación del volumen de hielo de los últimos ocho ciclos glaciares-interglaciares e incluso muchos detalles de esa señal perteneciente a la escala de 23 a 41 ka. Los buenos ajustes obtenidos sugieren que la densidad de las aguas profundas y su tasa de formación puede ser un factor importante que controla el pulso oceánico que desencadena los glaciaciones. *Schmittner* [2007] ha confirmado, con un modelo climático global, la sensibilidad del CO₂ atmosférico a los procesos que afectan a la estratificación en aguas del SO. En nuestro análisis, los pulsos oceánicos que dependen fuertemente, de una manera no lineal, de la estratificación del océano profundo son necesarios para desencadenar glaciaciones. Los pulsos obtenidos en los mejores modelos están siempre muy cerca de la función Heaviside propuesto por la obra original de PP04. Pulsos de CO₂ oceánico, con una duración de entre 10 y 20 ka se encontraron al comienzo de los nueve últimos glaciaciones de acuerdo con las mejores modelos analizados. Además, los diferentes tiempos de respuesta de emisión y absorción de CO₂ y para la acumulación y ablación de hielo son necesarios para obtener el mejor ajuste a los datos disponibles. La acumulación y ablación de hielo son diferentes mecanismos físicos que pueden tener diferentes tiempos característicos. Sin embargo, los dos tiempos de respuesta de emisión y absorción de CO₂ son más difíciles de explicar. Para decidir si estos dos tiempos de respuesta corresponden a mecanismos físicos reales, una comprensión más profunda de las tasas de transferencia a largo plazo en el ciclo del carbono debería **lograrse es** necesaria.

En resumen, hemos obtenido ocho ajustes diferentes con correlaciones de volumen de hielo entre 0.58 y 0.89 que muestran una buena concordancia cuantitativa y cualitativa con la serie temporal empírica, especialmente 4τ , EP, 3τ y LS; Aunque el evento de -490 ka no se reproduce correctamente por ningún modelo. El modelo 4τ mejora las correlaciones de PP04 (0.59 y 0.63) a 0.79 y 0.89 utilizando el mismo número de parámetros (a saber, 14). El modelo EP utiliza 15 parámetros, pero el

parámetro adicional, el cual fue dirigido a la mejora de la forma de la función de pulso oceánica, no mejora las correlaciones y puede considerarse inútil. El modelo 3τ obtiene casi las mismas correlaciones como 4τ utilizando sólo 13 parámetros. El modelo LS (15 parámetros) no mejora las correlaciones de 4τ , pero incorpora una forma funcional para la estratificación F que parece más consistente con los mecanismos sugeridos por *Paillard and Parrenin* [2004]. Si nuestro objetivo fuera seleccionar el modelo con la mayor varianza explicada por parámetro, la elección sería 3τ . Sin embargo, un segundo objetivo de este trabajo es determinar si los modelos con una varianza explicada similar a la obtenida por 3τ contienen parametrizaciones que se pueden de la forma más realista posible con mecanismos observados. LS puede ofrecer una información valiosa sobre el verdadero significado de la buena evolución de los modelos derivados de PP04. En el siguiente capítulo, la dinámica y mecanismos incorporados en 3τ y LS se analiza y compara.

C.3. Capítulo 2:

MECANISMOS FÍSICOS TRAS A LA DINÁMICA DE LOS CICLOS GLACIARES-INTERGLACIARES

En el primer capítulo, los modelos derivados de PP04 fueron calibrados para obtener un mejor ajuste a las series experimentales de $\delta^{18}\text{O}$ y CO_2 disponibles para los últimos 800 ka BP. Se observa que el rendimiento de PP04 se puede mejorar si su sensibilidad del CO_2 a la insolación se elimina y si diferentes tiempos de respuesta se consideran para la absorción y

la emisión de CO_2 , así como para la ablación y la acumulación de hielo. Las correlaciones entre las simulaciones y los datos experimentales aumentan de 0.59 a 0.79 para el CO_2 , y de 0.63 a 0.89 para el volumen de hielo V (modelo 4τ), respectivamente. Según los modelos, pulsos de CO_2 abruptos, con una duración de 10 a 20 ka, se llevan a cabo a principios de las últimas nueve glaciaciones.

El buen ajuste obtenido con los modelos derivados de PP04, especialmente con 3τ y LS, sugiere que los mecanismos que incorporan estos modelos pueden ser factores importantes que controlan las oscilaciones glacial-interglaciales. Los objetivos de este capítulo son identificar los mecanismos y dinámicas que se han incorporado en los modelos derivados de PP04, específicamente en 3τ y LS, que conducen a buen ajuste de datos; explorar las interpretaciones físicas más plausibles de las expresiones matemáticas incorporadas en estos modelos; y estudiar el grado en que los mecanismos y dinámicas previamente identificados son consistentes con los resultados de la dinámica observacional que supuestamente causa las oscilaciones glaciales-interglaciales.

El buen resultado de datos obtenidos con este conjunto de modelos refuerza la hipótesis de que algunos mecanismos intrínsecos de los modelos son los principales impulsores de oscilaciones glaciales interglacial, señalando a los mecanismos específicos que merecen un análisis más detallado.

C.3.1. Modelos 3τ y LS

Las ecuaciones de los dos modelos son:

3τ		LS	
$\frac{dV}{dt} = \frac{(V_r - V)}{\tau_V},$		$\frac{dV}{dt} = \frac{(V_r - V)}{\tau_V},$	c.7]
$\frac{dA}{dt} = \frac{(V - A)}{\tau_A},$		$\frac{dA}{dt} = \frac{(-C - A)}{\tau_A},$	c.8]

$$\frac{dC}{dt} = \frac{(C_r - C)}{\tau_C}, \quad \frac{dC}{dt} = \frac{(C_r - C)}{\tau_C}, \quad \text{c.9}$$

$$V_r = -x C - y I_{65} + z, \quad V_r = -x C - y I_{65} + z, \quad \text{c.10}$$

$$C_r = -\beta V + \gamma H(-F) + \delta, \quad C_r = \alpha I_{65} - \beta V + \gamma H(-F) + \delta, \quad \text{c.11}$$

$$F = a V - b A + d, \quad F = c C - b A + d, \quad \text{c.12}$$

En estas ecuaciones, las variables V , A y C , tienden exponencialmente a los estados de referencia V_r , A_r y C_r con tiempos característicos τ_V , τ_A y τ_C , respectivamente; estos tiempos característicos y el resto de parámetros se especifican en la Tabla C.1. Las series de tiempo de ambos modelos, así como los datos observacionales, se muestran en la Figura C.3.

Hay varias diferencias entre los modelos 3τ y LS. Una diferencia es el valor utilizado para la capa de hielo antártica de referencia, ya sea $-C$ (que representa el efecto inverso de la temperatura de la Antártida en la capa de hielo) para el modelo LS o V para el modelo de 3τ . Otra pequeña diferencia es la inclusión de I_{65} en el modelo LS cuando se especifica el valor de la concentración atmosférica de CO_2 de referencia, C_r . Sin embargo, la principal diferencia entre ambos modelos, es su parametrización de la estratificación, con $F = F(V, A)$ en el modelo 3τ y $F = F(C, A)$ en el modelo LS. Tanto V como C son buenas aproximaciones para la temperatura regional del SO y, por lo tanto, $F = F(V, A)$ o $F = F(C, A)$ son maneras plausibles de modelar la formación local de salmueras. El hecho de que la dependencia $F = F(V, A)$ se comporte mejor que $F = F(C, A)$ puede ser debido al papel no despreciable que V tiene en la estratificación a través de una teleconexión NH-SH (*García-Olivares and Herrero [2013]*) o a un posible efecto mayor del nivel del mar que la temperatura de la Antártida en la formación de salmuera.

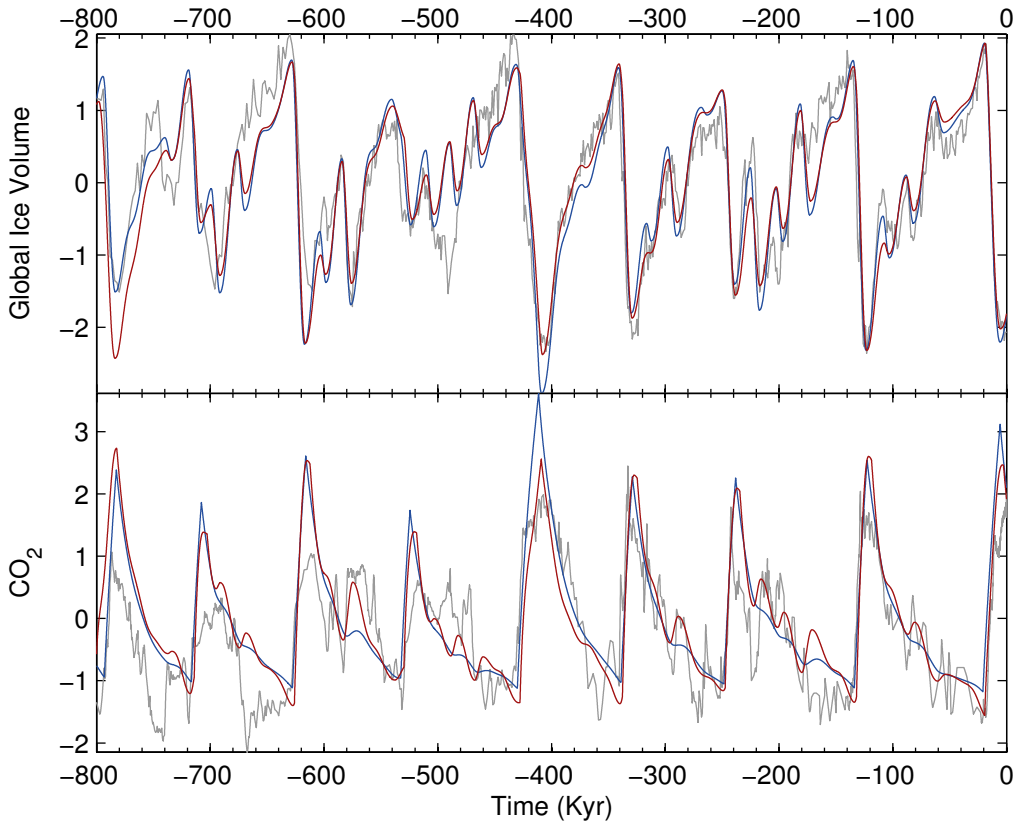


Figura
C.3

Panel superior: volumen de hielo normalizado por 3τ (línea azul) y LS (línea roja), y $\delta^{18}\text{O}$ de Lisiecki and Raymo [2005] (línea gris). Panel inferior: CO_2 normalizado por 3τ (línea azul) y LS (línea roja) y datos experimentales de CO_2 (Petit et al. [1999]; Indermuhle et al. [2000]; Monnin et al. [2001]; Siegenthaler et al. [2005]; Luthi et al. [2008]) (línea gris).

C.3.2. Dinámica de los modelos

La Figura C.4 muestra la variación de I_{65} (arriba), V (segundo panel), A (tercer panel), C (cuarto panel) y F (abajo) simuladas por 3τ (línea azul) and LS (línea roja) para los dos últimos ciclos glaciares. Debido al efecto de τ_C , C responde a las variaciones de I_{65} con un cierto retraso. Por esta razón, cada máximo (mínimo) de I_{65} en la figura es seguido por un máximo (mínimo) de C 5 kyr después. Las variaciones de C se reflejan en la F variable que tiene su máxima y mínima en contra-fase con C . Por otra parte, A responde a C siguiendo su tendencia de largo plazo (con un retraso de 7 kyr aproximadamente) pero amortiguando las oscilaciones de alta frecuencia. Cuando C es baja, como en el máximo glacial, A es grande, y F está cerca del disparador $F < 0$. En esta situación, cualquier nuevo máximo en I_{65} causa una disminución en F (a través de C y A) que activa el pulso CO_2 oceánico, disparando la deglaciación. En el caso de 3τ , una descripción prácticamente equivalente se puede hacer usando la variable V en lugar de C .

La doble condición para generar una deglaciación es, por tanto, la coincidencia de un máximo de I_{65} en un período en que V es grande. Esta doble condición ya fue observada e incorporada por Paillard en algunos modelos anteriores (Paillard [1998]).

La Figura C.5 muestra las contribuciones relativas a los niveles de CO_2 de los mecanismos implicados, en función del tiempo, para los modelos 3τ (arriba) y LS (abajo). La línea azul representa la $\delta - \beta V$ en la ecuación C.11; la línea roja representa la contribución del océano profundo ($H(-F)$) En la misma ecuación para el cambio en Cr . Una contribución inercial, definida como la diferencia instantánea entre C y su valor asintótico Cr , se ha incluido como una línea verde.

En los modelos 3τ y LS, Cr mantiene un crecimiento monótono después de -135 ka. En primer lugar, tras el aumento brusco de Cr causado por la conexión del pulso **oceánico**; entonces, tras el aumento de Cr causado por la respuesta positiva de T- CO_2 (V- CO_2 en nuestros modelos). La pendiente de este aumento de CO_2 depende de la tasa de disminución de V , que responde a una combinación de forzamiento

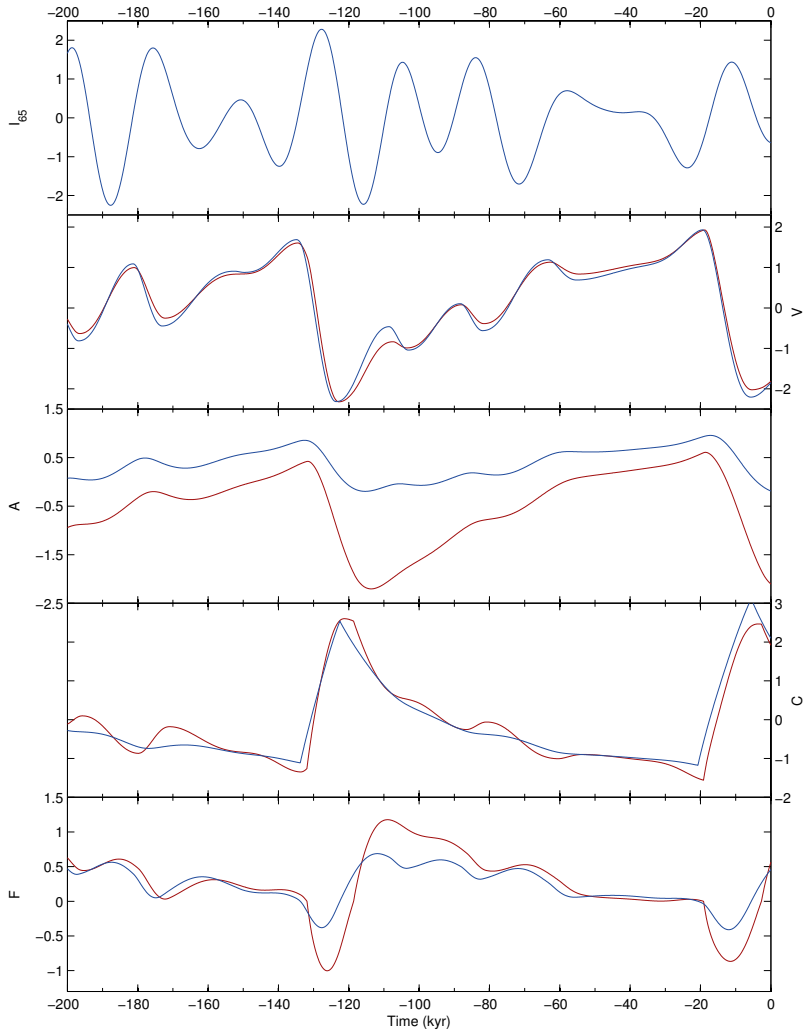


Figura
C.4

Variación de I_{65} (arriba), V (segundo panel), A (tercer panel), C (cuarto panel) y F (abajo) simuladas por 3τ (línea azul) and LS (línea roja) para los dos últimos ciclos glaciares.

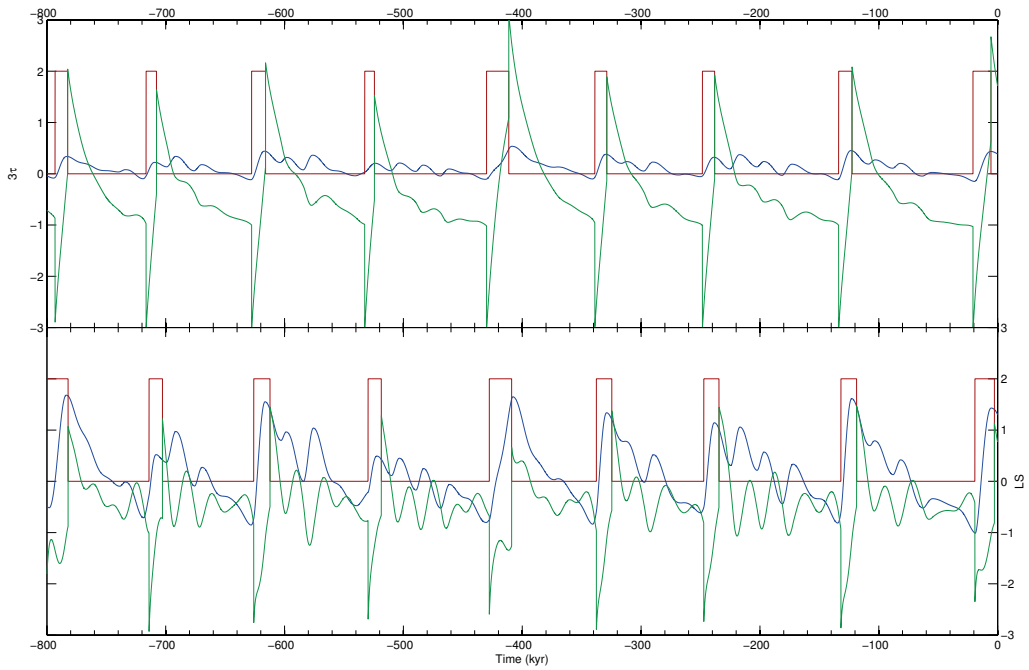


Figure
C.5

Contribuciones relativas a los niveles de CO₂ de los mecanismos implicados, en función del tiempo, para los modelos 3τ (arriba) y LS (abajo). La línea azul representa la $\delta - \beta V$ en la ecuación C.11; la línea roja representa la contribución del océano profundo ($H(-F)$) en la misma ecuación para el cambio en C_T . Una contribución inercial, definida como la diferencia instantánea entre C y su valor asintótico C_T , se ha incluido como una línea verde.

astronómico y a efecto invernadero. En estos modelos el período durante el cual el CO₂ aumenta es aproximadamente el período en que está conectado el pulso oceánico. Sin embargo, la introducción de un forzamiento directo de I_{65} en Cr en el modelo LS permite a las desglaciaciones comenzar con un pulso más corto de CO₂. Esta intercambiabilidad entre una fracción de la liberación oceánica y otras fuentes de CO₂ tiene lugar en momentos de calentamiento astronómico (como suele ser una terminación) y se deriva en última instancia de la extrema simplicidad de los mecanismos de liberación de CO₂ incorporadas en los modelos derivados de PP04. Después del final del pulso oceánico y las aportaciones astronómicas, C está por encima de su nivel asintótico y empieza a disminuir hacia niveles glaciales.

Dos conclusiones principales se pueden extraer de este análisis:

- (i) La oscilación en V que caracteriza los períodos de terminación se produce fundamentalmente por la misma retroalimentación positivas, CO₂-T y T-CO₂, que caracteriza a cualquier otra oscilación provocada por el cambio insolación; sin embargo, esta oscilación tiene pendientes más fuertes, tanto en Cr como en Vr debido a la contribución adicional generada por el pulso oceánico.
- (ii) Una liberación abrupta de CO₂ oceánico (similar a un pulso rectangular) parece necesario iniciar una desglaciación; esta liberación está controlada por la variable de la formación de aguas profundas, F , que depende principalmente de V y A (modelo 3τ) o en C y A (Modelo LS); y V , A y C son impulsados en la última instancia por la insolación.

¿Hasta qué punto son los modelos PP04 consistentes con la dinámica observacional? En primer lugar, la secuencia de activación de los procesos que liberan CO₂ durante las terminaciones, sugerido por la secuencia de activación, es muy diferente a la secuencia de pasos que reducen CO₂ durante la época glacial, y esta diferencia genera la forma de diente de sierra típica de las oscilaciones glaciales-interglaciales. La falta de un modelo completo para las bombas biológicas y de carbonatos en los modelos derivados de PP04 hace que sea imposible de reproducir con precisión la

serie de acontecimientos que caracterizan los períodos glaciales, y la utilización de diferentes tiempos de relajación para los momentos de aumento y disminución de CO₂ es la manera más fácil de tener en cuenta esta asimetría y reproducir el ciclo de doble vertiente.

Aunque el decaimiento glacial se simula sólo aproximadamente por los modelos derivados de PP04, la precisión de ajuste de ritmo y la intensidad del CO₂ interglacial que estos modelos generan es suficiente para obtener un buen ajuste de la evolución de volumen de hielo.

Una de las conclusiones de este estudio es que los modelos derivados de PP04 no son sensibles a la insolación sur, I_{60} . En estos modelos, C parece ser una mucho mejor proxy de temperatura de la Antártida que I_{60} . Esto refuerza indirectamente la conclusión de *Huybers and Denton* [2008] que la temperatura de la Antártida no es sensible a la insolación durante un día de verano en particular y que podría ser sensible a otro tipo de variables, tales como la duración del verano austral.

La función de la estratificación, F , es una variable fundamental de los modelos derivados de PP04, que debe ser interpretado como la estratificación producida por diferencia de densidad entre AABW y NADW con una posible contribución menor de la estratificación producida por diferencia de densidad entre NADW y aguas superficiales. F controla el afloramiento de CO₂ de una manera no lineal: una liberación brusca de CO₂ oceánico similar a un pulso rectangular de 10 a 20 por kyr, muy sensible a F , es necesaria en estos modelos para generar las terminaciones.

Los cambios en la circulación oceánica asociados con vientos del oeste, la estratificación del océano profundo, la expansión del hielo marino, la variación de la eficiencia de la AMOC, junto con las variaciones de la absorción biológica y de compensación de carbonatos parecen ser los principales impulsores de la diferencia atmosférica de CO₂ entre los estados glaciales e interglaciales. *Ferrari et al.* [2014] ha propuesto recientemente un nuevo mecanismo capaz de vincular la expansión del hielo marino antártico con el descenso de la temperatura, el reordenamiento de las masas de aguas profundas y el cambio de circulación en LGM, demostrando que no son mecanismos independientes, sino retroalimentaciones. El mecanismo exacto es liderado

por los isopiecnas del SO, que controlan el afloramiento y la mezcla de AABW y NADW, separando las células NMOC y SMOC. La pendiente y la posición de este cambio isopiecnico es función de la expansión del hielo marino de verano, mezclando activamente AABW y NADW en el período interglacial, pero limitando el afloramiento de mezcla impulsada por las aguas abisales en la LGM, cerrando el SMOC y previniendo la mezcla de NADW y AABW. Como resultado, las AABW llenan las cuencas oceánicas hasta 2 km de profundidad, en lugar de la actual profundidad de 4 km. Esta celda cerrada actuaría como un almacenamiento oceánico de carbono. Este enfoque, considera la expansión de casi permanente el hielo marino en el SH como el conductor de la terminación. Esto sugeriría que la extensión del hielo marino puede tener un efecto sobre la intensidad de liberación de CO₂, que trabaja en la misma dirección que la estratificación durante los períodos glaciales e interglaciales; por lo tanto, no podemos descartar una posible contribución paralela del área de hielo marino en la intensidad de la emisión de CO₂.

La conclusión más importante de este estudio es que una dinámica detallados de CO₂ es de poca relevancia para obtener un buen acuerdo entre el volumen de hielo simulado y $\delta^{18}\text{O}$. Todo lo que se necesita es una inestabilidad no lineal que se alcanza después de 80 a 100 ka y que permite que incluso una variación suborbital modesta pueda desencadenar una liberación repentina de CO₂ atmosférico. Esta inestabilidad no lineal parece estar controlada por V o C (aquí interpretado como temperatura de la Antártida) y por A (interpretado como capa de hielo de la Antártida) en los modelos derivados de PP04.

Una simulación precisa del conjunto detallado de los hechos que constituyen el desencadenante de la desglaciación requeriría la adición de algún modelo para la capa de hielo del Atlántico Norte, así como modelos de carbono más complejos. Los modelos derivados de PP04 producen buenos ajustes a pesar de su simplicidad en el modelado de la liberación de CO₂ oceánico, que depende sólo de la estratificación. Las otras contribuciones (compensación de carbonatos, la formación NADW, el cambio de la productividad en el SO y ralentización de la AMOC) no están incluidos en el modelo, pero deben incluirse en futuras mejoras para obtener una representación más cerca de todos los procesos físicos que al parecer están involucrados.

C.4. Capítulo 3:

IMPACTO DEL CO₂ ANTROPOGÉNICO EN EL PRÓXIMO CICLO GLACIAL

En este capítulo se utilizan los dos modelos, 3τ y LS, para predecir la respuesta glacial-interglacial de la Tierra durante los próximos 300 ka.

Como hemos visto en los capítulos anteriores, los modelos, utilizando los parámetros de la Tabla C.1, son capaces de reproducir los máximos y mínimos climáticos observados desde 800 ka BP hasta el presente tanto en volumen de hielo como en CO₂ (Figuras C.1, C.2 y C.3), así como algunas de las periodicidades suborbitales observados (Figura 2.2). La coherencia cross-wavelet y el análisis cross-recurrence (*Grinsted et al. [2004]; Marwan and Kurths [2002]; Marwan et al. [2007]*) muestran que tanto los registros de modelo como los datos experimentales muestran una dinámica similar (Figuras 2.3 a 2.19).

Estos resultados apoyan firmemente la idea de que los modelos de relajación, a pesar de su simplicidad, incluyen algunos de los mecanismos clave que están detrás de las oscilaciones climáticas del Pleistoceno. De hecho, la estructura de los modelos imitan algunas de las principales retroalimentaciones que se están produciendo plausiblemente en los mecanismos de control del sistema climático, tales como el efecto de la insolación norte en el volumen de hielo, la realimentación de CO₂-temperatura (a través del volumen de hielo, V), la retroalimentación volumen de hielo - CO₂, y la emisión de CO₂ del océano profundo como una función de la estratificación (la variable F) que depende del nivel del mar y la capa de hielo Antártica. Detalles adicionales sobre estos mecanismos, y la forma en que los modelos los representan, se pueden encontrar en *Paillard and Parrenin [2004]*, *Paillard [2010]* y *García-Olivares and Herrero [2013]*.

Bajo estas consideraciones, y siempre que el pulso de CO₂ antropogénico esté representado adecuadamente, los modelos pueden ser utilizados para predecir su efecto sobre la perturbación de la secuencia natural de glaciaciones y terminaciones.

C.4.1. Emisión de CO₂ y respuesta atmosférica

Un primer paso fundamental es estimar cuánto CO₂ antropogénico se emitirá a la atmósfera. Para ello, hemos utilizado los datos históricos de quema de combustibles fósiles (*Boden et al.* [2010]), complementado con datos de los últimos años del Global Carbon Project¹. Se ha aproximado la tasa total anual de emisiones de combustibles fósiles como una función de Lorentz:

$$E = \frac{U b e^{-b(t-tp)}}{[1 + e^{-b(t-tp)}]^2}, \quad \text{C.13}$$

donde U representa la Ultimate Recoverable Resources (URR) de combustibles fósiles en gigatoneladas de carbono equivalente (Gtce), tp es el año del máximo de emisiones (yr), y $Ub/4$ es la correspondiente tasa de emisiones (Gtce yr⁻¹).

Teniendo en cuenta la literatura y los últimos estudios realizados, se ha considerado una URR total de combustibles fósiles de 1300 Gtce, siendo éste nuestra mejor estimación para las emisiones antropogénicas integradas de carbono.

La Figura C.6 muestra los datos históricos sobre las emisiones de combustibles fósiles durante el período de 1800 a 2010 AD y el ajuste correspondiente utilizando una función de Lorentz (Ecuación C.13), obtenida considerando $U = 1300$ Gt, lo que corresponde a unas emisiones máximas en el año 2037 AD. Este ajuste se ha hecho de tal manera que la emisión de carbono integrado en 2010 AD tiene exactamente la misma área que la serie histórica hasta 2010 AD (líneas discontinuas en las figuras C.6 y C.7). Esta función de Lorentz modificada es la que utilizamos para producir

¹<http://www.globalcarbonproject.org/carbonbudget>

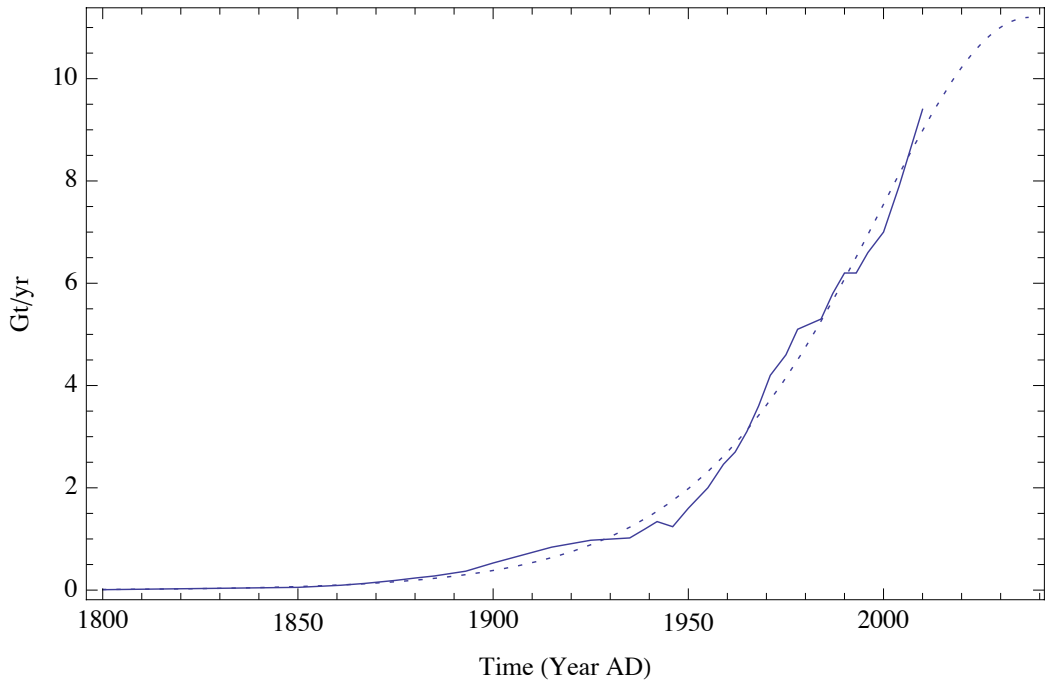


Figura
C.6

Datos históricos de las emisiones de combustibles fósiles durante el periodo 1800-2010 (línea continua) y la función de Lorentz ligeramente modificada de tal manera que el área hasta 2010 equivale a las emisiones históricas acumuladas (línea discontinua).

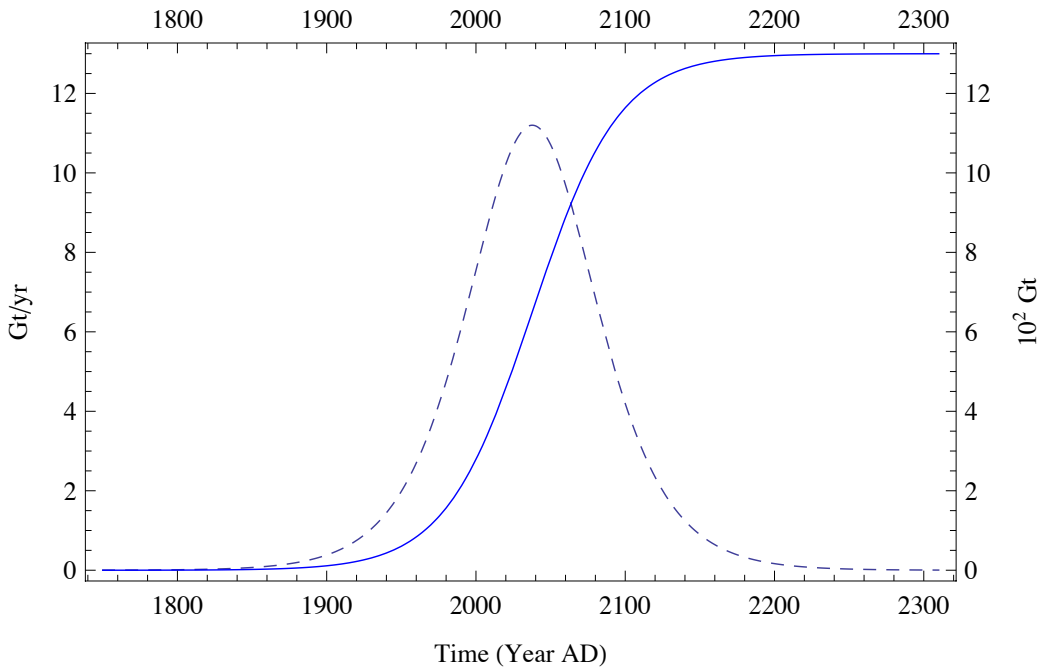


Figura C.7 Función de Lorentz modificada que ilustra la liberación antropogénica de carbono por año (línea discontinua) y la liberación de carbono acumulado (línea continua).

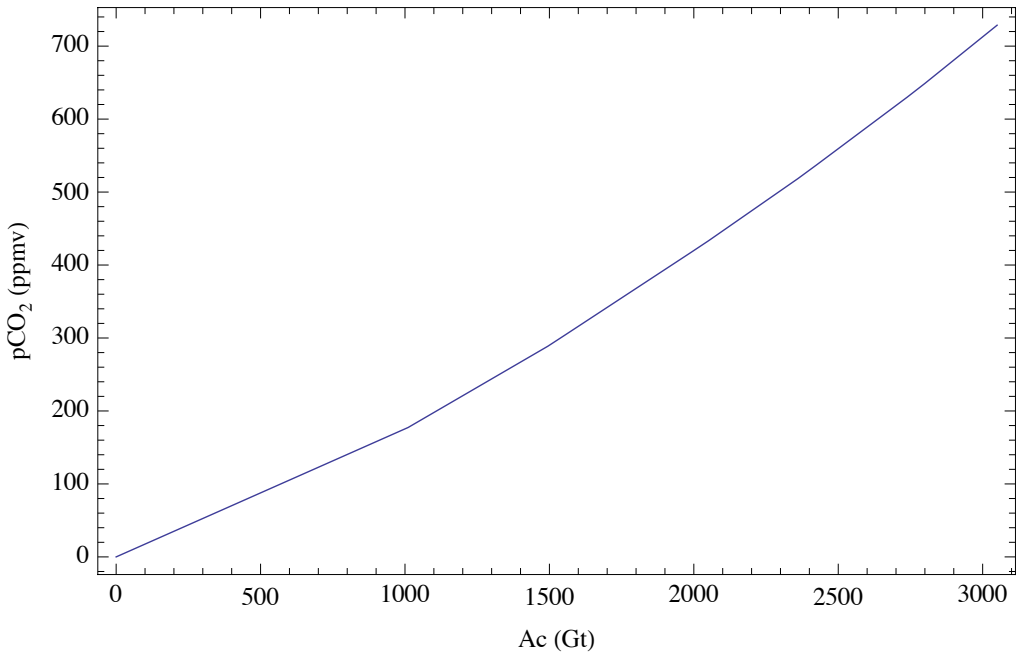


Figura
C.8

Relación entre las emisiones de carbono antropogénicas acumuladas (Ac) y la concentración atmosférica de CO_2 (pCO_2). Los datos se obtienen a partir de un agregado de escenarios A1T (*SRES* [2000]) predichos por el modelo ISAM (*Jain et al.* [1994]), disponible en <http://climate.atmos.uiuc.edu/isam2/>, para cada posible valor de la URR..

la serie temporal completa de emisiones antropogénicas acumuladas de los combustibles fósiles (Figura C.7). El pico de las emisiones se produce en el año 2037 AD, coincidiendo con el punto de inflexión de la curva acumulada, y tiende a cero cerca de año 2324 AD, cuando las emisiones acumuladas alcanzan sus valores máximos.

Las emisiones de CO₂ antropogénico relativamente rápidas, en la escala de 10 a 100 años, darán lugar a un aumento de la concentración atmosférica pero también producirá un aumento de la tasa de almacenamiento en el océano, la vegetación del suelo, árboles, detritus y el suelo (*Kheshgi and Jain* [2003]). Nuestros modelos no incluyen este tipo de mecanismos de retroalimentación climáticos relativamente rápida. Para tenerlas en cuenta que necesitamos una función de transferencia de las emisiones de carbono acumulados (Ac , en Gt) a concentración atmosférica de CO₂ (pCO_2 en ppmv). Con este objetivo hemos usado el modelo ISAM (*Jain et al.* [1994]; *Kheshgi and Jain* [2003]). En este modelo, las tasas de transferencia de la atmósfera a los cinco compartimentos superiores han sido calibradas para que coincida con las proyecciones promedio (**por seis modelos globales-vegetación dinámicos y 10 modelos acoplados océano-atmósfera**) para la absorción de CO₂ entre los años 2000 y 2200 AD.

Con el fin de obtener la función de transferencia de Ac a pCO_2 , utilizamos el modelo ISAM con los parámetros del escenario A1T, según lo propuesto por el IPCC (*SRES* [2000]). Corremos el modelo ISAM para valores de URR entre 0 y 3000 Gt, aumentado a intervalos URR de 100 Gt, sustituyendo los combustibles fósiles del escenario A1T con la función de Lorentz modificada. Para cada valor URR obtenemos la respuesta atmosférica correspondiente; estos puntos finales se interpolan linealmente con el fin de tener una curva continua (Figura C.8). La función de transferencia correspondiente debe ser adecuada para modelar el corto plazo (a escalas decenales y de siglos) la respuesta en el rango de 0 a 3000 Gt; en particular, puede ser utilizado para modelar los resultados con nuestra mejor estimación URR, $U = 1300$ Gt (Figuras C.6 y C.7). Tenga en cuenta que las contribuciones de la deforestación futura son considerados por el modelo ISAM, por lo tanto, que se reflejan en la función de transferencia de la Figura C.8.

C.4.2. Proyección para el futuro

Podemos ahora por fin estimar la evolución temporal del pulso CO₂ atmosférico antropogénico. Los datos históricos de las concentraciones atmosféricas se utilizan para el período entre 1750 y 2010 AD. A partir de entonces, y hasta el final de la emisión antropogénica en el año 2324 AD, el CO₂ atmosférico se estima utilizando las emisiones acumuladas predichos de la función de Lorentz modificado (Figuras C.6 y C.7) y la función de transferencia como se deduce a partir del modelo ISAM (Figura C.8). De esta manera la emisión de carbono acumulado es 361 Gt en el año 2010 AD, 642 Gt en el año 2037 AD, y alcanza un valor máximo de 1300 Gt el año 2324 AD, y las concentraciones atmosféricas en esas fechas se puede obtener de las ordenadas correspondientes en Figura C.8.

Antes de hacer una proyección para los próximos 300 ka hay que tener en cuenta si hay otros mecanismos plausibles que no están incorporados en nuestros modelos. En este trabajo se consideran dos posibles contribuciones: la weathering compensation, muy bien establecida, y la emisión de menos conocida de metano de los clatratos. Hemos elegido estos dos mecanismos, no sólo porque son de hecho los efectos pertinentes, sino también porque son ilustrativos del tipo de modificaciones que los mecanismos de retroalimentación pueden causar en la dinámica del Pleistoceno.

Las ecuaciones del modelo se integran hacia adelante, con el escenario de emisiones de carbono antropogénico en la Figura C.7 como la condición inicial y adecuadamente forzados por la insolación en 65°N (*Berger [1978b]*), para predecir la evolución de las transiciones interglaciares-glaciares durante los próximos 300 kyr.

La proyección para los próximos 300 ka se calcula tanto para el caso perturbado como las condiciones naturales usando ambos modelos imperturbable 3τ y LS; la Figura C.9 ilustra, como ejemplo, la evolución prevista de CO₂ atmosférico tras el pulso de CO₂ antropogénico. Ambos modelos presentan un decaimiento exponencial de CO₂ en la atmósfera, con la característica de tiempo de decaimiento algo más largo de 3τ que para LS. Los dos modelos, a pesar de tener diferentes parametri-

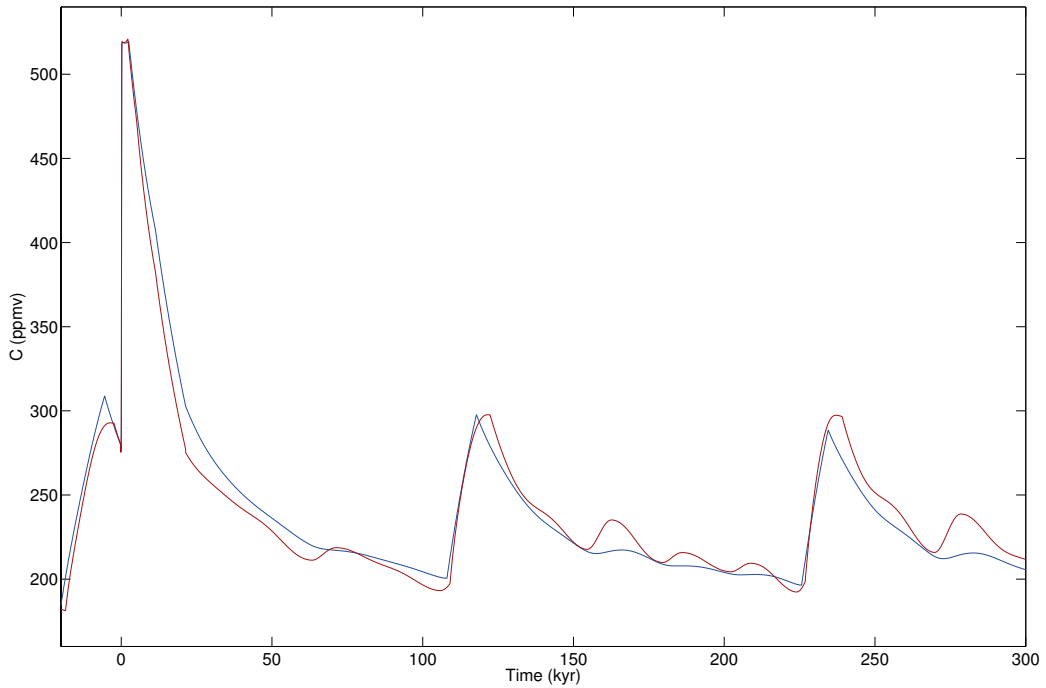


Figura C.9

Predicción de la concentración de CO₂ atmosférico sin dimensiones para los próximos 300 ka utilizando, como una condición inicial, el escenario de la liberación de carbono antropogénico mostrado en la Figura C.7. Las líneas azules y rojas corresponden a la proyección del modelo 3τ y LS, respectivamente.

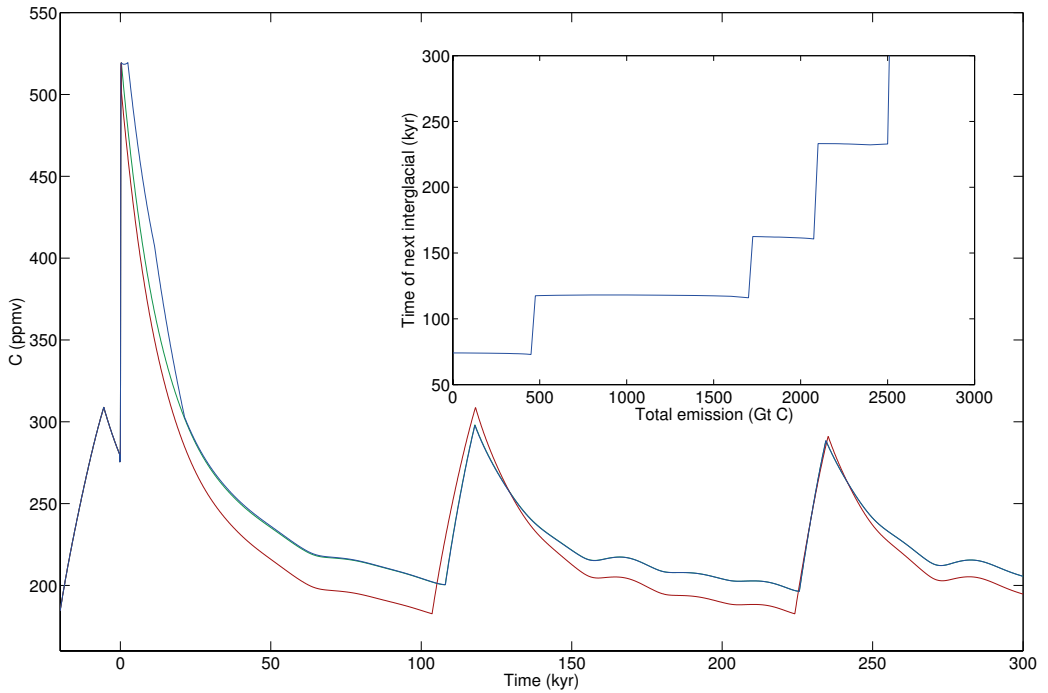


Figura
C.10

Concentración de CO₂ en la atmósfera para los próximos 300 ka según lo predicho por el modelo 3τ siguiendo el pulso corto plazo antropogénico (línea roja), después de añadir la weathering compensation a largo plazo (línea verde), y después de la incorporación de las emisiones de metano de los clatratos (línea azul). El recuadro muestra cómo varía el inicio de los próximos interglaciares en función de las emisiones totales de carbono.

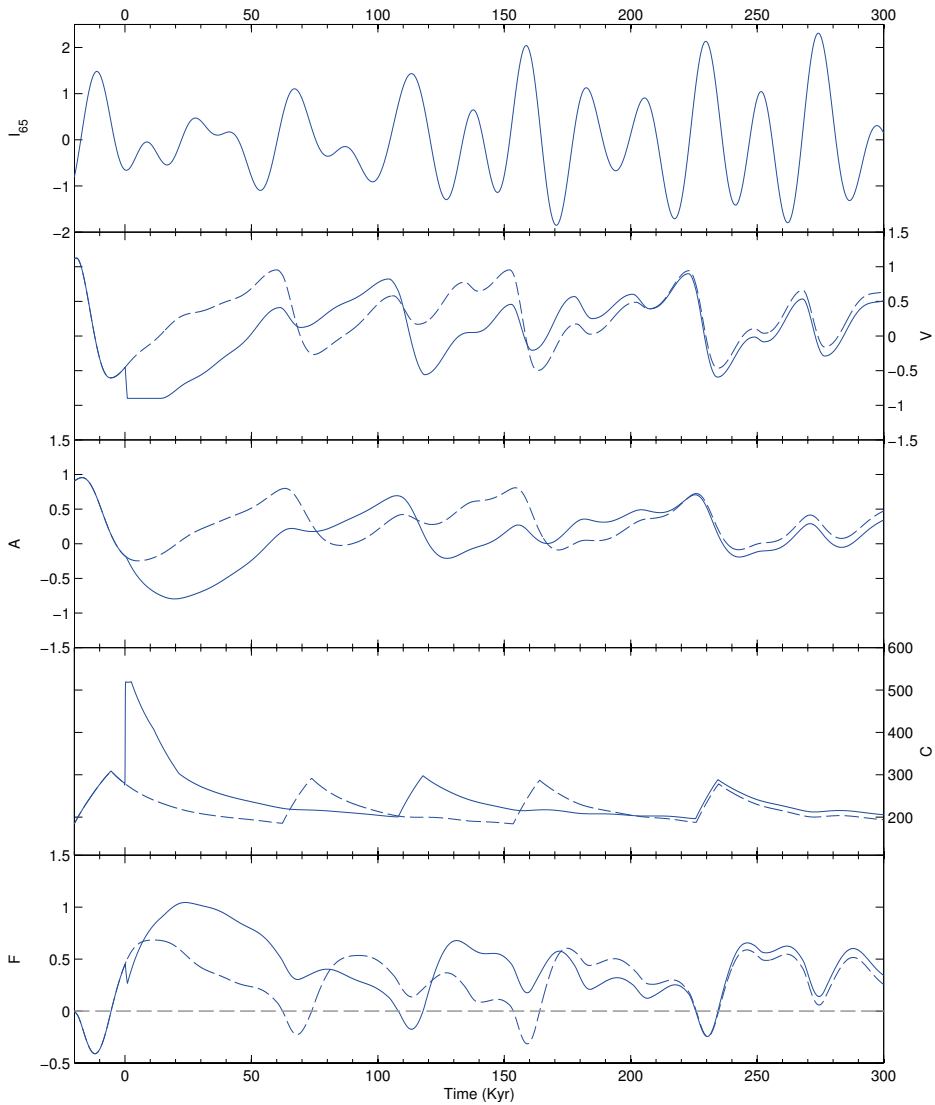


Figura C.11

Predicción de las variables climáticas para el futuro 200 ka obtenida mediante el modelo 3τ (incluida la weathering compensation y las emisiones de metano). El panel superior muestra la insolación I_{65} y los otros cuatro paneles presentan la proyección de volumen normalizado hielo (segundo panel), la extensión normalizada de la capa antártica del hielo (tercero), las concentraciones atmosféricas de CO₂ dimensionales, (cuarto) y la estratificación (parte inferior), con (línea continua) y sin (línea discontinua) la perturbación antropogénica en todos los casos.

zaciones para la estratificación del océano y la evolución capa de hielo, producen un resultado muy similar para el siguiente ciclo glacial. De ahora en adelante, nos centraremos en la proyección futura obtenido con el modelo 3τ , una comparación de los dos modelos muestra resultados análogos.

La Figura C.10 muestra la evolución de CO_2 predicha por el modelo 3τ siguiendo el pulso antropogénico a corto plazo, después de añadir el mecanismo de weathering compensation a largo plazo y que incluye además las emisiones de metano de los clatratos. Se puede observar que en todos los casos el tiempo para los próximos interglaciares no cambia sustancialmente. El principal efecto es causado por la weathering compensation que provoca concentraciones algo más altas y una duración ligeramente más largo de la presente interglacial. El efecto de la emisión de metano se reduce mucho a excepción de una meseta en los valores de CO_2 después de terminar el pulso antropogénico.

La introducción del pulso CO_2 antropogénico perturba claramente el ciclo natural de las cuatro variables del modelo en el próximo 300 ka (Figura C.11).

El modelo predice la desaparición de la próxima era interglacial, que debe comenzar en 64 ka AP. Esto es debido a la zona de volumen de hielo y capa de hielo anormalmente reducida predijo para el presente interglacial, que toma mucho tiempo para recuperarse. La capa de hielo, A , Sigue la evolución de V con un retraso de aproximadamente 7 kyr (Ecuación C.8 y valor de τ_A en la Tabla C.1). La función F , sin embargo, se vuelve negativo sólo cuando A es lo suficientemente grande. A los 64 ka AP, V disminuye (C se eleva) en respuesta a la forzamiento positivo del I_{65} pero A no es lo suficientemente alto como para que F se haga negativo. Si V y A fuesen grandes, como ocurre en el caso no perturbado, F sería cercana al valor de umbral ($F = 0$) y la disminución de V (ascenso de C), en ese momento F tomaría valores negativos, lo que provocaría el pulso oceánico. Este retraso en la recuperación del volumen de hielo V (y A) es causado por el pulso antropogénico introducido en el modelo, que produce 20 kyr de efecto invernadero anormalmente alto. Bajo estas condiciones, V necesita un tiempo más largo para alcanzar el máximo glacial y el

siguiente ciclo glacial mueve 44 kyr adelante en el tiempo. En 235 kyr AP los interglaciales perturbados y no perturbados coinciden de nuevo y la posterior evolución de todas las variables permanecen en fase, lo que sugiere que la recuperación de la periodicidad natural.

También hemos explorado cómo de sensibles son los resultados del modelo, en particular, la momento de inicio para el siguiente ciclo interglacial, a diferentes valores URR. Un resultado principal es que un aumento progresivo en el pulso antropogénico conduce a ciclos más pequeños, con valores de CO₂ más bajos. Un resultado muy relevante es que el momento del próximo interglacial cambia discretamente como U supera diferentes valores de umbral (inset en la Figura C.10). Por ejemplo $U = 475$ Gt representa el umbral más allá del cual la siguiente interglacial experimentará un retraso de 44 kyr; los siguientes umbrales se producirán en 1725 y 2100 Gt, con los correspondientes retrasos adicionales de 42 y 72 ka.

En este trabajo se ha ilustrado una aplicación de dos modelos de tipo relajación simples (*García-Olivares and Herrero [2013]*) para predecir la evolución futura de las variables de la Tierra a nivel mundial durante los próximos 300 ka, con y sin la perturbación atmosférica de CO₂ causadas por las emisiones de combustibles fósiles antropogénicas.

El anormalmente alta perturbación térmica del interglacial actual dará lugar a un retraso en el futuro avance de la capa de hielo sobre la plataforma de la Antártida. Como resultado, el máximo relativo de la insolación boreal 65 kyr AP no tendrá ningún efecto sobre la estabilidad de la glaciación en desarrollo. Sin embargo, el pico de insolación siguiente (115 ka AP) se llevará a cabo en un estado apropiado del sistema climático y será suficiente para inducir la nueva deglaciación. El próximo máximo glacial se llevará a cabo sobre 105 AP kyr y el siguiente interglacial será retrasado hacia adelante en el tiempo 44 kyr en relación con las condiciones no perturbadas. Nuestras proyecciones dependen del valor URR, siendo muy estable en el rango de 475 a 1700 Gt; para URR igual o mayor que 1725/2100 Gt se espera que el próximo interglacial para 160/232 kyr AP.

Creemos que los modelos **acoplados simples** de relajación tienen el atributo fun-

damental de que, a pesar de su estructura simple, retienen las principales interacciones climáticas de la Tierra, **que es capaz de dar cuenta** siendo capaces de capturar la evolución natural de un pulso de CO₂ atmosférico impuesto externamente. Sin embargo, con el fin de confirmar esta afirmación, nuestros resultados deben ser comparados con los obtenidos a partir de un modelo complejidad intermedia, que incluya la dinámica del carbono a largo plazo **mundial totalmente interactivo de largo plazo**. Una vez que esto se demuestre, los modelos acoplados simples pueden convertirse en una herramienta útil para examinar la evolución futura del clima en diferentes escenarios de emisiones antropogénicas de los combustibles fósiles.

C.5. Capítulo 4:

ESTUDIO DEL MIS-13 UTILIZANDO MODELOS DE RELAJACIÓN Y UN STACK DE NIVEL DEL MAR

Como hemos visto en el capítulo anterior, las oscilaciones de los glaciares-interglaciares en los últimos tiempos el clima del Pleistoceno (últimos 800 ka) revelan un ciclo de la edad de hielo de 100 ka, derivado principalmente de los parámetros orbitales y de evaluaciones internas del sistema climático (*Hays et al.* [1976]; *Archer et al.* [2000]; *Paillard* [2010, 2015]).

Siguiendo *Paillard and Parrenin* [2004], varios modelos de relajación, basados en simples parametrizaciones de la estratificación del océano profundo, se han desarrollado (*García-Olivares and Herrero* [2012, 2013]). Dos de estos modelos, 3τ y LS, tienen buenas habilidades que reproducen las condiciones durante los últimos ocho ciclos glaciales. La periodicidad de 100 ka glacial-interglacial se genera internamente a través de tres variables acopladas: la concentración de CO₂ en la atmósfera, el volumen del hielo global y la ampliación de la plataforma de hielo de la Antártida.

Los datos de foraminíferos bentónicos $\delta^{18}\text{O}$ (*Lisiecki and Raymo* [2005]) pueden ser utilizados como un proxy para el volumen de hielo (*Shackleton et al.* [2000]; *Shakun et al.* [2015]; *Waelbroeck et al.* [2002]), aunque el ratio $\text{O}^{18}/\text{O}^{16}$ se sabe depende

tanto de la composición isotópica y la temperatura del agua donde se desarrollan foraminifera. *Waelbroeck et al.* [2002] encontraron que la relación entre $\delta^{18}\text{O}$ y el volumen de hielo no es lineal, causando algunas incertidumbres en las variaciones de volumen de hielo.

Los cambios de volumen de hielo globales derivados del crecimiento y el retroceso de las capas de hielo continentales pueden estar asociados con las variaciones del nivel del mar en los ciclos glaciales-interglaciales (*Chappell and Shackleton* [1986]; *Waelbroeck et al.* [2002]; *Lambeck et al.* [2014]), un proxy con menos incertidumbres. Algunas reconstrucciones de nivel del mar a partir de los sedimentos oceánicos se han realizado utilizando diferentes representaciones y modelos, cada una de ellas limitada por el error de medición, las variaciones locales en la salinidad y la temperatura, y los supuestos particulares de cada técnica. *Spratt and Lisiecki* [2015] han elaborado una amplia representación de estas reconstrucciones, el desarrollo de un stack de nivel del mar, lo que representa el registro del nivel del mar eustático con más precisión que cada una de las reconstrucciones individuales.

Hay varias diferencias entre los modelos 3τ y LS (Figura C.12, panel inferior). Una diferencia es el valor utilizado para la capa de hielo antártica de referencia, ya sea $-C$ (que representa el efecto inverso de la temperatura de la Antártida en la capa de hielo) para el modelo LS o V para el modelo 3τ . Otra pequeña diferencia es la inclusión de $I65$ en el modelo LS cuando se especifica el valor de la concentración atmosférica de CO_2 de referencia, C_r . Sin embargo, la principal diferencia entre ambos modelos, es su parametrización del estado del océano, con $F = F(V, A)$ en el modelo 3τ y $F = F(C, A)$ en el modelo LS. Tanto V y C son buenos sustitutos para la temperatura regional del SO y $F = F(V, A)$ o $F = F(C, A)$ son plausiblemente maneras de modelar la formación local de salmueras. El hecho de que la dependencia $F = F(V, A)$ realiza algo mejor que $F = F(C, A)$ puede ser debido al papel no despreciable que V tiene en la estratificación través de teleconexiones; o para un posible efecto mayor del nivel del mar que la temperatura de la Antártida en la formación de salmuera (*García-Olivares and Herrero* [2013]; *Gildor and Tziperman* [2001]).

Los dos proxies diferentes, $\delta^{18}\text{O}$ de *Lisiecki and Raymo* [2005] y el nivel del mar

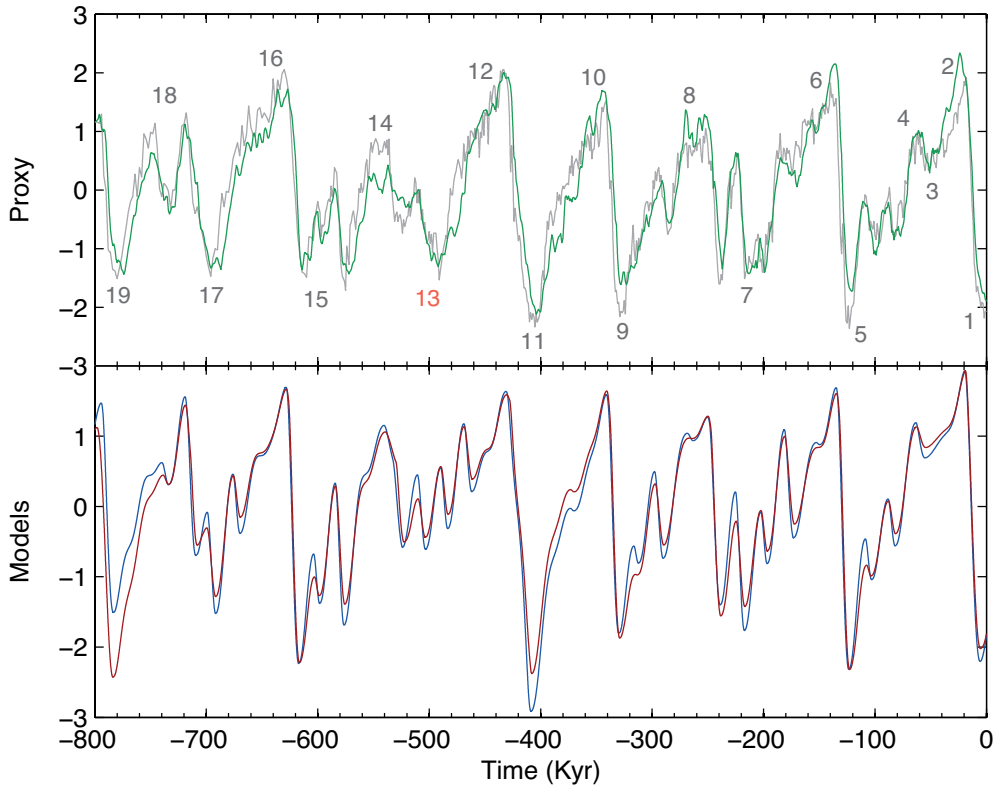


Figura
C.12

Panel superior: $\delta^{18}\text{O}$ de *Lisiecki and Raymo* [2005] (línea gris) y nivel del mar de *Spratt and Lisiecki* [2015] (línea verde); los números representan etiquetas de los Marine Isotopic Stage para el Plioceno temprano de *Lisiecki and Raymo* [2005]. Panel inferior: normalizado volumen de hielo como se predijo con 3τ (línea azul) y LS (línea roja).

de *Spratt and Lisiecki* [2015], tienen una dinámica similar pero el momento de glaciaciones se desplaza ligeramente en todos los casos, así como la profundidad de los ciclos glaciales, especialmente en los primeros cuatro ciclos (de -800 a -400 ka) (Figura C.12, arriba). La diferencia es, de alguna manera, más evidente alrededor de -500 ka, donde los datos de nivel del mar reconstruir el ciclo con menor varianza. Una comparación entre el nivel del mar y el $\delta^{18}\text{O}$ se ha realizado en *Spratt and Lisiecki* [2015], que muestra que la relación entre $\delta^{18}\text{O}$ y el nivel del mar está bien descrita por una función lineal en los primeros cuatro ciclos (de -800 a -400 kyr) y una función cuadrática en los últimos ciclos (de -400 a 0 ka).

C.5.1. Recalibración de los modelos

Teniendo en cuenta las diferencias dinámicas existentes entre el nivel del mar y el $\delta^{18}\text{O}$, una nueva calibración se ha hecho tanto para 3τ como para LS utilizando el nivel del mar (SL) de *Spratt and Lisiecki* [2015]. Esto ha derivado en dos nuevos modelos llamados $3\tau_{SL}$ y LS_{SL} de aquí en adelante.

La comparación entre los valores de los parámetros de todos los modelos se muestra en la Tabla C.3. Las correlaciones entre los modelos originales y los nuevos modelos no cambian mucho; para V , La correlación se ha incrementado de 0.88 (3τ) a 0.89 ($3\tau_{SL}$), sólo el 1%, mientras que no hay ningún cambio para el caso LS/ LS_{SL} . Para C sin embargo, la correlación ha disminuido ligeramente en ambos casos de 0.79 (3τ) a 0.77 ($3\tau_{SL}$) y de 0.76 (LS) a 0.73 (LS_{SL}), un 2% y un 3%, respectivamente. Este cambio en la correlación no debe ser importante, ya que las incertidumbres en $\delta^{18}\text{O}$ pueden producir una interpretación más de los datos, lo que significa que estas diferencias de correlación de menos de 4% se incluyen en la incertidumbre de observación. Sin embargo, la característica más notable de estas nuevas optimizaciones es un pico doble que se muestra en el volumen de hielo de $3\tau_{SL}$ alrededor de -500 kyr. Este doble pico no estaba presente en el modelo original, y no se muestra en ningún modelo LS, lo que sugiere que hay una diferencia significativa entre la dinámica tanto las delegaciones y/o en ambos modelos.

C.5.2. MIS-13

La Etapa Marina Isotópica 13 (MIS-13) ocurrió aproximadamente hace 500.000 años (-500 ka). Es de particular interés, ya que sufrió monzones graves de verano de forma simultánea con el aumento de isótopos de oxígeno marino y la disminución de los registros de núcleos de hielo de la Antártida en la temperatura en comparación con otros interglaciares (*Yin and Guo* [2008]; *Lang and Wolff* [2011]; *Muri et al.* [2012, 2013]). Todas estas anomalías indican un NH cálido y un SH fresco, y en consecuencia una fuerte asimetría de los climas continentales durante MIS-13 (*Guo et al.* [2009]).

La estratificación y la formación de aguas profundas en 3τ y $3\tau_{SL}$, donde $F = F(V, A)$, está parcialmente controlada por la temperatura de las aguas profundas del Atlántico Norte (NADW) y en parte por el nivel del mar, por lo que estos modelos son más afectados por los cambios y variaciones del nivel del mar temperatura NH. Por otro lado, los modelos LS y LS_{SL} tienen $F = F(C, A)$, lo que sugiere que la formación de las aguas antárticas (AABW) y la estratificación pueden ser controlada únicamente por la capa de hielo Antártico y la temperatura regional, todas las variables locales de la SH.

Los datos de $\delta^{13}C$ de *Lisiecki* [2010] pueden considerarse un buen indicador de almacenamiento de carbono del océano profundo, o en consecuencia, un proxy para la estratificación de profundidad. La Figura C.14 muestra los datos de $\delta^{13}C$ de *Lisiecki* [2010] y el parámetro océano, F , tanto para $3\tau_{SL}$ como para LS_{SL} . Los modelos representan con mayor precisión los últimos cuatro ciclos glaciales (de -400 a 0 ka), donde F se desplaza ligeramente en la estratificación, en lugar de los primeros (de -800 a -400 ka), donde F es claramente diferente de $\delta^{13}C$. Este comportamiento indica que F , que tiene el control del pulso de CO_2 y por lo tanto provoca la deglaciación, no podría ser lo que representa sólo la estratificación como *Paillard and Parrenin* [2004] sugirió. *Ferrari et al.* [2014] sugieren que las grandes emisiones de CO_2 oceánicas están relacionados con la capa de hielo antártica. Ambos mecanismos (estratificación y la cubierta de hielo de la Antártida) pueden ser representados en F en nuestros modelos, lo que sugiere que en los primeros cuatro ciclos glaciales los

PARÁMETROS	3τ	$3\tau_{SL}$	LS	LS _{SL}
τ_V	16585	20525.6	11325	15996.6
τ_{V_2}	3105.5	5826.5	2325	3179
τ_C	13505	8824.5	2793	2933.2
τ_{C_2}	-	-	8414	10069.4
τ_A	9004	11110	10266	13757.8
x	0.905	1.547	0.669	0.544
y	0.489	0.923	0.527	0.344
z	0.946	1.704	0.761	1.531
α	-	-	0.237	0.907
β	0.336	0.255	0.793	0.985
γ	2.044	1.538	1.955	2.242
δ	0.228	0.549	0.146	0.514
a	0.54	0.727	-	-
b	1.205	1.586	0.936	1.877
c	-	-	0.533	0.928
d	0.483	0.51	0.069	0.418
R_V	0.88	0.89	0.87	0.87
R_C	0.79	0.77	0.76	0.73

Cuadro C.3

Valores de los parámetros utilizados para los modelos originales 3τ y LS, y la nueva recalibración $3\tau_{SL}$ y LS_{SL}. R_V y R_C representan la correlación entre los proxies y los datos modelados para el volumen global hielo, V , y la concentración de CO₂ en la atmósfera, C , respectivamente.

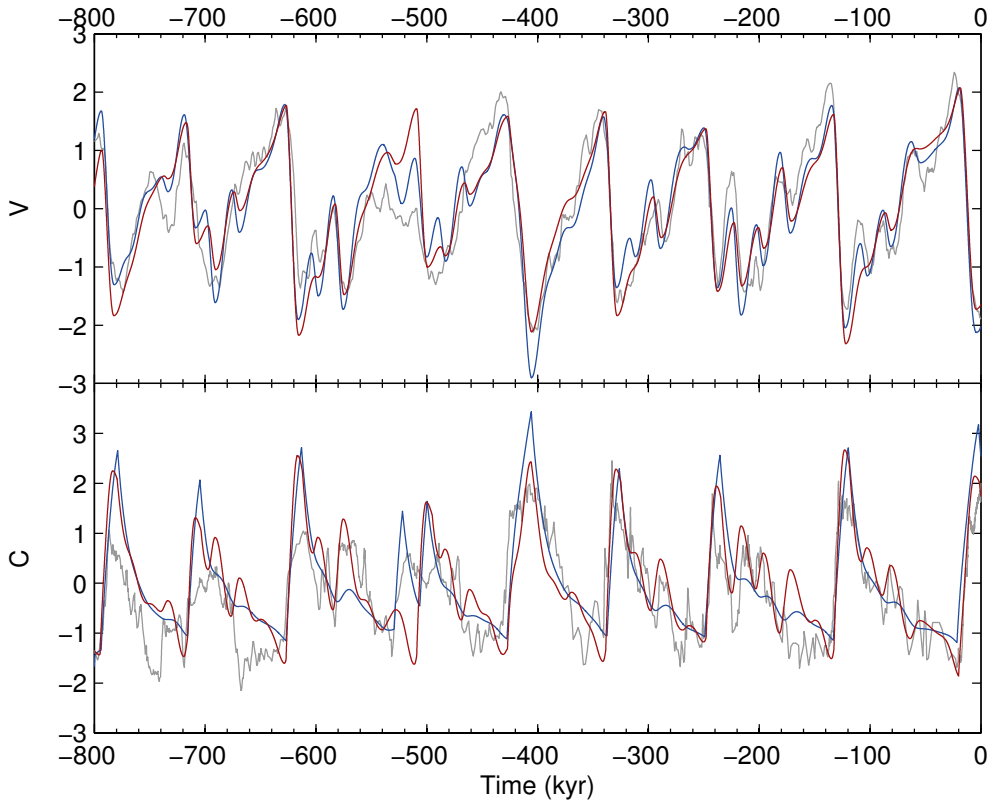


Figura C.13

Panel superior: mejor ajuste obtenido después de la optimización entre el nivel del mar de *Spratt and Lisiecki* [2015] (línea gris) y los modelos $3\tau_{SL}$ (línea azul) y LS_{SL} (línea roja). Panel inferior: mejor ajuste obtenido para la serie de tiempo de CO₂ después de la optimización: $3\tau_{SL}$ (línea azul), LS_{SL} (línea roja) y series temporales experimentales de CO₂ de *Petit et al.* [1999]; *Monnin et al.* [2001]; *Pepin et al.* [2001]; *Siegenthaler et al.* [2005]; *Luthi et al.* [2008] (línea gris).

dos mecanismos están fuera de sincronía, mientras que en los últimos cuatro ciclos están actuando en la misma dirección. Se necesitan más investigaciones para comprender los mecanismos de control de las emisiones de CO₂ oceánico y la causa de la anomalía MIS-13.

MIS-13 es un buen caso para evaluar esta posible doble dependencia de F , ya que los dos picos en el CO₂ son más como las mesetas, en lugar de la sierra de dientes común. Esto puede ser causado por la estratificación y la capa de hielo antártica actuando fuera de fase: la estratificación debilitada producirá un impulso vertical CO₂ para activar la deglaciación, pero a medida que la temperatura es especialmente baja en este interglacial, la cubierta de hielo de la Antártida es anormalmente amplia y actúa como una cubierta para la desgasificación esperada CO₂, control de la amplitud del pulso. Ambos modelos tienen formas muy similares pero LS_{SL} muestra un estado más profundo ($F < 0$) En todos los interglaciares, especialmente en MIS-13. Lo hace mostrar el inicio de un doble pico en MIS-13, pero la primera deglaciación es muy ligera y no produce suficiente pulso CO₂ para cambiar el estado, manteniendo el período glacial (Figura C.15). Después, el sistema está listo para cambiar dinámicamente el estado, produciendo un interglacial profundo y fuerte. Este profundo estado interglacial es más estable y genera un pulso de CO₂ lo suficientemente fuerte como para cambiar permanentemente de glacial para interglacial. En el caso $3\tau_{SL}$, el parámetro de la estratificación del océano profundo es más inestable (cerca del punto $F = 0$ inflexión) Y aunque el primer pulso de CO₂ genera un cambio de estado, no es lo suficientemente fuerte como para mantenerlo, retirarse a un estado glacial adicional. El segundo pulso es ligeramente más fuerte, por último generar un cambio estable de estado.

El primer intento de LS_{SL} de cambiar el estado puede no ser lo suficientemente fuerte, ya que no refleja la asimetría de los hemisferios, como el F parámetro sólo se ve afectado por variables SH. Por otro lado, $3\tau_{SL}$ se ve afectado por la dinámica de ambos NH y SH, capturando la asimetría entre los hemisferios que produce una más inestable la estratificación del océano profundo a través de una teleconexión de NADW (García-Olivares and Herrero [2013]; Gildor and Tziperman [2001]).

La comparación de $\delta^{13}C$ data de Lisiecki [2010] con el parámetro de estado del océa-

no, F , muestra una falta de coincidencia en los primeros ciclos (de -800 a -400 kyr), lo que sugiere que F podría representar no sólo la estratificación profunda (como sugiere *Paillard and Parrenin* [2004]), sino también otras variables, como la capa de hielo de la Antártida (como señala *Ferrari et al.* [2014]), lo que probablemente juegan un papel importante en las glaciaciones. En los últimos ciclos (de -400 a 0 ka), F parece estar en buen ritmo con la estratificación, aunque ligeramente desplazado, lo que sugiere que ambos mecanismos (estratificación y la cubierta de hielo de la Antártida) están actuando en la misma dirección.

La incapacidad de LS_{SL} en reproducir el pico doble de CO_2 a MIS-13 puede ser debido a la dependencia de F sobre las variables locales, que F no puede para capturar una asimetría entre los hemisferios. Por otra parte, $3\tau_{SL}$ reproduce correctamente esta doble pico y parece más preciso capturar la dinámica de MIS-13, lo que sugiere que la parametrización $F = F(V, A)$, afectado tanto por la dinámica de NH y SH, funciona mejor y es más apropiado para simular la dinámica del sistema climático.

C.6. CONCLUSIONES

En este capítulo final voy a revisar brevemente los resultados presentados en esta tesis. En el capítulo 1 varios modelos de relajación que incorporan una amplia representación de los mecanismos físicos, como el bombeo de CO_2 oceánico o los tiempos de respuesta de carbono y el volumen de hielo, se han desarrollado. Los parámetros de los modelos se han calibrado para proporcionar el mejor ajuste a datos experimentales de $\delta^{18}O$ y CO_2 para los últimos 800 ka BP. Hemos descrito ocho sub-modelos diferentes, todos derivados del modelo original de *Paillard and Parrenin* [2004], para evaluar cómo esas diferentes parametrizaciones afectan el ajuste de datos. Algunos de esos mecanismos como la producción de exportación biológico o un pulso oceánico de CO_2 exponencial no ofrecen nuevas perspectivas. Por otro lado, los sub-modelos con diferentes tiempos de respuesta para la acumulación y ablación de hielo, y/o emisión y absorción de CO_2 , muestran una buena concordancia cuantitativa y cualitativa con la serie de tiempo empírica, especialmente 4τ , EP,

C.6. CONCLUSIONES

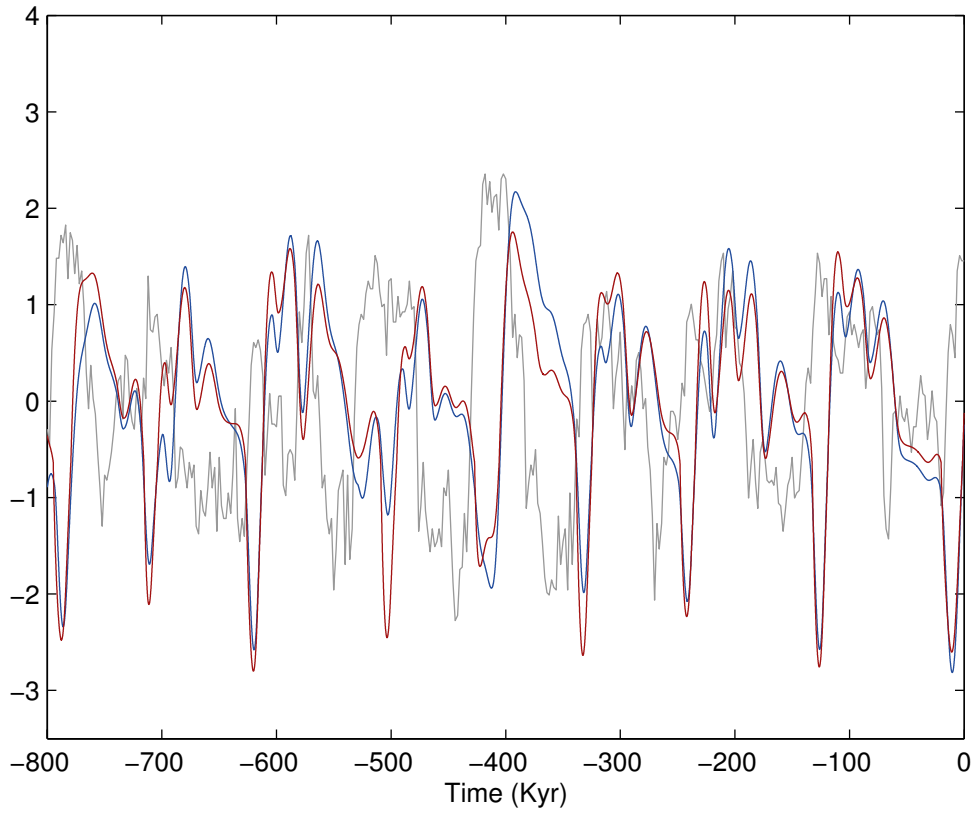


Figura C.14 Parámetro de la estratificación del océano profundo, F , derivado de $3\tau_{SL}$ (línea azul), de LS_{SL} (línea roja) y gradiente de $\delta^{13}C$ de *Lisiecki* [2010] (línea gris).

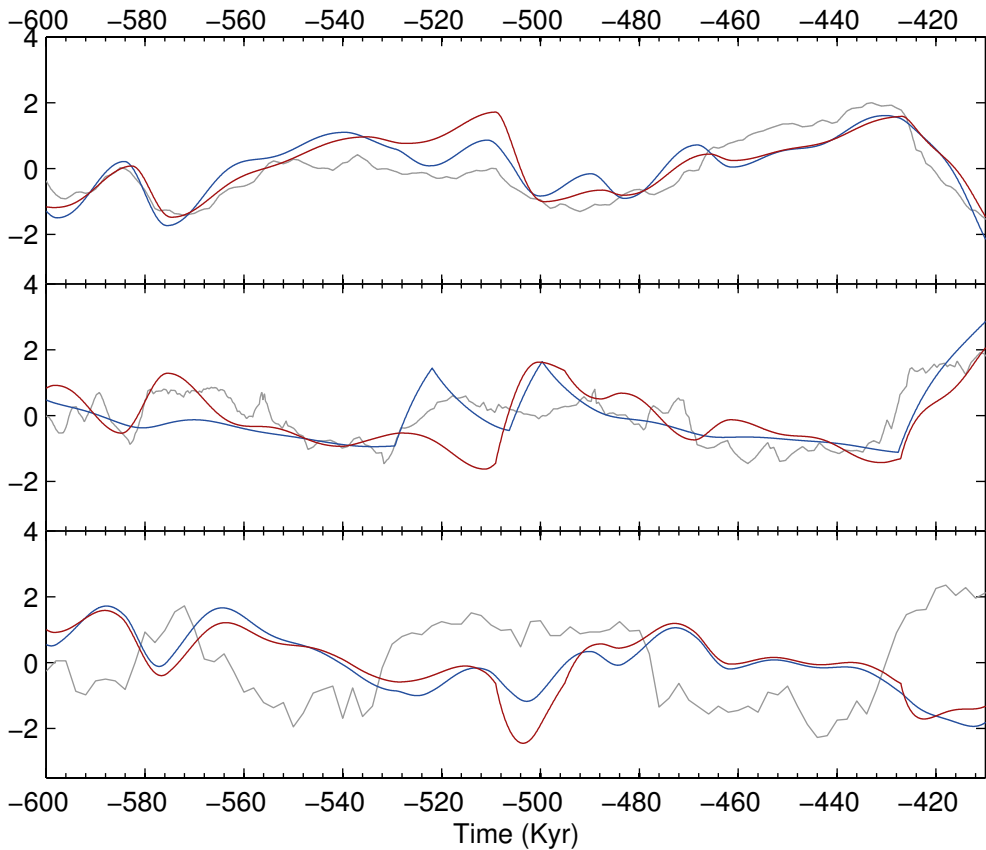


Figura C.15

El panel superior muestra el volumen de hielo se ajusta: modelo $3\tau_{SL}$ (línea azul) y el modelo LS_{GL} (línea roja), derivado de la optimización de *Spratt and Lisiecki* [2015] (línea gris). El mejor ajuste obtenido para la serie de tiempo de CO_2 : $3\tau_{SL}$ (línea azul) y el modelo LS_{GL} (línea roja), en comparación con el experimental de series temporales de CO_2 de *Petit et al.* [1999]; *Monnin et al.* [2001]; *Pepin et al.* [2001]; *Siegenthaler et al.* [2005]; *Luthi et al.* [2008] (línea gris) se muestran en el panel central. El parámetro de la estratificación del océano profundo, F , derivado de $3\tau_{SL}$ (línea azul) y el modelo LS_{GL} (línea roja) y gradiente $\delta^{13}C$ de *Lisiecki* [2010] (línea gris) se muestran en el panel inferior.

C.6. CONCLUSIONES

3τ y LS, lo que sugiere que diferentes tiempos de relajación son una posible manera de reproducir la asimetría en los ciclos glaciares y que los mecanismos que estos modelos incorporan pueden ser factores importantes que controlan las oscilaciones glaciares-interglaciares.

El modelo 4τ mejora las correlaciones de PP04 (0.59 y 0.63) a 0.79 y 0.89 utilizando el mismo número de parámetros (a saber, 14). El modelo EP utiliza 15 parámetros, pero el parámetro adicional, el cual fue dirigido a la mejora de la forma de la función de pulso oceánica, no mejora las correlaciones y puede considerarse inútil. El modelo 3τ obtiene casi las mismas correlaciones como 4τ utilizando sólo 13 parámetros. El modelo LS (15 parámetros) no mejora las correlaciones de 4τ , pero incorpora una forma funcional para la estratificación F que parece más consistente con los mecanismos sugeridos por *Paillard and Parrenin* [2004]. 3τ es el modelo con la mayor varianza explicada por parámetro, y LS, con una varianza explicada similar a la obtenida por 3τ , contiene parametrizaciones que se pueden relacionar de la forma más realista posible con mecanismos observados. Ambos modelos pueden ofrecer una información valiosa sobre el verdadero significado de la buena evolución de los modelos derivados de PP04.

En el Capítulo 2, la dinámica y mecanismos incorporados en 3τ y en LS y se han analizado y comparado para explorar las interpretaciones físicas más plausibles de las expresiones matemáticas. En primer lugar, hemos evaluado sus dinámicas no lineales utilizando wavelet transform, cross-wavelet transform, wavelet coherence, Fourier analysis, attractors y cross-recurrence plots. Hemos, por tanto, identificado los mecanismos y las dinámicas que llevan a buen ajuste de los datos y hemos comparado los resultados con la dinámica de observación que supuestamente causan oscilaciones glaciares-interglaciares.

Hemos demostrado que, de hecho, los modelos de relajación son una herramienta útil para analizar y estudiar los mecanismos físicos del sistema climático, así como para identificar las retroalimentaciones y las variables implicadas. Hemos demostrado que los modelos no son sensibles a la insolación sur; sino que responden a una variable diferente, C , que parece ser una mejor representación de la temperatura de la Antártida. Una conclusión importante es que la dinámica detallada del CO_2 no es importante

para obtener un buen ajuste entre los modelos y los datos indirectos. Lo realmente importante es la inestabilidad no lineal, alcanzada después de 80 a 100 kyr (permitiendo a V alcanzar un nivel máximo), permitiendo que cualquier aumento modesto de la insolación pueda provocar una liberación de CO_2 atmosférico.

La variable F es crucial en los modelos. Hemos señalado que una liberación abrupta oceánica de CO_2 , similar a un pulso rectangular de 10 a 20 ka, es necesario activar la terminación, y F es el control no lineal de este afloramiento de CO_2 . Se puede describir como un parámetro de control del océano profundo. Creemos que F puede ser considerado físicamente la estratificación sincrónicamente en combinación con las bombas biológicas y de carbonatos en la zona subantártica, y con la extensión del hielo marino que controla la circulación residual y la profundidad del agua de surgencia.

Una simulación precisa del conjunto detallado de los hechos que constituyen el disparador deglacial requeriría añadir una parametrización para la inestabilidad de la capa de hielo del Atlántico Norte a nuestros modelos, así como una dinámica del carbono más compleja. Los modelos derivados de PP04 producen buenos resultados a pesar de su simplicidad en el modelado de la liberación oceánica de CO_2 , y para obtener una representación más cerca de todos los procesos físicos que intervienen en el sistema climático, más mecanismos deben ser incluidos en futuras versiones.

En el Capítulo 3 hemos ilustrado una aplicación de los modelos de relajación, útil también para responder a preguntas dinámicas más directas. Hemos usado los modelos 3τ y LS para predecir la evolución futura de las variables globales de la Tierra durante los próximos 300 ka, con y sin la perturbación de CO_2 atmosférico causado por las emisiones antropogénicas de combustibles fósiles.

El pulso de CO_2 antropogénico produce 20 kyr de efecto invernadero anormalmente alto, implicando un retraso en el futuro avance de la capa de hielo sobre la plataforma de la Antártida. Como resultado, el pico correspondiente de la insolación, que causa una terminación en el escenario imperturbado, no tendrá ningún efecto sobre la estabilidad de la glaciación en desarrollo. Sin embargo, el siguiente pico de insolación se llevará a cabo en un estado apropiado del sistema climático y será suficiente para inducir la nueva desglaciación, moviendo, en consecuencia, el siguiente

C.6. CONCLUSIONES

ciclo glacial 44 kyr adelante en el tiempo. Después de tres ciclos, los interglaciales perturbados y no perturbados coinciden de nuevo y la posterior evolución de todas las variables permanecen en fase, lo que sugiere la recuperación de la periodicidad natural. Por otro lado, un aumento progresivo en el pulso antropogénico conlleva menores ciclos interglaciares, con valores inferiores de CO₂, y el timing del siguiente interglacial cambia discretamente a medida que U excede diferentes valores de umbral.

En el Capítulo 4 los modelos han sido re-calibrados usando nuevos datos del nivel del mar y se utilizan para comprender la dinámica de un evento interglacial muy particular, el MIS-13. Hemos comparado 3τ y LS con el nivel del mar de *Spratt and Lisiecki* [2015] para analizar e identificar las diferencias entre $\delta^{18}\text{O}$ (*Lisiecki and Raymo*, 2005) y el nivel del mar como los datos de indicadores para el volumen de hielo.

La comparación del parámetro del océano profundo, F , con un proxy de estratificación profunda (benthic $\delta^{13}\text{C}$, *Lisiecki* [2010]) muestra una falta de coincidencia en los primeros ciclos (de -800 a -400 kyr), lo que sugiere que F podría representar no sólo la formación de aguas profundas, sino también otras variables, como la capa de hielo antártica. En los últimos ciclos (de -400 a 0 ka), F parece estar en buen ritmo con la estratificación, aunque desplazado ligeramente, lo que sugiere una representación de un estado mixto de las profundidades del océano. Esto refuerza los resultados del capítulo 2, donde F representa no sólo la estratificación, sino también la extensión del hielo marino.

La aparición (o no) de un pico doble de CO₂ en MIS-13 en nuestros modelos, sugieren que la parametrización $F = F(V, A)$, afectada tanto por la dinámica de NH y SH, es más apropiado para simular el clima.

Podemos, por tanto, concluir que los modelos de relajación pueden ser herramientas muy útiles para caracterizar el complejo sistema climático, y útiles también para examinar cuestiones específicas como la evolución futura del clima bajo diferentes escenarios de emisiones antropogénicas de los combustibles fósiles. Los modelos de relajación pueden contribuir a ampliar el conocimiento de los mecanismos que con-

trolan la variabilidad de los ciclos glaciales del Pleistoceno; sin embargo, sus resultados deben ser comparados con los obtenidos a partir de un modelo de complejidad intermedia, que debe incluir ecuaciones de conservación, una geometría realista y la dinámica del carbono a largo plazo. El análisis de los resultados actuales bajo la perspectiva complementaria dada por estos modelos complejos sería una continuación natural de esta tesis. ┘



Bibliography

- Adhémar, J., *Révolutions de la mer*, 184 p, 1st ed., Déluges Périodiques, Paris, 1842.
- Adkins, J. F., K. McIntyre, and D. P. Schrag, The salinity, temperature, and $\delta^{18}\text{O}$ of the glacial deep ocean, *Science*, 298(5599), 1769–1773, 2002.
- Agassiz, L., Upon glaciers, moraines, and erratic blocks; address delivered at the opening of the Helvetic Natural History Society at Neuchatel, *New Philos. J. Edinb.*, (24), 864 – 883, 1838.
- Anderson, J. B., S. S. Shipp, A. L. Lowe, J. S. Wellner, and A. B. Mosola, The Antarctic ice sheet during the Last Glacial Maximum and its subsequent retreat history: a review, *Quaternary Science Reviews*, 21, 49–70, 2002.
- Anderson, R. F., S. Ali, L. I. Bradtmiller, S. H. H. Nielsen, M. Q. Fleisher, B. E. Anderson, and L. H. Burckle, Wind-Driven Upwelling in the Southern Ocean and the Deglacial Rise in Atmospheric CO_2 , *Science*, 323(5920), 1443–1448, 2009.
- Archer, D., Fate of fossil fuel CO_2 in geologic time, *J. Geophys. Res.*, 110, C09S05, 2005.
- Archer, D., and A. Ganopolski, A movable trigger: Fossil fuel CO_2 and the onset of the next glaciation, *Geochemistry, Geophysics, Geosystems*, 6(5), Q05,003, 2005.
- Archer, D., A. Winguth, D. Lea, and N. Mahowald, What caused the glacial/interglacial atmospheric pCO_2 cycles?, *Rev. Geophys.*, 38(2), 159–189, 2000.
- Archer, D., B. Buffett, and V. Brovkin, Ocean methane hydrates as a slow tipping point in the global carbon cycle, *Proceedings of the National Academy of Sciences*, 106(49), 20, 596–20, 601, 2009a.
- Archer, D., et al., Atmospheric lifetime of fossil fuel carbon dioxide, *Annual Review of Earth and Planetary Sciences*, 37(1), 117–134, 2009b.
- Arrhenius, S., On the influence of carbonic acid in the air upon the temperature of the ground, *Philos. Mag.*, 41, 237 – 276, 1896.
- Banderas, R., J. Alvarez-Solas, A. Robinson, and M. Montoya, An interhemispheric mechanism for glacial abrupt climate change, *Climate Dynamics*, 44 (9-10), 2897–2908, 2015.
- Bard, E., North-Atlantic sea surface temperature reconstruction, IGBP PAGES/World

- data center for paleoclimatology, *Data Contribution Series 2003-026*. NOAA/NGDC Paleoclimatology Program, Boulder CO, USA., 2003.
- Bard, E., B. Hamelin, M. Arnold, L. Montaggioni, G. Cabioch, G. Faure, and F. Rougerie, Deglacial sea-level record from tahiti corals and the timing of global meltwater discharge, *Nature*, 382(6588), 241–244, 1996.
- Barker, S., P. Diz, M. J. Vautravers, J. Pike, G. Knorr, I. R. Hall, and W. S. Broecker, In-terhemispheric atlantic seesaw response during the last deglaciation, *Nature*, 457(7233), 1097–1102, 2009.
- Berg, P., and A. Boland, Analysis of ultimate fossil fuel reserves and associated CO₂ emissions in ipcc scenarios, *Natural Resources Research*, 2013.
- Berger, A., *A simple algorithm to compute long term variations of daily or monthly insolation.*, vol. 18, 18 ed., Contribution de l'Institut d'Astronomie et de Geophysique, Universite Catholique de Louvain. Louvain-la-Neuve. Belgium, 1978a.
- Berger, A., Long term variations of daily insolation and quaternary climatic changes, *J. Atmos. Sci.*, 35(12), 2362–2367, 1978b.
- Berger, A., and M. Loutre, Insolation values for the climate of the last 10 million years, *Quaternary Science Reviews*, 10 (4), 297 – 317, 1991.
- Bintanja, R., R. van de Wal, and J. Oerlemans, Modelled atmospheric temperatures and global sea levels over the past million years, *Nature*, 437, 125–128, 2005.
- Björkström, A., *A model of CO₂ interaction between atmosphere, ocean and land biota.* In “*The Global Carbon Cycle*”, 403-457, B. Bolin, E. T. Degens, S. Kempe, and P. Ketner (eds.), 1979.
- Boden, A., G. Marland, and R. Andres, Global, regional, and national fossil-fuel CO₂ emissions, *Tech. rep.*, Carbon Dioxide Information Analysis Center, Oak Ridge National Laboratory, U.S. Department of Energy, 2010.
- Bond, G. C., and R. Lotti, Iceberg discharges into the North Atlantic on millennial time scales during the last glaciation, *Science*, 267(5200), 1005–1010, 1995.

Bouttes, N., D. Paillard, D. M. Roche, C. Waelbroeck, M. Kageyama, A. Lourantou, E. Michel, and L. Bopp, Impact of oceanic processes on the carbon cycle during the last termination, *Climate of the Past*, 8(1), 149–170, 2012.

Broecker, W. S., Paleocean circulation during the last deglaciation: A bipolar seesaw?, *Paleoceanography*, 13(2), 119–121, 1998.

Brovkin, V., J. Bendtsen, M. Claussen, A. Ganopolski, C. Kubatzki, V. Petoukhov, and A. Andreev, Carbon cycle, vegetation, and climate dynamics in the Holocene: Experiments with the CLIMBER-2 model, *Global Biogeochemical Cycles*, 16(4), 1139, 2002.

Burke, A., and L. F. Robinson, The Southern Ocean's role in carbon exchange during the last deglaciation, *Science*, 335(6068), 557–561, 2012.

Chappell, J., and N. J. Shackleton, Oxygen isotopes and sea level, *Nature*, 324(6093), 137–140, 1986.

Charbonneau, P., *An introduction of genetic algorithms for numerical optimization*, High Altitude Observatory, National Center for Atmospheric Research. Boulder, Colorado., 2002.

Cheng, H., R. L. Edwards, W. S. Broecker, G. H. Denton, X. Kong, Y. Wang, R. Zhang, and X. Wang, Ice age terminations, *Science*, 326(5950), 248–252, 2009.

Croll, J., On the eccentricity of the Earth's orbit, and its physical relations to the glacial epochs, *Philos. Mag.*, (33), 119 – 131, 1867.

Crucifix, M., How can a glacial inception be predicted?, *The Holocene*, 21(5), 831–842, 2011.

Denton, G. H., R. F. Anderson, J. R. Toggweiler, R. L. Edwards, J. M. Schaefer, and A. E. Putnam, The last glacial termination, *Science*, 328 (5986), 1652–1656, 2010.

Energy Watch Group, Coal: Resources and future production, *EWG-Series No 1/2007*, 1, 2007.

Ferrari, R., M. F. Jansen, J. F. Adkins, A. Burke, A. L. Stewart, and A. F. Thompson, Antarctic sea ice control on ocean circulation in present and glacial climates, *Proceedings of the National Academy of Sciences*, 111 (24), 8753–8758, 2014.

- Fischer, H., et al., The role of southern ocean processes in orbital and millennial CO₂ variations - a synthesis, *Quaternary Science Reviews*, 29 (1-2), 193 – 205, 2010.
- Ganopolski, A., R. Calov, and M. Claussen, Simulation of the last glacial cycle with a coupled climate ice-sheet model of intermediate complexity, *Climate of the Past*, 6(2), 229–244, 2010.
- García-Olivares, A., and C. Herrero, Fitting the last pleistocene $\delta^{18}\text{O}$ and CO₂ time-series with simple box models, *Sci. Mar.*, 76S1, 209–218, 2012.
- García-Olivares, A., and C. Herrero, Simulation of glacial-interglacial cycles by simple relaxation models: consistency with observational results, *Climate Dynamics*, 41 (5-6), 1307–1331, 2013.
- Gargett, A., Vertical eddy diffusivity in the ocean interior, *J. Mar. Res.*, 42(2), 359–393, 1984.
- Gassan-zade, O., National ghg emission factors in former soviet union countries, *TSU Internship Report, IPCC NGGIP/IGES*, p. 53pp, 2004.
- Gildor, H., and E. Tziperman, Physical mechanisms behind biogeochemical glacial- interglacial CO₂ variations, *Geophys. Res. Lett.*, 28(12), 2421–2424, 2001.
- Griffiths, M. L., et al., Increasing Australian-Indonesian monsoon rainfall linked to early Holocene sea-level rise, *Nature Geosci.*, 2(9), 636–639, 2009.
- Grinsted, A., J. Moore, and S. Jevrejeva, Application of the cross wavelet transform and wavelet coherence to geophysical time series, *Nonlin. Processes Geophys.*, 11, 561–566, 2004.
- Guo, Z. T., A. Berger, Q. Z. Yin, and L. Qin, Strong asymmetry of hemispheric climates during MIS-13 inferred from correlating China loess and Antarctica ice records, *Climate of the Past*, 5(1), 21–31, 2009.
- Haertel, P., and A. Fedorov, The ventilated ocean, *J. Phys. Oceanogr.*, 42(1), 141–164, 2011.
- Hain, M. P., D. M. Sigman, and G. H. Haug, Carbon dioxide effects of antarctic stratification, north atlantic intermediate water formation, and subantarctic nutrient drawdown during the last ice age: Diagnosis and synthesis in a geochemical box model, *Global Biogeochemical Cycles*, 24(4), 2010.

- Haken, H., *Advanced synergetics: instability hierarchies of self-organizing systems and devices*, Springer, Berlin, 1987.
- Hays, J. D., J. Imbrie, and N. J. Shackleton, Variations in the earth's orbit: Pacemaker of the ice ages, *Science*, *194*(4270), 1121–1132, 1976.
- Hodell, D. A., K. A. Venz, C. D. Charles, and U. S. Ninnemann, Pleistocene vertical carbon isotope and carbonate gradients in the South Atlantic sector of the Southern Ocean, *Geochemistry, Geophysics, Geosystems*, *4*(1), 1–19, 2004, 2003.
- Höök, M., A. Sivertsson, and K. Aleklett, Validity of the fossil fuel production outlooks in the IPCC emission scenarios, *Natural Resources Research*, *19*, 63–81, 2010.
- Huybers, P., Combined obliquity and precession pacing of late Pleistocene deglaciations *Nature*, *480*(7376), 229–232, 2011.
- Huybers, P., and G. Denton, Antarctic temperature at orbital timescales controlled by local summer duration, *Nature Geosci*, *1* (11), 787–792, 2008.
- IEA, World energy outlook, *Tech. rep.*, International Energy Agency, 2010. IEA, World energy outlook, *Tech. rep.*, International Energy Agency, 2012.
- Imbrie, J., et al., On the Structure and Origin of Major Glaciation Cycles 1. Linear Responses to Milankovitch Forcing, *Paleoceanography*, *7* (6), 701 – 738, 1992.
- Imbrie, J., et al., On the structure and origin of major glaciation cycles 2. The 100,000-year cycle, *Paleoceanography*, *8*(6), 699 – 735, 1993.
- Indermuhle, A., E. Monnin, B. Stauffer, T. F. Stocker, and M. Wahlen, Atmospheric CO₂ concentration from 60 to 20 kyr BP from the Taylor Dome Ice Core, Antarctica, *Geophys. Res. Lett.*, *27*(5), 735–738, 2000.
- IPCC, *Climate Change 2001: The Scientific Basis. Contribution of Working Group I to the Third Assessment Report of the Intergovernmental Panel on Climate Change*, Cambridge University Press, Cambridge, United Kingdom and New York, NY, USA, 2001.
- IPCC, *Contribution of Working Group I to the Fourth Assessment Report of the Intergovernmental Panel on Climate Change*, vol. 6: Paleoclimate, Fig. 6.3, Cambridge University

Press, Cambridge, United Kingdom and New York, NY, USA., 2007.

Jain, A., H. Kheshgi, and D. Wuebbles, Integrated science model for assessment of climate change model, in *Proceedings of Air and Waste Management Association 87th Annual Meeting*, Cincinnati, Ohio, 1994.

Jouzel, J., et al., Orbital and millennial antarctic climate variability over the past 800,000 years, *Science*, 317(5839), 793–796, 2007.

Karsten, R. H., and J. Marshall, Constructing the residual circulation of the ACC from observations, *J. Phys. Oceanogr.*, 32(12), 3315–3327, 2002.

Keeling, R. F., and B. B. Stephens, Antarctic sea ice and the control of Pleistocene climate instability, *Paleoceanography*, 16(1), 112–131, 2001.

Kennel, M. B., R. Brown, and H. D. I. Abarbanel, Determining embedding dimension for phase-space reconstruction using a geometrical construction, *Phys. Rev. A*, 45, 3403 – 3411, 1992.

Kheshgi, H. S., and A. K. Jain, Projecting future climate change: Implications of carbon cycle model intercomparisons, *Global Biogeochemical Cycles*, 17(2), 2003.

Kovacic, I., and M. J. Brennan, *The Duffing Equation: Nonlinear Oscillators and their Behaviour*, John Wiley & Sons, Ltd, 2011.

Laherrere, J., Fossil fuels: what future? Global Dialogue on Energy Security, The Dialogue International Policy Institute, China Institute of International Studies, Beijing, in *Proceedings*, 2006.

Laherrere, J., ASPO: Lessons learned: successes and challenges, in *10 years of ASPO: lessons learned*, 2012a.

Laherrere, J., Update on coal. the oil drum, 2012b.

Lambeck, K., H. Rouby, A. Purcell, Y. Sun, and M. Sambridge, Sea level and global ice volumes from the last glacial maximum to the holocene, *Proceedings of the National Academy of Sciences*, 111 (43), 15,296–15,303, 2014.

Lang, N., and E. W. Wolff, Interglacial and glacial variability from the last 800 ka in marine,

ice and terrestrial archives, *Climate of the Past*, 7 (2), 361–380, 2011.

Leduc, G., L. Vidal, K. Tachikawa, and E. Bard, ITCZ rather than ENSO signature for abrupt climate changes across the tropical Pacific?, *Quaternary Research*, 72(1), 123 – 131, 2009.

Lisiecki, L. E., A benthic $\delta^{13}C$ -based proxy for atmospheric pCO₂ over the last 1.5 myr, *Geophysical Research Letters*, 37 (21), 121708, 2010.

Lisiecki, L. E., and M. E. Raymo, A Pliocene-Pleistocene stack of 57 globally distributed benthic $\delta^{18}O$ records, *Paleoceanography*, 20(1), PA1003, 2005.

Loutre, M., and A. Berger, Future climatic changes: Are we entering an exceptionally long interglacial?, *Climatic Change*, 46, 61–90, 2000.

Luthi, D., et al., High-resolution carbon dioxide concentration record 650,000–800,000 years before present, *Nature*, 453 (7193), 379–382, 2008.

Marchitto, T. M., S. J. Lehman, J. D. Ortiz, J. Fluckiger, and A. van Geen, Marine radiocarbon evidence for the mechanism of deglacial atmospheric CO₂ rise, *Science*, 316(5830), 1456–1459, 2007.

Martin, J. H., and S. E. Fitzwater, Iron deficiency limits phytoplankton growth in the north-east pacific subarctic, *Nature*, 331(6154), 341–343, 1988.

Martinez-Boti, M. A., G. Marino, G. L. Foster, P. Ziveri, M. J. Henehan, J. W. B. Rae, P. G. Mortyn, and D. Vance, Boron isotope evidence for oceanic carbon dioxide leakage during the last deglaciation, *Nature*, 518(7538), 219–222, 2015.

Martínez-García, A., A. Rosell-Melé, W. Geibert, R. Gersonde, P. Masqué, V. Gaspari, and C. Barbante, Links between iron supply, marine productivity, sea surface temperature, and CO₂ over the last 1.1 ma, *Paleoceanography*, 24 (1), pA1207, 2009.

Marwan, N., and J. Kurths, Nonlinear analysis of bivariate data with cross recurrence plots, *Phys. Lett. A*, 302(5-6), 299–307, 2002.

Marwan, N., M. C. Romano, M. Thiel, and J. Kurths, Recurrence plots for the analysis of complex systems, *Physics Reports*, 438(5-6), 237–329, 2007.

McManus, J. F., R. Francois, J.-M. Gherardi, L. D. Keigwin, and S. Brown-Leger, Col- lapse

and rapid resumption of atlantic meridional circulation linked to deglacial climate changes, *Nature*, 428 (6985), 834–837, 2004.

Milankovitch, M., *Kanon der Erdbestrahlung und seine Anwendung auf das Eiszeitenproblem*, 663 p, 1941.

Monnin, E., A. Indermuhle, A. Dallenbach, J. Fluckiger, S. Bernhard, T. F. Stocker, D. Raynaud, and J.M. Barnola, Atmospheric CO₂ concentrations over the last glacial termination, *Science*, 291, 112–114, 2001.

Montenegro, A., V. Brovkin, M. Eby, D. Archer, and A. J. Weaver, Long term fate of anthropogenic carbon, *Geophys. Res. Lett.*, 34(19), L19,707, 2007.

Muri, H., A. Berger, Q. Yin, A. Voldoire, D. S. Y. Méliá, and S. Sundaram, SST and ice sheet impacts on the MIS-13 climate, *Climate Dynamics*, 39(7-8), 1739–1761, 2012.

Muri, H., A. Berger, Q. Yin, M. P. Karami, and P.-Y. Barriat, The Climate of the MIS-13 Interglacial according to HadCM3, *J. Climate*, 26(23), 9696–9712, 2013.

Mysak, L. A., Glacial inceptions: Past and future, *Atmosphere-Ocean*, 46(3), 317–341, 2008.

Paillard, D., The timing of pleistocene glaciations from a simple multiple-state climate model, *Nature*, 391(6665), 378–381, 1998.

Paillard, D., What drives the ice age cycle?, *Science*, 313(5786), 455–456, doi: 10.1126/science.1131297, 2006.

Paillard, D., Climate and the orbital parameters of the Earth, *Comptes Rendus Geoscience*, 342 (4-5), 273 – 285, 2010.

Paillard, D., Quaternary glaciations: from observations to theories, *Quaternary Science Reviews*, 107, 11 – 24, 2015.

Paillard, D., and F. Parrenin, The Antarctic ice sheet and the triggering of deglaciations, *Earth. Planet. Sci. Lett.*, 227 (3-4), 263 – 271, 2004.

Parrenin, F., and D. Paillard, Amplitude and phase of glacial cycles from a conceptual model, *Earth. Planet. Sci. Lett.*, 214(1-2), 243 – 250, 2003.

Peacock, S., E. Lane, and J. M. Restrepo, A possible sequence of events for the generalized glacial-interglacial cycle, *Global Biogeochemical Cycles*, 20(2), gB2010, 2006.

Pelegrí, J. L., A physiological approach to oceanic processes and glacial-interglacial changes in atmospheric CO₂, *Sci. Mar.*, 72, 185–202, 2008.

Pelegrí, J. L., P. De La Fuente, R. Olivella, and A. García-Olivares, Global constraints on net primary production and inorganic carbon supply during glacial and interglacial cycles, *Paleoceanography*, 28(4), 713 – 725, 2012PA002419, 2013.

Pepin, L., D. Raynaud, J. M. Barnola, and M. F. Loutre, Hemispheric roles of climate forcings during glacial-interglacial transitions as deduced from the Vostok record and LLN-2D model experiments, *Journal of Geophysical Reviews*, 106, 31,885–31,892, 2001.

Peterson, L. C., G. H. Haug, K. A. Hughen, and U. Röhl, Rapid changes in the hydrologic cycle of the tropical atlantic during the last glacial, *Science*, 290(5498), 1947–1951, 2000.

Petit, J. R., et al., Climate and atmospheric history of the past 420000 years from the Vostok ice core Antarctica, *Nature*, 399, 429–436, 1999.

Sagan, C., *Cosmos*, 1st ed., Random House Publishing Group, 1980.

Saikku, R., L. Stott, and R. Thunell, A bi-polar signal recorded in the western tropical pacific: Northern and southern hemisphere climate records from the pacific warm pool during the last ice age, *Quaternary Science Reviews*, 28 (23), 2374 – 2385, 2009.

Schmittner, A., Impact of the Ocean's Overturning Circulation on Atmospheric CO₂, *Geophysical Monograph Series*, 173, 2007.

Shackleton, N. J., M. A. Hall, and E. Vincent, Phase relationships between millennial-scale events 64,000-24,000 years ago, *Paleoceanography*, 15(6), 565–569, 2000.

Shakun, J. D., P. U. Clark, F. He, S. A. Marcott, A. C. Mix, Z. Liu, B. Otto-Bliesner, A. Schmittner, and E. Bard, Global warming preceded by increasing carbon dioxide concentrations during the last deglaciation, *Nature*, 484 (7392), 49–54, 2012.

Shakun, J. D., D. W. Lea, L. E. Lisiecki, and M. E. Raymo, An 800-kyr record of global surface ocean and implications for ice volume-temperature coupling, *Earth and Planetary*

Science Letters, 426, 58 – 68, 2015.

Siddall, M., B. Honisch, C. Waelbroeck, and P. Huybers, Changes in deep Pacific temperature during the mid-Pleistocene transition and Quaternary, *Quaternary Science Reviews*, 29(1-2), 170 – 181, 2010.

Siegenthaler, U., et al., Stable carbon cycle-climate relationship during the Late Pleistocene, *Science*, 310, 1313–1317, 2005.

Sigman, D. M., and E. A. Boyle, Glacial/interglacial variations in atmospheric carbon dioxide, *Nature*, 407(6806), 859–869, 2000.

Sigman, D. M., M. P. Hain, and G. H. Haug, The polar ocean and glacial cycles in atmospheric CO₂ concentration, *Nature*, 466(7302), 47–55, 2010.

Skinner, L. C., Glacial-interglacial atmospheric CO₂ change: a possible “standing volume” effect on deep-ocean carbon sequestration, *Climate of the Past*, 5(3), 537–550, 2009.

Spratt, R. M., and L. E. Lisiecki, A late pleistocene sea level stack, *Climate of the Past Discussions*, 11(4), 3699–3728, 2015.

SRES, Special Report on Emissions Scenarios, report prepared by the Intergovernmental Panel on Climate Change (IPCC) for the Third Assessment Report, *Tech. rep.*, UN, 2000.

Stephens, B. B., and R. F. Keeling, The influence of antarctic sea ice on glacial-interglacial CO₂ variations, *Nature*, 404(6774), 171–174, 2000.

Toggweiler, J. R., Variation of atmospheric CO₂ by ventilation of the ocean’s deepest water, *Paleoceanography*, 14 (5), 571–588, 1999.

Toggweiler, J. R., J. L. Russell, and S. R. Carson, Midlatitude westerlies, atmospheric CO₂, and climate change during the ice ages, *Paleoceanography*, 21 (2), PA2005–, 2006.

Truesdell, C., and R. Toupin, *Mathematics and its physical interpretation*, Springer - Verlag, 1960.

Tziperman, E., M. E. Raymo, P. Huybers, and C. Wunsch, Consequences of pacing the pleistocene 100 kyr ice ages by nonlinear phase locking to milankovitch forcing, *Paleoceanography*, 21(4), PA4206–, 2006.

+ Bibliography

Waelbroeck, C., L. Labeyrie, E. Michel, J. Duplessy, J. McManus, K. Lambeck, E. Balbon, and M. Labracherie, Sea-level and deep water temperature changes derived from benthic foraminifera isotopic records, *Quaternary Science Reviews*, 21(1-3), 295 – 305, 2002.

Wang, X., A. S. Auler, R. L. Edwards, H. Cheng, P. S. Cristalli, P. L. Smart, D. A. Richards, and C.-C. Shen, Wet periods in northeastern Brazil over the past 210 kyr linked to distant climate anomalies, *Nature*, 432(7018), 740–743, 2004.

Watson, A., and A. C. N. Garabato, The role of southern ocean mixing and upwelling in glacial-interglacial atmospheric CO₂ change, *Tellus B*, 58(1), 73 – 87, 2006.

Watson, A. J., D. C. E. Bakker, A. J. Ridgwell, P. W. Boyd, and C. S. Law, Effect of iron supply on southern ocean CO₂ uptake and implications for glacial atmospheric CO₂, *Nature*, 407(6805), 730–733, 2000.

Winograd, I. J., J. M. Landwehr, K. R. Ludwig, T. B. Coplen, and A. C. Riggs, Duration and structure of the past four interglacials, *Quatern. Res.*, 48, 141–154, 1997.

Yin, Q. Z., and Z. T. Guo, Strong summer monsoon during the cool MIS-13, *Climate of the Past*, 4(1), 29–34, 2008. ┘

A hundred years from now, people will look back on us and laugh. They'll say, 'You know what people used to believe? They believed in photons and electrons. Can you imagine anything so silly?' They'll have a good laugh, because by then there will be newer better fantasies... And meanwhile, you feel the way the boat moves? That's the sea. That's real. You smell the salt in the air? You feel the sunlight on your skin? That's all real. Life is wonderful. It's a gift to be alive, to see the sun and breathe the air. And there isn't really anything else.

— Michael Crichton, *The Lost World*